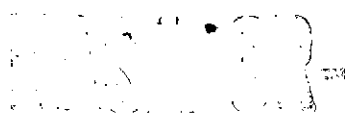


2mic



132888



Approved by
Special Engineer

Approved by
Special Engineer

Approved by
Special Engineer

(NASA-CR-132888) VHF COMMAND SYSTEM
STUDY Final Report, Jun, 1972 - Jun.
1973 (Radiation, Inc.) 202 p HC \$12.25
308

N75-12847

CSCL 17B

Unclas
24432

G3/07

TECHNICAL REPORT STANDARD TITLE PAGE

1. Report No.		2. Government Accession No.		3. Recipient's Catalog No.	
4. Title and Subtitle VHF COMMAND SYSTEM STUDY				5. Report Date June 1973	
				6. Performing Organization Code	
7. Author(s) T. H. Gee, PhD and J. M. Geist, PhD				8. Performing Organization Report No. 7620-73-001	
9. Performing Organization Name and Address Systems Engineering Department Radiation, Division of Harris Intertype Corp. Melbourne, Florida 32901				10. Work Unit No.	
				11. Contract or Grant No. NAS5-20358	
				13. Type of Report and Period Covered Final Report June 1972-June 1973	
12. Sponsoring Agency Name and Address NASA, Goddard Space Flight Center Greenbelt, Maryland 20771 Technical Officer: W. B. Poland, Jr.				14. Sponsoring Agency Code	
15. Supplementary Notes					
16. Abstract This study provides solutions to specific problems arising in the GSFC VHF-PSK and VHF-FSK Command Systems in support of establishment and maintenance of Data Systems Standards. Signal structures which incorporate transmission on the uplink of a clock along with the PSK or FSK data are considered. Strategies are developed for allocating power between the clock and data, and spectral analyses are performed. Bit error probability and other probabilities pertinent to correct transmission of command messages are calculated. Biphase PCM/PM and PCM/FM are considered as candidate modulation techniques on the telemetry downlink, with application to command verification. Comparative performance of PCM/PM and PSK systems is given special attention, including implementation considerations. Gain in bit error performance due to coding is also considered.					
17. Key Words (Selected by Author(s)) Command Systems Modulation Techniques Spectral Analysis Bit Error Probability				18. Distribution Statement	
19. Security Classif. (of this report) Unclassified		20. Security Classif. (of this page) Unclassified		21. No. of Pages 201	22. Price*

*For sale by the Clearinghouse for Federal Scientific and Technical Information, Springfield, Virginia 22161.

PRECEDING PAGE BLANK NOT FILMED

PREFACE

This is the Final Report submitted by Radiation on the VHF Command System Study, Contract Number NAS5-20358, with the Standards Office, Code 520.2, Goddard Space Flight Center. The Technical Officer for this contract is W. B. Poland, Jr.

The VHF Command System Study consists of six study tasks providing investigation and development of solutions to specific problems arising in the uplink and downlink portions of the GSFC PSK-VHF and FSK-VHF Command Systems. Results of the study are presented here in accordance with the task structure.

The authors wish to acknowledge the consultation rendered during this study by Dr. W. P. Osborne of Radiation. We also recognize the technical guidance and other considerations provided by Dr. F. A. Ford of Radiation. In addition, we are grateful to the Technical Officer, W. B. Poland, Jr. of NASA/GSFC for the technical coordination furnished throughout these contractual efforts. The authors also wish to thank R. E. Blackman and J. H. Behrens for their assistance during preparation of this report.

TABLE OF CONTENTS

<u>Paragraph</u>	<u>Title</u>	<u>Page</u>
1.0	INTRODUCTION	1-1
1.1	Background Information	1-1
1.1.1	RF Carrier Modulation	1-3
1.1.2	Command Formats and Subcarrier Modulation	1-4
1.1.2.1	Message Structure	1-4
1.1.2.2	Baseband	1-5
1.1.2.3	Subcarrier	1-6
1.1.2.4	Clock and Synchronization Format	1-7
1.1.2.5	Verification	1-7
1.1.3	Command Link Model	1-9
1.1.4	Performance Parameters	1-11
1.2	Task Descriptions and Summary of Results	1-11
1.2.1	Significant Features of FSK and PSK Command Systems	1-11
1.2.2	Carrier and Subcarrier Bandwidth Requirements	1-12
1.2.3	Selection of PSK Subcarrier Frequencies	1-13
1.2.4	Error Rates	1-13
1.2.5	Uplink Carrier Modulation	1-14
1.2.6	Downlink Carrier Modulation	1-14
1.3	References	1-15
2.0	SIGNIFICANT FEATURES OF FSK AND PSK COMMAND SYSTEMS	2-1
2.1	Error Probability with Perfect Bit Synchronization	2-1
2.1.1	No Clock	2-3
2.1.2	AM Clock	2-7
2.1.3	Summed Clock	2-10
2.1.4	Peak Signal Considerations	2-12
2.2	AM and Summed Clock Characteristics	2-16
2.2.1	Extraction of Summed Clock	2-16
2.2.2	Extraction of AM Clock	2-18
2.3	Optimum Power Allocation	2-21
2.4	AM Clock Phase Effects	2-27
2.4.1	Bandwidth Effects	2-27
2.4.2	Effects on Error Probability	2-27
2.5	Summary and Conclusions	2-32
2.6	References	2-33

TABLE OF CONTENTS (Continued)

<u>Paragraph</u>	<u>Title</u>	<u>Page</u>
3.0	CARRIER AND SUBCARRIER BANDWIDTH REQUIREMENTS . . .	3-1
3.1	Spectral Characteristics of PSK-AM Signal Structures	3-1
3.2	Spectral Characteristics of FSK-AM Signal Structures	3-10
3.3	RF Carrier Spectral Characteristics	3-21
3.3.1	Amplitude Modulation of the RF Carrier	3-25
3.3.2	PSK-AM/FM Spectral Characteristics	3-26
3.3.3	PSK-AM/PM Spectral Characteristics	3-30
3.3.4	FSK-AM/FM Spectral Characteristics	3-30
3.3.5	FSK-AM/PM Spectral Characteristics	3-36
3.4	Summary of Bandwidth Requirements	3-36
3.5	References	3-42
4.0	SELECTION OF PSK SUBCARRIER FREQUENCY	4-1
4.1	Selection on the Basis of Spectral Occupancy	4-1
4.1.1	Relationship of RF Bandwidth to Subcarrier Frequency	4-2
4.2	Selection on the Basis of Interference	4-3
4.2.1	AM Receiver - AM Interference	4-4
4.2.2	AM Receiver - Angle Modulated Interference	4-6
4.2.3	Angle Modulation Receiver - AM Interference	4-8
4.2.4	Angle Modulation Receiver - Angle Modulated Interference . .	4-13
4.3	Summary of Factors in Selection of PSK Subcarrier Frequency	4-15
4.4	References	4-16
5.0	ERROR RATES	5-1
5.1	PSK Demodulation Structures	5-1
5.1.1	Amplitude Modulated Clock	5-1
5.1.2	Summed Clock	5-4
5.2	Squelch Strategy and Analysis	5-7
5.2.1	Characteristics of the Squelch Filter Output	5-7
5.2.2	False Start and Message False Alarm Probabilities	5-10
5.2.3	Detection, Deletion, and Miss Probabilities	5-13
5.2.4	Design Considerations	5-15
5.2.5	Squelch Analysis in the Absence of RF Carrier	5-16
5.3	Bit Error Probability	5-20
5.3.1	Degradation Due to Subcarrier Phase Jitter	5-22

TABLE OF CONTENTS (Cont'd)

<u>Paragraph</u>	<u>Title</u>	<u>Page</u>
5.3.2	Degradation Due to Clock Phase Jitter	
5.3.3	Degradation Due to Use of Suboptimal	
5.4	Message Error Probability	
5.5	RFI Effects in the Subcarrier Bandpass	
5.5.1	Effects of RFI on Message False Alarm	
5.5.2	Effects of RFI on Message Deletion Probability	5-35
5.6	Coding for Error Detection and Correction	5-37
5.6.1	Uplink Coding	5-37
5.6.2	Downlink Coding	5-39
5.7	Performance Margin Criterion for PCM/PSK Demodulators	5-42
5.7.1	AM Clock System	5-43
5.7.1.1	Subcarrier and Clock Reference Phase Jitter	5-44
5.7.1.2	Effects of Bandlimiting Upon Bit Error Performance	5-45
5.7.1.3	Margin of Performance	5-45
5.7.2	Summed Clock System	5-47
5.7.2.1	Margin of Performance	5-48
5.7.3	Comparative Performance	5-49
5.8	Summary and Conclusions	5-49
5.9	References	5-50
6.0	UPLINK CARRIER MODULATION	6-1
6.1	AM Carrier Modulation	6-1
6.2	FM and Noncoherent FM Carrier Modulation	6-8
6.3	Coherent PM Carrier Modulation	6-16
6.4	Cross-Coupling Between RF Systems	6-21
6.4.1	Cross-Coupling Between Angle - and Amplitude - Modulation Systems	6-21
6.4.2	Cross-Coupling Between FM and PM	6-21
6.5	Doppler Considerations	6-23
6.6	Summary	6-26
6.7	References	6-26
7.0	DOWNLINK CARRIER MODULATION	7-1
7.1	Biphase PCM	7-1
7.2	PCM/PM	7-2
7.3	PCM/FM	7-7
7.4	Downlink Reliability Requirements	7-8
7.5	Summary	7-10
7.6	References	7-11

LIST OF ILLUSTRATIONS

<u>Figure</u>	<u>Title</u>	<u>Page</u>
1.1-1	Simplified Command System Configuration	1-2
1.1-2	Primary System Analysis Model	1-3
1.1.2.1	Command Message Format	1-5
1.1.2.4	Clock Modes	1-8
1.1.2.5	Verification Modes	1-10
2.1.1-1	Optimum Coherent PSK Detector	2-4
2.1.1-2	Optimum Noncoherent FSK Detector	2-6
2.1.1-3	DPSK Demodulator	2-7
2.1.1-4	P_e for Signals With No Clock	2-8
2.1.4	Effective Energy Used by Detector	2-15
2.3-1	Lower Bounds on P_e , Energy-Limited Signals	2-25
2.3-2	Lower Bounds on P_e , Amplitude-Limited Signals	2-26
2.4.2	Envelopes of Matched Filter Output	2-30
3.1-1	PSK-AM Spectra, (a) Spectral Density and (b) Cumulative Power Spectrum	3-5
3.1-2	PSK Spectral Envelope	3-8
3.1-3	Curves Representing (a) S_3 and (b) S_1	3-9
3.2-1	FSK-AM Spectra, (a) Spectral Density and (b) Cumulative Spectrum	3-17
3.2-2	FSK Spectral Envelope Levels as a Function of Normalized Frequency and Modulation Index	3-19
3.2-3	FSK Spectral Envelope	3-20
3.3.2-1	Power Spectrum and Cumulative Spectrum for Carrier Frequency Modulated by PSK-AM Subcarrier	3-27
3.3.2-2	PSK-AM/FM Spectra, (a) Line Spectrum Envelope and (b) Cumulative Spectrum	3-28
3.3.2-3	Peak Values of PSK-AM/FM Spectral Envelope	3-29
3.3.3-1	PSK-AM/PM Power Spectra, (a) Line Spectrum Envelope and (b) Cumulative Spectrum	3-31
3.3.3-2	Peak Values of PSK-AM/PM Spectral Envelope	3-32
3.3.4-1	FSK-AM/FM Power Spectra, (a) Line Spectrum Envelope and (b) Cumulative Spectrum	3-33
3.3.4-2	Peak Values of FSK-AM/FM Spectral Envelope	3-35
3.3.5-1	FSK-AM/PM Power Spectra, (a) Line Spectrum Envelope and (b) Cumulative Spectrum	3-37
3.3.5-2	Peak Values of FSK-AM/PM Spectral Envelope	3-38
3.4	99% Total Power RF Bandwidth, $m_{cl} = 0.5$ and $\theta_{cl} = \pi$	3-41

LIST OF ILLUSTRATIONS (Continued)

<u>Figure</u>	<u>Title</u>	<u>Page</u>
4.2.3	Sketch of Line Spectrum Corresponding to Convolution of Spectra for $\sin [x(t) - \theta_c]$ and $y(t)$	4-11
5.1.1-1	PSK Demodulator Configuration for AM Clock Signal Structure	5-2
5.1.1-2	Subcarrier Tracking Loop Bandwidth	5-5
5.1.2	PSK Demodulator Configuration for Summed Clock Signal Structure	5-6
5.2.1	One-Sided Power Spectral Density at Output of Square-Law Device	5-9
5.2.2-1	Markov Chain Model for Squelch in Absence of Signal	5-11
5.2.2-2	False Start Rate	5-14
5.2.4(a)	Detection and Deletion Probability	5-17
5.2.4(b)	Message Detection and Deletion Probability	5-18
5.2.4(c)	Message Detection and Deletion Probability	5-19
5.3.1	Degradation Due to Reference Subcarrier Phase Jitter	5-26
5.3.2	Degradation Due to Clock Phase Jitter	5-28
5.3.3	Degradation in Suboptimum PSK Detector Performance	5-29
5.4(a)	Probability of Correct Message	5-31
5.4(b)	Probability of Correct Message	5-32
5.4(c)	Probability of Correct Message	5-33
5.5.2	Degradation of Detection Probability Due to RFI in Subcarrier Passband	5-36
5.6.2-1	A Rate - $1/2$, $m = 2$ Convolutional Encoder (Generators: 101, 111)	5-40
5.6.2-2	Performance of Rate - $1/2$ Convolutional Codes with Viterbi Decoding	5-41
5.7.1.2	Upper Bounds on Bit Error Probability	5-46
6.1-1	AM Receiver	6-2
6.1-2	Noise Spectra Associated with AM Receiver (High C/N_oR)	6-3
6.1-3	Error Probability for AM Uplink Above Threshold, $m_c = 0.8$	6-6
6.1-4	Performance Curve for AM Receiver	6-8
6.1-5	Approximate Error Probability Curve for PSK/AM	6-9
6.2-1	FM Receiver	6-10

LIST OF ILLUSTRATIONS (Continued)

<u>Figure</u>	<u>Title</u>	<u>Page</u>
6.2-2	Approximate Bit Error Probability for FM Uplink with $\beta = 2$ and $p = 6$	6-13
6.2-3	Error Probability for PM Uplink Above Threshold, $\beta = 0.5$. . .	6-15
6.3-1	Coherent PM Receiver	6-16
6.3-2	$J_0(\beta)$ and $J_1(\beta)$, With Small- β Approximations	6-19
6.5	Error Probability for PSK/PM, $0.1 \leq \beta \leq 0.5$	6-24
7.1	Random Biphase PCM Power Spectrum	7-2
7.2-1	Power Spectra of PCM/PM	7-4
7.2-2	Signal Space Model for PCM/PM	7-6
7.3	PCM/FM Power Spectrum	7-8
7.4	Error Probabilities for PCM/PM and PCM/FM	7-9

LIST OF TABLES

<u>Table</u>	<u>Title</u>	<u>Page</u>
2.1.3	P_e for Energy-Limited Signals	2-11
2.1.4	P_e for Peak Amplitude-Limited Signals	2-14
3.4	Modulated Signal Bandwidths	3-39
6.4.2	Cross-Coupling Between FM and PM	6-22

LIST OF SYMBOLS

A_c	Unmodulated RF carrier amplitude
A_{sc}	Unmodulated subcarrier amplitude
a	Peak value of subcarrier signal
B_c	RF bandwidth
B_{cl}	Clock filter bandwidth
B_s	Squelch filter bandwidth
B_{sc}	Subcarrier bandwidth
C	RF carrier power
E_b	Energy per bit
E_{eff}	Effective energy used by detector
$e_c(t)$	RF signal
$e_{sc}(t)$	Subcarrier signal
$e_x(t)$	Subcarrier tracking loop filter output
f_0, f_1	FSK mark and space frequencies
f_c	RF carrier frequency
f_{cl}	Clock frequency
f_{sc}	Subcarrier frequency
$h_0(t), h_1(t)$	Matched filter impulse responses
k	Angle modulator proportionality constant
L_1, L_2	Squelch threshold levels
M	Number of noise samples per message

LIST OF SYMBOLS (Continued)

m_a	Average RF modulation index
m_{cl}	Clock modulation index
m_f	FSK modulation index
N_o	One-sided noise spectral density
$n_{sc}(t)$	Subcarrier noise
P_c	RF carrier power
P_{CORR}	Correct message probability
P_{DEL}	Message deletion probability
P_{DET}	Message detection probability
P_e	Bit error probability
$P_{e \tau}$	Bit error probability conditioned on timing error
P_{FS}	False start probability
P_{MFA}	Message false alarm probability
P_{MISS}	Message miss probability
$Q(\cdot)$	Complementary error function
R	Data rate
$S(\omega)$	Power density spectrum
$S_e(\omega)$	Power density spectrum envelope
SNR_{cl}	Clock signal-to-noise ratio
SNR_{sc}	Subcarrier signal-to-noise ratio

LIST OF SYMBOLS (Continued)

SNR_x	Subcarrier tracking loop signal-to-noise ratio
$s_0(t), s_1(t)$	General binary signals
T	Bit interval (1/R)
$W(\omega)$	RF power density spectrum
W_m	Discrete power spectral component
$x(t)$	Baseband data signal
β	RF angle modulation index
β_p	Average RF phase modulation index
β_f	Average RF frequency modulation index
η	Bit energy efficiency factor
θ_c	RF carrier phase
θ_{cl}	Clock phase
θ_{sc}	Subcarrier phase
μ_0	Mean of squelch filter output, signal absent
μ_1	Mean of squelch filter output, signal present
μ_{NC}	Mean of squelch filter output, carrier absent
ρ	Correlation coefficient
σ_0	Standard deviation of squelch output, signal absent
σ_1	Standard deviation of squelch output, signal present
σ_{NC}	Standard deviation of squelch output, carrier absent

LIST OF SYMBOLS (Continued)

τ	Clock synchronization error
$\phi(t)$	RF angle modulation function
ϕ	Phase jitter
ΔA_{pk}	Peak RF amplitude deviation
Δf	Peak FSK frequency deviation
Δf_{pk}	Peak RF frequency deviation
$\Delta \phi_{pk}$	Peak RF phase deviation

1.0

INTRODUCTION

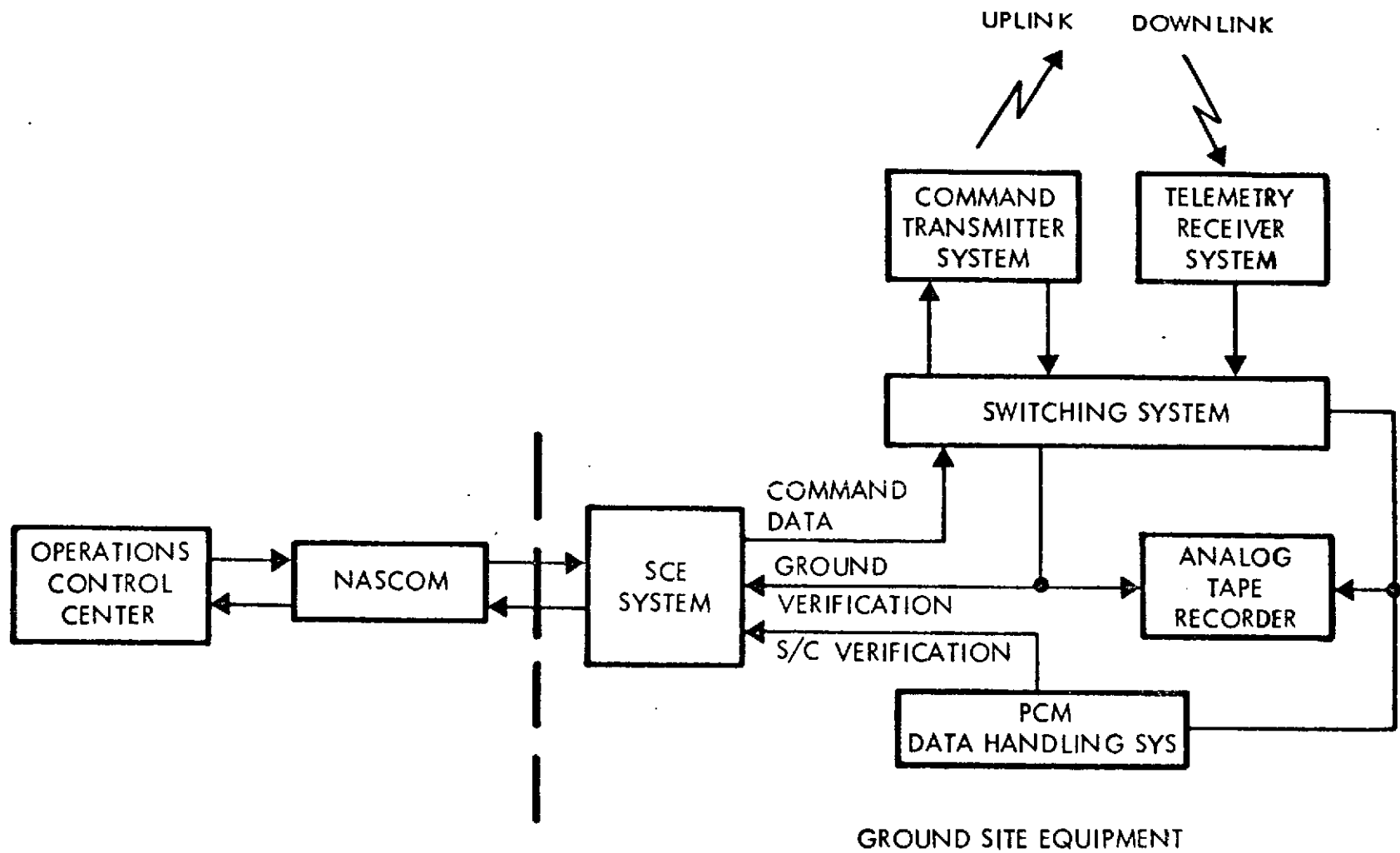
The variety of spacecraft supported by the NASA Unified Network requires development and maintenance of command systems standards. Establishment of such standards requires information on basic system performance characteristics, comparisons and evaluation of the various command modes. Towards this end, the VHF Command System Study under NASA Contract Number NAS5-20358 addresses specific tasks covering diverse areas pertinent to the establishment of such standards. It is not the purpose of this effort to conduct a general study of VHF Command Systems, but to provide answers to specific questions formulated by NASA. Under the task structure, the VHF Command System Study provides theoretical data and supporting analyses for PSK system standards and in several areas comparison of FSK and PSK command modes. In the following paragraphs, background information relevant to this study is presented, followed by brief statements of the various task objectives and summary of results.

1.1

Background Information

The information base which is considered prerequisite to addressing the VHF Command System Study is presented here. The primary subjects discussed include command generation and flow, modulation techniques and parameter ranges, command formats, performance criteria, and other key system considerations. Since the Spacecraft Command Encoder (SCE) system will be the heart of the command process in the future, the discussion here necessarily includes reference to the SCE system.

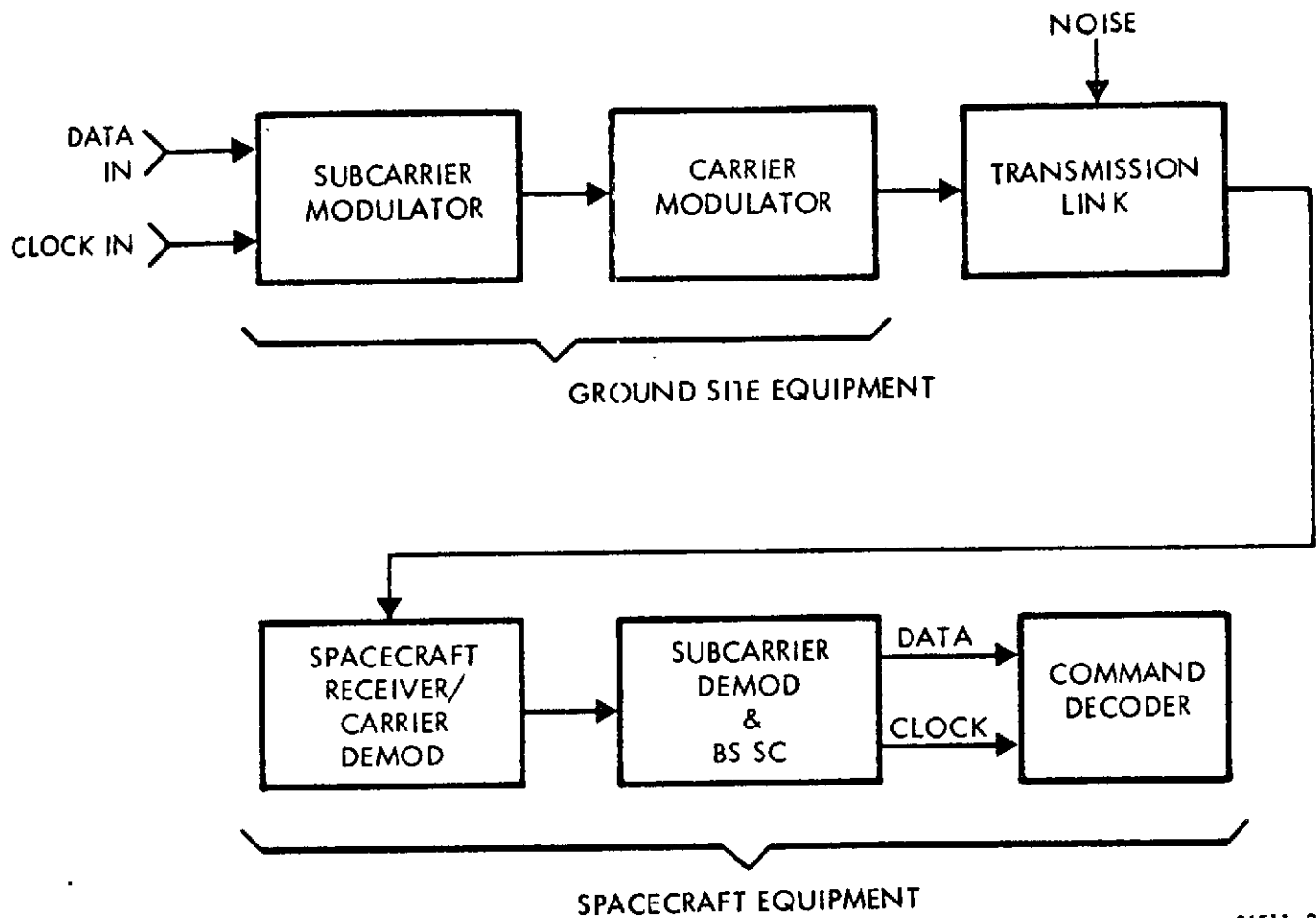
Figure 1.1-1 provides a simplified version of the overall command system configuration. Normally, commands originate at the Operations Control Center and are transmitted to the SCE at the appropriate ground site via NASCOM. This transmission is highly redundant and the SCE requests retransmission if errors are detected, or transmits verification data to the OCC if none are detected. For most passes the transmission of commands from the OCC to SCE occurs in a prepass mode and the commands are buffered within SCE. In special cases, commands can be transmitted from the OCC and processed by SCE in real time, or even originated by the local SCE operator. The SCE is a flexible device which can output commands in the tone, tone digital, PCM/PSK and PCM/FSK modes. SCE processes and formats the input command data providing the appropriate modulated subcarrier for modulation onto the carrier (which is in the 148-154 MHz range for this study) and transmission. In order to verify the success of the transmission, the transmitted signal is demodulated by a verification receiver and compared to the desired command signal in a "short loop" test. This verification is accomplished by SCE. An additional measure of assurance is provided on some commands by interrogating downlink telemetry data for spacecraft command response. This overall process provides maximum assurance of correct command transmission and reception by closing the command loop at its output terminal and finally with the spacecraft.



86411-1

Figure 1.1-1. Simplified Command System Configuration

Details of the command formats and modulation parameters possible with SCE are given below. Figure 1.1-2 presents the primary analysis model for the command system study.



86511-2

Figure 1.1-2. Primary System Analysis Model

1.1.1 RF Carrier Modulation

The NASA networks operate VHF command uplinks in the frequency band between 148 and approximately 154 MHz. Uplink signals around 120 MHz are also possible; however, the former constitutes the primary operating band and the one which is emphasized in this study. The modulation on the VHF carrier may be amplitude (AM), frequency (FM), or phase (PM) with AM being the most common.

Typically, for the VHF application the baseband subcarrier generated by SCE is modulated directly upon the carrier. This is contrasted to utilization of an intermediate subcarrier. The power output of the basic STADAN transmitters vary from 250 watts to 2.5 kw with antenna gains in the range from around 9 dB to 21 dB. Variable line losses are encountered between antenna and transmitter at the various ground sites.

The carrier frequency on the downlink is generally in the band from 136 to 138 MHz for VHF operation. Modulation of the carrier is most often accomplished by modulating the telemetry signal directly upon the VHF carrier utilizing FM or PM. Spacecraft are power limited; thus, the transmitter powers for the downlink are usually below 5 watts. Ground receiving antennas cover a range of possibilities for the VHF application. These include 85-foot and 40-foot antennas.

Verification data are often included in the downlink. These data are stripped from the downlink signal by the PCM Data Handling Equipment and transferred to SCE for verification. The verification process is discussed in more detail in a later paragraph.

1.1.2 Command Formats and Subcarrier Modulation

This section provides background information on the format of the signals which are generated within the Spacecraft Command Encoder, SCE, and which interface with the RF facilities at each site. This background, in conjunction with the RF modulation, provides the basis for the VHF Command System Study. Primary emphasis is given to the PCM/FSK and PCM/PSK modes for VHF commands. Pertinent information contained within the available Command Standards [1-1] and Guidelines [1-2] is briefly summarized below.

1.1.2.1 Message Structure

A message consists of an uninterrupted data transmission for a Command or a Memory Load instruction. The format for the Command Message is a preamble followed by one or more frames of data, each frame consisting of a message address and a command instruction. The format for the Memory Load Message is a preamble followed by a frame (address plus memory load instruction command) followed by the actual Memory Load Data itself.

The bit structure for these different message constituents is determined by the specified format and by the information data. The preamble, which initiates each new message is termed the Message Synchronization and contains thirteen or more "0's" followed by one "1". The address part of each frame is a 7-bit code word

selected because of its Hamming distance properties from other code words. The command part of each frame contains the actual instructions and is constrained by format to have a number of bits such that the frame length is less than 64 bits. (The Memory Load Instruction command is also selected based on its code word distance properties.) The Memory Load Data consists of the actual data bits but is format constrained to be an integer number of frame bits up to a maximum of 4096 bits. The subcarrier is turned off at the end of each message for at least a 20-bit interval after which new messages can be accommodated. An example of the bits in a message structure is given in the Command Message Format example of Figure 1.1.2.1 (a).

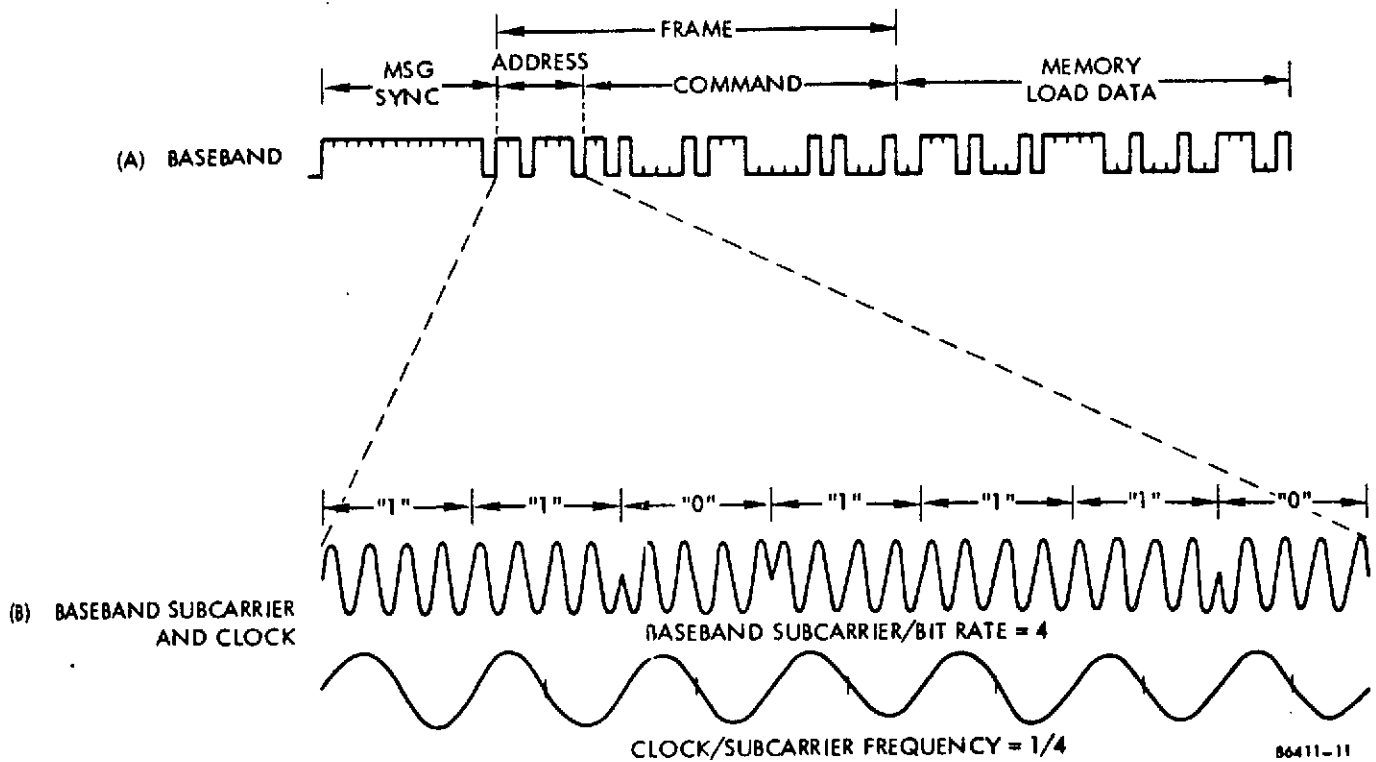


Figure 1.1.2.1. Command Message Format

1.1.2.2 Baseband

The baseband digital bit stream is generally an NRZ-level (or NRZ-change) signal in which the actual level of voltage or current specifies the "1" - "0" state. In addition, Biphasic Level (or Split Phase) is accommodated by the VHF PCM/PSK Command System and is a requirement for the SCE performance; however, this mode is not referenced in the VHF PCM/PSK Standard Guidelines.

The data rates are integer multiples of two or ten with the following limitations:

$$2^n \text{ where } n = 3, 4, 5, \dots, 10 \text{ and}$$

$$n \cdot 10^2 \text{ where } n = 1, 2, \dots, 12$$

and thus extend over the range from 8 b/s to 1200 b/s. An example of the baseband signal is given in Figure 1.1.2.1 (a).

1.1.2.3 Subcarrier

The baseband signal is FSK'ed or PSK'ed onto a baseband subcarrier to form the composite PCM/FSK or PCM/PSK modulated signal. In accordance with the FSK standards, the subcarrier frequency is chosen in the range between 7 kHz and 12 kHz. In accordance with the PSK guidelines, the subcarrier is chosen such that the sidebands are contained within the 7 kHz to 15 kHz frequency range. The SCE system has capabilities of generating any subcarrier between 2 kHz and 16 kHz with a resolution of 1 Hz for frequencies from 2-10 kHz and of 2 Hz for frequencies from 10-16 kHz.

The ratio of baseband subcarrier to bit rate is limited to an integer between 6 and 512 by the PSK guidelines; a minimum of 6 cycles/bit is specified. For the FSK Standards, the frequency deviation is given as greater than 200 Hz and not less than twice bit rate with a shifting time less than 1 cycle of the subcarrier frequency. The specifications of SCE allow a greater choice of parameters since for PSK, a minimum of 2 cycles per bit is allowable while for FSK, any frequency assignments for "1" and "0" may be made within this subcarrier frequency range. The transient time for the FSK signals is near instantaneous - appreciably less than one cycle.

The subcarrier frequency in the SCE system can be chosen with a resolution of 1 Hz (or 2 Hz for the higher frequencies) and with an accuracy of $\pm 0.02\%$ as determined by the digital timing. This frequency tolerance is somewhat better than the $\pm 0.1\%$ value given in the PCM/FSK Command Standards reference.

An example of a PCM/PSK baseband subcarrier modulation is given in Figure 1.1.2.1 (b). For convenience in drawing the figure, only four cycles per bit are shown in the example.

1.1.2.4 Clock and Synchronization Format

The bit timing and synchronization of a received bit stream is an important element in the performance of a command link and is one of the considerations for the VHF Command Study. Although several modes for transmission of clock information are available in the VHF Command System, the one of primary interest is the 50 percent AM case as specified by both the PCM/FSK Standard and the VHF PCM/PSK Guideline. However, the case of transmitting summed clock and data and the case of transmitting no separate clock are capabilities of the system as determined by SCE. These three modes are briefly discussed in the following paragraphs and an example of each mode is given in Figure 1.1.2.4.

For the AM case, the clock sinewave equal to the bit rate is amplitude modulated onto the baseband subcarrier to produce a composite waveform out of SCE and into the RF modulator. Although emphasis is given to the 50 percent AM case, SCE has provisions of AM'ing with modulation indices of 0, 10, 20, 90 percent with a tolerance of $\pm 5\%$. The 50 percent AM case is illustrated in Figure 1.1.2.4 (a) for the case where the subcarrier is four times the bit rate, or clock frequency. The phase of the clock is chosen such that the positive going crossover point of the waveform is selected at the 0, $1/4$ or $1/2$ position of the bit interval (half the bit interval is shown in the example). This selection is a design parameter of the system and even greater selection is permitted by SCE - each 45-degree phase increments for the FSK mode and each 5.625 degree phase increment for the PSK case.

For the summed case, both data and clock are added together to give the composite baseband subcarrier signal. The two signals are generally summed with equal levels; i.e., 1:1 although again the SCE capabilities provide considerably more flexibility with clock to subcarrier ratios of 4:1, 3:1, 2:1, 1:1, 2,3,4, 10, controlled by attenuator settings. The analogous example of this mode is given in Figure 1.1.2.4 (b).

If no clock signal is transmitted, this corresponds to the mode of operation illustrated by Figure 1.1.2.4 (c).

1.1.2.5 Verification

Several different verification modes are available and even required by the Common Standards and Guidelines as provided for the PCM/FSK System. These verification modes are ground, spacecraft and/or ground-spacecraft checks. Each mission is required to have ground check and either the S/C or the Ground-S/C check for the verification of the command data.

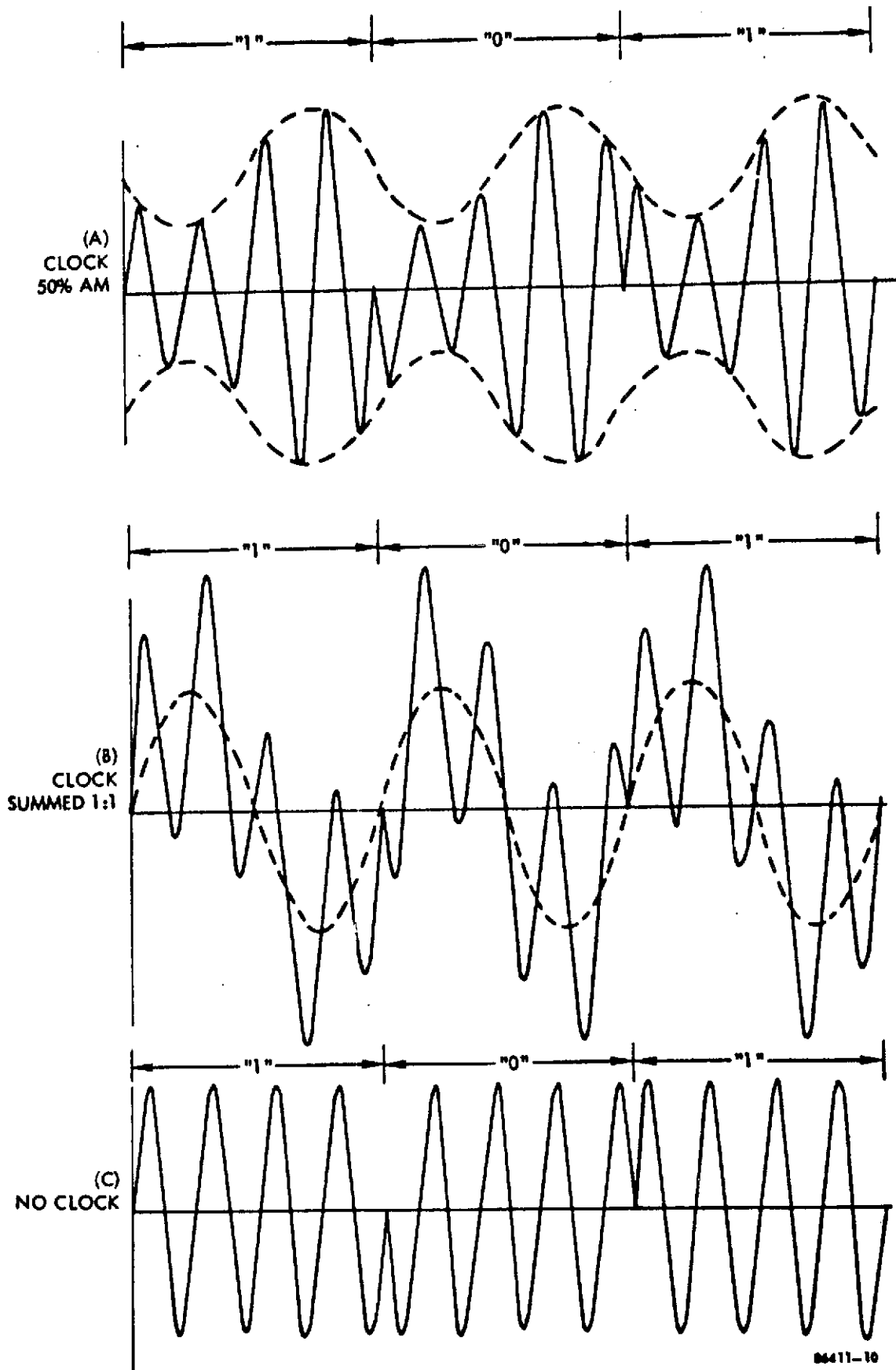


Figure 1.1.2.4. Clock Modes

The ground verification is accomplished by comparing the signal actually being transmitted (via the antenna probe output) with the correct command word. The comparison may be a bit-by-bit correlation (bit feedback check) or checking a peculiarity of the codewords, such as parity, etc., (code check). This helps assure that invalid command words are not transmitted and if they are, detection is immediate such that corrections can be implemented.

Spacecraft verifications are provided by transmitting redundancy in the command format. This redundancy may be simple frame repetitions or, alternatively, may provide error detection capabilities in the code words themselves. In either case, the spacecraft can detect an invalid command such that no action results from the invalid command.

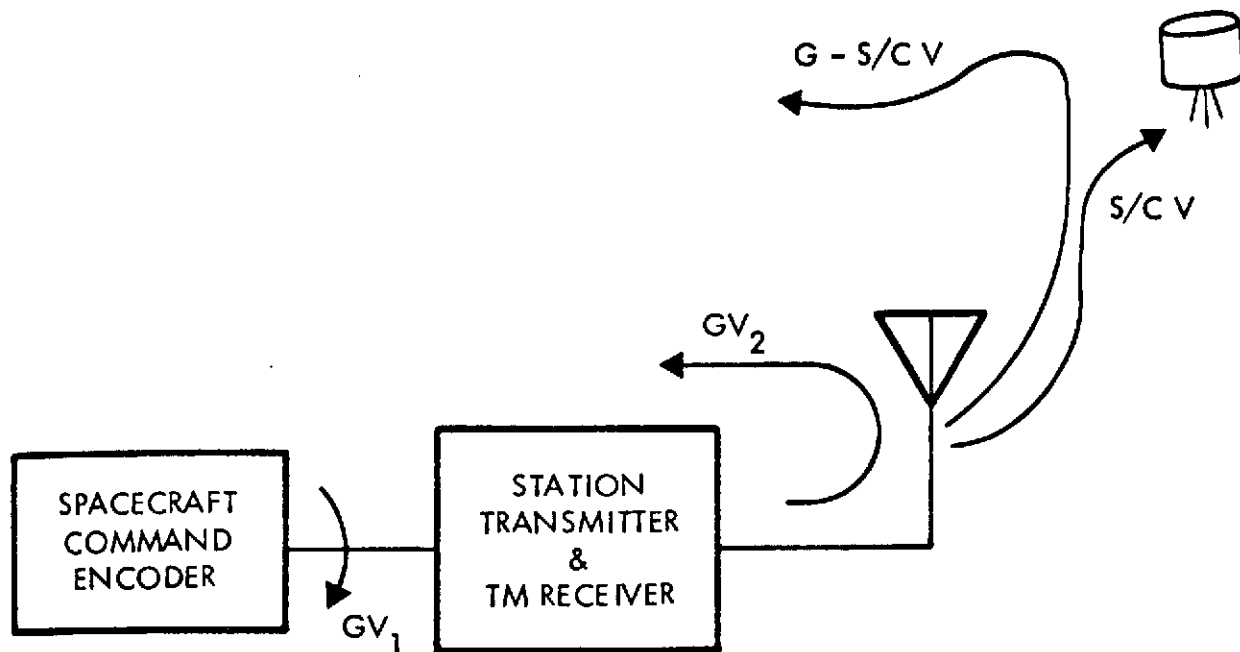
The third mode of verification is Ground-Spacecraft and involves the complete duplex link. In the frame feedback case, the command words are returned by the S/C to the ground (SCE) for verification. Alternatively, the S/C may make a decision that correct detection has occurred and only the results of this decision are returned to the ground for the verification check (decision feedback). This mode of operation is required for those commands which require verification prior to their execution and provide the greatest degree of security to the Command System.

These modes of verification are illustrated by the block diagram of Figure 1.1.2.5. One additional ground verification mode is shown in the figure which is provided by SCE and provides a verification check on the baseband sub-carrier signal itself.

1.1.3 Command Link Model

The signal path for the commands extend from the output of SCE through the RF transmitter to the spacecraft wherein command detection and execution takes place. In addition, for some operational modes, the return link - spacecraft to TM receiver to SCE - is included for the verification.

The deterministic effects of the channel model include primarily the filtering performed in the signal paths. For the command uplink, this filtering includes baseband subcarrier filters at the output of SCE and the input of the RF transmitter, and includes VHF filters at the transmitter output and the spacecraft receiver input. These filters may act to reduce the amount of signal power in the transmitted signal, and more importantly, to cause interdependence, or correlation, between adjacent bits.



86411-12

Figure 1.1.2.5. Verification Modes

Another source of error in the channel is due to the tolerances on the desired modulation and demodulation parameters. For the modulation parameters, for example, tolerance of 5 percent of the AM'ing or summing values is specified, ± 3 degrees on the clock to subcarrier phase relationship, and $\pm .02$ percent on the clock and subcarrier frequencies themselves. Additional parameter tolerances are specified for the RF modulator and transmitter. For the spacecraft receiver and command decoder, such tolerances are not defined for specific equipment; however, nominal values can be assumed for different generic classes of implementation.

The random effects of the VHF link are primarily those of Gaussian noise and/or interference at the spacecraft receiver input. The Gaussian noise is readily modelled, with contributions due to the spacecraft antenna, RF losses, and receiver noise figure. This effect is important because it is a fundamental limitation upon which link parameters are budgeted and upon which link performance is often predicted. Interference in the link is more difficult to model unless the specific source is known; however, simplifications are sometimes useful to evaluate the capabilities of the command transmissions against potential interference. In these simplifications, the interference is generally modelled as a CW signal at a given carrier frequency or perhaps a pulsed CW signal whose pulse width is short compared to a bit time. These effects of noise and interference are of primary importance in calculating the predicted performance of the VHF Command System.

1.1.4 Performance Parameters

The criterion of goodness which describes the command system performance must account for the individual bit errors which occur due to link disturbances as well as the effect of these errors on the overall performance. The Bit Error Probability (BER) is the most fundamental error criterion to evaluate since this is the primary result of additive noise or interference.

The relationship of bit errors to message errors is important in order to evaluate the effects of the errors on the system. The actual command format, the location of the error(s), and the command decoder are utilized in assessing the effects of an error (i.e., no effect, a message error and command rejection, or a message error and erroneous command reception). It is desirable to choose the command format such that erroneous command reception is prevented and no signal errors are allowed undetected. The probability of not getting a command message through the system becomes an important parameter when the command decoder does not allow any single errors and when complete ground-spacecraft verification is required for a correct transmission. This parameter can be calculated, at least under certain simplifying assumptions, based upon bit and message errors on each successive command.

1.2 Task Descriptions and Summary of Results

The VHF Command System Study consists of six tasks as set forth in the Statement of Work of Contract Number NAS5-20358. Here, a brief description of each task along with the principal results obtained from each task study are presented. The remainder of this report is organized into Sections 2 through 7 corresponding respectively to the six tasks.

1.2.1 Significant Features of FSK and PSK Command Systems

This task is concerned with determination of performance of FSK and PSK systems, with emphasis given to aspects of system performance related to transmission of the clock along with the data.

Classical expressions of bit error probability are modified to account for the AM Clock and Summed Clock signal structures which are of primary interest here. In addition, it is shown in Section 6 that the RF uplink modulation subsystems impose a peak subcarrier amplitude limitation as opposed to the energy limited condition normally encountered in determination of PSK and FSK bit error probabilities. Applicable bit error probability expressions are developed and tabulated in Tables 2.1.3 and 2.1.4 for energy limited and peak amplitude limited signals respectively.

The optimum division of total subcarrier power between clock and data is determined to be approximately 1:9. This corresponds to an AM Clock modulation index of 0.5, or a clock-to-data amplitude ratio of 1:3 for a Summed Clock. Under peak amplitude limited conditions and optimum power division, the Summed Clock demodulator's bit error performance is approximately 1.0 dB better than that of the AM Clock.

Finally, for an AM Clock system, it is shown that a clock phase corresponding to a positive-going zero crossing at time $T/4$ results in least sensitivity to small bit synchronization errors.

1.2.2 Carrier and Subcarrier Bandwidth Requirements

Determination of spectral characteristics and signal bandwidths at subcarrier and RF are basic to the overall objectives of this study. Expressions for constant envelope FSK and PSK signals for NRZ-L data are well known. It is then required to address the cases presented by amplitude modulation of the FSK and PSK subcarrier by the clock, where three possibilities exist relating the phase of the clock to the bit transitions. Spectral characteristics of AM, FM, and PM carriers modulated by the composite subcarrier are also of interest.

Power spectral density analyses have been carried out for PCM/PSK-AM and PCM/FSK-AM signals with representative data presented in Sections 3.1 and 3.2 respectively. It is shown that cases where the clock signal's positive-going zero crossing occurs at time $T/4$ yields the most narrow bandwidth for a given AM Clock modulation index. Specifically, for a clock modulation index of 0.5, the respective spectral envelopes at frequencies removed from the subcarrier lie 6 dB below those of pure PSK or FSK.

Spectral characteristics of RF carriers modulated by the composite PCM/PSK-AM and PCM/FSK-AM have also been determined. For AM carriers, the RF spectra are obtained by simple translation of the subcarrier spectra to the carrier frequency. In the FM and PM case, discrete spectral analyses are employed to compute representative RF spectral characteristics as a function of both subcarrier and carrier modulation parameters. These data are graphically presented in Section 3.3. Approximate relationships between required bandwidth and the various modulation parameters are developed and summarized in Table 3.4. In addition, 99% total RF power bandwidth data are given as a function of modulation index in Section 3.4.

1.2.3 Selection of PSK Subcarrier Frequencies

The objective of this task is to establish criteria for selection of PSK subcarrier frequencies. Of particular interest are selection based upon RF spectral occupancy and selection from the viewpoint of minimizing the effects of interference due to two command systems sharing a common RF channel.

It is shown in Section 3.3 that the RF bandwidth is primarily dependent upon the value of the subcarrier frequency and that the bit rate plays a secondary role. The RF bandwidth is approximately an even integer multiple of the subcarrier frequency. Thus, minimization of subcarrier frequency results in conservation of RF spectral occupancy.

The results of Sections 6.1 and 6.2 indicate that the ability to establish threshold at the receiver's first detector is strongly dependent upon the RF bandwidth and consequently the value of subcarrier frequency. Thus, detector threshold considerations also support selection of the subcarrier frequency as small as practical.

Consideration is given to the possible selection of PSK subcarrier frequencies which results in reducing the risk of interference due to two command systems sharing a common RF channel, including various combinations of AM, FM, and PM modulation. A first order analysis shows that the interference in or near the desired subcarrier passband can be representative of subcarrier and/or carrier spectra of the desired and/or interfering signal. It is seen that the difference frequency between desired and interfering RF carriers serves to translate the interfering spectrum. In the case where this is a Doppler difference frequency, the frequency band of the interfering spectrum can vary with time. The Doppler generated difference can be on the order of the subcarrier frequency or less. It is found that under conditions of near-zero difference frequency, an AM receiver with AM interference yields more readily than an angle modulation receiver to attempts to reduce interference through a judicious choice of subcarrier frequency. On the other hand, an angle modulation receiver exhibits a capture effect and will therefore operate under lower signal-to-interference levels than an AM receiver.

1.2.4 Error Rates

The objective of this task is a detailed analysis of the bit error probability and message error probability performance of PSK command systems. Simple demodulators for PSK-AM and PSK-Summed signals are postulated. The demodulators include, besides the PSK detector, a squelch circuit, and circuitry for obtaining bit and subcarrier synchronization. In connection with the squelch strategy, formulas and curves are presented in Section 5.2 indicating how the choice of squelch parameters affects message detection and deletion probability

and the probability that the decoder starts to decode a spurious message. It is shown that the condition where the RF carrier is absent must be considered in setting the squelch threshold. Effects of selected RFI signal structure upon squelch operation is presented in Section 5.5.

The clock and subcarrier synchronization schemes are analyzed and the degradation in performance due to synchronization error is shown in Section 5.3 to be only a fraction of a decibel for signal-to-noise ratios in the range of interest. These and other considerations, such as implementation loss and power division between data and clock, are collected to develop a performance margin for AM and Summed Clock type PSK demodulators. The margin for each system is approximately 3 dB.

1.2.5 Uplink Carrier Modulation

In this task the overall system performance of PSK or FSK subcarrier signals in conjunction with AM, FM or PM carrier modulation is studied. For AM and narrowband PM uplink, formulas are obtained which relate bit error probability to carrier power and noise spectral density. Representative data are graphically presented in Sections 6.1 and 6.2 for AM and narrowband PM uplinks, respectively. For an FM uplink, a bound on error probability is obtained which shows that the wideband FM improvement usually found in FM systems cannot be exploited. Exact relationships between error probability and RF signal-to-noise ratios for FM uplinks cannot be determined. However, a method of approximating the error probability is discussed, and approximate values are obtained and plotted in Section 6.2. It is seen that the bit error performance of systems employing a Summed Clock is about 1 dB superior to those employing an AM Clock when the RF modulation is AM or narrowband PM. When the RF modulation is FM, this difference is about 0.5 dB.

Effect of Doppler shift at RF and subcarrier are considered. It is shown that the Doppler shift at RF is significant (i.e., ≤ 6.5 kHz) compared to the subcarrier frequency and therefore, has some impact on receiver design. Influence of Doppler shift upon bit error performance is discussed in Section 6.5. The Doppler shift at subcarrier is not significant.

1.2.6 Downlink Carrier Modulation

This task is concerned with those aspects of the telemetry downlink which relate to its function in the command verification loop. Error probability expressions for biphase PCM/PM and PCM/FM are developed. In the PCM/PM case a modulation index of $\beta = \pi/2$, resulting in antipodal PSK signals, is shown to require least signal power to achieve a given error probability. However, the bit error performance is degraded by only 0.5 to 1 dB when 10 to 20 percent of the

total power is put in the carrier to facilitate synchronization (corresponding to values of β in the range 1.25 to 1.1). This could be a desirable trade for decreased receiver complexity realized by tracking the carrier directly. Drawing on results of Section 5.6, it is shown that the error probabilities necessary for efficient operation of the verification loop can be achieved at intermediate signal-to-noise ratios (~ 7 dB) through the use of encoding and decoding equipment of moderate complexity.

1.3

References

- [1-1] Aerospace Data System Standard, Part II, Section 3, PCM/FSK Command Data System Standard, GSFC, Greenbelt, Maryland, July 1, 1971.
- [1-2] VHF PCM/PSK Command System Standard Guidelines: Memorandum from R. J. Coates to Distribution, GSFC, Greenbelt, Maryland, October 6, 1971.

2.0 SIGNIFICANT FEATURES OF FSK AND PSK COMMAND SYSTEMS

Comparative analyses of various systems are performed in this section, with particular emphasis on the fundamental differences between PSK and FSK systems, and the effects on performance when various synchronization options are used.

Initially PSK and FSK systems are compared on the basis of bit error probability P_e for given bit energy-to-noise ratio E_b/N_o . Consideration is given to the effect on P_e of removing some energy from the data and using it to transmit the bit rate clock.

Next, methods of clock recovery at the receiver are discussed and output signal-to-noise ratios are derived. Following this, an attempt is made to determine the optimum division of transmitted energy between data and clock.

Finally, the effects of varying the phase of an amplitude-modulated clock on power spectra and receiver performance are discussed.

2.1 Error Probability with Perfect Bit Synchronization

In this section, the probability of bit error as a function of transmitted energy is determined for PSK and FSK with a variety of bit synchronization schemes. For the present, it is assumed that whatever the synchronization strategy, perfect synchronization is obtained. The effects of bit timing errors will be studied in Section 2.3, and from a different point of view in Section 5.

Three methods of deriving bit synchronization will be considered. The first method involves no separate transmission of a clock; the receiver estimates bit timing from the received PSK or FSK signal. The principal advantage of this method is that all the transmitted energy is used to convey information, with none "wasted" in transmitting a clock. The price of this efficiency is a high degree of complexity in synchronizing circuitry at the receiver.

A second approach is to transmit timing information by amplitude modulating the PSK or FSK signal by a sinusoid whose frequency is the bit rate and whose phase is in a known relation to the switching times. This clock signal is recovered at the receiver by one of the conventional AM detection techniques. With this method, the synchronization circuitry is much simpler than with the first method, but when the simplest receiver is used, the transmitted energy associated with the clock is ignored in making bit decisions, so that there is some loss of efficiency. However, it will be shown that when a more complex receiver is used, this loss of efficiency does not occur.

Finally, synchronization can be obtained by transmitting a sinusoidal clock added to the PSK or FSK signal. The synchronization circuitry is simple, but the clock power is "wasted". Unlike the AM clock case, there is no way that the waste can be avoided by using a more complicated receiver.

PSK and FSK systems employing all three synchronization strategies will be compared on the basis of error probability as a function of signal power. The PSK guidelines [2-1] specify that the subcarrier frequency f_{sc} should be an integer multiple of the data rate R . No comparable condition is imposed by the FSK standard [2-2], and the results given are, except as noted, valid for any choice of mark and space frequencies f_1 and f_0 .

A key formula in this section is that for the probability of error for coherent detection of equally likely signals $s_0(t)$ and $s_1(t)$ of equal energy E_b in the presence of additive white Gaussian noise of spectral density $N_0/2$. Let

$$\rho = \frac{1}{E_b} \int_0^T s_0(t) s_1(t) dt$$

then [2-3]

$$P_e = Q\left(\sqrt{\frac{(1-\rho) E_b}{N_0}}\right) \quad (2.1-1)$$

where

$$Q(X) = \frac{1}{\sqrt{2\pi}} \int_X^\infty e^{-u^2/2} du$$

A case of particular importance is $\rho = -1$, in which case the signals are called antipodal.

Another useful error probability formula is that for noncoherent detection of orthogonal signals. To say that $s_0(t)$ and $s_1(t)$ are orthogonal means that $\rho = 0$. Under this condition, a noncoherent detector exhibits error probability [2-3]

$$P_e = \frac{1}{2} e^{-E_b/2N_o} \quad (2.1-2)$$

This relation applies to receivers which make decisions on a bit-by-bit basis; we shall note subsequently that better performance can sometimes be obtained by using receivers which take advantage of dependence among adjacent bit intervals of the transmitted signal.

2.1.1 No Clock

When there are no constraints on equipment complexity and receiver design is allowed to be as elaborate as necessary, synchronization can be derived from the pure PSK or FSK signal alone, without the transmission of a separate clock. In such a scheme, all transmitted power is used in communicating data, so that the most efficient use of power is made. In addition, it can be shown [2-4] that in cases of practical interest, an estimate of bit timing derived from the data signal itself is superior to one derived from a separate clock transmission.

The major disadvantage of receivers which synchronize directly from the data signal is that fairly complex synchronization circuitry is required (details of the receiver designs and analysis of their performance are given by Stiffler [2-5]). In particular, for FSK systems, where no subcarrier synchronization is necessary, the addition of circuitry to derive bit synchronization from the FSK signal is a significant increase in receiver complexity. In PSK systems, the subcarrier must be extracted in order to detect, and since $f_{sc} = pR$, p an integer, the clock could be obtained by dividing down the extracted subcarrier. However, a p -fold ambiguity must be resolved, and since p can be quite large, ($6 \leq p \leq 512$) this problem is not simple. The situation is complicated by the fact that the form of the preamble (thirteen zeros followed by a one) allows only one sign change before the data sequence begins; this complication could be overcome by changing the form of the preamble or by using biphasic rather than NRZ PCM*.

In the absence of a transmitted clock, the NRZ-L PCM/PSK signals (over one bit interval) have the form

*The terms "biphase", "NRZ" and related terms are used in this report as defined in [2-6].

$$s_0(t) = \sqrt{\frac{2E_b}{T}} \cos(\omega_{sc} t + \theta_{sc}), \quad 0 \leq t \leq T$$

$$s_1(t) = -s_0(t)$$

PSK must be coherently detected since the information resides in the subcarrier phase. The signal energy is E_b , and since $s_0(t) = -s_1(t)$, $\rho = -1$; therefore using Equation 2.1-1,

$$P_e = Q\left(\sqrt{\frac{2E_b}{N_o}}\right) \quad (2.1.1-1)$$

The optimum receiver is the correlation device shown in Figure 2.1.1-1.[†]

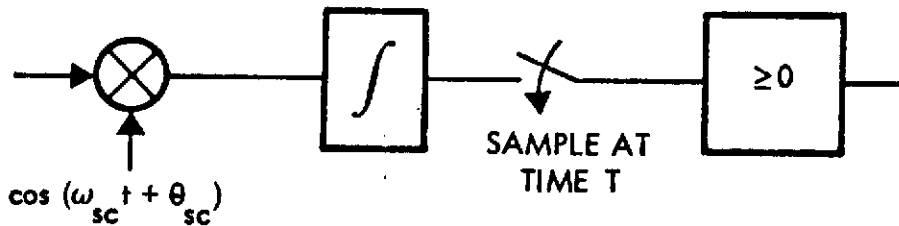


Figure 2.1.1-1. Optimum Coherent PSK Detector

If the baseband signal is biphase PCM, the resulting PSK signals have the form

$$s_0(t) = \begin{cases} \sqrt{\frac{2E_b}{T}} \cos(\omega_{sc} t + \theta_{sc}), & 0 \leq t < T/2 \\ -\sqrt{\frac{2E_b}{T}} \cos(\omega_{sc} t + \theta_{sc}), & T/2 \leq t \leq T \end{cases}$$

[†]Derivation of the optimum receiver structures can be found in [2-7].

$$s_1(t) = -s_0(t)$$

Since the signals are antipodal with energy E_b , error probability is still given by Equation 2.1.1-1. The form of the optimum receiver is essentially that of Figure 2.1.1-1 except that the received signal should be correlated with the biphase sinusoid

$$f(t) = \begin{cases} \cos(\omega_{sc} t + \theta_{sc}) & , 0 \leq t < T/2 \\ -\cos(\omega_{sc} t + \theta_{sc}) & , T/2 \leq t \leq T \end{cases}$$

Biphase PSK and NRZ PSK are seen to be equally good in terms of error probability. However, biphase PSK facilitates extraction of the bit clock from the data since at least one sign change per bit is guaranteed. In addition, a biphase PCM signal contains negligible power near dc, which is important in certain practical situations.

The NRZ-L PCM/FSK signals have the form:

$$s_i(t) = \sqrt{\frac{2E_b}{T}} \cos(\omega_i t + \theta) \quad , \quad 0 \leq t \leq T \quad , \quad i = 0,1$$

where the phase θ over each bit interval depends on previous bits in such a way as to make the phase of the FSK signal continuous.

While FSK can be coherently detected, this is not often done since a non-coherent FSK detector performs nearly as well (at high signal-to-noise ratios) and is more simply implemented because no synchronization to subcarrier frequency is required. Such a non-coherent receiver is implemented as shown in Figure 2.1.1-2. The filters $h_0(t)$ and $h_1(t)$ are matched to $s_0(t)$ and $s_1(t)$ without regard to phase; that is

$$h_i(t) = \cos \omega_i t \quad , \quad 0 \leq t \leq T \quad , \quad i = 0,1$$

The error probability when this receiver is used is given by Equation 2.1-2, provided that the signals are orthogonal. The FSK Command System Standard [2-2] requires that $|f_0 - f_1| \geq 2R$, and under this condition the correlation coefficient ρ is sufficiently small that Equation 2.1-2 is quite accurate. The exact form for P_e for any ρ can be found in [2-3].

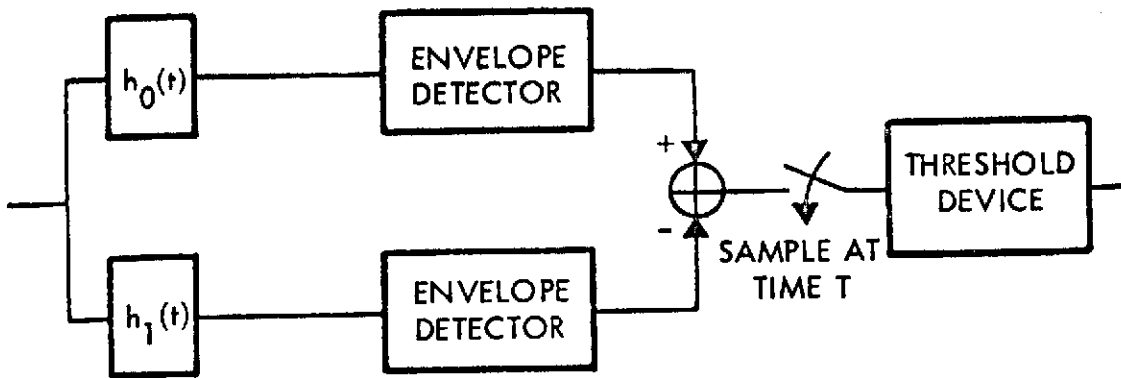


Figure 2.1.1-2. Optimum Noncoherent FSK Detector

A continuous phase FSK signal can also be demodulated by a discriminator, and when the ratio $|f_0 - f_1|/R$ is small and the IF bandwidth is properly chosen, performance is better than Equation 2.1-2 indicates [2-8]. The reason for this superiority is that discriminators take advantage of a "differential phase coherence" [2-9] introduced by the phase continuity. Since the phase over any bit interval depends on (and contains information about) previous bits, receivers which are allowed to make use of this information should perform better than bit-by-bit receivers. Receivers which use this memory explicitly have been devised [2-10] and shown to perform better than Equation 2.1-2 indicates, but these receivers are considerably more complex than the receiver of Figure 2.1.1-2, and are not likely to be used in this application.

Biphase PCM can be used in conjunction with FSK. In this case, the non-coherent receiver is similar to that of Figure 2.1.1-2 except that the filters are matched to biphase FSK pulses. Alternatively, a receiver can be implemented consisting of filters matched to f_0 and f_1 over half a bit interval, followed by envelope detectors, with post detection combining of the outputs after the two half-bit intervals. Performance of the former receiver is given by Equation 2.1-1; the latter receiver is slightly inferior, having twice the P_e at $E_b/N_0 = 8.0$.

Finally, for comparison purposes we present the performance of a scheme which combines some of the advantages of PSK and FSK, namely differential PSK. In DPSK a signal $s_0(t)$ is transmitted if the corresponding data bit agrees with the bit immediately preceding it, and $s_1(t) = -s_0(t)$ is transmitted if the corresponding bit is the complement of its predecessor. What is gained by this is that a receiver can be realized which does not require subcarrier coherence; instead, the received signal is correlated with a time-delayed version of itself, as shown in Figure 2.1.1-3. The error probability of this scheme is given by [2-11]

$$P_e = \frac{1}{2} e^{-E_b/N_o}$$

This is 3 dB better than noncoherent orthogonal FSK, and only slightly worse than PSK at high signal-to-noise ratios.

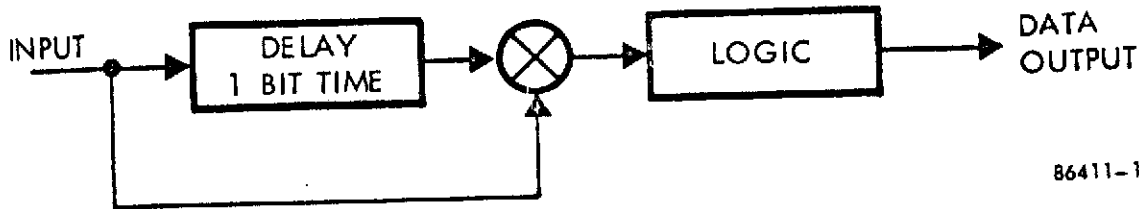


Figure 2.1.1-3. DPSK Demodulator

The bit error probability results we have noted are plotted in Figure 2.1.1-4. We remark again that these results are valid under the assumption of perfect synchronization. Degradation due to clock and subcarrier phase jitter will be considered later.

In what follows, we will, for purposes of simplicity, consider only coherent PSK and non-coherent FSK, with NRZ-L PCM baseband signals.

2.1.2 AM Clock

Convenient expressions for the NRZ-L PSK signals with AM Clock are

$$s_0(t) = \sqrt{\frac{2E_b}{T(1+q^2)}} \left[1 + \sqrt{2}q \cos(\omega_{cl}t + \theta_{cl}) \right] \cos(\omega_{sc}t + \theta_{sc}) \quad 0 \leq t \leq T$$

and $s_1(t) = -s_0(t)$, where $\omega_{cl} = 2\pi/T$ is the clock frequency in radians per second, θ_{cl} is the clock phase, and $\sqrt{2}q$ is the AM modulation index. The signals are antipodal, so the optimum receiver is similar to that of Figure 2.1.1-1, except that the received signal should be correlated with an amplitude modulated sinusoid with the form of $s_0(t)$, rather than the pure sinusoid. The signals are antipodal with energy

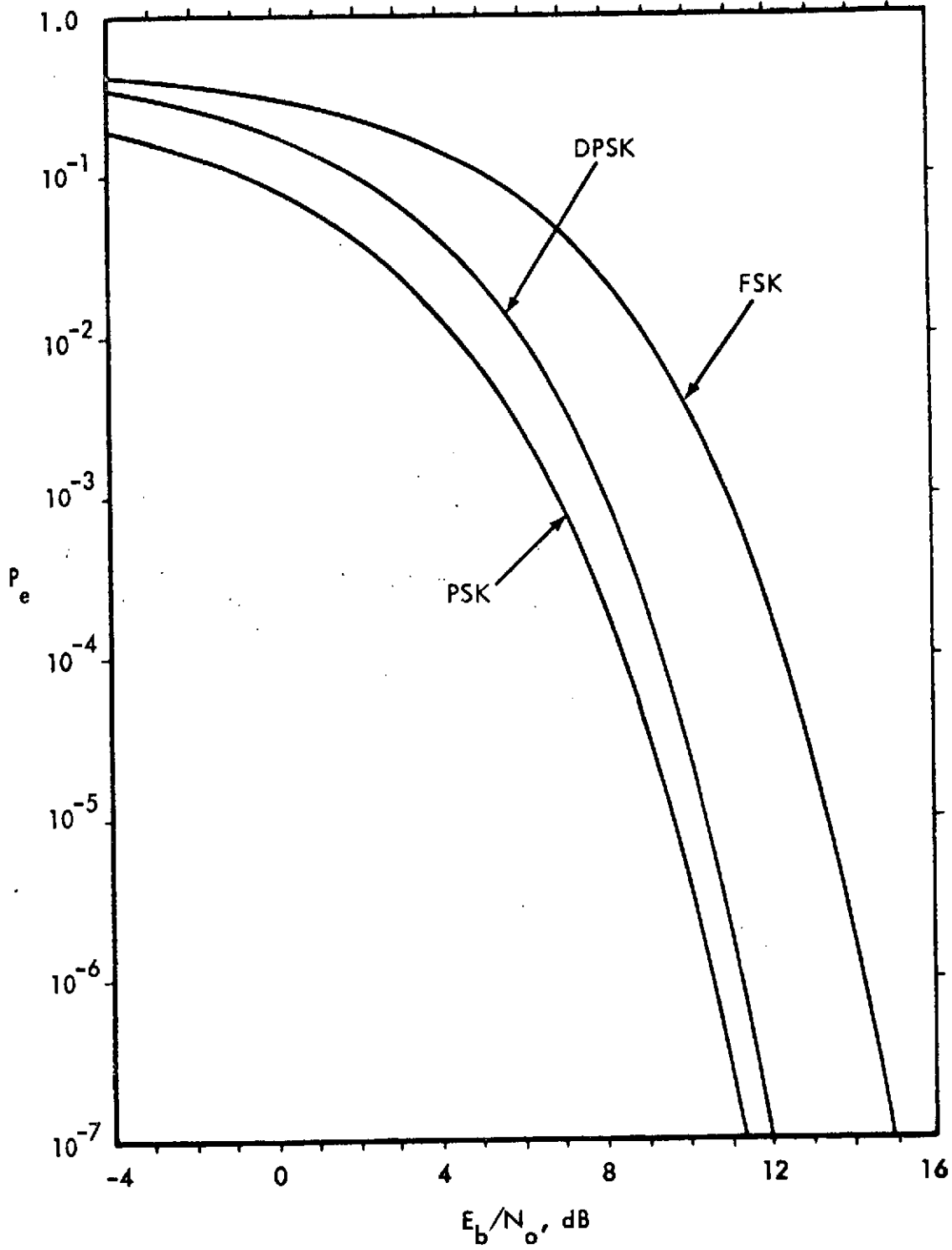


Figure 2.1.1-4. P_e for Signals With No Clock

E_b , so that when the optimum receiver is used, P_e is given by Equation 2.1.1-1. Thus there is no increase in error probability when the clock is transmitted by amplitude modulation of the PSK, provided that the optimum receiver is used.

It is also possible to detect the PSK-AM signal with the receiver of Figure 2.1.1-1 as shown; i.e., by correlating with the pure sinusoid rather than the amplitude-modulated sinusoid. This is attractive for reasons of receiver simplicity and we will see later that very little loss is suffered. To see the effect of this, note that the signals can be rewritten

$$s_i(t) = (-1)^i \sqrt{\frac{2E_b}{T(1+q^2)}} \cos(\omega_{sc}t + \theta_{sc}) + (-1)^i \sqrt{\frac{4q^2 E_b}{T(1+q^2)}} \cos(\omega_{cl}t + \theta_{cl}) \cos(\omega_{sc}t + \theta_{sc}), \quad 0 \leq t \leq T, \quad i = 0, 1$$

Since $\omega_{sc} = 2p\pi/T$, p an integer, the response of the correlator at time T to the second term is zero. Therefore at the sampling instant the threshold device sees the same quantity it would see if $s_i(t)$ had consisted of the first term alone. But the first term is a pure PSK pulse of energy $E_b/(1+q^2)$, and this receiver is optimum for pure PSK. Defining $\eta = 1/(1+q^2)$,

$$P_e = Q\left(\sqrt{\frac{2\eta E_b}{N_o}}\right) \quad (2.1.2-1)$$

Since η is the fraction of energy associated with the pure PSK term, it can be thought of as a measure of efficiency. If m_{cl} denotes the AM Clock modulation index, the relationship between η and m_{cl} is

$$\eta = \frac{1}{1+m_{cl}^2/2} \quad (2.1.2-2)$$

Since $0 \leq m_{cl} \leq 1$, the efficiency of a signal with an AM Clock satisfies

$$\frac{2}{3} \leq \eta \leq 1$$

When the data modulation is FSK, the signals have the form

$$s_i(t) = \sqrt{\frac{2E_b}{T(1+q^2)}} \left[1 + \sqrt{2q} \cos(\omega_{cl}t + \theta_{cl}) \right] \cos(\omega_i t + \theta),$$

$$0 \leq t \leq T, \quad i = 0, 1$$

There exist optimum and suboptimum non-coherent detectors for FSK, corresponding to the cases in which the filters $h_0(t)$ and $h_1(t)$ are matched to the amplitude-modulated FSK signals, and the constant-amplitude FSK signals, respectively. Analysis of the suboptimum receiver in Section 2.4 shows that the clock terms have no effect on the envelope at time T , so that the probability of error is what it would be for pure FSK of energy ηE_b , namely

$$P_e = \frac{1}{2} e^{-\eta E_b / 2N_0} \quad (2.1.2-3)$$

For the optimum receiver, error probability is still given, at least to a good approximation, by Equation 2.1-2.

Whether the system is PSK or FSK, the signals can be written as the sum of a pure PSK or FSK term of energy ηE_b and a sideband term due to the clock, with energy $(1 - \eta) E_b$. The sideband term contains PSK or FSK information as well as clock information. The difference between the optimum and suboptimum receivers in each case is that the suboptimum receiver uses only the pure PSK or FSK signal to make bit decisions, while the optimum receiver uses both the pure PSK or FSK and the sidebands.

2.1.3 Summed Clock

When the data and clock are summed, the signals can be written

$$s_i(t) = \sqrt{\frac{2\eta E_b}{T}} \cos \phi_i(t) + \sqrt{\frac{2(1-\eta) E_b}{T}} \cos(\omega_{cl}t + \theta_{cl}),$$

$$0 \leq t \leq T, \quad i = 0, 1 \quad (2.1.3-1)$$

where $\phi_c(t)$ indicates either PSK or FSK data modulation. The first term, a pure data signal, has energy ηE_b while the second, a pure clock, has energy $(1 - \eta)E_b$.

Since the clock term carries no information about the data, the optimum receiver is one which ignores the clock and is optimum for the pure PSK or FSK term. The response of the correlator of Figure 2.1.1-1 to a pure sinusoid of frequency R is zero because of the integer relationship between f_{sc} and R . In the FSK receivers of Figure 2.1.1-2 the filters $h_0(t)$ and $h_1(t)$ are narrowband filters centered at f_0 and f_1 , respectively, and hence have negligible response to a tone of frequency R . Therefore, the receivers which were optimum for no clock are also optimum for Summed Clock, but only a fraction η of the total energy is used in making decisions. Therefore, P_e for PSK is given by Equation 2.1.2-1, and for FSK by Equation 2.1.2-3.

The error probability results for no clock, AM Clock, and Summed Clock, for both FSK and PSK are collected for future reference in Table 2.1.3.

Table 2.1.3. P_e for Energy-Limited Signals

	Coherent PSK	Non-coherent FSK (near-orthogonal)
No Clock	$Q\left(\sqrt{\frac{2E_b}{N_o}}\right)$	$\frac{1}{2} e^{-E_b/2N_o}$
AM Clock, Optimum Receiver	$Q\left(\sqrt{\frac{2E_b}{N_o}}\right)$	$\frac{1}{2} e^{-E_b/2N_o}$
AM Clock, Suboptimum Receiver	$Q\left(\sqrt{\frac{2\eta E_b}{N_o}}\right)$	$\frac{1}{2} e^{-\eta E_b/2N_o}$
Summed Clock	$Q\left(\sqrt{\frac{2\eta E_b}{N_o}}\right)$	$\frac{1}{2} e^{-\eta E_b/2N_o}$

2.1.4 Peak Signal Considerations

It will be shown in Section 6 that in the systems under study the sub-carrier signals are subject to a peak amplitude constraint. It is therefore of interest to obtain expressions for P_e as a function of peak signal amplitude rather than signal energy.

For a Summed Clock the subcarrier signal is given by Equation 2.1.3-1. The peak value of the signal occurs when both $\cos \phi(t) = 1$ and $\cos(\omega_{cl}t + \theta_{cl}) = 1^*$. Thus the peak value is given by

$$a = \sqrt{\frac{2E_b}{T}} \left[\sqrt{\eta} + \sqrt{1-\eta} \right]$$

so that

$$E_b = \frac{a^2 T}{2 [1 + 2\sqrt{\eta(1-\eta)}]} \quad (2.1.4-1)$$

Therefore the error probability for a Summed Clock system (with perfect synchronization) under a peak signal amplitude constraint is found by substituting Equation 2.1.4-1 into the appropriate formula from Table 2.1.3.

For an AM Clock, $s_i(t)$, $i = 0, 1$, has peak value**

$$a = \sqrt{\frac{2E_b}{T}} \left[\sqrt{\eta} + \sqrt{2(1-\eta)} \right]$$

*It may happen that the cosines do not assume their maxima simultaneously, but since the subcarrier frequency is much higher than R , there must be a time at which $\cos \phi(t) = 1$ and $\cos(\omega_{cl}t + \theta_{cl}) \approx 1$.

**The same observation concerning simultaneous maxima of the cosines just made applies here also.

where the substitutions

$$\eta = \frac{1}{1+q^2}$$

and

$$1-\eta = \frac{q^2}{1+q^2}$$

have been used. Thus

$$E_b = \frac{a^2 T}{2 [2-\eta + 2 \sqrt{2\eta(1-\eta)}]} \quad (2.1.4-2)$$

Table 2.1.4 shows the error probability expressions obtained by inserting Equations 2.1.4-1 and 2.1.4-2 into the corresponding entries of Table 2.1.3. The form of the results suggests defining an "effective energy" used in making bit decisions as

$$E_{\text{eff}} = \begin{cases} \frac{a^2 T}{2 [2-\eta + 2 \sqrt{2\eta(1-\eta)}]} & \text{AM Clock,} \\ & \text{Optimum receiver} \\ \\ \frac{a^2 T \eta}{2 [2-\eta + 2 \sqrt{2\eta(1-\eta)}]} & \text{AM Clock,} \\ & \text{Suboptimum receiver} \\ \\ \frac{a^2 T \eta}{2 [1+2 \sqrt{\eta(1-\eta)}]} & \text{Summed Clock,} \\ & \text{Optimum receiver} \end{cases}$$

Table 2.1.4. P_e for Peak Amplitude-Limited Signals

	Coherent PSK	Non-coherent FSK (near-orthogonal)
No Clock	$Q\left(\sqrt{\frac{a^2 T}{N_0}}\right)$	$\frac{1}{2} e^{-a^2 T / 4 N_0}$
AM Clock, Optimum Receiver	$Q\left(\sqrt{\frac{a^2 T}{N_0 [2 - \eta + 2\sqrt{2\eta(1-\eta)}]}}\right)$	$\frac{1}{2} e^{-\frac{a^2 T}{4 N_0 [2 - \eta + 2\sqrt{2\eta(1-\eta)}]}}$
AM Clock, Suboptimum Receiver	$Q\left(\sqrt{\frac{a^2 \eta T}{N_0 [2 - \eta + 2\sqrt{2\eta(1-\eta)}]}}\right)$	$\frac{1}{2} e^{-\frac{a^2 \eta T}{4 N_0 [2 - \eta + 2\sqrt{2\eta(1-\eta)}]}}$
Summed Clock	$Q\left(\sqrt{\frac{a^2 \eta T}{N_0 [1 + 2\sqrt{\eta(1-\eta)}]}}\right)$	$\frac{1}{2} e^{-\frac{a^2 \eta T}{4 N_0 [1 + 2\sqrt{\eta(1-\eta)}]}}$

With E_{eff} so defined, we have

$$P_e = \begin{cases} Q\left(\sqrt{\frac{2E_{\text{eff}}}{N_o}}\right) & \text{PSK} \\ \frac{1}{2} e^{-E_{\text{eff}}/2N_o} & \text{FSK} \end{cases}$$

Figure 2.1.4 shows how E_{eff} varies with the efficiency parameter η for the three cases of interest, indicating a superiority of the Summed Clock over the AM Clock with suboptimum receiver for all η , and over the AM Clock with optimum receiver for $\eta > 0.76$.

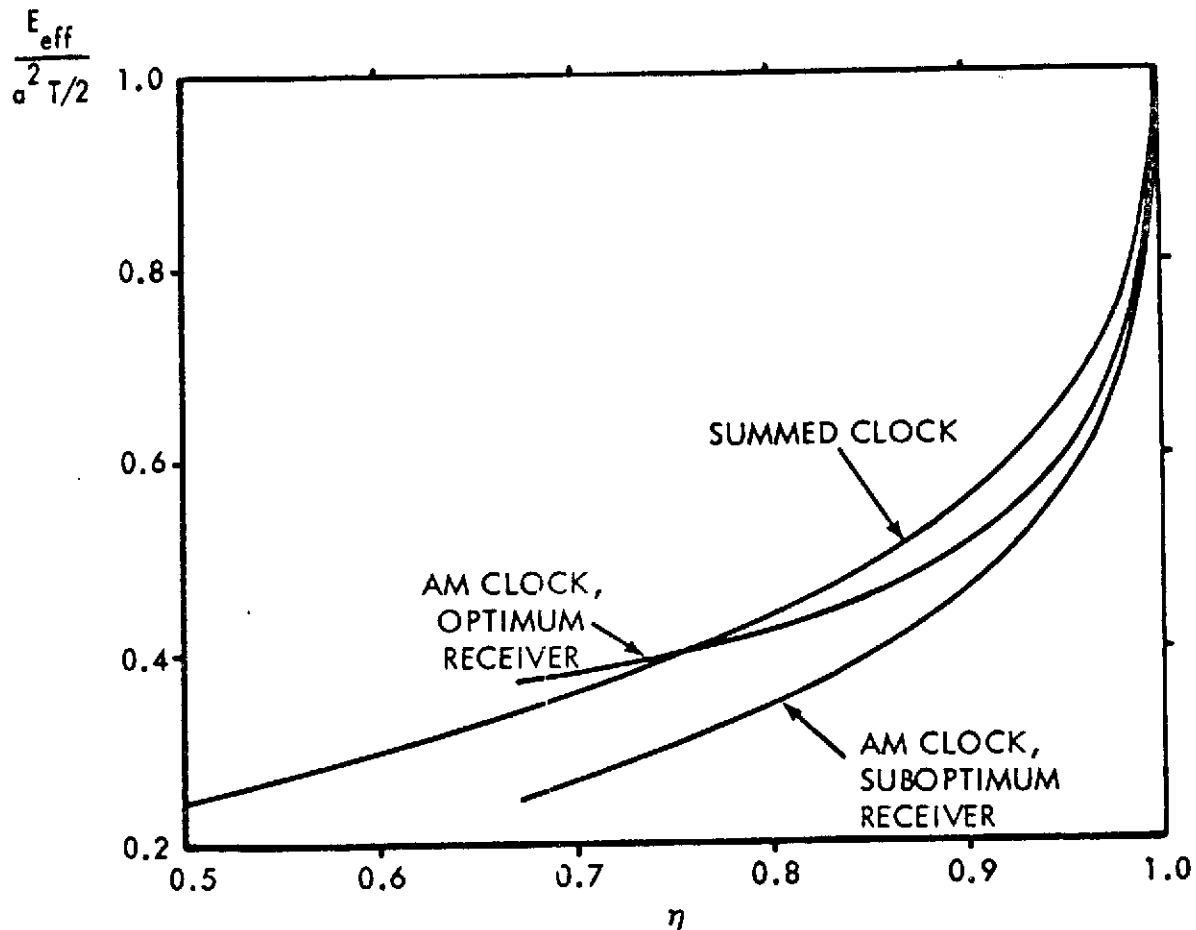


Figure 2.1.4. Effective Energy Used by Detector

2.2 AM and Summed Clock Characteristics

Schemes for recovering the clock signal transmitted with PSK data are analyzed in this section. It is shown that when the ratio of f_{sc} to R is large and SNR in the clock is large, the output of the clock extracting circuit is essentially the same whether AM or Summed Clock is used. When the ratio of f_{sc} to R is small, difficulties may exist with both clock schemes. In an AM Clock system with small p , a simple envelope detector cannot track the clock without considerable distortion of the signal. In a Summed Clock system, the clock extracting circuit may contain significant response to the data when p is small.

In this analysis, the filters are assumed to be ideal, with unity gain and zero phase (or linear phase) in the passband. In practice, linear phase is rarely achieved over broad bands and delay distortion may result. For a Summed Clock the clock spike is separated in frequency from the PSK by a substantial amount, and it is probable that the clock and data are shifted in time relative to one another due to filter phase nonlinearities. When R and f_{sc} are fixed, it is possible that the delay distortion can be compensated, but if either R or f_{sc} is variable, several different compensators will have to be provided.

When the clock is AM, the clock information is in the same frequency range as the data and delay distortion is not likely to be a significant problem.

2.2.1 Extraction of Summed Clock

When the clock signal is added to the PSK signal, it can be recovered by passing the received signal through a narrowband filter centered at frequency R . The received signal has the form

$$\sqrt{\frac{2(1-\eta) E_b}{T}} \cos(\omega_{cl} t + \theta_{cl}) + \sqrt{\frac{2\eta E_b}{T}} x(t) \cos(\omega_{sc} t + \theta_{sc}) + n_{sc}(t)$$

where $x(t)$ has the value ± 1 over each bit interval, indicating the corresponding data bit, and $n_{sc}(t)$ is white Gaussian noise of spectral density $N_0/2$. By linearity, the response of the clock filter is the sum of the responses to the three terms individually.

The first term, which is the clock signal, passes unchanged. The response to the second term can be thought of as interference from the PSK signal, and the response to the third term as noise. It is of interest to determine the relative power in the three terms.

Considering the signal interference term first, it will be shown in Section 3 that the PSK power spectrum has the form

$$S(\omega) = \frac{P_{sc}}{2T} \left| h(\omega - \omega_{sc}) - h(\omega + \omega_{sc}) \right|^2$$

where P_{sc} is the power in the pure PSK signal, and

$$h(\omega) = \frac{\sin(\omega T/2)}{\omega T/2} \exp(-j\omega T/2)$$

Using the coarse overbound

$$S(\omega) \leq \frac{P_{sc}}{2T} 2 \left| h(2\pi \frac{3}{2} R - \omega_{sc}) \right|^2$$

for $S(\omega)$ near $\omega = 2\pi R$, it can be shown after some manipulation that the interference power is upperbounded by

$$\frac{2\eta E_b B_{cl}}{\pi^2 \left(p - \frac{3}{2}\right)^2}$$

where B_{cl} is the bandwidth of the filter used to extract the clock. The power in the response to noise alone is $N_0 B_{cl}$, and the power in the signal response is $(1-\eta)E_b R$. Hence, the output signal to noise-and-interference ratio exceeds

$$\frac{(1-\eta) E_b R}{N_o B_{cl} + \frac{2\eta E_b B_{cl}}{\pi^2 \left(p - \frac{3}{2}\right)^2}}$$

The interference term can be neglected if

$$N_o B_{cl} \gg \frac{2\eta E_b B_{cl}}{\pi^2 \left(p - \frac{3}{2}\right)^2}$$

or

$$p \gg \frac{3}{2} + \frac{1}{\pi} \sqrt{\frac{2\eta E_b}{N_o}}$$

It should be noted that the bounding technique used in estimating the interference power was somewhat loose, and even if the condition above is marginal, interference probably is still negligible.

When the interference can be ignored, the output signal to noise ratio is

$$\text{SNR}_{cl} = (1-\eta) \frac{E_b}{N_o} \frac{R}{B_{cl}}$$

2.2.2 Extraction of AM Clock

An amplitude modulated clock can ordinarily be detected by an envelope detector, although problems may be encountered when p is small, as will be discussed later. For the present, assume the received amplitude-modulated PSK plus noise is passed through a bandpass filter centered at f_{sc} with bandwidth B_{sc} , wide enough to pass the signal with negligible distortion. The output of this filter is then

$$\begin{aligned}
y_1(t) &= A(t) \cos(\omega_{sc} t + \theta_{sc} + \phi(t)) \\
&+ n_c(t) \cos(\omega_{sc} t + \theta_{sc} + \phi(t)) \\
&+ n_s(t) \sin(\omega_{sc} t + \theta_{sc} + \phi(t))
\end{aligned}$$

where

$$A(t) = \sqrt{\frac{2E_b}{T(1+q^2)}} \left[1 + \sqrt{2q} \cos(\omega_{cl} t + \theta_{cl}) \right] \quad (2.2.2-1)$$

The phase $\phi(t)$ is varied by the data, and the quadrature noise components $n_c(t)$ and $n_s(t)$ each have power spectral density

$$S_n(\omega) = \begin{cases} N_0, & |\omega| \leq 2\pi \frac{B_{sc}}{2} \\ 0, & |\omega| > 2\pi \frac{B_{sc}}{2} \end{cases}$$

The envelope of $y_1(t)$ is, therefore

$$E(t) = \sqrt{\left[A(t) + n_c(t)\right]^2 + n_s^2(t)}$$

When the signal-to-noise ratio is high, the second term can be neglected in comparison with the first, yielding

$$E(t) \approx A(t) + n_c(t)$$

The output of the envelope detector is passed through a narrowband filter of bandwidth B_{cl} centered at R ; this filter blocks the dc component of $A(t)$ and passes the pure sinusoid, yielding

$$y_2(t) = \sqrt{\frac{4q^2 E_b}{T(1+q^2)}} \cos(\omega_{cl}t + \theta_{cl}) + n(t)$$

The output signal to noise ratio is thus

$$\text{SNR}_{cl} = \frac{\frac{2q^2 E_b}{T(1+q^2)}}{2N_o B_{cl}} = (1 - \eta) \frac{E_b}{N_o} \frac{R}{B_{cl}} \quad (2.2.2-2)$$

This is the same signal-to-noise ratio as derived previously for the Summed Clock. Moreover, since $B_{cl} \ll B_{sc}$, the noise process $n(t)$ is approximately Gaussian. Thus, whether an AM Clock or Summed Clock is used, the output of the clock extracting circuit can be satisfactorily modelled as a sinusoid plus Gaussian noise, with SNR_{cl} given by Equation 2.2.2-2.

As before, we are interested in comparing the clock schemes under a peak signal amplitude constraint. To do this, we substitute Equations 2.1.4-1 and 2.1.4-2 into our expression, yielding

$$\text{SNR}_{cl} = \begin{cases} \frac{a^2}{2N_o B_{cl}} \frac{1-\eta}{1+2\sqrt{\eta(1-\eta)}} & \text{Summed Clock} \\ \frac{a^2}{2N_o B_{cl}} \frac{1-\eta}{2-\eta+2\sqrt{2\eta(1-\eta)}} & \text{AM Clock} \end{cases}$$

Since

$$2-\eta+2\sqrt{2\eta(1-\eta)} > 1+2\sqrt{\eta(1-\eta)},$$

the Summed Clock exhibits somewhat higher SNR (e.g., 0.9 dB for $\eta = 0.89$).

In order for an envelope detector to work properly, the signal into the detector must display a well-defined envelope. This puts a restriction on the relative size of f_{sc} and R . For example, if the envelope detector is simply a full-wave rectifier followed by a low-pass filter, the separation between f_{sc} and R must be great enough that the filter output can track the variations in the clock signal, but not the variations in the rectified subcarrier. If p is large, a simple RC low-pass filter will perform satisfactorily, but if p is small, a filter with a sharper cutoff must be used or substantial distortion of the signal may result.

2.3 Optimum Power Allocation

It was demonstrated in the last section that whether the clock is added to the data or amplitude modulated onto it, the output of the clock extracting circuit can be adequately modelled as a sinusoid plus Gaussian noise, with SNR proportional to $1-\eta$. Reducing η thus increases the reliability of the synchronization, but decreases the reliability of the bit decisions conditioned on perfect synchronization. The objective of this section is to determine the value of η for which bit error probability is minimum. An exact solution is not obtained, but a lower bound on P_e is found, and from the form of the bound and certain other considerations, an estimate of the optimum η can be made with some confidence.

Let τ be the difference between the actual end of the bit interval and receiver's estimate of the end. If $p(\tau)$ is the probability density function of τ , and $P_{e|\tau}$ is the probability of bit error conditioned on timing error τ , then the overall error probability is

$$P_e = \int P_{e|\tau} p(\tau) d\tau \quad (2.3-1)$$

When the synchronization error is τ , the normalized output of the correlator at the sampling instant $T + \tau$ is*

$$z(T+\tau) = \frac{\sqrt{\eta E_b}}{T} \int_{\tau}^{T+\tau} x(t) dt + n$$

where $x(t)$ is the message, and n is a zero-mean Gaussian random variable with variance $N_0/2$.

For $0 \leq |\tau| \leq T$, the integral includes the last $T - \tau$ seconds of the correct bit interval and the first τ seconds of an adjacent interval. If the adjacent bit is the same as the bit in the correct interval the value of the integral is the same as if there were no error, namely $\pm \sqrt{\eta E_b}$. However, if the adjacent bit is the complement, the value of the integral becomes $\pm \sqrt{\eta E_b} (1 - 2|\tau|/T)$. Since the two possibilities are equally likely,

$$P_{e|\tau} = \frac{1}{2} Q \left(\sqrt{\frac{2\eta E_b}{N_0}} \right) + \frac{1}{2} Q \left(\sqrt{\frac{2\eta E_b}{N_0}} \left(1 - 2 \frac{|\tau|}{T} \right) \right),$$

$$0 \leq |\tau| \leq T$$

When $|\tau| > T$ the correlator output is statistically independent of the bit being detected so $P_{e|\tau} = 1/2$.

*The derivation presented here is for the Summed Clock case. The derivation for AM Clock is similar, except that $P_{e|\tau}$ depends on clock phase $\theta_{c|}$, as will be shown in Section 2.4. The results presented for AM Clock are for the best choice of $\theta_{c|}$.

Using these expressions in Equation 2.3-1, and making the reasonable assumption the $p(\tau)$ is an even function, we obtain

$$P_e = Q \left(\sqrt{\frac{2\eta E_b}{N_o}} \right) \int_0^T p(\tau) d\tau + \int_0^T Q \left(\sqrt{\frac{2\eta E_b}{N_o}} \left(1 - 2 \frac{|\tau|}{T} \right) \right) p(\tau) d\tau + \int_T^\infty p(\tau) d\tau \quad (2.3-2)$$

If $p(\tau)$ were known it could be substituted into Equation 2.3-2 and the resulting expression minimized analytically or numerically with respect to η . Here $p(\tau)$ is not known, but since the bit timing is established by observing the phase of a sinusoid (the clock) plus narrowband Gaussian noise, the timing jitter is related to the phase ϕ of a sinusoid plus narrowband Gaussian noise by

$$\frac{\tau}{T} = \frac{\phi}{2\pi} \quad (2.3-3)$$

(where ϕ is not reduced modulo 2π).

For $|\phi| \geq \pi$, then a timing error in excess of $T/2$ occurs. If we now regard ϕ as being reduced modulo 2π to a value satisfying $-\pi \leq \phi \leq \pi$, then Equation 2.3-3 indicates that τ is the timing error reduced modulo T to a value satisfying $-T/2 \leq \tau \leq T/2$. Letting $p_\phi(\phi)$ denote the density function of the phase reduced modulo 2π , the density function of the variable $x = \tau/T$, where τ is reduced modulo T , is given by

$$p_x(x) = 2\pi p_\phi(2\pi x)$$

Note that $p_x(x) = 0$ for $|x| > 1/2$.

Making the change of variable $x = \tau/T$ in Equation 2.3-2, and interpreting τ as reduced modulo T , we obtain an expression for error probability subject to the condition that timing errors of magnitude exceeding $T/2$ are reduced modulo T to a value satisfying $-T/2 \leq \tau \leq T/2$. We will denote this conditional error probability \tilde{P}_e

$$\tilde{P}_e = \frac{1}{2} Q \left(\sqrt{\frac{2\eta E_b}{N_o}} \right) + 2\pi \int_0^{1/2} Q \left(\sqrt{\frac{2\eta E_b}{N_o}} (1 - 2x) \right) p_\phi (2\pi x) dx \quad (2.3-4)$$

The density function $p_\phi (\phi)$ is given by [2-12]

$$p_\phi (\phi) = \frac{1}{2\pi} e^{-u^2/2} + \frac{u \cos \phi}{\sqrt{2\pi}} e^{-(u^2 \sin^2 \phi)/2} [1 - Q(u \cos \phi)]$$

where

$$u = \sqrt{2 \text{SNR}_{cl}}$$

Equation 2.3-4 was evaluated by computer for $E_b/N_o = 5, 10$ and 20 , with $R = 5B_{cl}$. Results are shown in Figure 2.3-1. The analogous equation to Equation 2.3-4 for an AM Clock was also derived, and results for $\theta_{cl} = \pi$ are also shown in Figure 2.3-1.

Because the conditioning on \tilde{P}_e excludes large synchronization errors, \tilde{P}_e is a lower bound on the actual error probability P_e . However, since such large synchronization errors are exceedingly rare when the clock signal-to-noise ratio is reasonable, the bound $P_e \geq \tilde{P}_e$ should be quite tight away from the extreme right end of the curves. The shape of the curves, the fact that they are lower bounds, and the expected tightness of the bound suggest the existence of a minimum for η between 0.8 and 0.9 . For $m_{cl} = 0.5$, $\eta = 0.89$, so that the suggested 50% modulation index appears to be near-optimum; for Summed Clock, a 3:1 amplitude ratio of data signal to clock (resulting in a 9:1 ratio of power) appears to be appropriate.

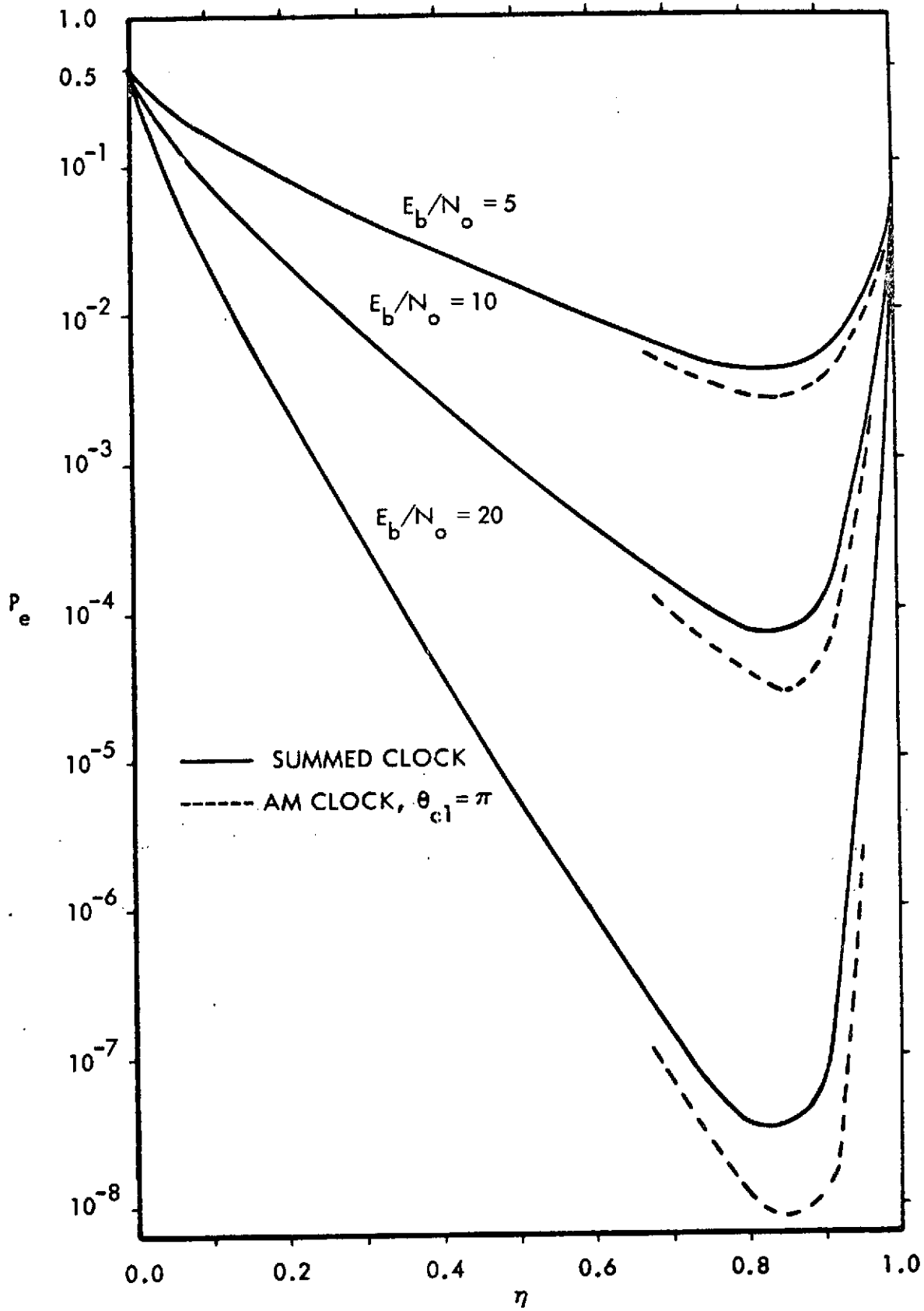


Figure 2.3-1. Lower Bounds on P_e , Energy-Limited Signals

Using Equations 2.1.4-1 and 2.1.4-2, lower bounds on P_e can be obtained for peak amplitude limited systems. Bounds are plotted in Figure 2.3-2 for both clock schemes and $a^2T/2N_o = 10, 20$. Here the Summed Clock looks better than the AM Clock, because as noted in Section 2.1, for given η and peak value, a Summed Clock signal has greater E_b than an AM Clock signal. Note also that the minimum shifts slightly to the right. This is to be expected since Equations 2.1.4-1 and 2.1.4-2 indicate that for a small increase in η , considerable increase in E_b results.

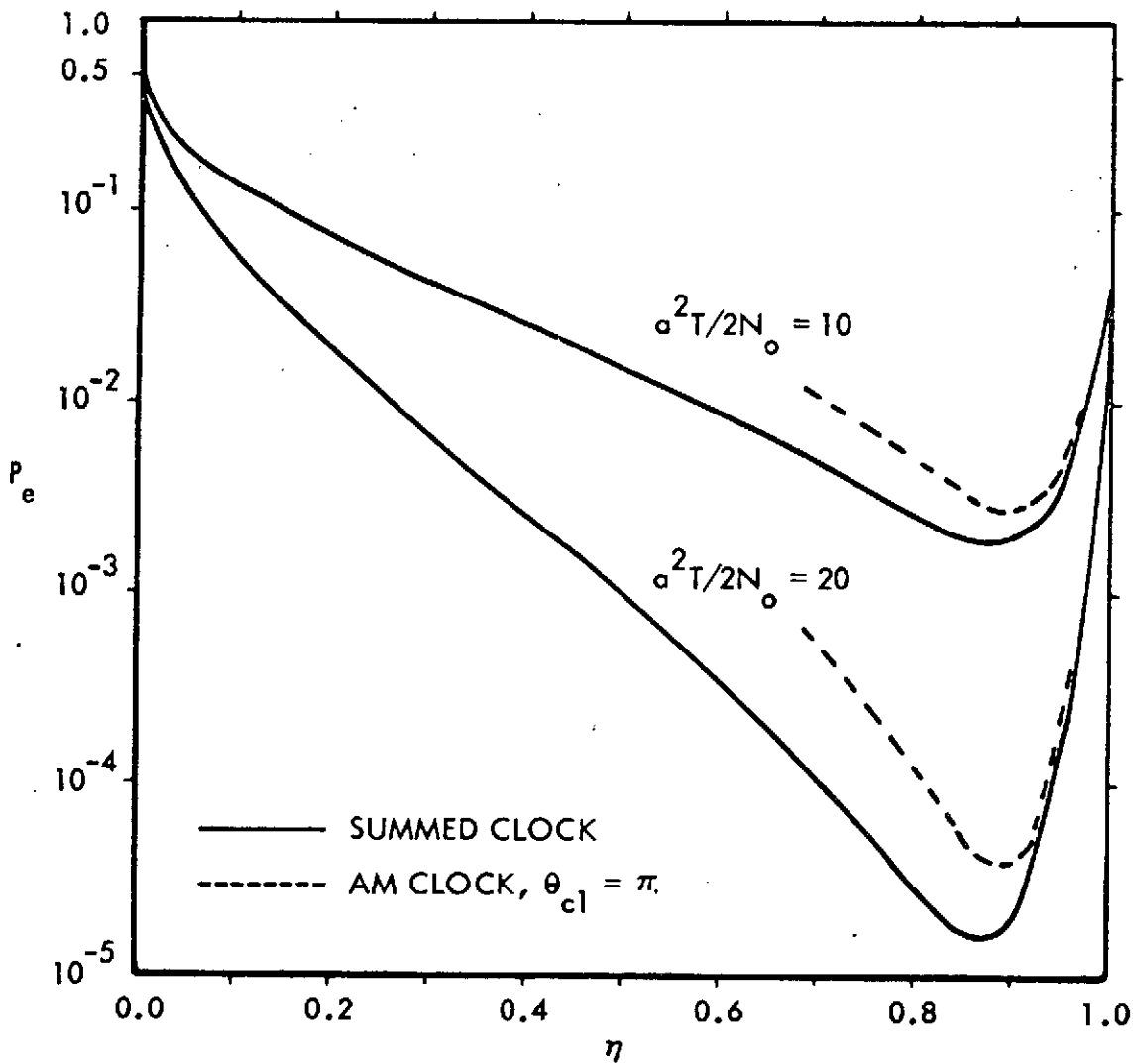


Figure 2.3-2. Lower Bounds on P_e , Amplitude-Limited Signals

2.4 AM Clock Phase Effects

Both the FSK standards and the PSK guidelines allow three choices of phase θ_{cl} for the clock: $-\pi/2$, π , and $\pi/2$, corresponding to positive-going zero crossings at time 0, $T/4$ and $T/2$ respectively. The choice of phase has various effects on the system behavior, which are determined in this section.

2.4.1 Bandwidth Effects

The effects of θ_{cl} on the power spectrum of the signal are discussed in detail in Section 3. Generally, the conclusion is that $\theta_{cl} = \pi$ yields minimum subcarrier bandwidth, and that the bandwidth with $\theta_{cl} = \pm\pi/2$ is the same as the bandwidth when no clock is transmitted. The reason for this is that when $\theta_{cl} = \pi$ the bit switching occurs at a time when the signal amplitude is minimum while with $\theta_{cl} = \pm\pi/2$, the signal level at switching time is the same as if no clock were present. If $\theta_{cl} = 0$ were an allowable choice of phase, a signal with this clock phase would exhibit maximum bandwidth.

2.4.2 Effects on Error Probability

The discussion in Section 2.1 indicates that the error probability is independent of θ_{cl} if the detector output is sampled at time T . However the choice of θ_{cl} does affect the system's sensitivity to small bit synchronization errors. For example, when the synchronization error is τ , the normalized output of the sub-optimum PSK detector at the sampling time is

$$z(T+\tau) = \frac{2}{T} \sqrt{\frac{E_b}{1+q}} \int_{T-\tau}^{T+\tau} \left[1 + \sqrt{2} q \cos(\omega_{cl} t + \theta_{cl}) \right] x(t) \cos^2(\omega_{sc} t + \theta_{sc}) dt$$

After some manipulation, this becomes

$$\begin{aligned}
z(T+\tau) = & \frac{\sqrt{\eta E_b}}{T} \int_0^T x(t) dt \\
& + \frac{\sqrt{\eta E_b}}{T} \left[\int_T^{T+\tau} x(t) \left[1 + m_{cl} \cos(\omega_{cl} t + \theta_{cl}) \right] dt \right. \\
& \left. - \int_0^\tau x(t) \left[1 + m_{cl} \cos(\omega_{cl} t + \theta_{cl}) \right] dt \right]
\end{aligned}$$

where the double-frequency terms have been dropped.

If $|\tau| < T$ and the adjacent bit differs from the bit being detected, this reduces to

$$z(T+\tau) = \pm \sqrt{\eta E_b} \left[1 - 2 \frac{|\tau|}{T} - \frac{2}{\pi} m_{cl} \cos(\pi \frac{\tau}{T} + \theta_{cl}) \sin \pi \frac{|\tau|}{T} \right]$$

For small values of timing error, $|\tau| \ll T$, this can be approximated as

$$z(T+\tau) = \pm \sqrt{\eta E_b} \left[1 - 2 (1 + m_{cl} \cos \theta_{cl}) \frac{|\tau|}{T} \right] \quad (2.4.2-1)$$

The reduction in magnitude of the detector output is seen to be least when $\theta_{cl} = \pi$; this clock phase therefore exhibits least sensitivity to small bit synchronization errors.

Now consider the non-coherent FSK detector shown in Figure 2.1.2-2. The filters $h_0(t)$ and $h_1(t)$ are matched to rectangular sinusoidal pulses of frequencies f_0 and f_1 , respectively:

$$h_i(t) = \begin{cases} \cos \omega_i t & 0 \leq t \leq T \\ 0 & t > T \end{cases}, \quad i = 0, 1$$

Suppose that the input signal is at frequency f_1 on the interval $(0, T)$, and at frequency f_0 in the adjacent intervals on each side. The output of filter $h_1(t)$ for any t in the interval $0 \leq t \leq T$, is then

$$y_1(t) = \int_{t-T}^0 A(s) \cos(\omega_0 s + \theta) \cos \omega_1(t-s) ds \\ + \int_0^t A(s) \cos(\omega_1 s + \theta) \cos[\omega_1(t-s)] ds$$

where $A(t)$ is as defined in Equation 2.2.2-1.

The first integral is negligible and the second, after discarding a double frequency term, is a sinusoid of frequency f_1 amplitude modulated by an envelope

$$\frac{1}{2} \int_0^t A(s) ds = \frac{1}{2} \sqrt{\frac{2E_b}{T(1+q^2)}} \int_0^t \left[1 + \sqrt{2} q \cos(\omega_{cl}s + \theta_{cl}) \right] ds \\ = K \left[\frac{t}{T} + \frac{m_{cl}}{2\pi} \left(\sin\left(2\pi \frac{t}{T} + \theta_{cl}\right) - \sin \theta_{cl} \right) \right]$$

This envelope is plotted for $m_{cl} = \sqrt{2q} = 1/2$ and $\theta_{cl} = \pi, \pm\pi/2$ in Figure 2.4.2. At $t = T$, the envelope is independent of θ_{cl} , so that if the sampling is done at the end of the interval and the synchronization is perfect, it is immaterial which value of clock phase is used. However, if the sampling time is chosen to be some time before time T (in order to reduce the probability that jitter drives the sampling point into the next interval), then $\theta_{cl} = \pi$ yields maximum response as long as the sampling time is $\geq 3T/4$.

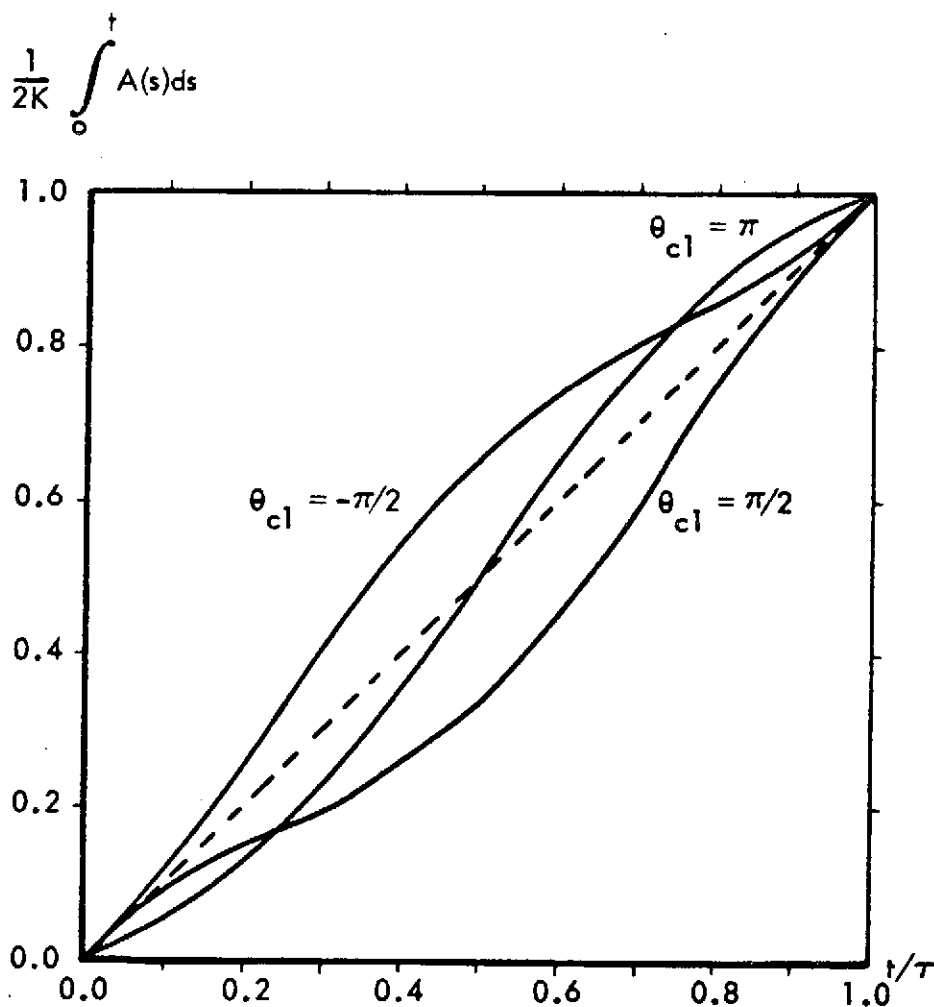


Figure 2.4.2. Envelopes of Matched Filter Output

To see the effect of small synchronization errors, suppose that the received signal is shifted in time by an amount τ relative to the receiver's time origin, where $0 \leq \tau \ll T$. At sampling time $t = T$, the output of $h_1(t)$ is

$$y_1(T) = \int_0^{T-\tau} A(s+\tau) \cos(\omega_1(s+\tau) + \theta_1) \cos \omega_1(T-s) ds$$

$$+ \int_{T-\tau}^T A(s+\tau) \cos(\omega_0(s+\tau) + \theta_2) \cos \omega_1(T-s) ds$$

As before the second term contributes no significant amount, while the first consists of a negligible double-frequency and an amplitude-modulated sinusoid with envelope

$$\frac{1}{2} \int_0^{T-\tau} A(s+\tau) ds = K \left[1 - \frac{\tau}{T} + \frac{m_{cl}}{2\pi} \left(\sin \theta_{cl} - \sin(\omega_{cl}\tau + \theta_{cl}) \right) \right]$$

The best choice of θ_{cl} is that which maximizes this value, or equivalently, that which maximizes

$$f(\theta_{cl}) = \sin \theta_{cl} - \sin(\omega_{cl}\tau + \theta_{cl})$$

For the available choices of θ_{cl} ,

$$f(\theta_{cl}) = \begin{cases} 1 - \cos(\omega_{cl}\tau) & \theta_{cl} = \pi/2 \\ \sin(\omega_{cl}\tau) & \theta_{cl} = \pi \\ -1 + \cos(\omega_{cl}\tau) & \theta_{cl} = -\pi/2 \end{cases}$$

For small values of synchronization error, $\tau \ll T$,

$$\sin(\omega_{cl}\tau) \approx \omega_{cl}\tau$$

and

$$1 - \cos(\omega_{cl}\tau) \approx \frac{1}{2}(\omega_{cl}\tau)^2$$

Thus $\theta_{cl} = \pi$ yields the largest output at the sampling time. The analysis for $-T \ll \tau < 0$ is similar and leads to the same choice of θ_{cl} . Hence, $\theta_{cl} = \pi$ yields least sensitivity to small bit synchronization errors.

2.5 Summary and Conclusions

Comparative analyses of FSK and PSK systems and various bit synchronization techniques have been considered. The principal criterion by which comparisons are made is bit error probability P_e . Well-known expressions for P_e with PSK and non-coherent FSK are modified to account for the power allocated to transmit a clock. This is done by defining an efficiency parameter η as the fraction of the total energy which is used by the receiver in making bit decisions.

Methods of extracting the two kinds of clock are considered. The principal result is that if the signal-to-noise ratio into the clock extracting circuit is high, the output is a sinusoid of clock frequency plus narrowband Gaussian noise. The output SNR is determined for AM and Summed Clock.

Using these results, an attempt is made to determine the optimum choice of η to minimize P_e , taking both additive Gaussian noise effects and synchronization error effects into account. This analysis is carried out only for PSK, since the FSK standard allows no choice; an analogous approach would apply FSK. The exact behavior of P_e as a function of η is not determined but a lower bound on P_e is derived which is thought to be reasonably tight. From the bound it is concluded that the optimum efficiency lies between 0.8 and 0.9. That is, 10% to 20% of the power should be dedicated to the clock and the rest to the pure PSK.

When the system is bit-energy constrained (or average power constrained), the bound on P_e (and probably P_e itself) is less when the AM Clock with optimum clock phase is used; but when the system is peak constrained the Summed Clock has a smaller bound on P_e . The reason for this is that when E_b is fixed, the AM Clock signal has less sensitivity to small synchronization errors than the added clock signal. However, when the peak value is fixed, the added clock signal has substantially higher value of E_b than the AM Clock signal.

Finally, the effects of varying the phase of the AM Clock are considered. It is shown that for both PSK and FSK, the phase which makes the envelope minimum at the ends of the bit interval (i.e., the positive-going zero crossing at the $T/4$ point) yields the least sensitivity to synchronization error.

2.6 References

- [2-1] VHF PCM/PSK Command System Standard Guidelines: Memorandum from R. J. Coates to Distribution, GSFC, Greenbelt, Maryland, October 6, 1971.
- [2-2] Aerospace Data System Standards, Part II, Section 3, PCM/FSK Command Data System Standard, GSFC, Greenbelt, Maryland, July 1, 1971.
- [2-3] Viterbi, A. J., Principles of Coherent Communication, McGraw Hill, New York, 1966, Chapter 7.
- [2-4] Stiffler, J. J., Theory of Synchronous Communications, Prentice Hall, Englewood Cliffs, New Jersey, 1971, Section 9.6.

- [2-5] ibid., Chapters 7-9.
- [2-6] IRIG Telemetry Standards, January 1971.
- [2-7] Wozencraft, J. M., and I. M. Jacobs, Principles of Communication Engineering, Wiley, New York, 1965.
- [2-8] Smith, E. F., "Attainable Error Probabilities in Demodulation of Random Binary PCM/FM Waveforms," IRE Trans on Space Electronics and Telemetry, VOL. SET-8, pp. 290-297, December 1963.
- [2-9] Darlington, S., "Demodulation of Wideband, Low-Power FM Signals," B.S.T.J., Vol. 43, pp. 339-374, January 1964.
- [2-10] Pelchat, M. G., and S. L. Adams, "Non-Coherent Detection of Continuous Phase Binary FSK," Proc. I. C. C., June 1971.
- [2-11] Viterbi, op. cit., pp. 212-214.
- [2-12] Davenport, W. B., and W. L. Root, An Introduction to the Theory of Random Signals and Noise, McGraw Hill, New York, 1958, pp. 165-167.

3.0

CARRIER AND SUBCARRIER BANDWIDTH REQUIREMENTS

Spectral characteristics of the modulated subcarrier and carrier are developed in this section for the signal structures described in the VHF PCM/PSK Command System Guidelines [3-1] and VHF PCM/FSK Command Data System Standard [3-2]. These characteristics are employed here to specify subcarrier and RF carrier bandwidth requirements. In a later task, the subcarrier spectral characteristics are employed to aid in selection of the subcarrier frequency and to investigate the effects of common RF channel interference.

The signal structures of interest here include subcarrier modulation via binary PSK with AM Clock (PSK-AM) and continuous-phase, binary FSK with AM Clock (FSK-AM). Each of these composite signals is subsequently considered as the modulating signal for an AM, FM, and PM RF carrier.

The approach to analysis adopted here consists of development of expressions of the power density spectrum for PSK-AM and FSK-AM. It is assumed that the binary baseband signal in each case consists of random, statistically independent, equally probable +1's and -1's. Amplitude modulation of the RF carrier is dealt with by simply translating the spectrum at subcarrier to the carrier frequency, since AM is a linear modulation process. In the cases involving FM or PM carrier modulation, the resulting RF bandwidths are not so easily obtained. In these cases, a periodic composite subcarrier signal is assumed and the line spectra relevant to FM and PM of the RF carrier are determined. This approach provides a tight bound on the required bandwidths.

3.1

Spectral Characteristics of PSK-AM Signal Structures

Spectral density expressions for PSK-AM signal structures are developed here. Letting the AM Clock be introduced via $c(t)$, the general expression for a subcarrier modulated by PSK and AM Clock can be written as

$$e_{sc}(t) = \sqrt{2 P_{sc}} c(t) x(t) \cos(\omega_{sc} t + \theta_{sc}) \quad (3.1-1)$$

with

$$c(t) = 1 + m_{cl} \cos(\omega_{cl} t + \theta_{cl}) , \quad (3.1-2)$$

and $x(t)$ represents the PSK, 0 or π radians phase shift occurring with equal probability in each bit interval. In the above, P_{sc} represents the average unmodulated subcarrier power with ω_{sc} and θ_{sc} denoting the subcarrier angular frequency and phase, respectively. The parameters, m_{cl} , ω_{cl} and θ_{cl} respectively denote clock amplitude modulation index, clock angular frequency and phase. Recall from Section 1.1.2.4 that the ratio of subcarrier frequency to bit rate, $R = 1/T$, equals an integer, p . Also, the clock phase is chosen such that the clock waveform crosses zero, positive-going, at 0, $T/4$ or $T/2$; that is, $\theta_{cl} = -\pi/2, \pi$ and $\pi/2$ respectively.

Considering the signal of Equation 3.1-1 as the sum of non-overlapping pulses of the form

$$x_n(t) = \begin{cases} e_{sc}(t), & nT \leq t \leq (n+1)T, \\ 0, & \text{otherwise} \end{cases}$$

where $x_n(t)$ denotes the pulse in the n^{th} bit interval. The factor $x(t)$ in Equation 3.1-1 becomes $a_n = \pm 1$, with equal probability, and the power density spectrum is given by [3-3]

$$S(\omega) = \lim_{N \rightarrow \infty} \frac{1}{NT} \sum_{m=0}^{N-1} \sum_{n=0}^{N-1} E \left\{ F_n(\omega) F_m^*(\omega) \right\} \quad (3.1-3)$$

with $F_n(\omega)$ representing the Fourier transform of the pulse $x_n(t)$. Above, the asterisk denotes the conjugate of a complex quantity and the averaging operator, E , implies an average over all a_i .

The Fourier transform of $x_n(t)$ can be expressed in the form

$$F_n(\omega) = \frac{\sqrt{2P_{sc}}}{2} \left\{ a_n \exp(j\theta_{sc}) h(\omega - \omega_{sc}) + a_n \exp(-j\theta_{sc}) h(\omega + \omega_{sc}) \right\} \exp(-jn\omega T),$$

where

$$h(\omega) = \int_0^T c(t) \exp(-j\omega t) dt. \quad (3.1-4)$$

Since

$$E \left\{ a_n a_m \right\} = \begin{cases} 1, & n = m \\ 0, & n \neq m \end{cases},$$

we have

$$E \left\{ F_n(\omega) F_m^*(\omega) \right\} = 0, \quad n \neq m.$$

After some straightforward mathematical manipulation,

$$E \left\{ F_n(\omega) F_m^*(\omega) \right\} = \frac{P_{sc}}{2} \left| h(\omega - \omega_{sc}) - h(\omega + \omega_{sc}) \right|^2, \quad n = m.$$

Here, we have set $\theta_{sc} = \pi/2$ radians since the phase shift takes place at a zero crossing of the subcarrier. Making the following substitutions for normalization purposes,

$$x = f/R$$

$$p = f_{sc}/R = \text{integer}$$

$$f_{cl}/R = 1,$$

the spectral density can be expressed in terms of these parameters as

$$S(x) = \frac{P_{SC}}{2T} \left| h(x-p) - h(x+p) \right|^2. \quad (3.1-5)$$

Evaluation of Equation 3.1-4 yields

$$h(x) = T \left\{ \frac{\sin(\pi x)}{\pi x} - \frac{m_{cl}}{2} \exp(j\theta_{cl}) \frac{\sin[\pi(x-1)]}{\pi(x-1)} \right. \\ \left. - \frac{m_{cl}}{2} \exp(-j\theta_{cl}) \frac{\sin[\pi(x+1)]}{\pi(x+1)} \right\} \exp(-j\pi x). \quad (3.1-6)$$

Curves depicting representative spectra are presented in Figure 3.1-1 (a). These curves are plots of normalized density spectra in the range centered at the subcarrier frequency (i.e., $x - p = 0$). Typical effects of clock modulation index and phase are noted in the figure. The special case, $m_{cl} = 0$, yields spectral characteristics pertinent to PSK-Summed Clock signal structures as well as representing the lower limit of clock modulation index. Part (b) of Figure 3.1-1 shows cumulative spectra corresponding to those cases included in part (a) of the figure. The cumulative spectra curves give the percent of total power in any specified bandwidth; thus, they aid in specifying the required bandwidth. Extensive analysis of data such as those represented by Figure 3.1-1 shows that a signal bandwidth of $4R$ contains at least 94% of the total power of the modulated subcarrier for PSK-AM signal structures. Additional bandwidth related data are summarized in Table 3.4.

In addition to the spectral characteristics in the vicinity of the subcarrier, interest also exists in the distribution of energy at frequencies removed from the subcarrier frequency. Such information aids in the determination of interference effects in adjacent channels. For this purpose, we now consider the rate at which the spectrum rolls-off in the range $|x - p| \gg 1$. This is accomplished here by means of a spectral envelope. That is, if one imagines a monotonically decreasing curve drawn through the peaks of the spectral distributions of Figure 3.1-1 (a), all values of spectral density lie on or below such a curve. In the range of interest, an approximate expression for the spectral envelope can be written as

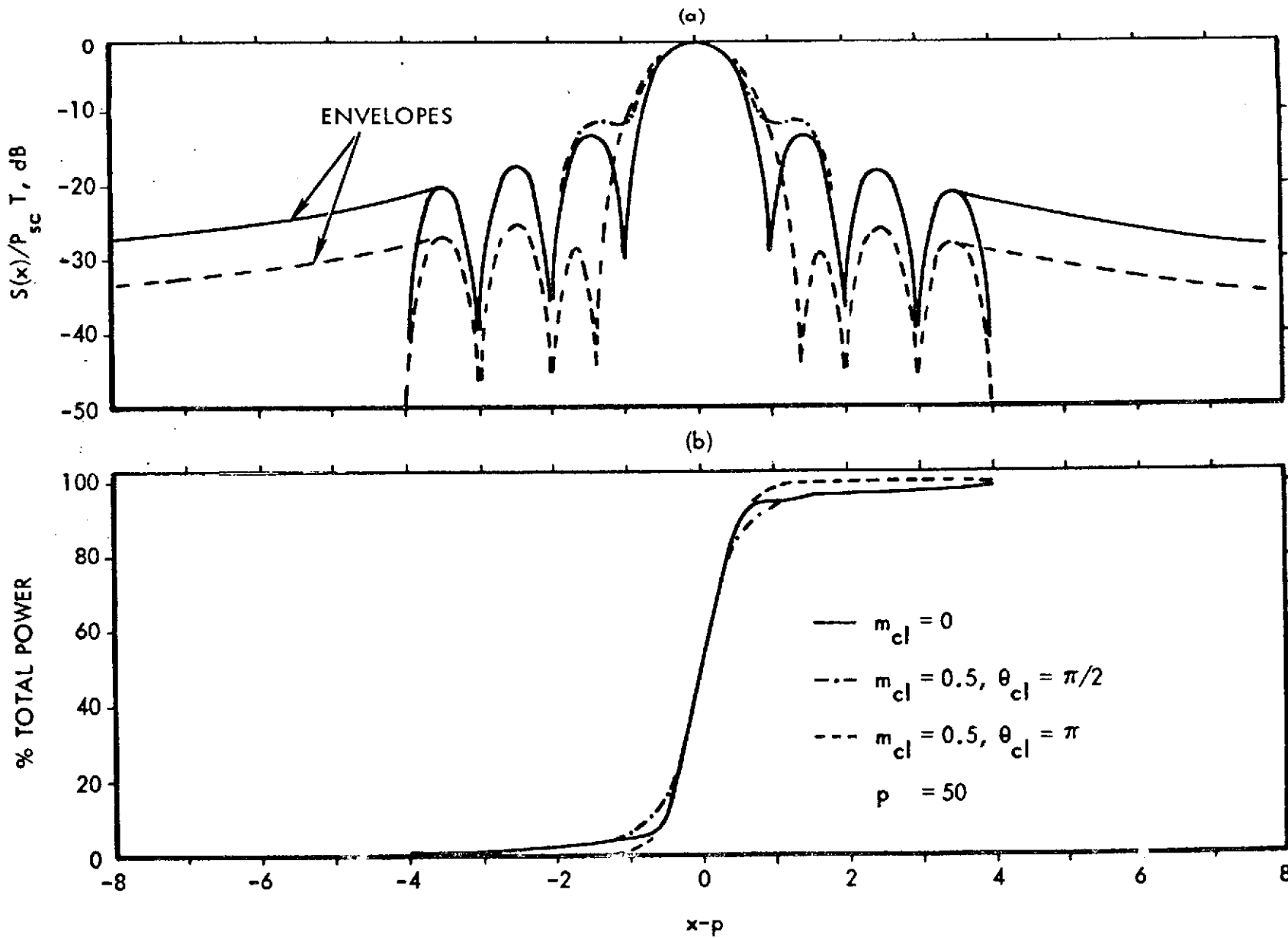


Figure 3.1-1. PSK-AM Spectra, (a) Spectral Density and (b) Cumulative Power Spectrum

$$\frac{S_e(x)}{P_{sc} T} \approx \left[1 + m_{cl} \cos(\theta_{cl}) \right]^2 \left[\frac{1}{\pi(x-p)} - \frac{1}{\pi(x+p)} \right]^2 \quad (3.1-7)$$

with the restriction

$$|x - p| \gg 1.$$

Examination of the above expression is quite revealing. We note that the spectral envelope for a PSK-AM signal structure is expressible as the spectral envelope for PSK (i.e., the right-most factor above) times a multiplicative factor which is a function of the clock modulation index and phase. Further, it is seen that the spectral envelope for PSK-AM with $0 \leq m_{cl} \leq 1$ and $\theta_{cl} = \pm\pi/2$ equals that for PSK (i.e., $m_{cl} = 0$). Finally, Equation 3.1-7 shows that clock phase equal to π radians yields the most narrow signal bandwidth. In contrast with the latter case, we note that $\theta_{cl} = 0$ yields the worst case for a given value of m_{cl} , a value disallowed by the VHF PCM/PSK Command System Guidelines.

It is apparent that the PSK and PSK-AM signal bandwidth is a function of the parameter p , depending of course upon the bandwidth selection criterion. Such dependence is especially significant for small values of p , and in the range $x - p < 0$. This fact complicates presentation of spectral data for general usage. In an effort to alleviate this problem, we write Equation 3.1-7 in the following form where the normalized spectral envelope is expressed in decibels.

$$\left. \frac{S_e(x)}{P_{sc} T} \right)_{dB} = S_1 + S_2 + S_3, \quad |x - p| \gg 1, \quad (3.1-8)$$

where

$$S_1 = 10 \log \left\{ \left[1 + m_{cl} \cos(\theta_{cl}) \right]^2 \right\} \quad (3.1-9)$$

$$S_2 = -10 \log(p^2) \quad (3.1-10)$$

and

$$S_3 = 10 \log \left\{ \left[\frac{1}{\pi(x/p - 1)} - \frac{1}{\pi(x/p + 1)} \right]^2 \right\}. \quad (3.1-11)$$

Figure 3.1-2 is a plot of Equation 3.1-11, plotted as a function of x/p . An expanded view of this curve, in the range $0.9 \leq x/p \leq 1.1$, is shown in Figure 3.1-3 (a). Part (b) of the latter figure is a plot of Equation 3.1-9, plotted as a function of m_{c1} with $\theta_{c1} = \pi$. Figures 3.1-2 and its expanded view in Figure 3.1-3 (a) can be interpreted as the spectral envelope corresponding to $p = 1$ and $m_{c1} = 0$. For other values of p and m_{c1} , the values obtained from either of these curves must be subsequently modified according to Equation 3.1-8. If $\theta_{c1} = \pm\pi/2$, S_1 of Equation 3.1-9 equals zero; otherwise, the appropriate value of S_1 can be found from Figure 3.1-3 (b).

Further explanation regarding the use of Figures 3.1-2 and 3.1-3 can best be given via several examples.

Example:

We determine the -30 dB bandwidth of the signal structure characterized by the parameter values $p = 100$, $m_{c1} = 0.5$ and $\theta_{c1} = \pi$.

Substituting into Equation 3.1-8,

$$-30 \text{ dB} = -6 \text{ dB} - 40 \text{ dB} + S_3$$

From Figure 3.1-3 (a), $S_3 = 16 \text{ dB}$ corresponds to $x/p = 0.949$ and 1.05 . Thus, the 30 dB signal bandwidth is $x = 105 - 94.9 = 10.1$, normalized to the bit rate. The bandwidth can otherwise be expressed as 10.1R hertz for any value of bit rate.

A second example follows which is representative of wideband signal structures.

Example:

We determine the 15 dB bandwidth of the signal structure characterized by the parameters, $p = 6$, $m_{c1} = 0.5$ and $\theta_{c1} = \pi/2$.

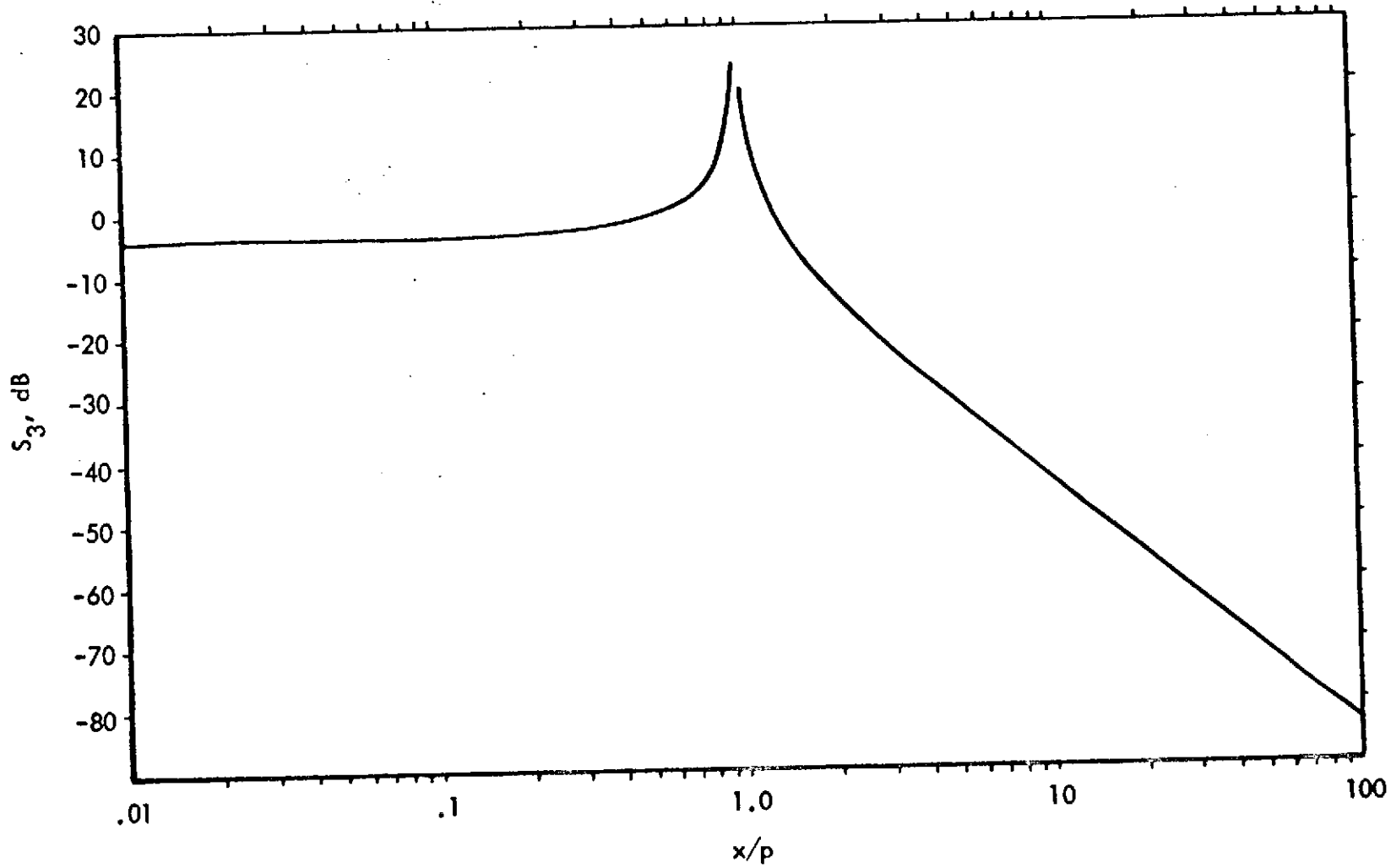


Figure 3.1-2. PSK Spectral Envelope

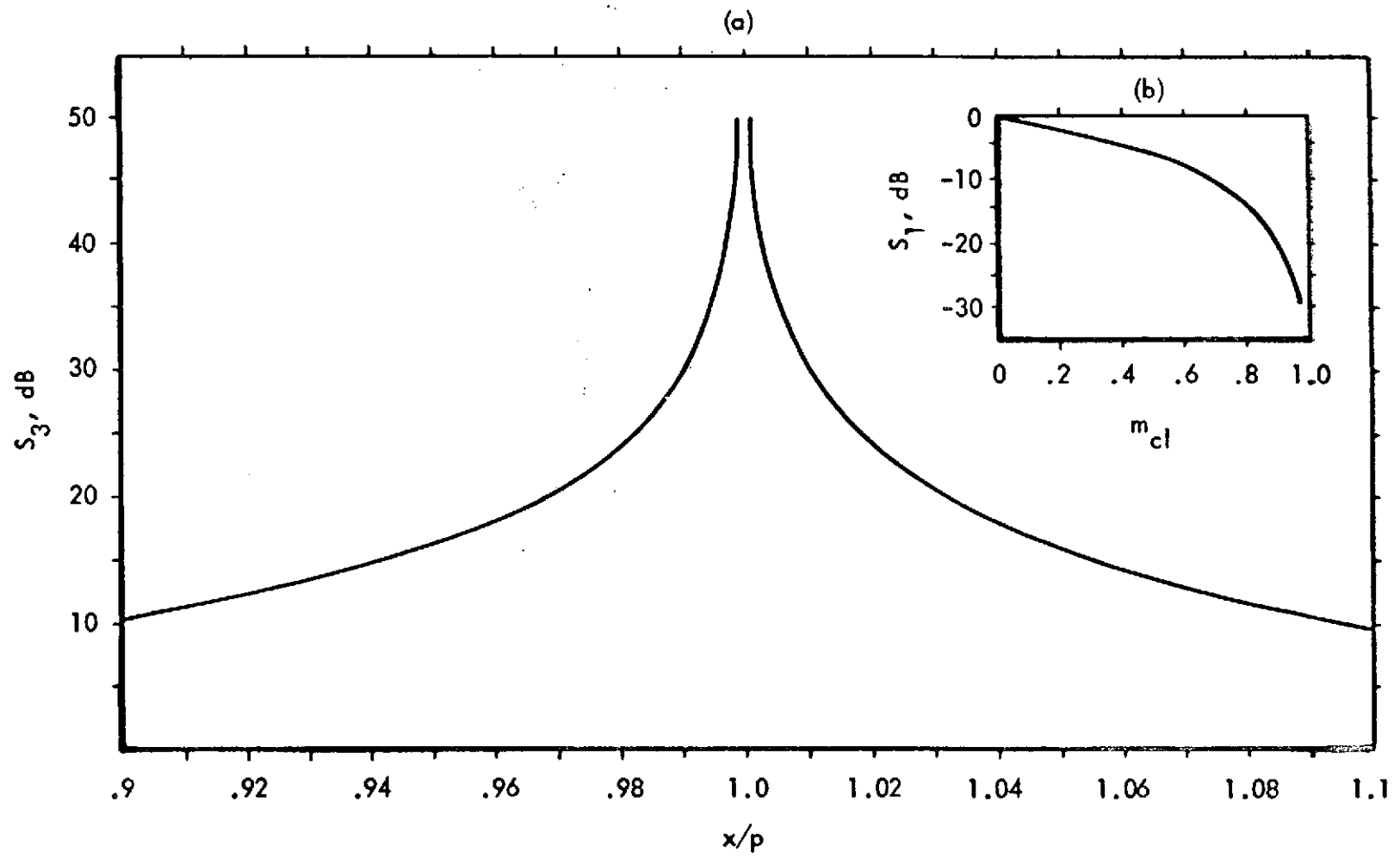


Figure 3.1-3. Curves Representing (a) S_3 and (b) S_1

Since $S_1 = 0$, substitution in Equation 3.1-8 gives

$$-15 \text{ dB} = -15.56 \text{ dB} + S_3$$

From Figure 3.1-2, $S_3 = 0.56 \text{ dB}$ corresponds to $x/p \approx 0.6$ and 1.25 , and the normalized 15 dB signal bandwidth is $x \approx 3.9$. The bandwidth expressed in hertz is therefore approximately $3.9 R$.

The latter example depicts the most extreme case allowed by the Guidelines with regards to wideband-ness of PSK-AM signal structures. This case also is a marginal one with regards to applicability of the spectral envelope concept, since Equation 3.1-7 is restricted to $|x - p| \gg 1$. However, the results obtained above are quite accurate as proven by data computed for this special case. Figure 3.1-1 indicates the range of applicability of Equation 3.1-7.

As demonstrated by the examples presented above, Figures 3.1-2 and 3.1-3 are extremely useful in that they allow one to determine spectral characteristics for a wide range of parameter values. Finally, it should be pointed out that the PSK and PSK-AM signal structures are wideband in spectral structure for values of $p < 50$, approximately. The extent to which this statement is true depends upon the bandwidth of interest. For $p = 6$, $m_{cl} = 0$, the spectral envelope is down to -20.5 dB at dc, corresponding to $x - p = -6$. Above the subcarrier frequency at $x - p = 6$, the spectral envelope has a value of -31 dB , exhibiting wideband spectral characteristics. In the range of x/p covered by Figure 3.1-3 (a), the spectral characteristics exhibit a narrowband nature as indicated by the symmetrical form of this curve about $x/p = 1$. In contrast, the curve of Figure 3.1-2 is quite unsymmetrical in the range removed from $x/p = 1$, being indicative of wideband spectral characteristics.

3.2 Spectral Characteristics of FSK-AM Signal Structures

The power density spectrum for continuous phase, binary FSK has been analyzed by Bennett and Rice [3-4] and Pelchat [3-3]. The problem here is to incorporate the AM Clock into such an analysis. Since the clock is not independent of the PCM code, the results which these authors present do not apply directly to determination of PCM/FSK-AM spectra (i.e., via convolution of spectra). Solution of the PCM/FSK-AM problem is presented in the following paragraphs. Pelchat's approach is followed with appropriate modifications and extension.

Letting the AM Clock be introduced via $c(t)$ as in Equation 3.1-2, the PCM frequency modulated subcarrier is given by

$$e_{sc}(t) = \sqrt{2 P_{sc}} c(t) \cos [\omega_{sc} t + \phi(t)] . \quad (3.2-1)$$

Over the n^{th} bit interval the instantaneous phase $\phi(t)$ can be expressed as

$$\phi(t) = a_n \Delta \omega (t-nT) + \sum_{i=0}^{n-1} a_i \Delta \omega T + \theta_{sc} , \quad nT \leq t < (n+1) T , \quad (3.2-2)$$

where θ_{sc} is a random variable assumed to be uniformly distributed over the range 0 to 2π radians and $\Delta \omega$ is the peak deviation from the subcarrier frequency.

For the purpose of computing the power spectrum, it is convenient to consider Equation 3.2-1 as a sum of nonoverlapping pulses

$$x_n(t) = \begin{cases} e_{sc}(t) , & nT \leq t < (n+1) T \\ 0 , & \text{otherwise} . \end{cases}$$

With $F_n(\omega)$ denoting the Fourier transform of $x_n(t)$, as before, the power density spectrum is given by Equation 3.1-3.

Letting

$$k(a_m, \omega) = \int_0^T c(t) \exp (j a_m \Delta \omega t) \exp (-j \omega t) dt , \quad (3.2-3)$$

the Fourier transform of $x_m(t)$ is

$$F_m(\omega) = \frac{\sqrt{2 P_{sc}}}{2} \left\{ \exp \left[j (\omega_{sc} - \omega) mT + \Delta \omega T \sum_{i=0}^{m-1} a_i + \theta_{sc} \right] \right. \\ \cdot k(a_m, \omega - \omega_{sc}) \\ + \exp \left[-j (\omega_{sc} + \omega) mT - \Delta \omega T \sum_{i=0}^{m-1} a_i - \theta_{sc} \right] \\ \left. \cdot k^*(a_m, -\omega - \omega_{sc}) \right\} ,$$

where the asterisk denotes complex conjugate. For signal structures of interest here, where

$$E \left\{ \exp(j \theta_{sc}) \right\} = 0 ,$$

$$F_m(\omega) F_n^*(\omega) = \frac{P_{sc}}{2} \left[G_{m,n}(\omega) + G_{m,n}^*(-\omega) \right] .$$

Letting

$$G(\omega) = \lim_{N \rightarrow \infty} \frac{P_{sc}}{2NT} \sum_{m=0}^{N-1} \sum_{n=0}^{N-1} E \left\{ G_{m,n}(\omega) \right\} ,$$

the power spectrum can be expressed by

$$S(\omega) = G(\omega) + G^*(-\omega) \quad (3.2-4)$$

In cases where the narrowband approximation can be made, only the $G(\omega)$ term above significantly contributes to the power spectrum.

It is helpful at this point to make the following substitutions:

$$\begin{aligned} p &= f_{sc}/R \\ m_f &= 2\Delta f/R \\ x &= f/R \end{aligned} \quad (3.2-5)$$

Note that the parameter, p , is not restricted to integer values. Here, m_f denotes the modulation index associated with the frequency shift modulation, where Δf is the peak deviation from the subcarrier. Employing the above substitutions,

$$G_{m,n}(x) = \exp \left\{ j2\pi \left[(p-x)(m-n) + \frac{m_f}{2} \left(\sum_{i=0}^{m-1} a_i - \sum_{i=0}^{n-1} a_i \right) \right] \right\} \\ \cdot k(a_m, x-p) k^*(a_n, x-p)$$

After some manipulations, following Pelchat,

$$G(x) = \frac{P_{sc}}{2T} \left\{ K_o(x-p) + 2 \operatorname{Re} \left[\frac{K_c(x-p)}{1 - C_1 \exp[-j2\pi(x-p)]} \right] \right\} \quad (3.2-6)$$

with the restriction

$$C_1 \exp \left[-j2\pi (x - p) \right] \neq 1 \quad , \quad (3.2-7)$$

where

$$C_1 = E \left\{ \exp (j a m_f \pi) \right\} \quad ,$$

$$K_o(x) = E \left\{ \left| k(a, x) \right|^2 \right\}$$

and

$$K_c(x) = \exp(-j2\pi x) E \left\{ k(a_m, x) \right\} \\ \cdot E \left\{ \exp(j a_n m_f \pi) k^*(a_n, x) \right\} \quad .$$

The restriction given in Equation 3.2-7 requires m_f be noninteger. In the case where $|C_1| = 1$, corresponding to m_f equal to an integer,

$$G(x) = \frac{P_{sc}}{2T} \left\{ K_o(x-p) - K_1(x-p) \right\} \quad , \quad (3.2-8)$$

with

$$C_1 \exp \left[-j2\pi (x - p) \right] \neq 1 \quad .$$

Here

$$K_1(x) = \left| E \left\{ k(a, x) \right\} \right|^2 \quad .$$

At frequencies, $x = x_d$, such that

$$|C_1| = 1 \text{ and } C_1 \exp \left[-j2\pi (x_d - p) \right] = 1 ,$$

$$G(x) = \frac{P_{sc}}{2T^2} K_1 (x - p) \delta (x - x_d) , \quad (3.2-9)$$

spectral lines, or impulses of power density, appear in the power spectrum.

In terms of the normalized frequency variable, x , evaluation of Equation 3.2-3 yields

$$\begin{aligned} k(a_m, x) = T & \left\{ \frac{\sin \left[\pi (x - a_m m_f/2) \right]}{\pi (x - a_m m_f/2)} \right. \\ & + \frac{m_{cl}}{2} \left[\frac{\exp(j\theta_{cl})}{\pi (x - a_m m_f/2 - 1)} + \frac{\exp(-j\theta_{cl})}{\pi (x - a_m m_f/2 + 1)} \right] \\ & \left. \cdot \sin \left[\pi (x - a_m m_f/2) \right] \right\} \exp \left[-j\pi (x - a_m m_f/2) \right] . \end{aligned} \quad (3.2-10)$$

If the parameter T is factored out of Equation 3.2-10, Equations 3.2-6 and 3.2-8, and subsequently Equation 3.2-4, can be expressed in normalized form independent of the bit rate. The single-sided spectral density thus becomes

$$\frac{S(x)}{P_{sc} T} = \frac{G(x)}{P_{sc} T} + \frac{G(-x)}{P_{sc} T} \quad (3.2-11)$$

normalized to the average energy per bit of the unmodulated subcarrier. It is also noted that the terms $G(x)$ and $G(-x)$ are real functions.

The spectral density of FSK signal structures takes varying forms as the modulation index, m_f , varies between integer values, being most significant in the frequency range existing between the mark and space frequencies, f_0 and f_1 . This fact is brought out in the work of Bennett and Rice. Similar effects are likewise present in the case of FSK-AM signal structures. Curves of the normalized spectral density are illustrated in Figure 3.2-1 (a), corresponding to $m_f = 4.5$ and several values of m_{cl} and θ_{cl} . Only that portion of the curves above the subcarrier frequency ($x - p \geq 0$ in the figure) are shown here since the spectral density is symmetrically distributed about the subcarrier frequency in the range encompassing the mark and space frequencies. As noted in Figure 3.2-1, spectral data for $\theta_{cl} = \pi/2$ is identical to that for $\theta_{cl} = -\pi/2$. Also, the clock phase, $\theta_{cl} = \pi$, yields the most narrow signal bandwidth as illustrated in Figure 3.2-1. This is to be expected since the signal amplitude at the frequency-shift instant is smaller than that corresponding to all other values of clock phase. It should be noted that the phase which results in the greatest signal bandwidth is $\theta_{cl} = 0$, a phase disallowed by the Standards.

Further characteristics of the FSK-AM spectral density are similar to those noted by Bennett and Rice. As m_f varies from a multiple of one-half towards an integer value, the peak values of spectral density at or near f_0 , $f_0 \pm f_{cl}$ and f_1 , $f_1 \pm f_{cl}$ become larger and more sharp. When m_f equals an integer, an impulse of spectral density develops at these frequencies. The latter case reflects the fact that the phase at the start of each bit interval is independent of the keying.

Part (b) of Figure 3.2-1 shows the cumulative power spectrum for each case presented in part (a) of the figure. From the cumulative spectrum, the percent total average power in a given bandwidth can be obtained. Analysis of data provided by cumulative spectra computations for a broad range of parameters lead to the percent total power-bandwidth relations presented in Table 3.4. The information in the table can be employed as the basis for specifying signal bandwidth requirements.

Further interest in FSK-AM spectral characteristics lies in determination of the manner in which the spectrum rolls-off at frequencies removed from the subcarrier. In the frequency range corresponding to $|x - p| \gg m_f/2 + 1$, we can consider the spectral envelope which is given approximately by

$$\frac{S_e(x)}{P_{sc} T} \approx \left[1 + m_{cl} \cos(\theta_{cl}) \right]^2 f(x, p, m_f) \quad (3.2-12)$$

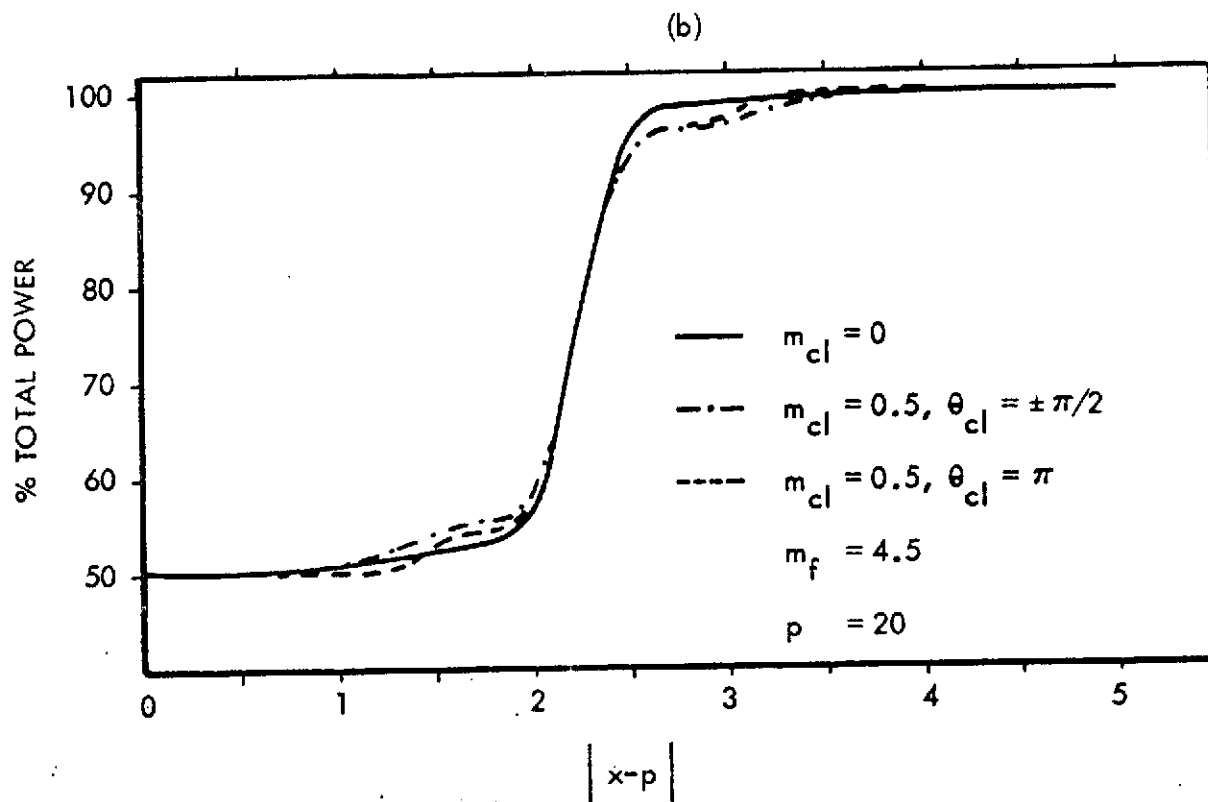
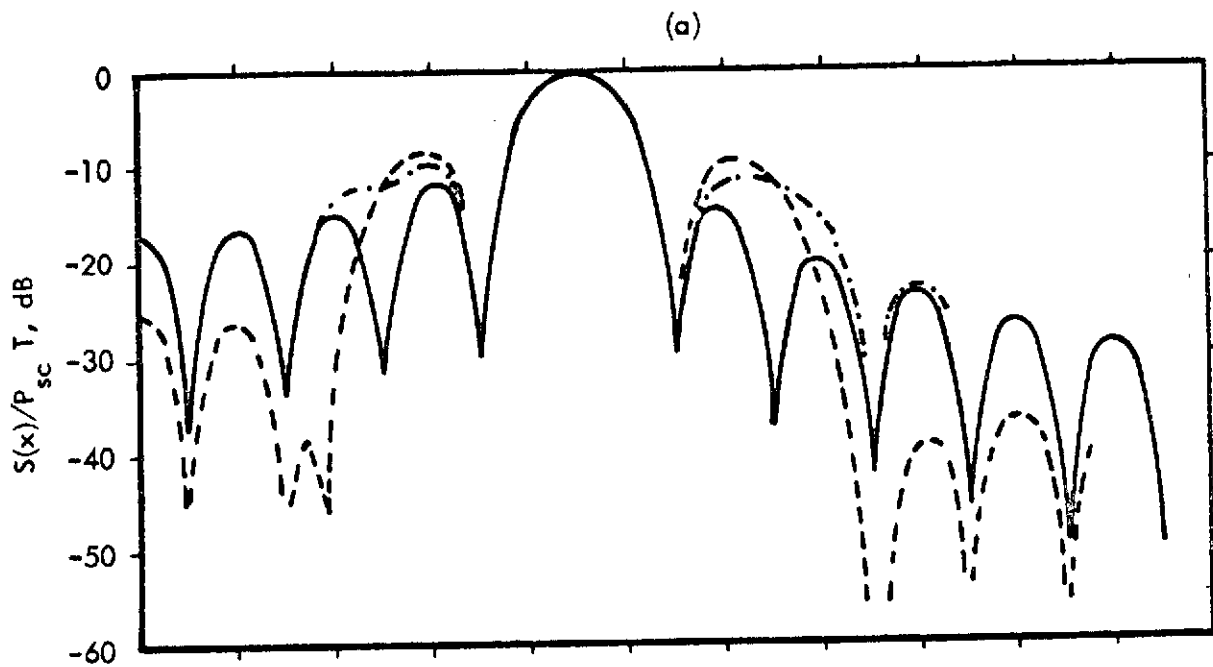


Figure 3.2-1. FSK-AM Spectra, (a) Spectral Density and (b) Cumulative Spectrum

where $f(x, p, m_f)$ represents the spectral envelope function for pure FSK signal structures. The above expression provides considerable visibility into the effect of the AM Clock. We note that clock phases $\theta_{cl} = \pm\pi/2$ produce spectral envelopes equal to that of FSK, while $\theta_{cl} = \pi$ provides the most narrow signal bandwidth.

The frequency shift modulation index, m_f , can vary over a wide range of values ($2 \leq m_f \leq 625$) as allowed by the VHF PCM/FSK Command Data Systems Standard. Thus, it is not practical to attempt presentation of data covering all values of m_f of possible interest. An alternative approach has been adopted; namely, curves are presented which depict the frequency where the envelope, $f(x, p, m_f)$, is down relative to the unmodulated subcarrier by a specified number of decibels. These curves are plotted in Figure 3.2-2 as a function of m_f with envelope levels of -30, -40, -50, and -60 dB acting as a parameter. Linear interpolation can be applied with reasonably good accuracy between the curves shown. The family of curves presented in Figure 3.2-2 were actually computed using Equation 3.2-6 with $m_{cl} = 0$. Cases of interest where $m_{cl} \neq 0$ and $\theta_{cl} = \pi$ can be evaluated by adding the appropriate value obtained from Figures 3.1-3 (b) to that obtained from Figure 3.2-2.

Further explanation of the use of the curves presented in Figure 3.2-2 is in order. These curves are directly applicable in the frequency range which is characteristic of narrowband signals; that is, where the envelope is symmetrical about the subcarrier frequency. In such a case, the signal bandwidth is twice the value obtained from Figure 3.2-2 for a given value of p . However, in cases characterized by wideband signal structure, data given by these curves must be adjusted to compensate for frequency foldover. Such modification of the data is illustrated in the following example in conjunction with Figure 3.2-3.

Example:

We determine the -50 dB bandwidth of an FSK-AM signal structure characterized by the parameter values, $p = 20$, $m_f = 4.5$, $m_{cl} = 0.5$ and $\theta_{cl} = \pi/2$.

From Figure 3.2-2, we find that the envelope is down 50 dB at $x-p = 15$. Below the subcarrier at $x-p = -15$, we experience foldover effects. That is, since $x-p = -20$ corresponds to dc, the magnitude of the envelope at $x-p = -25$ (-59 dB or 1.26×10^{-6}) adds to the value corresponding to -50 dB (i.e., 1×10^{-5}) at $x-p = -15$. The adjusted value of the envelope at $x-p = -15$ is therefore 1.126×10^{-5} or -49.5 dB. We conclude that the -50 dB bandwidth is slightly larger than $2 \times 15 R$ hertz or approximately 31 R hertz. Since $\theta_{cl} = \pi/2$ in this example, we note from Equation 3.2-12 that no adjustment to the above value as a result of the AM Clock is necessary.

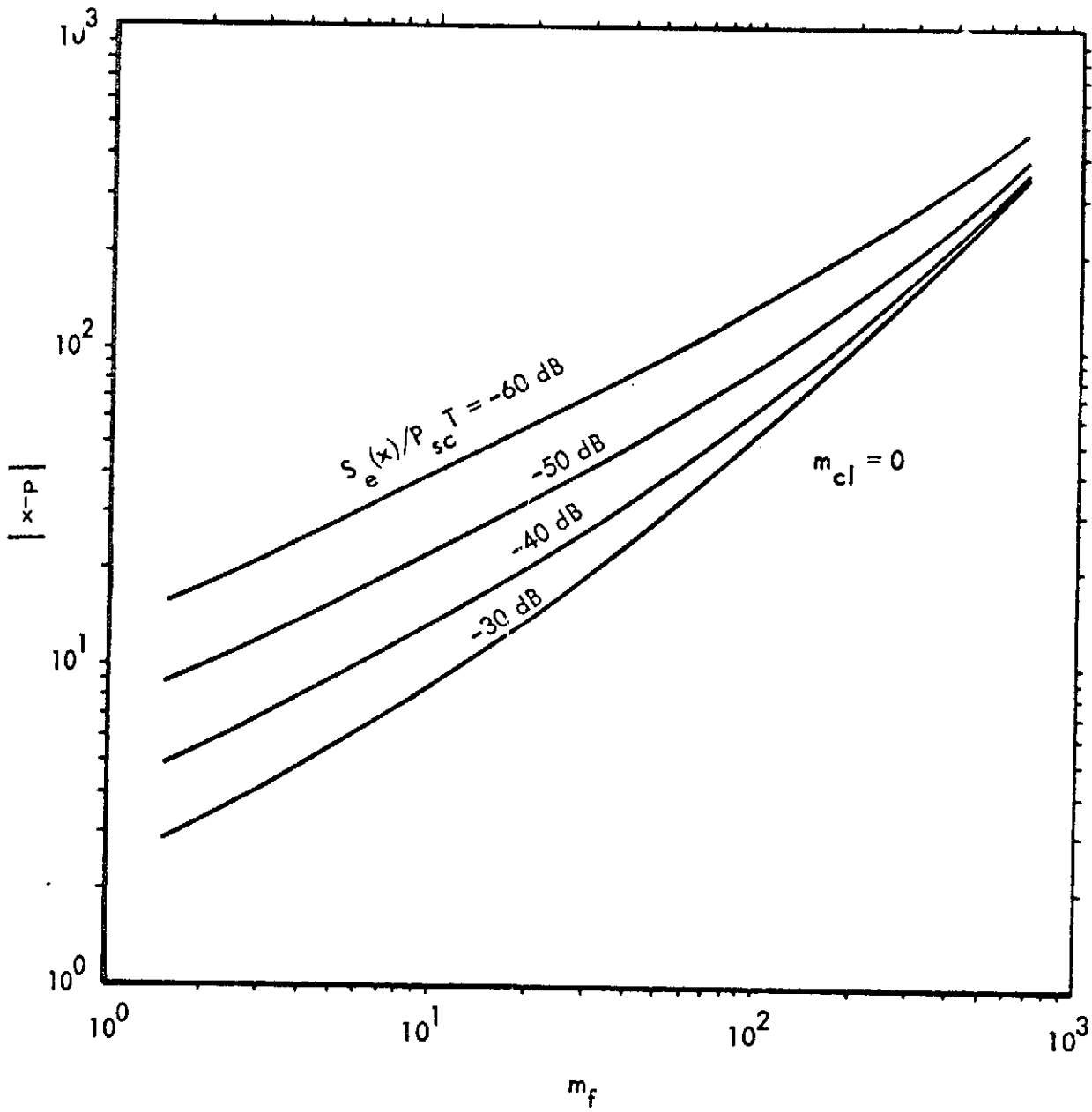


Figure 3.2-2. FSK Spectral Envelope Levels as a Function of Normalized Frequency and Modulation Index

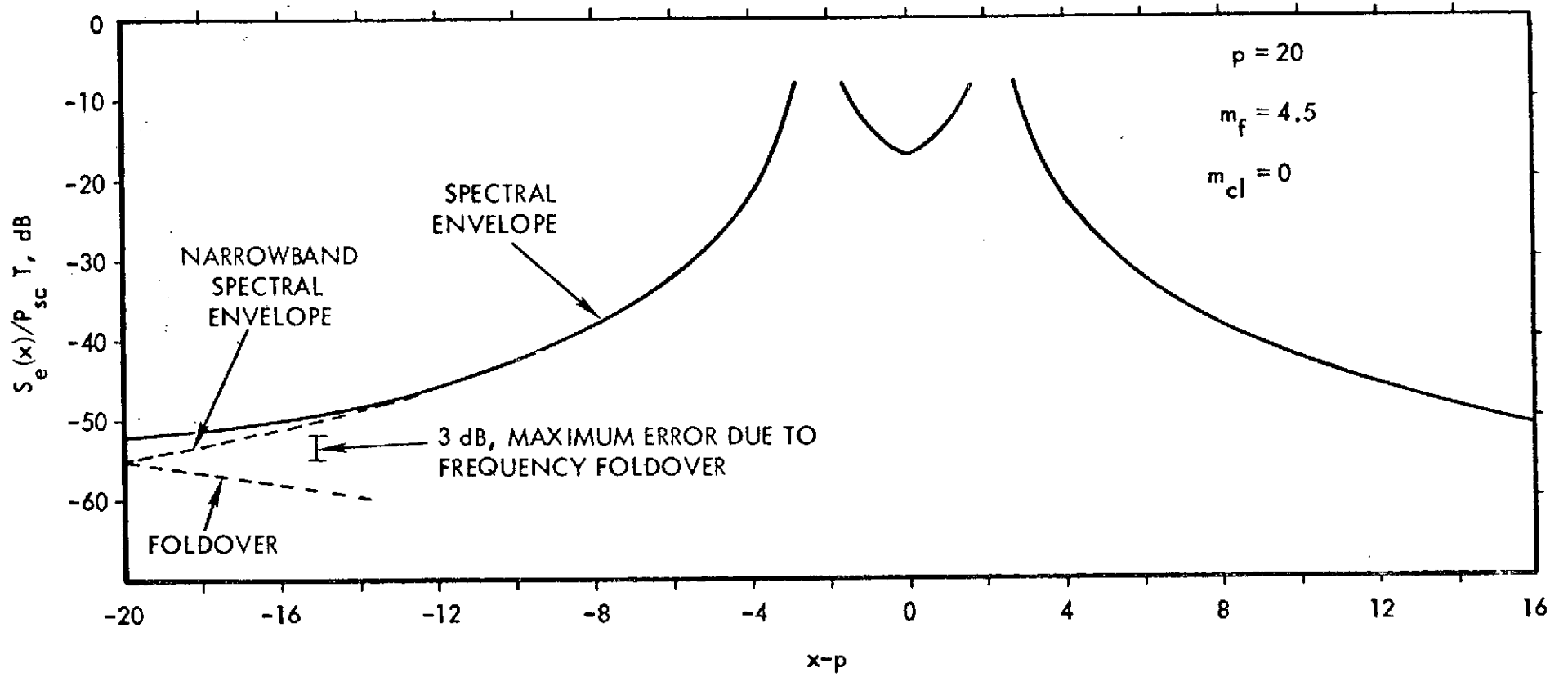


Figure 3.2-3. FSK Spectral Envelope

Since the magnitude of the effect of foldover is a function of p , it is difficult to generalize the effects of such. The above example illustrates the necessary considerations, and the significant effects of foldover can be readily estimated by sketching an envelope curve similar to that shown in Figure 3.2-3 from data obtainable from Figure 3.2-2.

Of practical significance, we note that the worst case effect of foldover occurs at dc, where the magnitude of the spectral envelope is doubled as a result of foldover. Therefore, the maximum adjustment ever required is to increase the envelope level by 3 dB, a value which is not significant in most cases of practical interest.

3.3 RF Carrier Spectral Characteristics

Further spectral characteristics relevant to VHF Command Systems are presented in the following paragraphs where the composite subcarrier signal structures act as the RF modulating signal. Specifically, RF carrier modulation techniques which are considered include amplitude, phase and frequency modulation by the PSK-AM and FSK-AM subcarrier. Emphasis is placed upon general RF spectral characteristics and bandwidth requirements at RF.

Amplitude modulation of the carrier is considered by translation of the subcarrier spectrum up to the carrier frequency, this approach being possible since AM is a linear modulation process. RF spectral characteristics and bandwidth requirements are therefore obtained in a straightforward manner without further analysis.

Frequency and phase modulation, or general angle modulation, are nonlinear modulation processes and are not as easily handled as amplitude modulation. The approach adopted here assumes periodic subcarrier modulation, and subsequently line spectra pertinent to the modulated RF carrier are calculated through the use of a Fast Fourier Transform (FFT) Algorithm [3-5]. Angle modulation of the RF carrier can be expressed by

$$e_c(t) = \sqrt{2 P_c} \cos \left[\omega_c t + \phi(t) + \theta_c \right] , \quad (3.3-1)$$

where P_c , ω_c and θ_c denote average unmodulated carrier power, carrier angular frequency and phase, respectively. In the above expression, $\phi(t)$ represents the modulation function for angle modulation. It is assumed that the PCM baseband signal consists of alternate plus and minus ones denoted by $a_n = \pm 1$ in the n^{th} bit interval. In general, we have a sequence of N bits, $n = 0, 1, 2, \dots, N - 1$, with N equal to an even integer such that the modulation function repeats identically for each N bit sequence.

In the case of PSK-AM subcarrier modulation the ratio p is an integer and the value of N equals two. Otherwise, in the case of FSK-AM subcarrier modulation, the value of p is not necessarily an integer value and N is therefore an even integer equal to or greater than two, dependent upon the value of p . In terms of a Fourier series representation, Equation 3.3-1 can be expressed as

$$e_c(t) = \sqrt{2 P_c} \sum_{m=-\infty}^{\infty} |F_m| \cos \left[(\omega_c + m\omega_r) t + \theta_m + \theta_c \right], \quad (3.3-2)$$

with the complex Fourier coefficients for narrowband signals given by

$$F_m = \frac{1}{NT} \int_0^{NT} \exp \left[j \Phi(t) \right] \exp (-jm \omega_r t) dt \quad . \quad (3.3-3)$$

Thus, the Fourier coefficients, F_m , can be found from the modulation function via the FFT technique. The fundamental frequency, relative to the carrier frequency, is given by

$$f_r = 1/NT = R/N$$

The power spectrum can be represented by

$$W_m = |F_m|^2 \quad . \quad (3.3-4)$$

The modulated subcarriers employed in the angle modulation RF spectral analysis can be represented as follows employing the change of variable, $t' = \omega_r t$;

$$e_{sc}(t') = \sqrt{2 P_{sc}} a_n c(t') \cos (N p t' + \theta_{sc}) \quad , \quad \text{PSK-AM} \quad (3.3-5)$$

$$e_{sc}(t') = \sqrt{2 P_{sc}} c(t') \cos \left[N (p + a_n m_f) t' + \pi \sum_{i=0}^{n-1} a_i m_f + \theta_{sc} \right], \quad \text{FSK-AM} \quad (3.3-6)$$

where the AM Clock is introduced via

$$c(t') = 1 + m_{cl} \cos (Nt' + \theta_{cl})$$

The summation in Equation 3.3-6 requires that the FSK-AM subcarrier signal be continuous phase at each frequency transition.

The modulation function of Equation 3.3-3 for the FM and PM carriers becomes

$$\phi(t') = \frac{k}{\omega_r} \int_0^{t'} e_{sc}(u) du, \quad 0 \leq t' \leq 2\pi; \quad \text{FM} \quad (3.3-7)$$

$$= k e_{sc}(t'), \quad 0 \leq t' \leq 2\pi; \quad \text{PM}, \quad (3.3-8)$$

where k is a proportionality constant representative of the respective modulator. The subcarrier signal indicated above is the appropriate expression from Equation 3.3-5 or 3.3-6 for PSK-AM or FSK-AM, respectively.

We note that the actual peak frequency deviation from the carrier in the FM case is

$$\Delta \omega_{pk} = k \sqrt{2 P_{sc}} (1 + m_{cl}) \quad (3.3-9)$$

and we define the deviation ratio as[†]

$$\frac{\Delta f_{pk}}{f_{sc}} = \beta_f (1 + m_{cl}) \quad (3.3-10)$$

Similarly, in the PM case the peak phase deviation is given by

$$\begin{aligned} \Delta \phi_{pk} &= k \sqrt{2 P_{sc}} (1 + m_{cl}) \\ &= \beta_p (1 + m_{cl}) \end{aligned} \quad (3.3-11)$$

The parameters β_f and β_p are recognized as the FM and PM modulation indices, respectively, in the absence of an AM Clock.

This summarizes the mathematical formulation necessary to compute RF line spectra using Equations 3.3-7 and 3.3-8 in conjunction with Equation 3.3-3 which can be rewritten in terms of the variable t' as

$$F_m = \frac{1}{2\pi} \int_0^{2\pi} \exp \left[j \phi (t') \right] \exp (-jmt') dt' \quad (3.3-12)$$

The FFT algorithm is employed to evaluate F_m .

Spectral characteristics and bandwidth requirements are presented in the following paragraphs via line spectra envelopes and cumulative spectra curves. Representative curves are included for each type of angle modulation of interest here. In addition, families of curves are presented which relate the manner in which the skirts of the RF spectra roll-off. From these data, bandwidth requirements are easily obtained for any desired bandwidth definition.

[†]In the FSK-AM case, f_{sc} is the average of the mark and space frequencies.

3.3.1 Amplitude Modulation of the RF Carrier

Amplitude modulation of the RF carrier can be expressed as

$$e_c(t') = \sqrt{2 P_c} \left[1 + m_a e_{sc}(t') / \sqrt{2 P_{sc}} \right] \cos(\omega_c t + \theta_c) \quad (3.3.1-1)$$

where P_c , ω_c and θ_c denote average unmodulated carrier power, carrier angular frequency and phase, respectively. The parameter m_a is the RF modulation index, defined as

$$m_a = \sqrt{P_{sc}/P_c} \quad (3.3.1-2)$$

However, the value of m_a here does not represent the peak deviation of the carrier amplitude because of the presence of the AM Clock. The actual peak deviation of the carrier amplitude is given by

$$\Delta A_{pk} = m_a (1 + m_{cl}) \quad (3.3.1-3)$$

a value which must be maintained less than or equal to unity to prevent envelope distortion. Hence, we have the following relationship which must be observed,

$$m_a \leq 1 / (1 + m_{cl}) \quad (3.3.1-4)$$

It is well known that the RF carrier spectrum consists of the subcarrier spectrum translated to ω_c and multiplied by $m_a^2/2$. In addition, a spectral line exists at the carrier frequency. In terms of the spectral densities developed in Section 3.1 and 3.2 for PSK-AM and FSK-AM, respectively, the single-sided power spectral density becomes

$$W(\omega) = P_c \left\{ \delta(\omega - \omega_c) + \frac{m_a^2}{2} S(\omega - \omega_c) \right\} \quad (3.3.1-5)$$

In order to determine any defined bandwidth at RF, we only need to determine the upper cutoff frequency corresponding to the subcarrier spectral density, and double that value. Thus, the spectral characteristics developed at subcarrier are directly applicable here by simple translation according to Equation 3.3.1-5.

Relationships between bandwidth and pertinent parameters which describe the signal structure are summarized in Table 3.4.

3.3.2 PSK-AM/FM Spectral Characteristics

Frequency modulation of the RF carrier by the composite PSK-AM subcarrier signal is considered here, where the subcarrier is assumed to be periodically phase-shift-keyed, with period $2T$.

Computation of the power spectrum defined by Equation 3.3-4 for a wide range of parameter values has been carried out by means of an FFT computer program. In addition, corresponding cumulative power spectra have been computed. A representative result is shown in Figure 3.3.2-1. In this figure, and subsequent figures, only that portion of the spectrum above the carrier is pictured since the spectrum is symmetrically distributed about the carrier frequency. Similarly, the effect of the clock modulation index upon the FM spectrum is illustrated in Figure 3.3.2-2 (a) via line spectrum envelopes. The latter figure depicts envelopes for the two extreme values of m_{cl} (i.e., zero and unity). Part (b) of Figure 3.3.2-1 and 3.3.2-2 shows the cumulative spectra which correspond to part (a) of these figures. Examination of these two figures indicate the dependence of the spectrum upon the clock modulation index and phase for small values of β_f . Data analysis has revealed that the gross spectral structure (e.g., the envelope) is not critically dependent upon clock modulation index or clock phase.

Restricting attention to the peaks of the line spectrum envelope, we now consider the FM spectrum in a more general sense. Analysis of computed spectral data leads to the following results and conclusions:

1. Line spectrum envelope peaks occur at approximately integer multiples of the subcarrier relative to the carrier frequency.
2. For given values of β_f , m_{cl} and θ_{cl} , the peak values are independent of the parameter p , and the subcarrier frequency.

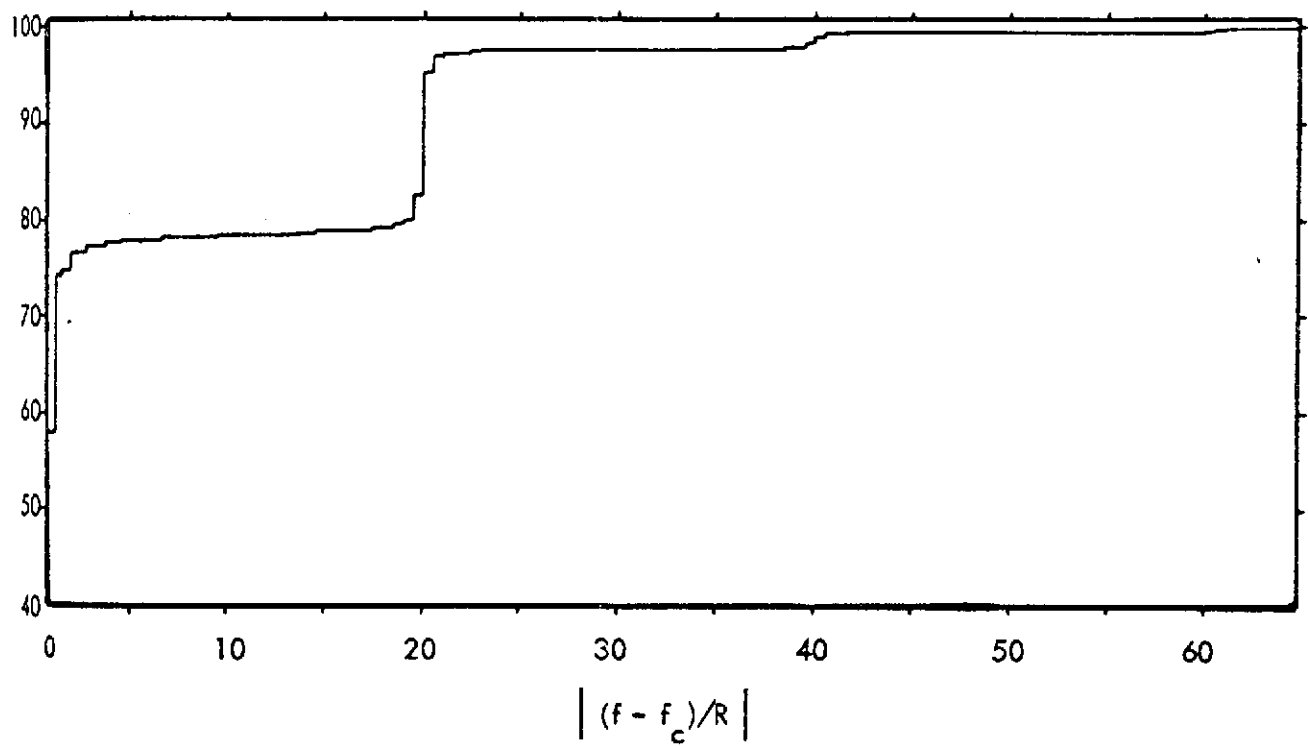
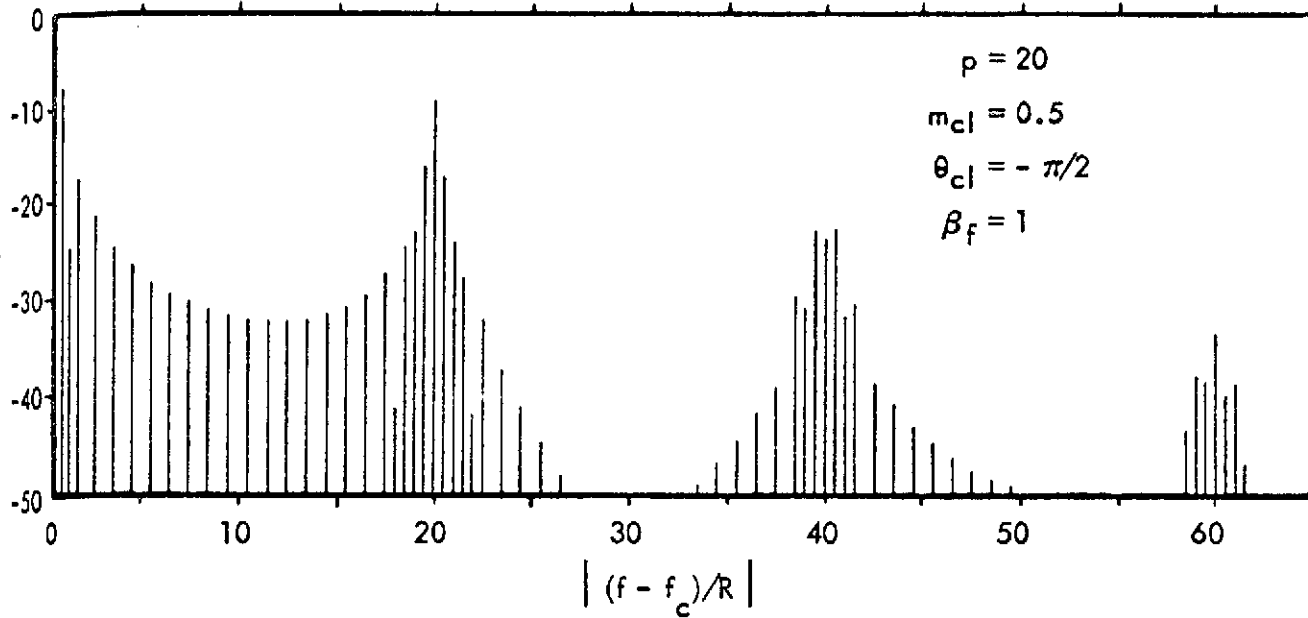
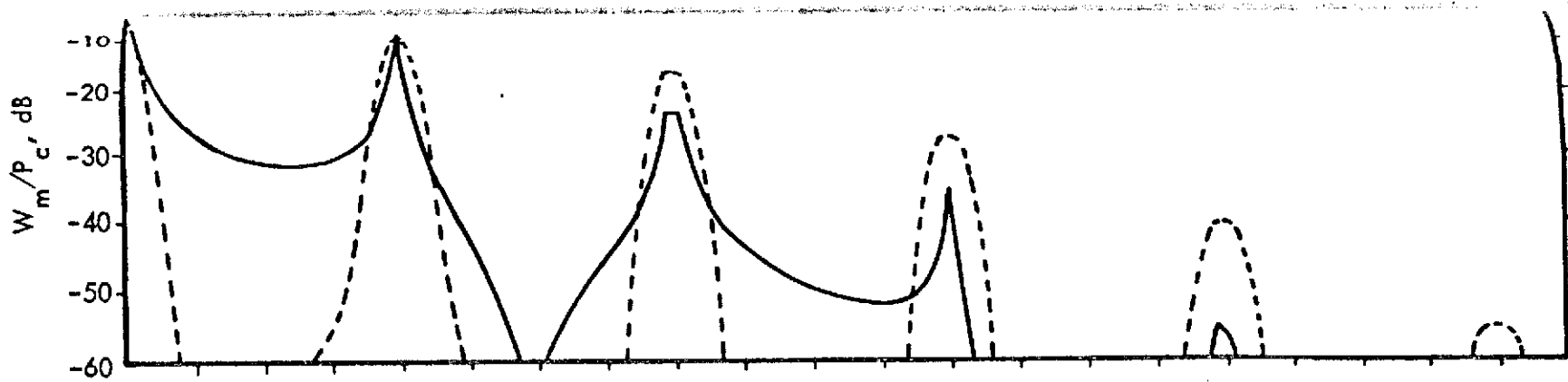


Figure 3.3.2-1. Power Spectrum and Cumulative Spectrum for Carrier Frequency Modulated by PSK-AM Subcarrier



(b)

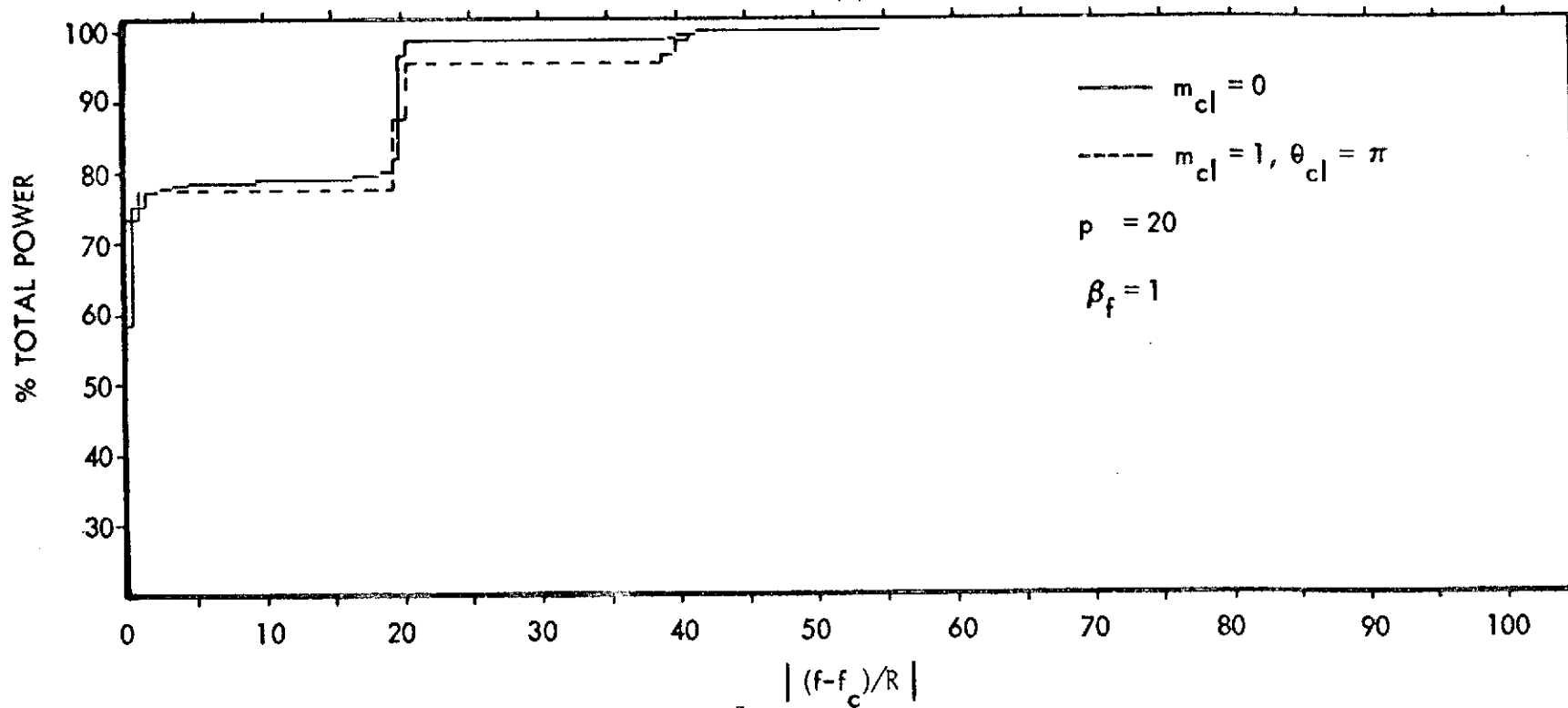


Figure 3.3.2-2. PSK-AM/FM Spectra, (a) Line Spectrum Envelope and (b) Cumulative Spectrum

In anticipation of the clock modulation index being equal to or less than one-half in practice, the following considerations are restricted to cases where $m_{cl} = 0.5$ and $\theta_{cl} = \pi$. Extensive data analysis justifies this parameter selection as representative of cases where $m_{cl} \leq 0.5$ and $\theta_{cl} = \pm\pi/2$ or π . In Figure 3.3.2-3, values of spectral envelope peaks which occur at multiples of the subcarrier, relative to the carrier frequency, are plotted for various values of β_f . These data provide information regarding the manner in which the FM spectrum rolls-off. In addition, the FM spectral envelope peaks which correspond to 96% and 99% of the total RF power are indicated in Figure 3.3.2-3. Based upon results of data analysis, an empirical expression of bandwidth has been determined as

$$B_c = 2 (\beta_f + 1) (f_{sc} + R) , \beta_f \leq 5 \quad (3.3.2-1)$$

An ideal filter with the bandwidth given above would pass 94% or more of the total RF power. For values of $\beta_f < 3$, this figure is approximately 98% and subsequently decreases for larger values of β_f . Due to the structure of the RF spectral envelope, noninteger values of $(\beta_f + 1)$ should be rounded to the nearest integer value.

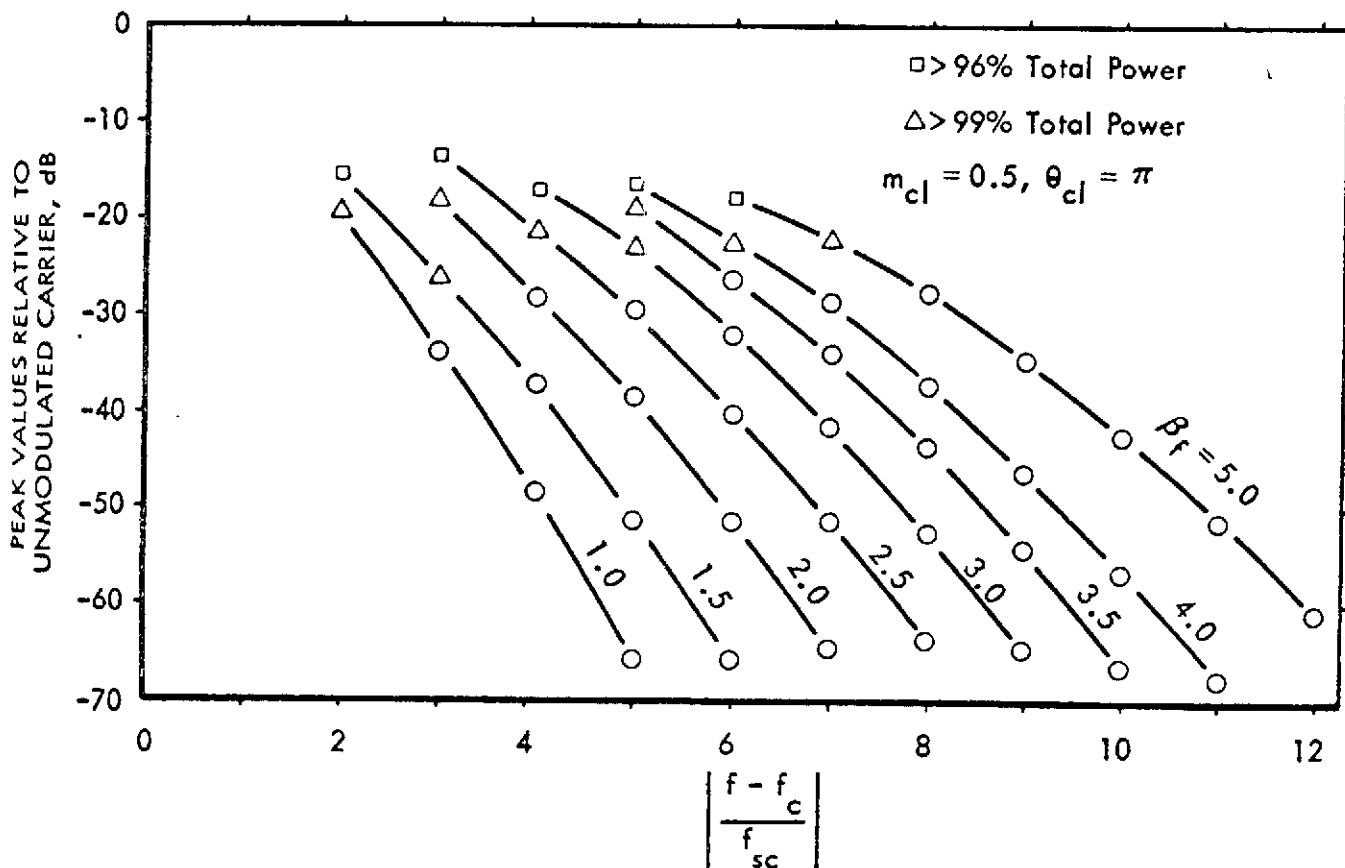


Figure 3.3.2-3. Peak Values of PSK-AM/FM Spectral Envelope

3.3.3 PSK-AM/PM Spectral Characteristics

Phase modulation of the RF carrier is considered here in a manner similar to that of the FM carrier. In this case, the modulation function corresponds to a periodic phase-shift-keyed subcarrier with period $2T$. Figure 3.3.3-1 illustrates the line spectrum via envelope curves for the extreme values of clock modulation index. The dependence of the spectrum upon clock modulation index and clock phase are small for values $m_{cl} \leq 0.5$, as in the FM case. Part (b) of this figure shows the corresponding cumulative power spectra.

Analysis of computed data corresponding to peak phase deviations of $\pi/2$ radians or less reveals that peaks of the line spectrum envelopes again occur at approximately integer multiples of the subcarrier, relative to the carrier frequency. Also, for given values of the parameters β_p , m_{cl} and θ_{cl} , the values of the envelope peaks are independent of p , and the subcarrier frequency. Therefore, as in the FM case, we can present data relevant to the envelope peak values which are applicable for all values of the parameter p . These data are shown in Figure 3.3.3-2.

In the range $\beta_p < \pi/2$, the 95%, or greater, total power bandwidth is given by

$$B_c = 2 (f_{sc} + R) , \quad \beta_p < \pi/2 \quad . \quad (3.3.3-1)$$

Again, more power is encompassed in this passband for smaller values of β_p . For $\beta_p \geq \pi/2$, the expression would necessarily have to reflect the effect of β_p as in the PSK-AM/FM case.

3.3.4 FSK-AM/FM Spectral Characteristics

In general, the FSK-AM/FM spectrum results from combined effects of many parameters, including FSK subcarrier, AM Clock and RF modulation parameters. An FFT computer program has been utilized to gather discrete spectral data which are representative of the most significant effects which these parameter values introduce. The waveforms of interest here are continuous phase at subcarrier and RF. Application of the technique employed here to compute line spectra is restricted by the continuous phase requirements. Specifying N_p equal to an integer satisfies the continuous phase subcarrier condition. Conditions for maintaining continuous phase of the modulation function from one period, NT , to another are complicated functions of subcarrier and carrier modulation parameters. The most trivial solution to this problem is to set $N = 2$ and $p \pm m_f/2$ equal to an integer. Such conditions have been imposed to compute the data presented here.

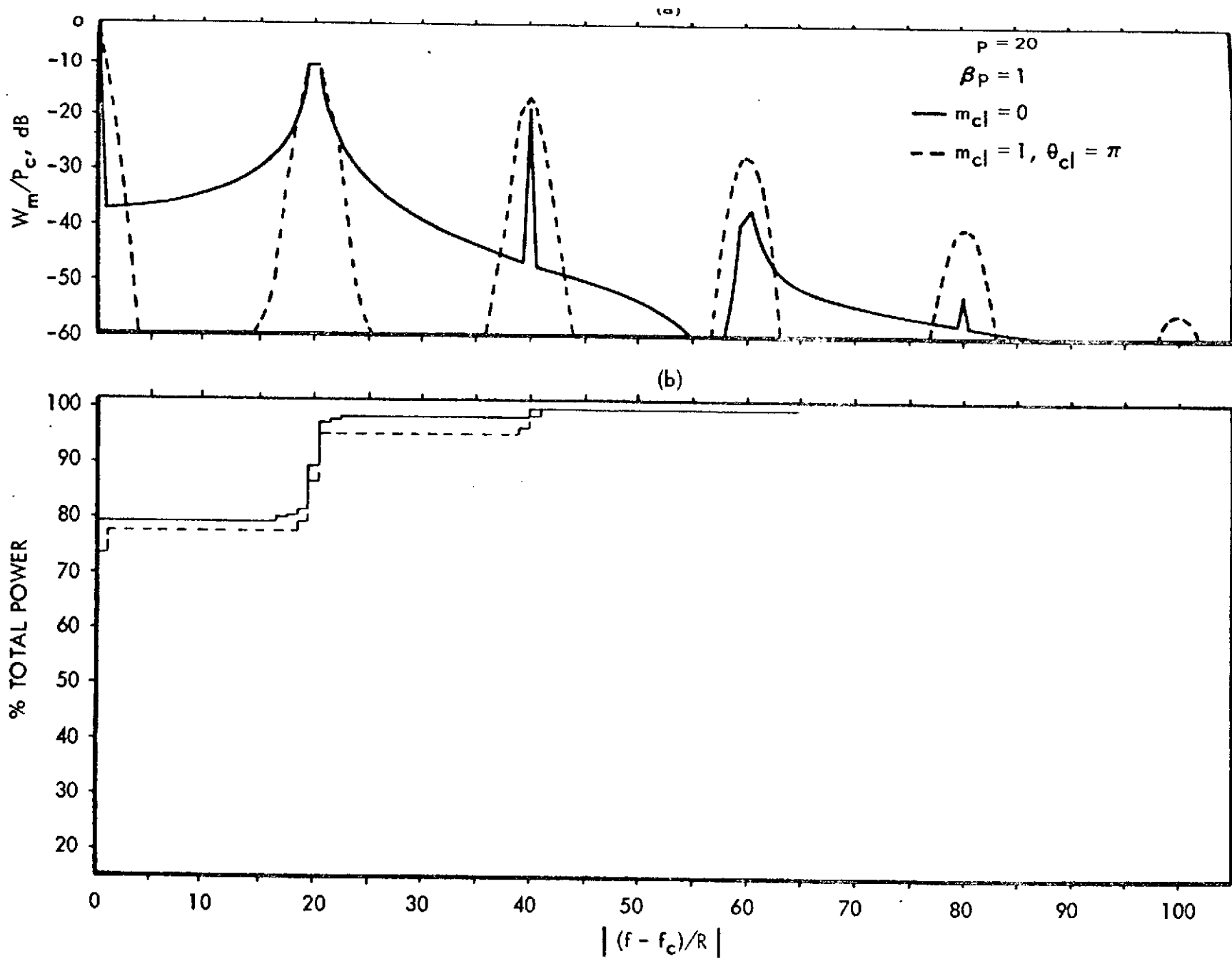


Figure 3.3.3-1. PSK-AM/PM Power Spectra, (a) Line Spectrum Envelope and (b) Cumulative Spectrum

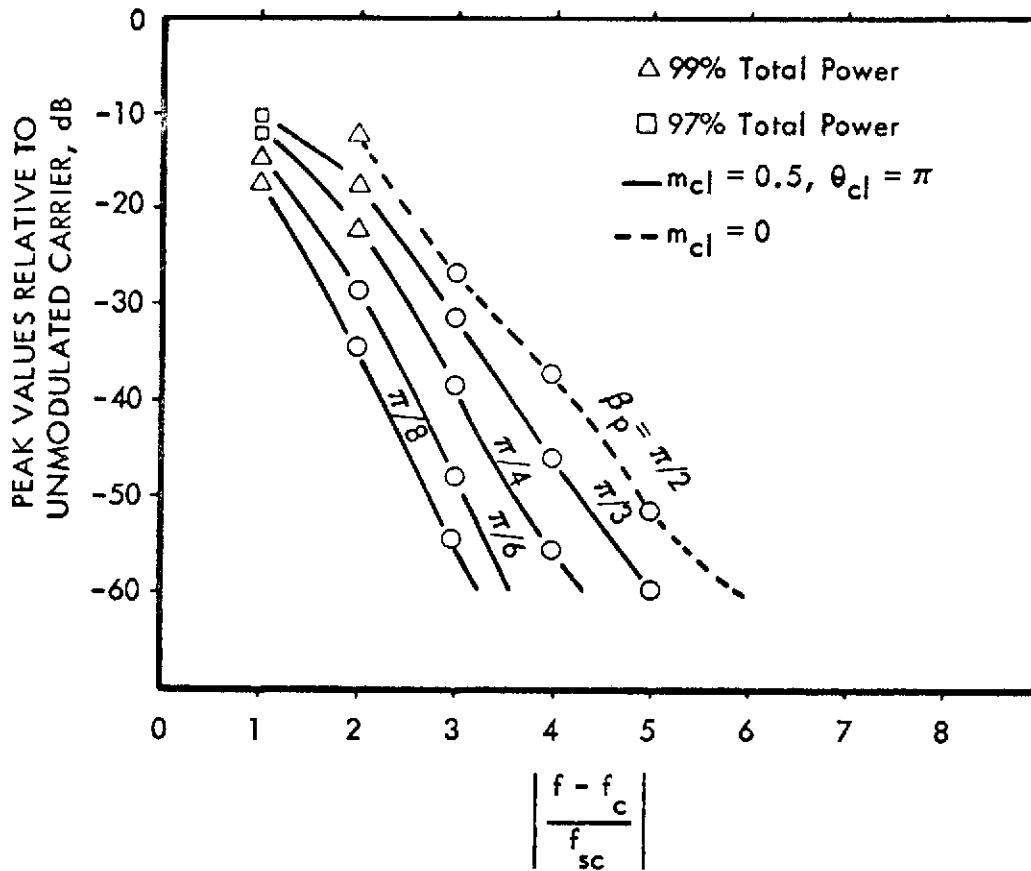


Figure 3.3.3-2. Peak Values of PSK-AM/PM Spectral Envelope

Data presented in Figure 3.3.4-1 are illustrative of FSK-AM/FM spectral characteristics, these data including RF spectral envelopes and associated cumulative spectra. Analysis of computed data shows the following characteristics to exist:

1. Figure 3.3.4-1 is representative of the effect of the AM Clock modulation index at RF. The presence of the AM Clock has a small RF bandwidth "broadening" effect.

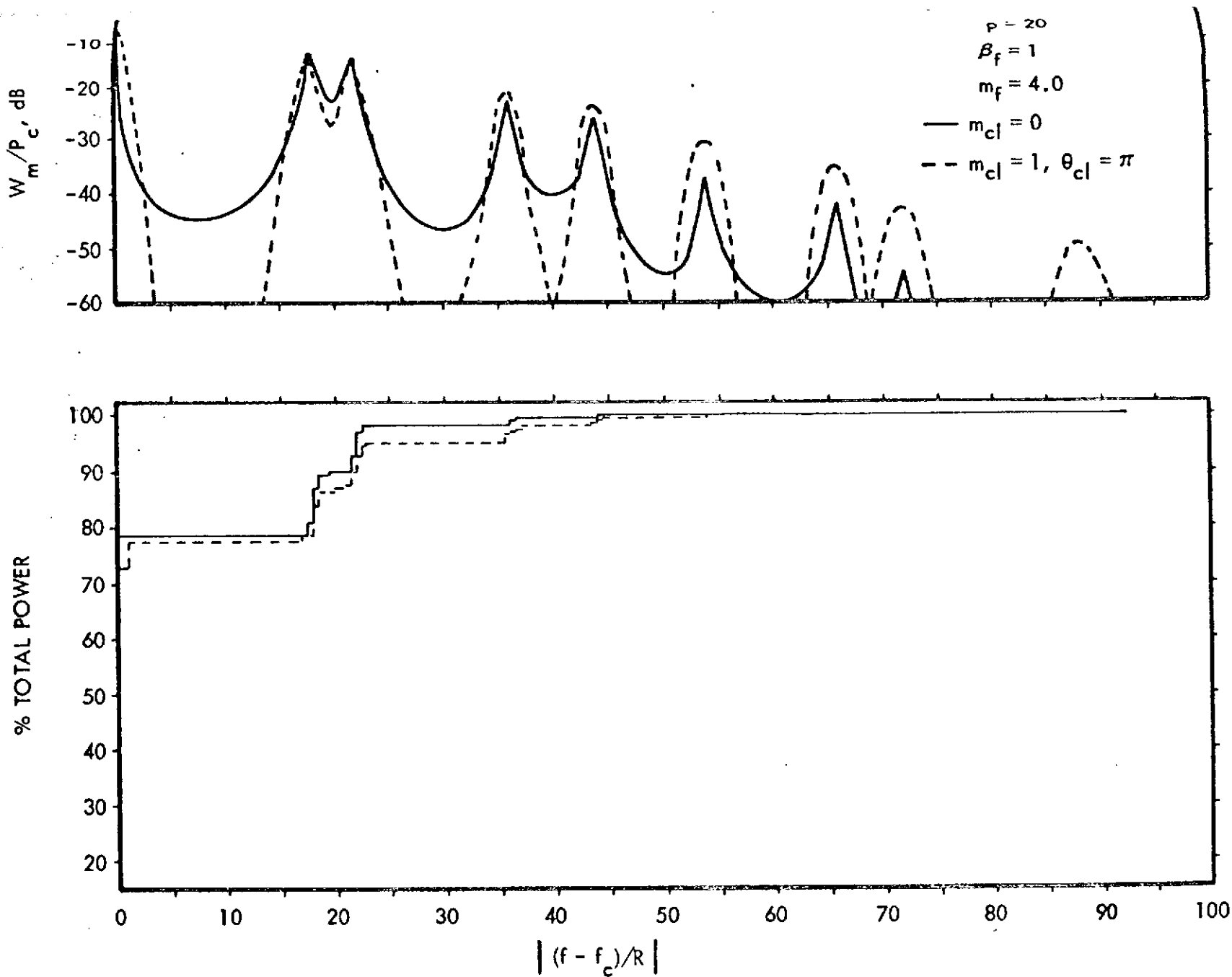


Figure 3.3.4-1. FSK-AM/FM Power Spectra, (a) Line Spectrum Envelope and (b) Cumulative Spectrum

2. Under the conditions imposed here, selection of the subcarrier phase to yield frequency shifts at a zero crossing of the subcarrier yields the most broad RF bandwidth; however, this effect is small.
3. The power at the RF carrier is a function of $\beta_f (1 + m_{cl})$, with small dependence upon the clock modulation index for $m_{cl} \leq 0.5$. In this range, the carrier power can be predicted quite accurately by assuming sinusoidal FM with modulation index β_f .
4. In general, peaks of the spectral envelopes occur at integer multiples of $f_{sc} \pm \Delta f$ (i.e., the mark and space frequencies). The values of the peak at mark and space are generally unequal because the actual deviation ratio varies from mark to space bits while the average value, $\beta_f (1 + m_{cl})$, remains fixed.

Figure 3.3.4-2 depicts values of the spectral envelope peaks which occur at $f_{sc} + \Delta f$ relative to the RF carrier, plotted for several values of β_f equal to or less than five. In anticipation of an ultimate choice of $m_{cl} = 0.5$ and $\theta_{cl} = \pi$ radians, the data in this figure correspond to these clock modulation parameter values. It should be emphasized that only the discrete data points in Figure 3.3.4-2 have meaning, and the broken lines connecting such points only serve to establish those points which are associated with a given value of β_f . Also, these data relate to values of half-bandwidth at RF since the data shown appear symmetrically about the RF carrier.

Based upon analysis of a number of cases (i.e., modulation parameter values) for which data have been computed, the envelope peak value data shown in Figure 3.3.4-2 for $p = 20$ and $m_f = 2$ are representative of all $p/m_f = 10$. Further, it appears that these data present an approximate upper bound for $p/m_f < 10$. A possible exception to the latter statement might exist when

$$m (p - m_f/2) = (m - n) (p + m_f/2) \quad ,$$

where m and n are integers. This condition corresponds to a harmonic of f_0 coinciding with a different harmonic of f_1 . Such a condition would normally have greatest significance for larger values of β_f (e.g., $\beta_f > 3$).

As before, an empirical expression of RF bandwidth has been determined to be

$$B_c = 2 (\beta_f + 1) (f_{sc} + \Delta f + R) \quad , \quad \beta_f \leq 5 \quad , \quad (3.3.4-1)$$

a bandwidth which would pass 94% or more of the total RF power.

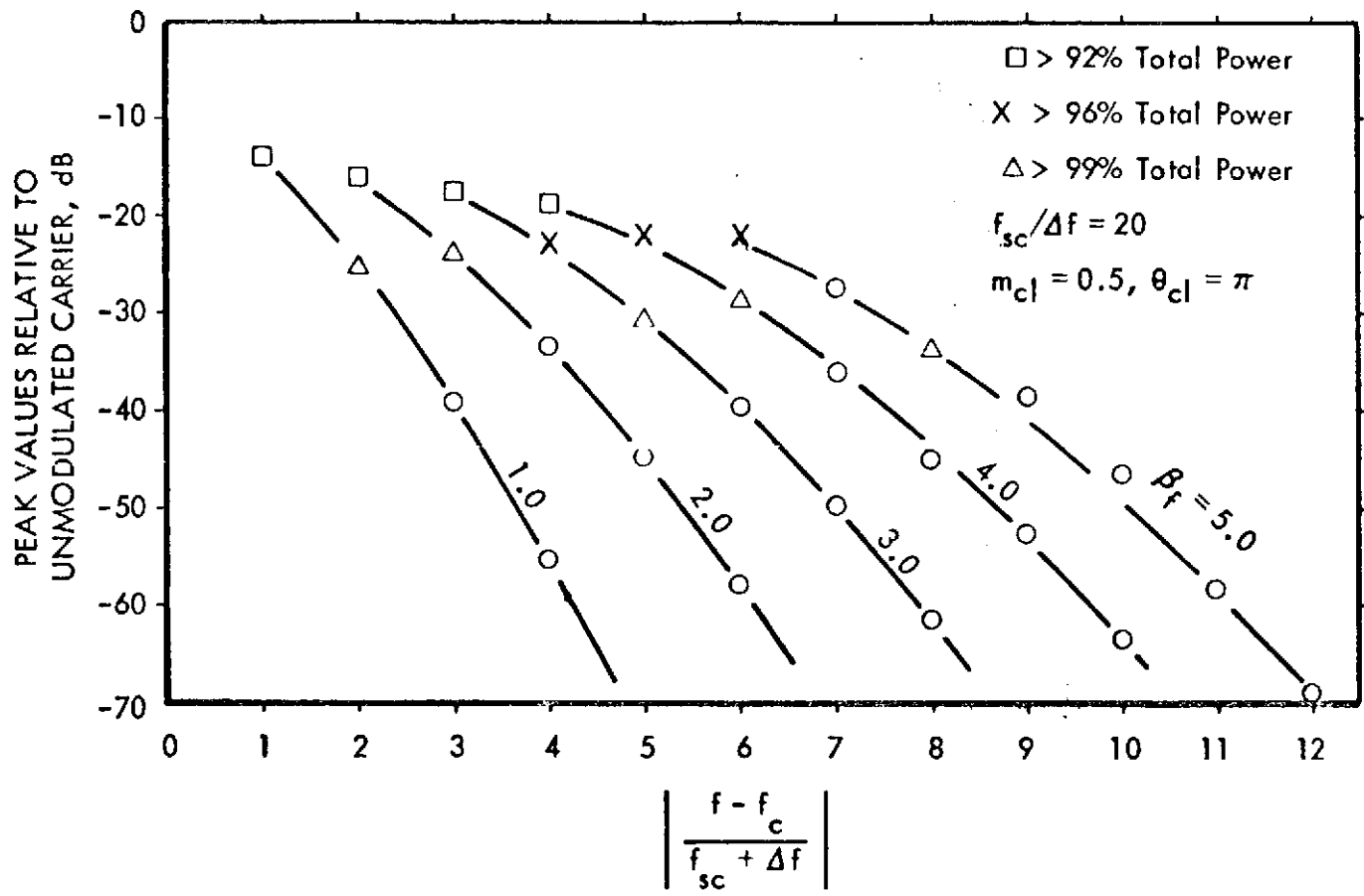


Figure 3.3.4-2. Peak Values of FSK-AM/FM Spectral Envelope

3.3.5 FSK-AM/PM Spectral Characteristics

Phase modulation of the RF carrier is considered here in a manner similar to that for the FSK-AM/FM carrier. Continuous phase requirements at subcarrier and RF are satisfied in this case by setting N_p equal an integer. Data have been computed which correspond to peak phase deviations of $\pi/2$ and smaller. Figure 3.3.5-1 shows spectral envelopes and associated cumulative spectra representative of the effects of an AM Clock as well as the more general characteristics of the FSK-AM/PM spectrum. The characteristics itemized 1 through 4 in Section 3.3.4 are applicable here also.

Figure 3.3.5-2 depicts values of the spectral envelope peaks for various values of β_p , providing RF bandwidth information in addition to showing the rate at which the spectrum rolls-off. Analysis of computed data indicates that the FSK-AM/PM spectral characteristics are generally independent of integer relationships between the mark and space frequencies and the bit rate. Further, the peak values shown in Figure 3.3.5-2 present approximate upper bounds for values of p and m_f of interest here.

In this case, the 95%, or greater, total power bandwidth is given as

$$B_c = 2(f_{sc} + \Delta f + R) \quad , \quad \beta_p < \pi/2 \quad . \quad (3.3.5-1)$$

Similar to the PSK-AM/PM case, an expression of bandwidth covering $\beta_p \geq \pi/2$ must include the effect of β_p as with FM.

3.4 Summary of Bandwidth Requirements

Expressions of power spectrum density have been developed here for PSK-AM and FSK-AM signal structures. Spectral densities and cumulative power spectra were computed and analysed to yield approximate relationships between defined signal bandwidths and the parameters which characterize the signal. When these composite subcarrier signals are employed to amplitude modulate an RF carrier, the RF bandwidths are readily determined by translation of the subcarrier spectra. Table 3.4 summarizes the bandwidth-parameter relationships for the various modulation techniques considered.

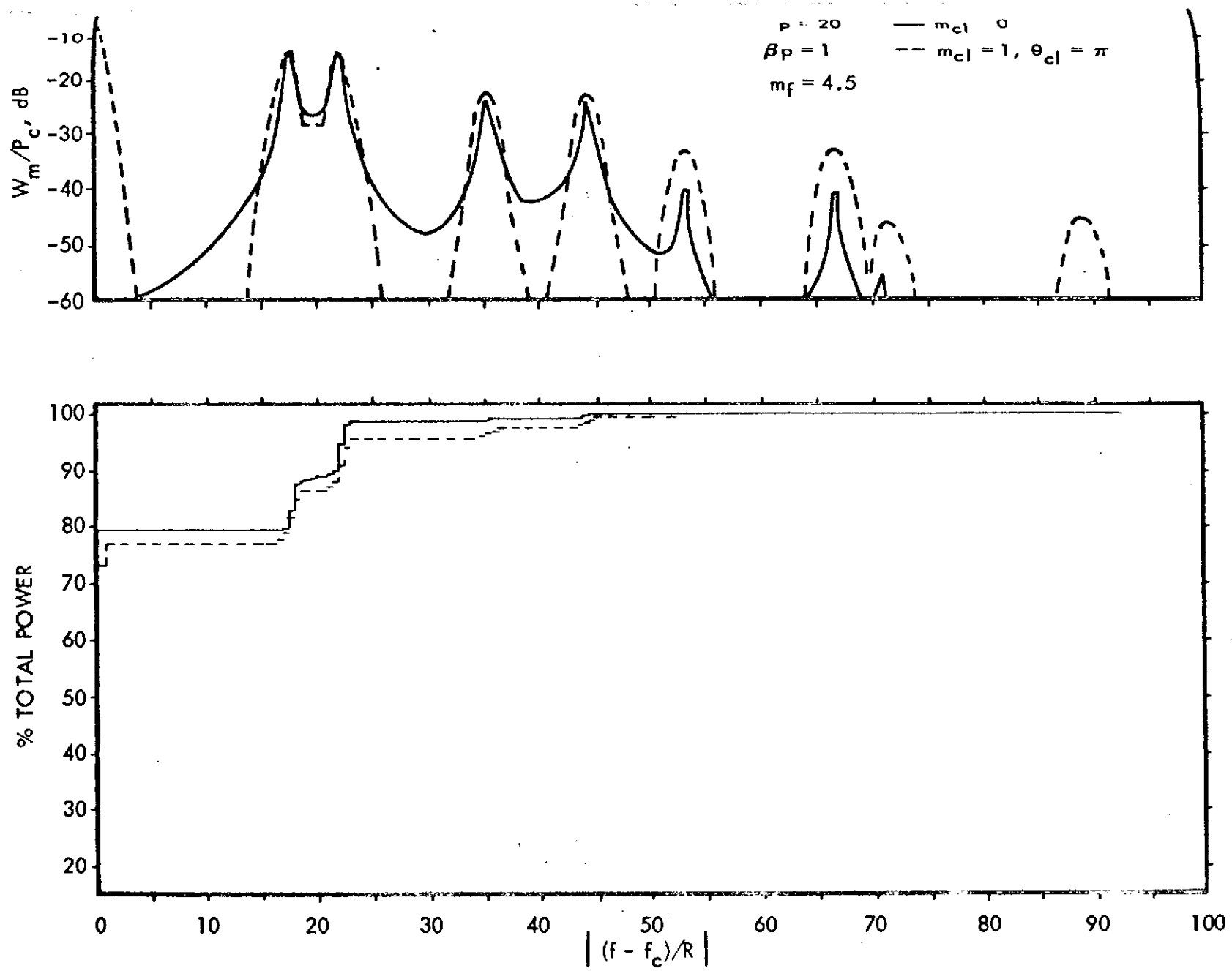


Figure 3.3.5-1. FSK-AM/PM Power Spectra, (a) Line Spectrum Envelope and (b) Cumulative Spectrum

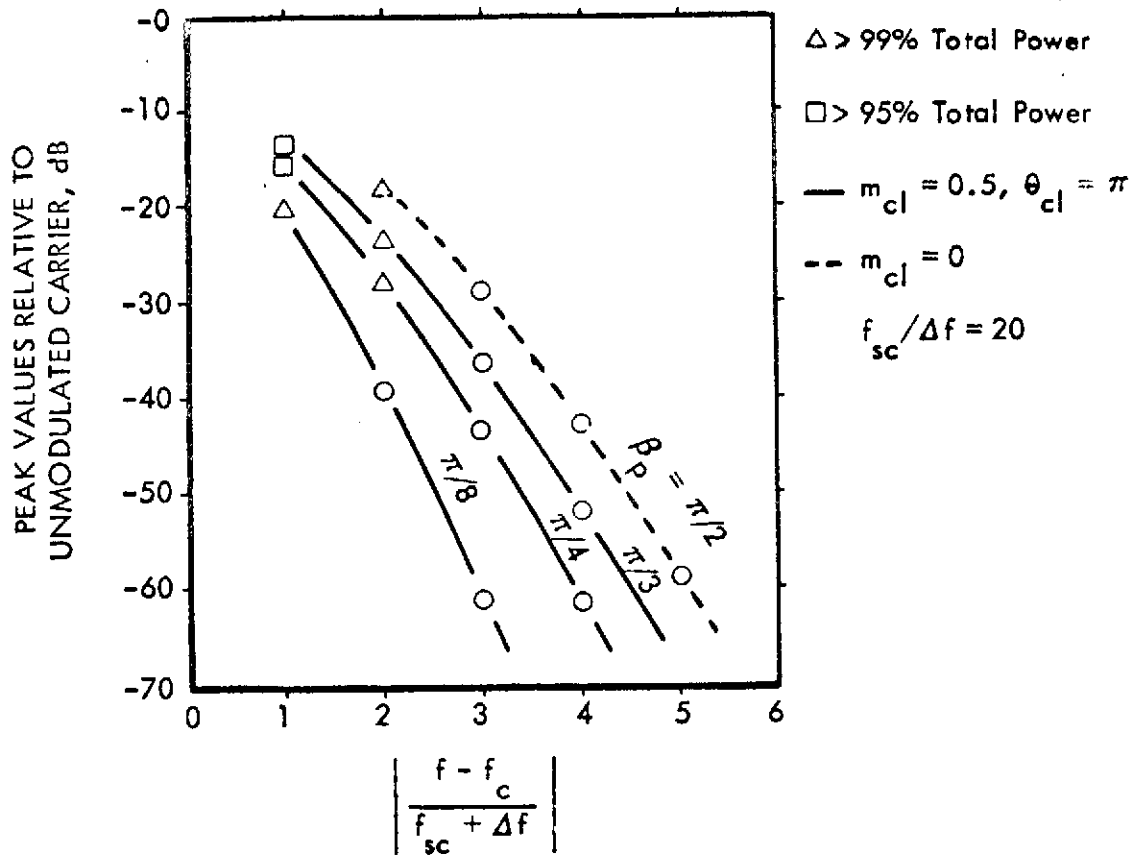


Figure 3.3.5-2. Peak Values of FSK-AM/PM Spectral Envelope

In the cases where the PSK-AM subcarrier is used to FM or PM the RF carrier, numerical methods have been employed to compute line spectra and cumulative power spectra. Analysis of these data culminated in sets of curves which depict the bandwidth in terms of relevant signal parameters. These curves also show the manner in which the RF spectrum rolls-off at frequencies removed from the carrier.

Although PSK signals with Summed Clock have not been considered directly, the subcarrier spectra results presented here, corresponding to a clock modulation index equal zero, can be applied to such signal structures. This is accomplished by simply adding an impulse of spectral density at the clock frequency to the PSK spectral density for $m_{cl} = 0$.

Table 3.4. Modulated Signal Bandwidths

Modulation			Bandwidth	% Total Power
Subcarrier/ Carrier	m_{cl}	θ_{cl}		
PSK-AM	0	—	2 R	≥ 89
			4 R	≥ 94
	.5	$\pm \pi/2$	2 R	≥ 86
			4 R	≥ 94
			8 R	≥ 96
	.5	π	2 R	≥ 98
FSK-AM	0	—	$2 (\Delta f + R)$	≥ 98
	.5	$\pm \pi/2$	$2 \Delta f + 3 R$	≥ 98
	.5	π	$2 (\Delta f + R)$	≥ 98
PSK-AM/AM	0	—	$2 (f_{sc} + 2 R)$	≥ 94
	.5	$\pm \pi/2$	$2 (f_{sc} + 2 R)$	≥ 94
	.5	π	$2 (f_{sc} + R)$	≥ 98
FSK-AM/AM	0	—	$2 (f_{sc} + \Delta f + R)$	≥ 98
	.5	$\pm \pi/2$	$2 f_{sc} + 2 \Delta f + 3 R$	≥ 98
	.5	π	$2 (f_{sc} + \Delta f + R)$	≥ 98
PSK-AM/FM	.5	π	$2 (\beta_f + 1) (f_{sc} + R), \beta_f \leq 5$	≥ 94
PSK-AM/PM	.5	π	$2 (f_{sc} + R), \beta_p < \pi/2$	≥ 95
FSK-AM/FM	.5	π	$2 (\beta_f + 1) (f_{sc} + \Delta f + R), \beta_f \leq 5$	≥ 94
FSK-AM/PM	.5	π	$2 (f_{sc} + \Delta f + R), \beta_p < \pi/2$	≥ 95

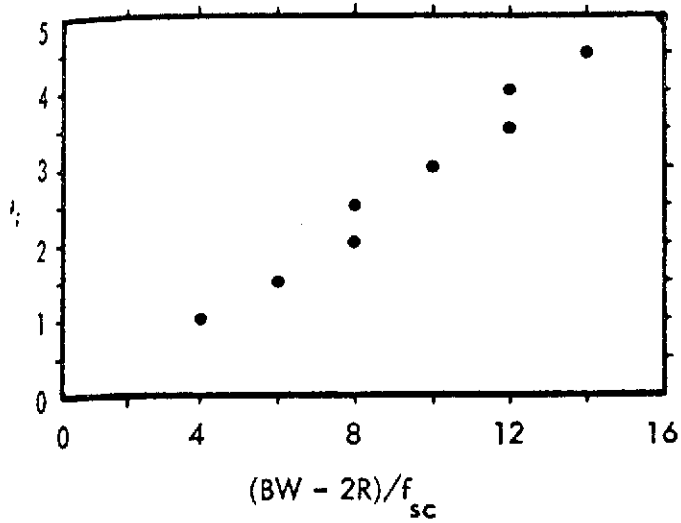
Similar to the cases involving a PSK-AM subcarrier, RF spectral data for an FM and PM carrier modulated by the composite FSK-AM subcarrier have been computed. The RF spectral information of interest is a function of many parameters, including FSK subcarrier, AM Clock and RF modulation parameters. Data are presented illustrative of the most significant effects of these parameters, corresponding to selected parameter values. Since the RF spectral analysis conducted here involves computation of discrete spectra, periodic subcarrier modulation is employed. The need to maintain continuous phase at subcarrier and RF between successive bits and periods of subcarrier modulation places some restrictions upon allowable modulation parameter values in computing the spectral data. However, during this investigation, no evidence was found to indicate that the general results obtained are critically dependent upon the imposed restrictions.

Data presented in conjunction with FM and PM RF modulation provide reasonably tight bounds on these RF spectral characteristics relevant to specification of bandwidth requirements and subsequent filter design. Expressions of RF bandwidth typically represent 94%, or greater, total RF power bandwidths when employed in conjunction with ideal filters. A complicating factor in relating RF bandwidth to subcarrier modulation parameters and the peak deviation at RF is the AM Clock. For example, the peak deviation defined by Equation 3.3-9 as

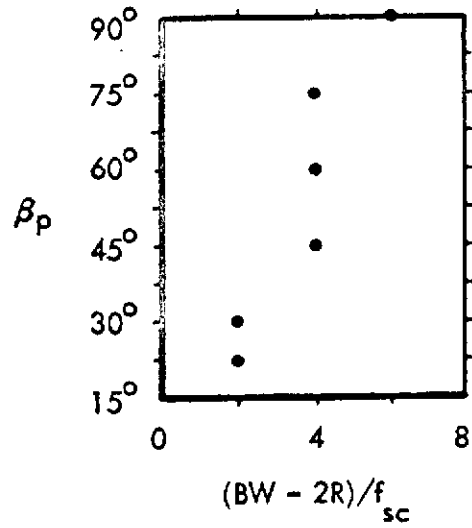
$$\begin{aligned} \Delta\omega_{pk} &= k \sqrt{2 P_{sc}} (1 + m_{cl}) \\ &= k' (1 + m_{cl}) \end{aligned}$$

in conjunction with subcarrier frequency, does not uniquely determine the RF bandwidth. That is, if we maintain the subcarrier frequency and Δf_{pk} fixed, and vary k' and m_{cl} within the fixed Δf_{pk} constraint, the RF bandwidth varies in a manner which is not easily related to k' and m_{cl} . Thus, the RF bandwidth expressions presented here are not as general as might be desired. Recently established international standards refer to a 99% total power bandwidth. From the data presented in Section 3.1, we determine that the ideal filter bandwidth which encompasses 99% of the total sideband power, plus carrier power, for PSK-AM/AM is given by $2(f_{sc} + R)$, with $m_{cl} = 0.5$ and $\theta_{cl} = \pi$ radians. Similarly, from Section 3.2, the bandwidth for FSK-AM/AM is given by $2(f_{sc} + \Delta f + R)$. Regarding FM and PM carriers, Figure 3.4 summarizes 99% total power bandwidths corresponding to PSK-AM and FSK-AM type modulating signals. These data are presented as a function of the appropriate RF modulation index. It should be noted that the data corresponding to FSK-AM/FM in Figure 3.4 were computer under conditions where harmonics of the mark (or space) frequency, relative to the carrier, do not coincide with or overlap different order harmonics of the space (or mark) frequency within the bandwidth of interest.

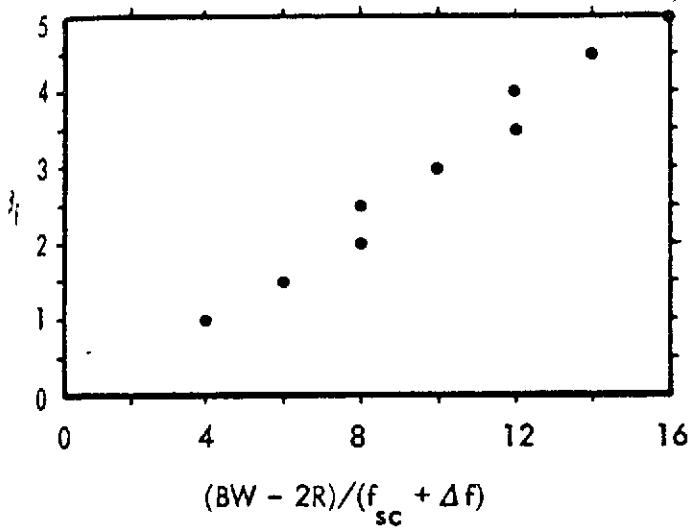
(a) PSK-AM/FM



(b) PSK-AM/PM



(c) FSK-AM/FM



(d) FSK-AM/PM

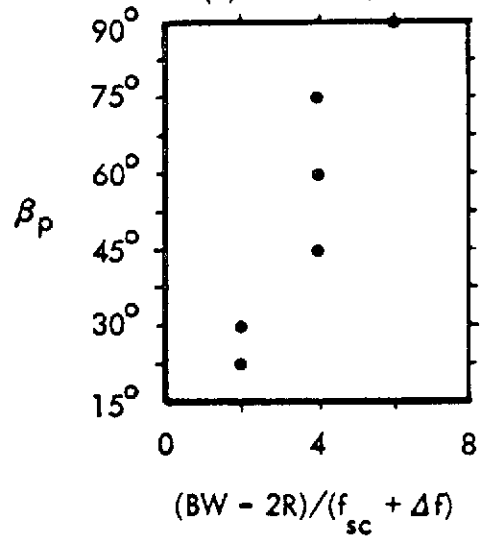


Figure 3.4. 99% Total Power RF Bandwidth, $m_{cl} = 0.5$ and $\theta_{cl} = \pi$

Data and results generated during this task effort have been employed here to provide a basis for specification of signal bandwidth. In the following section, these results will be employed to assist in the selection of subcarrier frequencies and to investigate effects of common RF channel interference.

3.5 References

- [3-1] VHF PCM/PSK Command System Standard Guidelines; Memorandum from R. J. Coates to Distribution, GSFC, Greenbelt, Maryland, October 6, 1971.
- [3-2] Aerospace Data System Standards, Part II, Section 3, PCM/FSK Command Data System Standard, GSFC, Greenbelt, Maryland, July 1, 1971.
- [3-3] Pelchat, M. G., "Power Spectrum of PAM/FM and PAM/PM", IEEE Transactions on Space Electronics and Telemetry, pp. 70, June 1965.
- [3-4] Bennett, W. R. and S. O. Rice, "Spectral Density and Autocorrelation Functions Associated with Binary Frequency-Shift Keying", BSTJ, pp. 2355, September 1963.
- [3-5] Gold, B. and C. M. Rader, Digital Processing of Signals, McGraw-Hill Book Co., New York, 1969.

4.0 SELECTION OF PSK SUBCARRIER FREQUENCY

Factors which enter into the selection of subcarrier frequencies for PCM/PSK which are pertinent to VHF PCM/PSK Command Systems are presented here. Consideration is given to bit rates, types of RF carrier modulation and associated carrier bandwidth requirements. In addition, the possible selection of subcarrier frequencies which reduce the risk of interference due to other systems sharing a common RF channel with the PCM/PSK command system is considered.

The spectra of the PCM/PSK command signals were determined and presented in the previous section. The dependence of RF bandwidth upon the PSK subcarrier modulation parameters for AM, FM, and PM carrier modulation was likewise determined. This information forms the basis for selection of PSK subcarrier frequencies from a spectral occupancy viewpoint.

A further consideration associated with selection of the subcarrier frequency which is included in this study task concerns interference in the subcarrier passband due to two systems sharing a common RF channel. The Tone-Digital, PCM/FSK and PCM/PSK Command Systems share the lower portion of the 7-15 kHz band, a situation which can give rise to interference between two such systems sharing a common RF channel. Recognizing the consequences of the presence of interference levels which are on the order of or larger than the desired signal level, we attempt here to show the first order effects upon receiver operation of interference whose level is lower than that of the desired signal. That is, under conditions of high desired-to-interference signal ratios where the AGC of an AM receiver is not dominated by interference, or where the interference does not capture an angle modulation receiver, we show the relationship between the interfering signal in the subcarrier passband, the subcarrier frequency and other RF modulation parameters. Under certain restrictive conditions, criteria are established which reduce the risk of interference.

Another factor to be considered in selection of the subcarrier frequency concerns achieving threshold in the first detector or RF demodulator of a command receiver. This matter is dealt with in Section 6 during consideration of uplink modulation. The results there indicate that the subcarrier frequency should be selected as small as feasible in order to obtain efficient operation.

4.1 Selection on the Basis of Spectral Occupancy

The ratio of subcarrier frequency-to-bit rate, p , is specified by the PCM/PSK Command System guidelines as an integer number, $6 \leq p \leq 512$. This wide range of values encompass both wideband and narrowband signal structures, with narrowband signal characteristics restricted to approximately $p > 20$.

Table 3.4 shows that the subcarrier bandwidth requirements for PCM/PSK-AM is given as two to four times the bit rate, depending upon the clock modulation index and phase. The presence of the AM Clock does not expand the subcarrier bandwidth requirement, but tends to cause a decrease when the optimum clock phase is employed. The subcarrier bandwidth translates linearity in the case of an amplitude modulated RF carrier, but in a nonlinear manner when the RF carrier is frequency or phase modulated. From a spectral occupancy viewpoint, one would generally want to select a value p as small as possible. In the following paragraphs, each of the three types of RF modulation and the associated bandwidth requirements as a function of subcarrier frequency are discussed.

4.1.1 Relationship of RF Bandwidth to Subcarrier Frequency

Concerning amplitude modulation of the RF carrier by the composite PSK-AM subcarrier, Table 3.4 shows that the bandwidth which encompasses 98% of the total PSK-AM/AM RF power is given by

$$B_c = 2 (f_{sc} + R)$$

Since $p \geq 6$, the influence of the bit rate upon the required bandwidth is typically small. Thus, for $p \gg 1$, we note that the bandwidth varies directly as the subcarrier frequency.

As in the case of an AM carrier, it is desirable to relate the FM spectral occupancy to the subcarrier frequency and bit rate, and in addition, to the FM deviation ratio. It has been noted previously that the presence of the AM Clock tends to complicate development of a bandwidth relationship which provides the accuracy of Carson's Rule as applied to sinusoidal angle modulation. However, Equation 3.3.2-1 provides an expression of bandwidth which passes 94% or more of the total RF power when applied to an ideal filter. From this expression, we again note that the bandwidth increases directly as the subcarrier frequency for $p \gg 1$.

The dependence of the PM RF bandwidth upon bit rate and subcarrier frequency for peak phase deviations less than $\pi/2$ radians is given by Equation 3.3.3-1. The bandwidth defined there encompasses at least 95% of the total RF power when applied to an ideal filter. As expected, for small values of βp , the bandwidth here is approximately equal to that for an AM carrier.

In each case of RF modulation considered, it is seen that the required bandwidth increases with increasing values of the subcarrier frequency. Bandwidth dependence upon bit rate is approximately 15% of the total when p takes on its lower value, and this dependence decreases as the value of p increases. Thus, it is the subcarrier frequency which primarily determines the RF bandwidth. Since the RF bandwidth is approximately an even integer multiple of the subcarrier frequency, the value of the subcarrier frequency can have a significant affect upon the resulting RF bandwidth. It is therefore desirable from this viewpoint to maintain the subcarrier frequency small.

4.2 Selection on the Basis of Interference

In addition to the foregoing considerations, other factors which enter into selection of the PSK subcarrier frequency include interference effects. Regarding general consideration of the effect of interference upon system operation, it should be emphasized that this problem is best handled via simulation or experimentation. This is due to the fact that the desired results are dependent upon the signal structures of interest; and in angle modulation systems, inherent nonlinearities make analytical solutions difficult. Related to the latter point we recognized the work of Davenport [4-1] and Jones [4-2], for example, who studied the problems of hard limiting one sinusoid plus Gaussian noise and two sinusoids plus Gaussian noise, respectively. Jones presents results of signal suppression, as a function of signal-to-signal ratio and signal-to-noise ratio, which show that the weaker signal can be suppressed by as much as 6 dB under high signal-to-noise conditions (i.e., > 10 dB). Little treatment is given in the literature on the effects of modulated signals. Tyree and Bailey [4-3] have investigated the bit error rate of multiple PSK signals through a hard limiter via computer simulation.

Concerning the possible selection of subcarrier frequencies to reduce the risk of interference due to two command systems sharing a common RF channel, we adopt an analytical approach similar to that typically followed in first order demodulator performance analyses [4-4]. We do not attempt to deal with the problems of signal suppression and intermodulation noise effects. Further, recognizing the consequences of small desired-to-interfering signal ratio, we restrict attention here to conditions of small interference levels. We initially assume the presence of desired and interfering RF carriers at near equal frequencies such that both carriers are within the receiver's predetection passband. In this case, the output of an amplitude or angle modulation detector will exhibit the difference frequency of the RF carriers. The interfering spectrum can be representative of subcarrier and/or carrier spectra. It can be seen from the development here that the difference frequency serves to translate the interference spectrum in all types of modulation considered, in addition to producing other deleterious effects. A situation of particular interest here concerns the existence of a

difference frequency resulting from the Doppler effect. At VHF frequencies, the range of difference frequencies due to Doppler is of the order of the subcarrier frequency and less. In addition, this source causes the difference frequency to be time varying, making it difficult to select the subcarrier frequency such that effects of interference due to two system sharing a common RF channel are avoided. Attempts to determine the effects of such interfering signals upon system performance are further complicated by frequency foldover when the difference frequency is smaller than the average frequency of the interference spectrum which it translates.

Although restrictive in practice, the considerations of interference due to two systems sharing a common RF channel are presented for the case where the difference frequency is zero. Such an approach indicates the nature of the interference and leads to criteria which allows the risk of interference to be reduced in several special circumstances. Desired signal-interfering signal combinations due to the various RF modulation techniques of interest are considered. If we imagine in this development that the phase θ_c is replaced by

$$\omega_d t + \theta_c ,$$

where ω_d represents the difference frequency, the role of the difference frequency becomes apparent. In each case, we denote the RF carrier modulation for the desired and interfering signals as $x(t)$ and $y(t)$, respectively. Associated with the two signals are the subcarrier frequencies f_x and f_y , bandwidths B_x and B_y , RF carrier amplitude modulation indices m_x and m_y , RF carrier angle modulation indices β_x and β_y , and RF carrier power P_x and P_y . Due to the existence of various subcarrier and carrier modulation parameters, and different possible types of subcarrier modulation, it is impractical to consider each possible combination independently. In some cases it is sufficient to assume general bandwidth characteristics, and in other cases it is sufficient to assume RF carrier modulation by a sinusoidal modulating signal.

4.2.1 AM Receiver - AM Interference

The composite signal at the receiver frontend resulting from an AM desired and interfering signal can be expressed as

$$C(t) = \sqrt{2 P_x} [1 + x(t)] \cos(\omega_c t) + \sqrt{2 P_y} [1 + y(t)] \cos(\omega_c t + \theta_c) , \quad (4.2.1-1)$$

where f_c is the received RF carrier frequency, the carriers being amplitude modulated by $x(t)$ and $y(t)$. With the input $C(t)$, the output of an envelope detector is given by

$$R(t) = \left\{ \left[\sqrt{2 P_x} x(t) \right]^2 + 2 \left[\sqrt{2 P_x} x(t) \right] \left[\sqrt{2 P_y} y(t) \cos(\theta_c) \right] + \left[\sqrt{2 P_y} y(t) \right]^2 \right\}^{1/2} \quad (4.2.1-2)$$

If the undesired carrier level is approximately equal to or greater than the desired carrier level, the response of the receiver's AGC will be significantly affected or even dominated by the interference. Thus, we only consider here the case where

$$R(t) \approx \sqrt{2 P_x} x(t) + \sqrt{2 P_y} y(t) \cos(\theta_c) \quad ,$$

$$m_x \sqrt{2 P_x} \gg m_y \sqrt{2 P_y} \quad (4.2.1-3)$$

yielding the desired signal plus interference. To avoid overlap of the two spectra,

$$\left| f_x - f_y \right| > \frac{1}{2} (B_x + B_y) \quad . \quad (4.2.1-4)$$

In practice, a guard band would be included in addition to the above requirement.

Both PSK and FSK subcarrier spectra were determined in Section 3.0 where bandwidth as a function of bit rate was presented, thus providing information for use in Equation 4.2.1-4 for situations involving interference related to either PSK or FSK subcarrier.

In the case where the interfering signal represents a Tone Command [4-5], it suffices to select f_x greater than the highest tone frequency by an amount $B_x/2$ plus a small guard band which includes half the bandwidth occupied by keying the highest frequency tone. In this case, let f_y represent the highest tone frequency, then Equation 4.2.1-4 would apply by letting B_y be approximately four times the inverse of the tone duration. For a 0.5 second tone duration, $B_y \sim 8$ hertz.

Finally, if the interfering signal represents a Tone Digital [4-6] Command, this subcarrier bandwidth can be bounded by a value approximately four times the inverse of the shortest tone duration (i.e., corresponding to a zero having an $18/f_y$ second duration). Equation 4.2.1-4 again applies by letting $B_y \approx 4f_y/18$, yielding

$$f_x > \frac{10}{9} f_y + B_x/2 \quad . \quad (4.2.1-5)$$

4.2.2 AM Receiver - Angle Modulated Interference

In this case, the desired command is received by way of an AM RF carrier, and the interfering signal is on an angle modulated carrier. Here, the composite signal is given by

$$C(t) = \sqrt{2 P_x} \left[1 + x(t) \right] \cos (\omega_c t) + \sqrt{2 P_y} \cos \left[\omega_c t + y(t) + \theta_c \right], \quad (4.2.2-1)$$

and the output of the AM detector becomes

$$R(t) \approx \sqrt{2 P_x} x(t) + \sqrt{2 P_y} \cos \left[y(t) + \theta_c \right],$$

$$m_x \sqrt{2 P_x} \gg \sqrt{2 P_y} \quad (4.2.2-2)$$

The first term on the right in Equation 4.2.2-2 represents the desired modulated subcarrier with its spectrum centered at f_x . The second term represents interference due to the presence of the angle modulated RF carrier. Assuming that the interfering RF carrier is modulated by a periodic signal of fundamental frequency f_r , the Fourier series representation of this modulated carrier is given by

$$\cos \left[\omega_c t + y(t) + \theta_c \right] = \sum_{n=-\infty}^{\infty} |F_n| \cos \left[(\omega_c + n\omega_r) t + \theta_n + \theta_c \right], \quad (4.2.2-3)$$

with complex Fourier coefficients

$$F_n = f_r \int_0^{1/f_r} \exp \left[i y(t) \right] \exp (-jn\omega_r t) dt. \quad (4.2.2-4)$$

Under the assumed conditions, the Fourier series representation of the interference term in Equation 4.2.2-2 is

$$\cos \left[y(t) + \theta_c \right] = \sum_{n=-\infty}^{\infty} |F_n| \cos (n\omega_r t + \theta_n + \theta_c) \quad (4.2.2-5)$$

This is equivalent to translation of the RF line spectrum which is centered at f_c down to dc, according to Equation 4.2.2-5.

If we neglect the subcarrier modulation for the present, $y(t)$ represents sinusoidal modulation of the RF carrier and the discrete spectrum of Equation 4.2.2-4 consists of lines at integer multiples of the subcarrier frequency, f_y . The magnitudes of these spectral lines are governed by the Bessel functions $J_n(\beta_y)$, where β_y is the appropriate angle modulation index. In order to place the desired subcarrier spectrum above that of the interference, f_x must be at least twice f_y even for small β_y . This requirement would be difficult to realize if the interference represents either PSK or FSK subcarrier modulation occupying the lower portion of the 7-15 kHz band.

Alternatively, we can consider a selection of f_x which tends to minimize the interference in cases where the interfering subcarrier signal is narrow-band. An example is that of a PCM/PSK-AM subcarrier angle modulating the RF carrier, where the ratio of subcarrier frequency-to-bit rate $p = f_y/R \approx 20$ or greater. With reference to Figure 3.3.2-2 and 3.3.3-1, we note that "holes" exist approximately midway between interger multiples of f_y relative to the carrier. The width and depth of these holes increase with increasing values of p . As discussed above, the spectrum of the assumed interference has this property; thus, a desired PCM/PSK-AM subcarrier can be placed at the location of a hole. That is, selecting $f_x \approx f_y/2$ or $3 f_y/2$ tends to minimize interference effects. In addition to the ratio P_y/P_x , the interference level is a function of each data rate, data clock modulation index and phase (if applicable), and the modulation index of the interfering carrier.

Although a very restrictive case, it is recognized that the above described method for selecting subcarrier frequencies is not particularly well suited in the case where the desired signal is representative of a PCM/PSK-Summed command. It is desirable to place the Summed Clock spectral line in a hole of the PCM/PSK-AM interference spectrum, in addition to the desired subcarrier.

4.2.3 Angle Modulation Receiver - AM Interference

The composite signal which consists of the desired command on an angle modulated RF carrier with an interfering command on an AM carrier can be expressed by

$$C(t) = \sqrt{2 P_x} \cos \left[\omega_c t + x(t) \right] + \sqrt{2 P_y} \left[1 + y(t) \right] \cos (\omega_c t + \theta_c) . \quad (4.2.3-1)$$

Assuming ideal limiter action, the output of the angle modulation detector for the cases of PM and FM follows.

PM

In this case, the instantaneous phase deviation from the carrier is obtained from Equation 4.2.3-1 to yield the PM detector output

$$\theta(t) = \tan^{-1} \left\{ \frac{\sin [x(t) + \sqrt{P_y/P_x} [1 + y(t)] \sin (\theta_c)]}{\cos [x(t) + \sqrt{P_y/P_x} [1 + y(t)] \cos (\theta_c)]} \right\}$$

(4.2.3-2)

Rewriting the above in the form of desired signal plus interference gives

$$\theta(t) = x(t) - \tan^{-1} \left\{ \frac{[1 + y(t)] \sin [x(t) - \theta_c]}{\sqrt{P_x/P_y} + [1 + y(t)] \cos [x(t) - \theta_c]} \right\}$$

(4.2.3-3)

Next, assuming a high desired signal-to-interference ratio, the detector output can be written as

$$\theta(t) \approx x(t) - \sqrt{P_y/P_x} \left\{ \sin [x(t) - \theta_c] + y(t) \sin [x(t) - \theta_c] \right\}, \quad \sqrt{P_x/P_y} \gg (1 + m_y)$$

(4.2.3-4)

In the above expression $x(t)$ represents the desired, modulated subcarrier (i.e., PCM/PSK), with its spectrum centered at f_x . The remaining terms represent interference. We only need to consider the second term on the right in Equation 4.2.3-4 to see that no choice of subcarrier frequencies exists which allows the desired subcarrier to be placed out-of-band of the interference. The interference in question has spectral characteristics of the desired RF spectrum (see Figure 3.3.3-1) clustered about $f_c \pm f_x$ and translated into the desired subcarrier passband via the second term in Equation 4.2.3-4. The interference power is dependent upon P_y/P_x in addition to β_x , the peak phase deviation in this case. We note here that a value of β_x exists which tends to reduce the effect of this interfering component. For example, if we consider $x(t)$ to represent an unmodulated subcarrier, selecting $\beta_x \approx 4$ yields $J_1(4) \approx 0$, thus reducing the interference at f_x , and in B_x , to approximately zero.

The last term in Equation 4.2.3-4 represents additional interference at frequencies resulting from the convolution of the spectrum of $y(t)$ with that of the desired spectrum translated to dc. If $x(t)$ and $y(t)$ represent unmodulated subcarriers, the resulting convolved spectra will have spectral lines at

$$\left| n f_x \pm f_y \right|, \quad n = 0, 1, 2, \dots \quad (4.2.3-5)$$

Figure 4.2.3 illustrates the spectrum resulting from convolution of the two spectra. To reduce interference in the subcarrier band B_x , centered at f_x , it is required to maximize the difference frequency,

$$\left| f_x - \left| n f_x \pm f_y \right| \right|, \quad n = 0, 1, 2, \dots \quad (4.2.3-6)$$

We are only interested in the values of n which yields the components adjacent to f_x .

In summary, the foregoing analysis shows the presence of interference at the desired subcarrier in addition to that at frequencies given by Equation 4.2.3-5. Such is the case for interfering signals representative of Tone, Tone Digital, PCM/PSK and PCM/FSK Commands transmitted on an AM RF carrier.

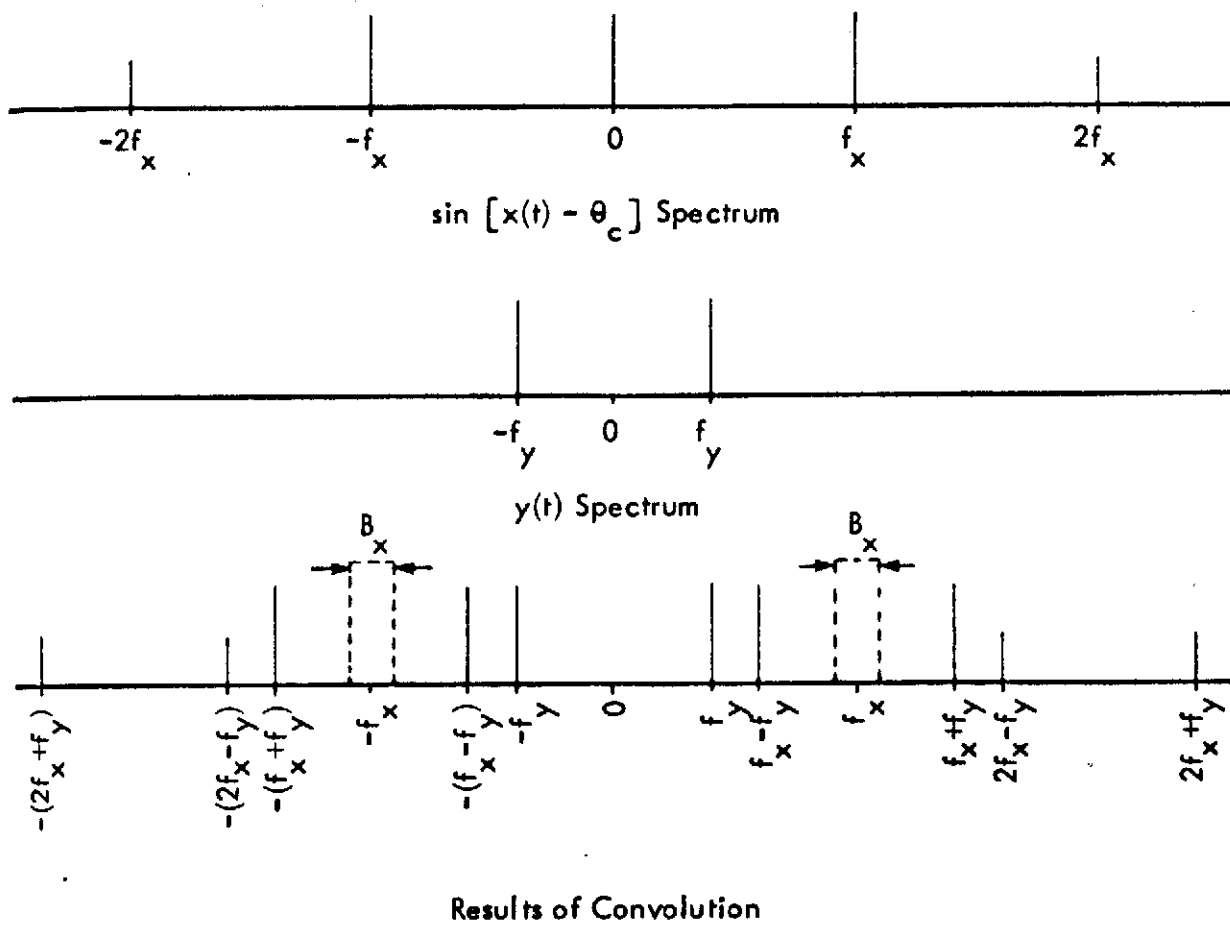


Figure 4.2.3. Sketch of Line Spectrum Corresponding to Convolution of Spectra for $\sin [x(t) - \theta_c]$ and $y(t)$

FM

The output of an FM detector is given by the first time derivative of Equation 4.2.3-4, with $\dot{x}(t)$ representing the desired, modulated (PCM/PSK) subcarrier. We have

$$\begin{aligned} \dot{\theta}(t) \approx & \dot{x}(t) - \sqrt{P_y/P_x} \dot{x}(t) \cos \left[x(t) - \theta_c \right] \\ & - \sqrt{P_y/P_x} \left\{ y(t) \dot{x}(t) \cos \left[x(t) - \theta_c \right] \right. \\ & \left. + \dot{y}(t) \sin \left[x(t) - \theta_c \right] \right\}, \quad \sqrt{P_x/P_y} \gg (1 + m_y). \end{aligned} \quad (4.2.3-7)$$

The desired signal out of the detector is represented by the first term on the right side of the above expression. The remaining three terms represent interference. The second term in this expression yields interference which is again distributed about f_x and integer multiples of f_x as a result of the indicated convolution of the desired subcarrier spectrum, $\dot{x}(t)$, and the translated RF spectrum associated with $x(t)$. Again, as in the PM case, the effect of this term can be minimized by an appropriate choice of the frequency modulation index.

The interference contributed by the last two terms in Equation 4.2.3-7 is similar to that of the last term in Equation 4.2.3-4 which corresponds to the PM case. Again there exists interference distributed in clusters about frequencies specified by Equation 4.2.3-5, and the interference in the band B_x can be reduced by maximizing the difference frequency of Equation 4.2.3-6. The major difference in this case and that pertaining to PM is due to the different bandwidths of the individual signals under convolution. The effectiveness of maximizing the difference frequencies is of course dependent upon carrier and subcarrier modulation parameters as well as the type of subcarrier modulation in each case.

4.2.4 Angle Modulation Receiver - Angle Modulated Interference

The final combination of desired and interfering signal involves both signals on angle modulated RF carriers sharing a common RF channel. Here, the composite signal at the frontend of the receiver is given as

$$C(t) = \sqrt{2 P_x} \cos \left[\omega_c t + x(t) \right] + \sqrt{2 P_y} \cos \left[\omega_c t + y(t) + \theta_c \right] .$$

(4.2.4-1)

As before, assuming use of an ideal limiter, the output of a PM or an FM detector consists of desired signal plus interference.

PM

The output of the PM detector is

$$\theta(t) = x(t) - \tan^{-1} \left\{ \frac{\sin \left[x(t) - y(t) - \theta_c \right]}{\sqrt{P_x/P_y} + \cos \left[x(t) - y(t) - \theta_c \right]} \right\} \quad (4.2.4-2)$$

With the assumption of high desired-to-interfering signal ratio,

$$\theta(t) \approx x(t) - \sqrt{P_y/P_x} \left\{ \sin \left[x(t) \right] \cos \left[y(t) + \theta_c \right] - \cos \left[x(t) \right] \sin \left[y(t) + \theta_c \right] \right\} , \quad \sqrt{P_x/P_y} \gg 1 .$$

(4.2.4-3)

Both interference terms above have spectra resulting from the convolution of RF spectra translated to dc. The interference therefore tends to cluster about the sum and difference frequencies

$$\left| n f_x \pm m f_y \right|, \quad n = 0, 1, 2, \dots; \quad m = 0, 1, 2, \dots \quad (4.2.4-4)$$

We note that there exists no choice of subcarrier frequencies, f_x and f_y , in this case which avoids interference in the subcarrier band B_x . In addition to the ratio P_y/P_x , the interference level is a function of each RF carrier angle modulation index as well as the desired and interfering data rates.

FM

The output of an FM detector is obtained by taking the first time derivative of Equation 4.2.4-3, where $\dot{x}(t)$ now represents the desired subcarrier signal.

$$\begin{aligned} \dot{\theta}(t) \approx & \dot{x}(t) + \sqrt{P_y/P_x} \left\{ \dot{y}(t) \sin [x(t)] \sin [y(t) + \theta_c] \right. \\ & + \dot{y}(t) \cos [x(t)] \cos [y(t) + \theta_c] \\ & - \dot{x}(t) \cos [x(t)] \cos [y(t) + \theta_c] \\ & \left. - \dot{x}(t) \sin [x(t)] \sin [y(t) + \theta_c] \right\}, \quad \sqrt{P_x/P_y} \gg 1 \end{aligned} \quad (4.2.4-5)$$

Again, the interference tends to cluster about the sum and difference frequencies given by Equation 4.2.4-4, and potentially each interference term in Equation 4.2.4-5 contributes interference in the band B_x . Certain choices of the RF modulation

indices for the desired and interfering signals in conjunction with maximization of $|f_x - f_y|$ lead to a reduction in the risk of interference under the conditions assumed here. Concerning the first two interference terms in Equation 4.2.4-5, the value of β_x can be selected to suppress the RF power in the vicinity of $f_c \pm f_x$, and reduce the effects of these terms in the subcarrier passband, B_x . Similarly, interference represented by the last two terms in Equation 4.2.4-5 can be reduced by selecting β_y to suppress the power in the vicinity of the carrier in the interfering RF spectrum.

In order to apply the approach here for reduction of the risk of interference in the presence of a nonzero difference frequency, conditions must exist which limits the difference frequency to a value much less than $|f_x - f_y|$.

4.3 Summary of Factors in Selection of PSK Subcarrier Frequency

Considerations pertaining to selection of the PSK subcarrier frequencies on the basis of spectral occupancy have been discussed. Approximate empirical formulas are presented which show the dependence of required bandwidth upon subcarrier frequency, bit rate and RF modulation index. These bandwidth requirements show that the RF bandwidth increases with subcarrier frequency. Therefore, from a spectral occupancy viewpoint, it is desirable to make the PSK-AM subcarrier frequency small. It should be noted that a 98% total power bandwidth, for example, does not necessarily guarantee any specific system bit error performance, but it is an indicator of such. In Section 5, which is concerned with determination of a performance margin criterion, additional consideration of the effect of bandlimiting is presented. In addition to the desire to minimize the subcarrier frequency from a spectral occupancy point of view, the results of Section 6 indicate that detector threshold requirements also support selection of the subcarrier frequency as small as practical.

Possible selection of the PSK subcarrier which results in reducing the risk of interference due to two command systems sharing a common RF channel has been investigated, with consideration given to the various combinations of AM, FM and PM carrier modulation. It is shown in this first order analysis that the interfering spectrum in or near the desired PSK subcarrier passband is representative of subcarrier and/or carrier spectra of the desired and/or interfering signals. Furthermore, it is seen that the difference frequency between the desired and interfering RF carriers serves to translate the interfering spectrum; and when this difference frequency is the result of Doppler, the frequency band location of the interference varies with time, in general. The Doppler difference can be in the range of zero to a value on the order of the subcarrier frequency. Under conditions of near-zero difference frequency, an AM receiver with AM interference yields more readily to efforts to reduce interference through a judicious choice of subcarrier frequency. If the interference represents an angle modulated carrier,

the interfering spectrum is broad and leaves little latitude for reduction of interference via subcarrier frequency selection. With an angle modulation receiver, no subcarrier frequency choice exists which avoids the presence of interference in the desired subcarrier passband. In the latter case, the interference power in the desired subcarrier passband can be reduced somewhat through selection of RF modulation indices.

Although little promise exists for significantly reducing interference in an angle modulation receiver through selection of subcarrier frequency, it should be noted that a demodulator exhibiting the capture effect can operate at a relatively low signal-to-interference ratio provided the signal-to-noise ratio is high. It cannot be expected that an AM receiver will do as well.

4.4 References

- [4-1] Davenport, W. B., Jr., "Signal-to-Noise Ratios in Bandpass Limiters", Journal of Applied Physics, Vol. 24, June 1953, pp. 720-727.
- [4-2] Jones, J. J., "Hard Limiting of Two Signals in Random Noise", IEEE Trans. on Information Theory, Vol. IT-9, January 1963, pp. 34-42.
- [4-3] Tyree, B. E. and J. F. Bailey, "An Investigation of the Effects of the Error Rate of Multiple Phase-Shift-Keyed Signals Through a Hard Limiter", IEEE Trans. on Communications, Vol. Com-20, No. 3, June 1972, pp. 361-372.
- [4-4] Panter, P. F., Modulation, Noise and Spectral Analysis, McGraw-Hill Book Co., New York, New York, 1965, Chaps. 6 and 7.
- [4-5] Aerospace Data Systems Standards, Tone Command Standard, prepared by GSFC Data Systems Requirements Committee, GSFC, Greenbelt, Maryland, August 1966.
- [4-6] Aerospace Data Systems Standards, Tone Digital Command Standard, prepared by GSFC Data Systems Requirements Committee, GSFC, Greenbelt, Maryland, July 1971.

5.0 ERROR RATES

In this section, analyses pertinent to the determination of error rates are presented along with resulting theoretical data. Attention is restricted to PSK subcarrier demodulation and a basic squelch strategy as it affects false alarm and detection probabilities. The effects of clock and subcarrier reference signal quality upon bit error rate are determined as a function of signal-to-noise ratio. In addition, consideration is given to error detection and correction coding and comparative data are presented for various coding schemes.

5.1 PSK Demodulation Structures

Basic subcarrier PSK (NRZ-L) demodulation configurations are presented and discussed in the following paragraphs for two cases of primary interest. The two cases include subcarrier signal structures where (1) the clock is amplitude modulated on the PSK subcarrier (PSK-AM), and (2) the clock is added to the PSK subcarrier (PSK-Summed).

5.1.1 Amplitude Modulated Clock

The PSK receiver for this case is shown in Figure 5.1.1-1. As discussed in Section 2, this receiver is suboptimum but it is easier to implement than the optimum receiver, and it will be shown that its performance is only 0.5 dB inferior to that of the optimum receiver for a clock AM modulation index of 0.5. The receiver includes a subcarrier tracking loop, envelope detection of the clock, a basic squelch circuit, and the suboptimum PSK detector configuration. The filters shown in this figure are assumed to be ideal rectangular filters with the exception of the filter in the squelch, it being a simple RC low pass filter. The choice of a real filter in the latter case is made because it is desirable to know the step response of this filter, on which the squelch operation is based. The input to the subcarrier demodulator is assumed to be the demodulated RF carrier signal plus white Gaussian noise with two-sided spectral density $N_0/2$.

$$\begin{aligned} y(t) &= e_{sc}(t) + n_{sc}(t) \\ &= A_{sc} \left[1 + m_{cl} \cos(\omega_{cl}t + \theta_{cl}) \right] x(t) \cos(\omega_{sc}t + \theta_{sc}) + n_{sc}(t) \end{aligned} \quad (5.1.1-1)$$

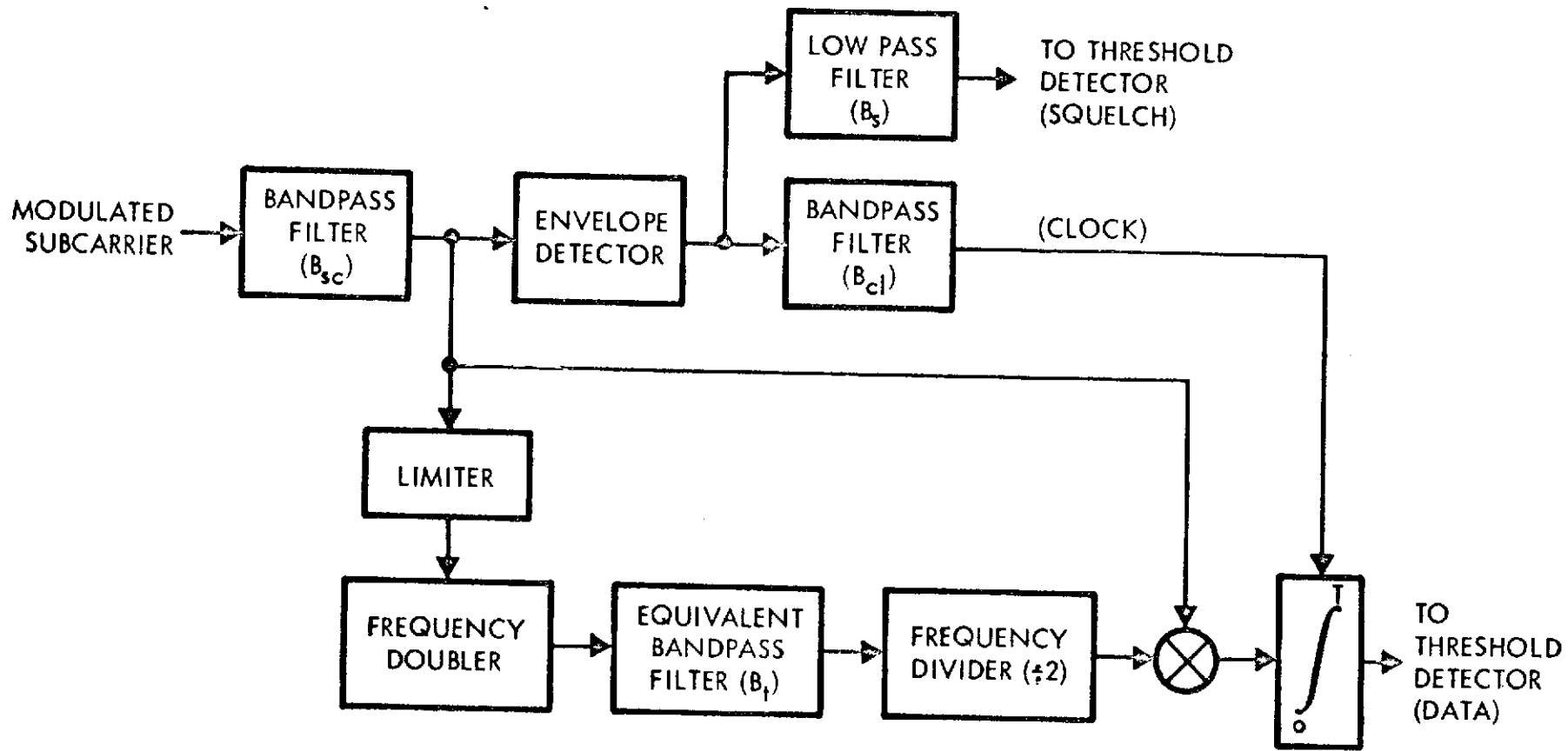


Figure 5.1.1-1. PSK Demodulator Configuration for AM Clock Signal Structure

In this expression, A_{sc} , ω_{sc} , m_{cl} and ω_{cl} denote the subcarrier amplitude, subcarrier angular frequency, clock AM modulation index and clock angular frequency, respectively. Also, $x(t) = \pm 1$ over each bit interval and additive noise is denoted by $n_{sc}(t)$.

Consideration is now given to the bandwidth requirements for each of the filters shown in Figure 5.1.1-1. The signal spectrum for the AM Clock case is determined in Section 3. The bandwidth of the signal, and hence the required filter bandwidth B_{sc} , depends on m_{cl} and θ_{cl} , but would be in the neighborhood of $4R$. Concerning the bandpass filter in the clock branch of Figure 5.1.1-1, two factors must be considered in determining its bandwidth. It is desired to make this bandwidth small in order to yield a high clock signal-to-noise ratio. However, when a message is initiated, the clock signal must be up (essentially in the steady state) prior to the end of the preamble (13 "zeros" followed by a "one"). Assuming that three bits (zeros) are required to start the decoder, the clock should be up at the tenth zero of the preamble. A bandpass bandwidth, $B_{cl} = R/5$ will provide the appropriate transient response for the desired conditions. Obviously, a longer preamble offers potential improvement in clock signal-to-noise ratio.

The equivalent bandpass filter shown in the subcarrier tracking loop of Figure 5.1.1-1 requires additional consideration. Typically, this filter would be representative of a phase-locked-loop (PLL). The actual bandwidth of the PLL must be chosen to allow loop acquisition within ten bits of the preamble. At the frequency of interest here (i.e., twice the subcarrier frequency, or on the order of 20 kHz) Doppler effects are negligible. With the prescribed frequency stability of 0.02% (SCE characteristics), the PLL must acquire over a range of approximately ± 4 Hz. Using the expressions given by Gardner [5-1] for maximum lock-in frequency, lock-up transient time and noise bandwidth we have

$$\Delta \omega_L \approx 2 \delta \omega_n$$

$$T_L \approx 1/\omega_n$$

and

$$\begin{aligned} B_L &= \frac{\omega_n}{2} (\delta + 1/4 \delta) \\ &= B_t/2. \end{aligned}$$

In the above expressions, δ and ω_n are the loop damping factor and natural frequency, respectively. Two factors must be considered in determining the equivalent noise bandwidth; (1) required transient time ($< 10/R$), and (2) the frequency stability. These considerations lead to two constraints on bandwidth; namely

$$B_f/R \geq 4\pi \times 10^{-4} (1 + 1/4\delta^2)/p$$

and

$$B_f/R \geq (\delta + 1/4\delta)/10$$

with the larger of the two possible values being the appropriate selection. Alternatively, we can consider a fix-tuned filter with $B_f = R/5$ following the same arguments employed to establish the clock bandwidth, except in the range where the bandwidth is determined by frequency stability ($p > 250$). Both fix-tuned and equivalent PLL bandwidths are shown in Figure 5.1.1-2.

Finally, the bandwidth B_s of the RC low pass filter in the squelch circuit of Figure 5.1.1-1 is considered. The considerations previously stated in conjunction with the clock are again applicable, except that whereas the clock filter output must be a close replica of the clock signal after the tenth bit, here the output need only have reached some substantial fraction of its steady state value. We consider here that steady state is established when time equals $0.5/B_s = \pi RC$. If this point corresponds to ten bits, we have $B_s = R/20$. The philosophy here can vary somewhat. It should be pointed out however, that the threshold level will ultimately be set at a value corresponding to the fifth bit or so of the preamble.

5.1.2 Summed Clock

The Summed-Clock demodulator is shown in Figure 5.1.2. This configuration differs from that of Figure 5.1.1-1 only in the manner in which the clock is extracted. The composite subcarrier signal is given by

$$y(t) = A_{sc} x(t) \cos(\omega_{sc} t + \theta_{sc}) + A_{cl} \cos(\omega_{cl} t + \theta_{cl}) + n_{sc}(t) \quad (5.1.2-1)$$

Concerning filter bandwidth requirements in this configuration, they are the same as established in the AM Clock case.

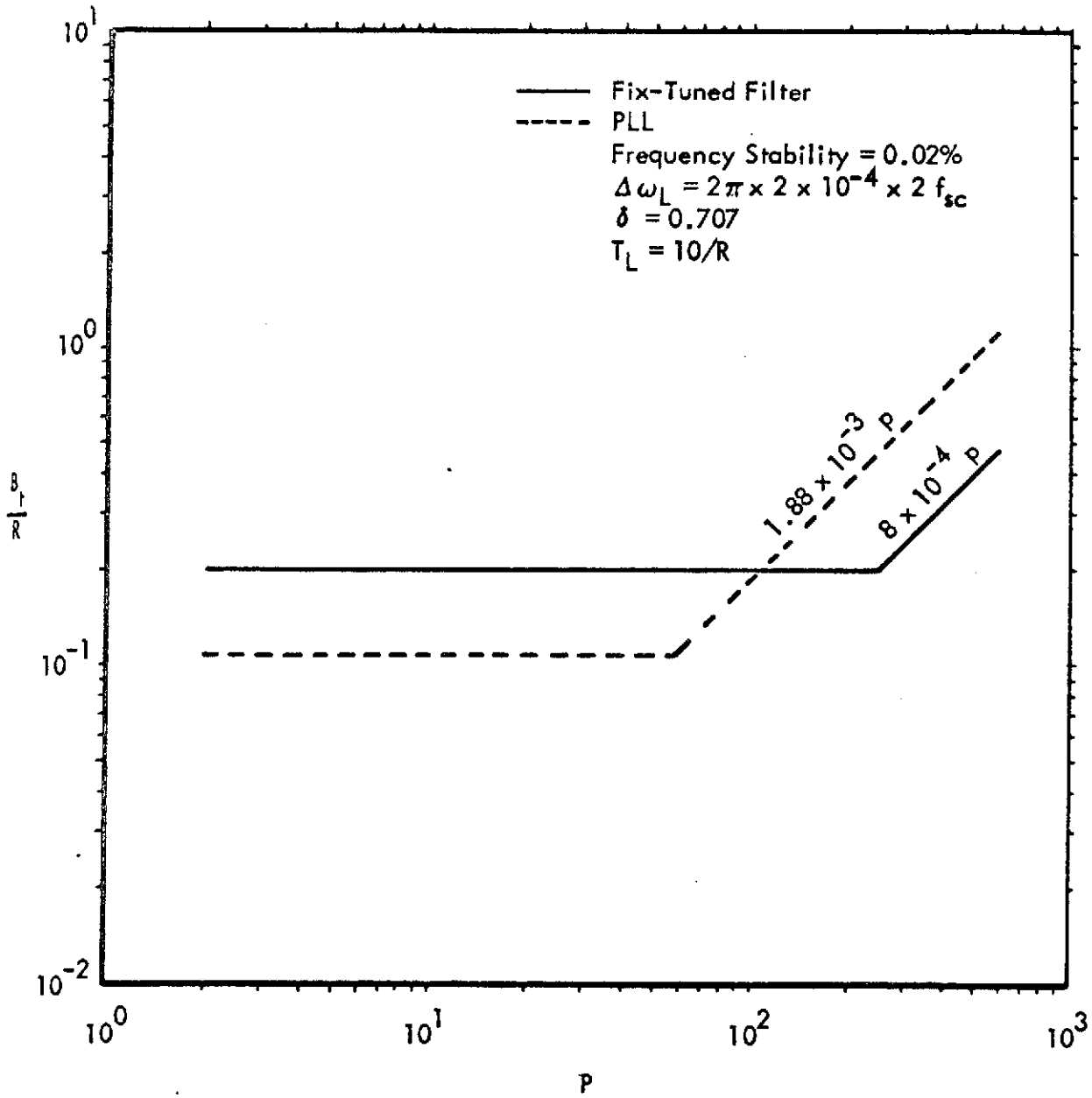


Figure 5.1.1-2. Subcarrier Tracking Loop Bandwidth

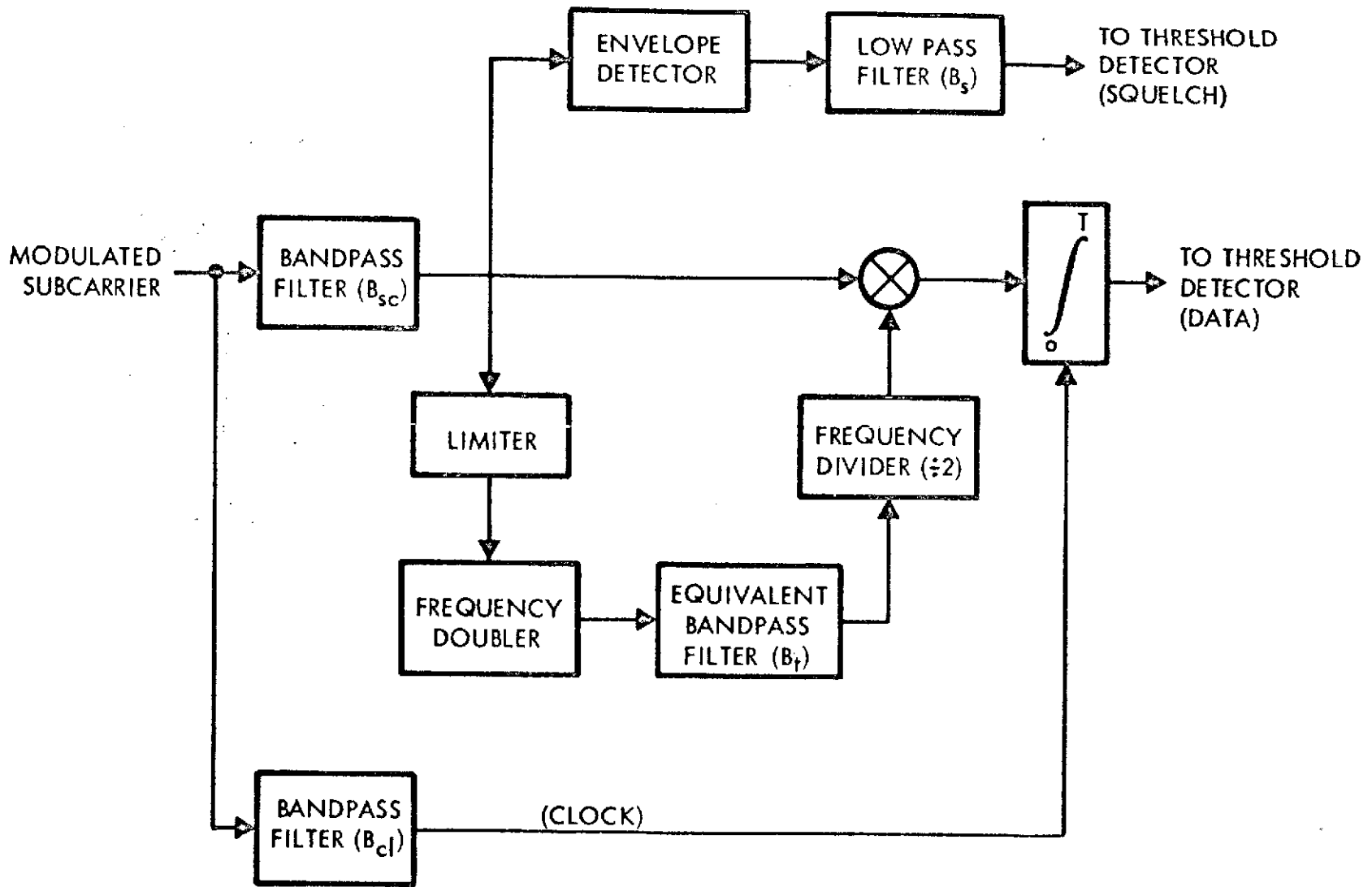


Figure 5.1.2. PSK Demodulator Configuration for Summed Clock Signal Structure

5.2 Squelch Strategy and Analysis

The squelch strategy suggested by the receiver block diagrams of Figures 5.1.1-1 and 5.1.2 is to use the envelope of the signal at subcarrier to determine the presence or absence of a command message. When a command is present, the signal envelope is approximately the envelope of the command signal, and when no command is present, the envelope is the envelope of noise. The simplest squelch tests the envelope against a threshold L and decides "command present" if the envelope exceeds L . The value of the threshold depends on specified probabilities of false alarm, detection, and so forth.

A more sophisticated strategy employs two thresholds, L_1 and L_2 , $L_1 \geq L_2$. The squelch goes "up" when the envelope exceeds L_1 , but once up it does not go "down" until the envelope drops below L_2 . Since the first strategy is a special case of the second (with $L_1 = L_2 = L$), we will analyze the second strategy. First we define and assign labels to some quantities of interest.

The probability of a false start by the decoder, denoted P_{FS} , is the probability that, given no message present, the squelch filter output goes above L_1 and the decoder begins to decode a spurious command. The great majority of the time, the squelch will shortly drop again, so that the decoder is engaged only briefly. With small but nonzero probability the squelch stays up for the length of a message. We call this event a message false alarm and denote its probability P_{MFA} .

When a message is present, it is detected if the squelch is up by the tenth bit of the preamble and remains up for the duration of the message. The probability of detection is denoted P_{DET} . If at some time during transmission, the squelch goes down, then part of the message is lost. In this case the message is said to be deleted and the probability of deletion is P_{DEL} . Finally it is possible that the squelch may never go up, so that the receiver is oblivious to the message; this is called a miss and happens with probability P_{MISS} . The major difference between a miss and a deletion is that with a deletion the receiver believes a message was present, but was unable to decode it completely, while with a miss, the receiver is unaware that a message was sent.

5.2.1 Characteristics of the Squelch Filter Output

In this section we attempt to characterize statistically the process at the output of the squelch filter under the two conditions of interest, message present and message absent. The analysis here applies to the case in which the RF carrier is up, whether a command message is being transmitted or not. The possibility that the RF carrier may not be present should also be considered in choosing parameters in the squelch strategy; this case is discussed separately in Section 5.2.5.

For the purpose of this analysis, we will replace the RC squelch filter by an ideal low-pass filter of the same equivalent noise bandwidth; this bandwidth is found to be $\pi B_s/2$. Because $B_s \ll B_{sc}$, we assume that the output process of the squelch filter is Gaussian.

Determination of the probabilities discussed above reduces to the problem of evaluating the probability that a certain random process exceeds a given value for all times in an interval. General solutions to such problems are unknown; we present an approximate solution based on the intuitive reasoning that samples of the process taken at frequency πB_s are sufficient to determine the process. Moreover, these samples are uncorrelated, and since the process is Gaussian, they are independent.

Suppose that the envelope detector is realized as a square-law device. The input to the device when a message is present consists of a PSK signal, possibly with AM or Summed Clock, plus narrowband Gaussian noise. Since $B_s \ll R$, the clock terms will not be present in the squelch filter output, so we ignore the clock. In addition, since the envelope of the PSK signal is the same as the envelope of the pure (unkeyed) sinusoid, we ignore the keying. Thus the input to the square-law device is reduced to

$$A_{sc} \cos(\omega_{sc} t + \theta_{sc}) + n_{sc}(t)$$

When no message is present the input has the same form, with $A_{sc} = 0$. Thus by analyzing the response to the above signal we can obtain results for both signal present and signal absent cases.

The power spectral density at the output of the square-law device can be shown to have the form illustrated in Figure 5.2.1. The mean (dc) value of the output is the square root of the impulse area and the variance (ac power) of the filter output is the shaded area. Letting $B_{sc} = 4R$ and $B_s = R/20$, we obtain for the mean and variance with signal present,

$$\mu_1 = \left(\frac{A_{sc}^2}{2N_o R} + 4 \right) N_o R \quad (5.2.1-1)$$

$$\sigma_1^2 \approx \frac{\pi}{10} \left(\frac{A_{sc}^2}{2N_o R} + 2 \right) \left(N_o R \right)^2 \quad (5.2.1-2)$$

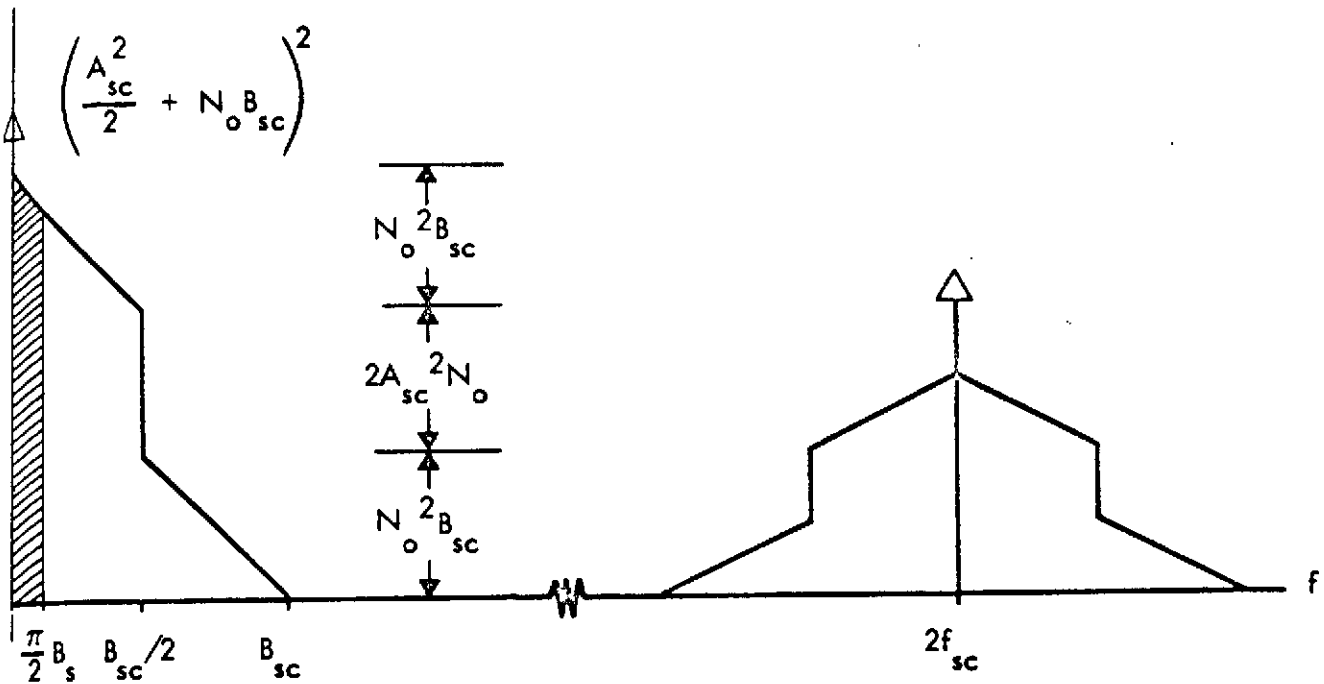


Figure 5.2.1. One-Sided Power Spectral Density at Output of Square-Law Device

The mean and variance with signal absent are obtained by setting $A_{sc} = 0$ in Equations 5.2.1-1 and 5.2.1-2. Therefore

$$\mu_o = 4N_o R$$

$$\sigma_o^2 \approx \frac{\pi}{5} (N_o R)^2$$

(Note that μ_1 and σ_1 as given here are steady-state values; in the sequel we ignore the fact that the first sample in a message envelope has mean value only approximately 95% of the steady-state value.)

5.2.2

False Start and Message False Alarm Probabilities

Let $P_F(m)$ denote the probability that at some fixed sample time, with no message present, the squelch goes up, remains up for exactly m samples (including the first), then drops after the m^{th} sample. Since L_1 must be exceeded by the first sample and L_2 by the next $m - 1$ samples, and since the samples are independent Gaussian random variables with mean μ_0 and standard deviation σ_0 , we have

$$P_F(m) = Q\left(\frac{L_1 - \mu_0}{\sigma_0}\right) \left[Q\left(\frac{L_2 - \mu_0}{\sigma_0}\right) \right]^{m-1} \left[1 - Q\left(\frac{L_2 - \mu_0}{\sigma_0}\right) \right]$$

It is convenient to normalize the threshold, mean and standard deviation by $N_0 R$; then defining

$$\alpha_0 = Q\left(\frac{L_1/N_0 R - 4}{\sqrt{\pi/5}}\right)$$

$$\beta_0 = Q\left(\frac{L_2/N_0 R - 4}{\sqrt{\pi/5}}\right)$$

we have

$$P_F(m) = \alpha_0 \beta_0^{m-1} (1 - \beta_0)$$

A false start has been defined as the event that the squelch goes up when no message is present, regardless of how long it stays up. Hence

$$P_{FS} = \sum_{m=1}^{\infty} P_F(m) = \alpha_0 (1 - \beta_0) \sum_{m=1}^{\infty} \beta_0^{m-1} = \alpha_0$$

Under the assumptions we have made, the sequence of samples with no message present can be modelled as the two-state Markov chain shown in Figure 5.2.2-1. Letting π_{UP} denote the equilibrium probability that the squelch is up and π_{DOWN} the equilibrium probability that the squelch is down, the equilibrium distribution satisfies the simultaneous equations

$$\pi_{UP} = \alpha_0 \pi_{DOWN} + \beta_0 \pi_{UP}$$

$$\pi_{UP} = 1 - \pi_{DOWN}$$

Combining yields

$$\pi_{UP} = \frac{\alpha_0}{1 + \alpha_0 - \beta_0} \quad (5.2.2-1)$$

This probability can be interpreted as the fraction of time the squelch is up when no message is present. Its design significance is that if the squelch is already up when an actual message begins, the receiver output sequence will have the message shifted to the right with meaningless bits inserted at the beginning. Thus an incorrect or invalid sequence is presented to the command decoder, resulting in a message deletion.

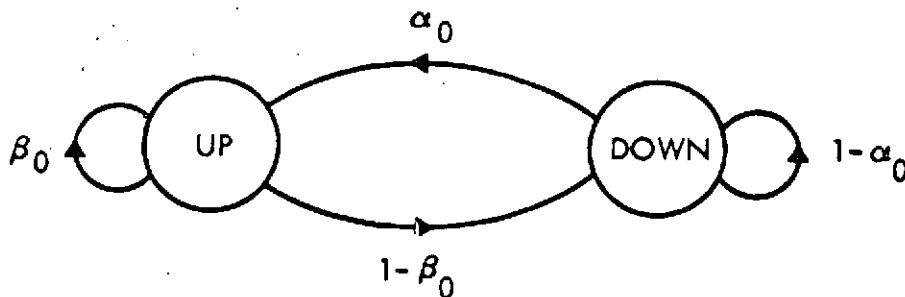


Figure 5.2.2-1. Markov Chain Model for Squelch in Absence of Signal

A related quantity of interest is the average length of time the squelch stays up after a false start. To calculate this, note that

$$\begin{aligned} E \{ m | FS \} &= \sum_{m=1}^{\infty} m P_F(m | FS) = \frac{1}{P_{FS}} \sum_{m=1}^{\infty} m P_F(m) \\ &= \frac{1}{\alpha_0} \alpha_0 (1 - \beta_0) \sum_{m=1}^{\infty} m \beta_0^{m-1} \end{aligned}$$

But

$$\sum_{m=1}^{\infty} m \beta_0^{m-1} = \frac{1}{(1 - \beta_0)^2}$$

Hence $E \{ m | FS \} = 1/(1 - \beta_0)$. This indicates that once the squelch goes up, the receiver will be operating for $1/(1 - \beta_0)$ sample times, on the average. The separation between samples is $1/\pi B_s = 20/\pi R$ so that the average duration of false starts is $N = 20/\pi (1 - \beta_0) = 6.37/(1 - \beta_0)$ bit times.

The average number of false starts per hour, termed the false start rate FSR can be estimated by

$$\begin{aligned} FSR &= \frac{P_{FS} \cdot \# \text{ samples/hr}}{\text{average } \# \text{ samples/false start}} \\ &= \frac{\alpha_0 \cdot \pi B_s \cdot 3600}{1/(1 - \beta_0)} \\ &= \alpha_0 (1 - \beta_0) \frac{\pi}{20} \cdot R \cdot 3600 \end{aligned}$$

Since $\beta_0 \ll 1$ in well-designed systems, we can approximate this by

$$FSR \approx 180 \pi \alpha_0 R \quad .$$

False start rates as a function of R for various values of P_{FS} are plotted in Figure 5.2.2-2.

Finally, the message false alarm probability is given by

$$P_{MFA} = \sum_{m=M}^{\infty} P_F(m)$$

where M is the number of samples in a message length. Since the shortest message is 64 bits long and since one sample time is 6.37 bit times, $M = 10$ for the shortest message. Thus

$$P_{MFA} = \alpha_0 (1 - \beta_0) \sum_{m=10}^{\infty} \beta_0^{m-1} = \alpha_0 \beta_0^9$$

For reasonable values of β_0 , P_{MFA} is an extremely small number, and of little design significance.

5.2.3 Detection, Deletion, and Miss Probabilities

The probability of detection, given a signal present, is

$$\begin{aligned} P_{DET} &= Q\left(\frac{L_1 - \mu_1}{\sigma_1}\right) Q\left(\frac{L_2 - \mu_1}{\sigma_1}\right)^{M-1} \\ &= \alpha_1 \beta_1^{M-1} \end{aligned}$$

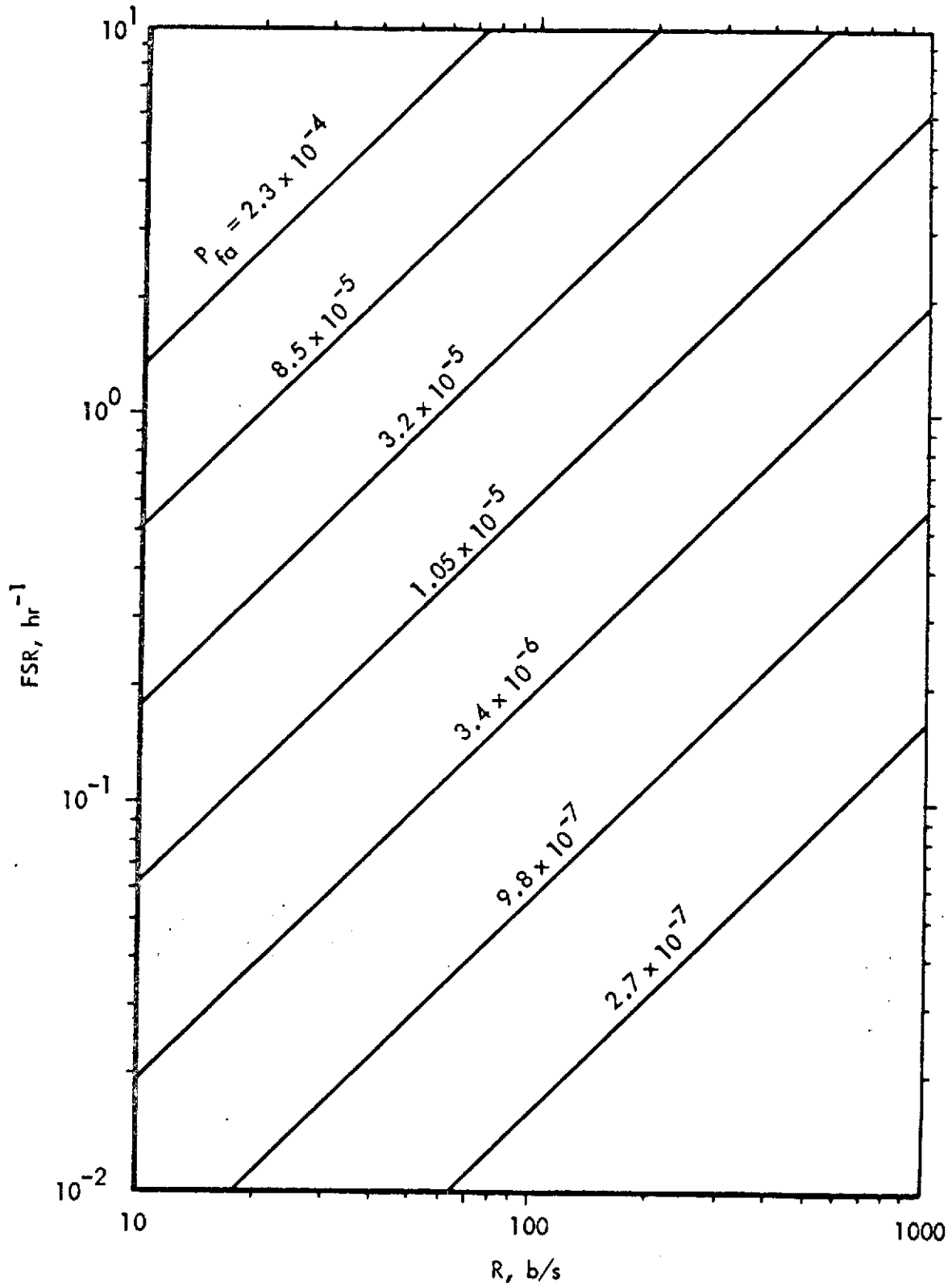


Figure 5.2.2-2. False Start Rate

where α_1 and β_1 are, normalizing as before,

$$\alpha_1 = Q \left(\frac{L_1/N_o R - 4 - A_{sc}^2/2N_o R}{\sqrt{\frac{\pi}{10} \left(\frac{A_{sc}^2}{2N_o R} + 2 \right)}} \right) \quad (5.2.3-1)$$

$$\beta_1 = Q \left(\frac{L_2/N_o R - 4 - A_{sc}^2/2N_o R}{\sqrt{\frac{\pi}{10} \left(\frac{A_{sc}^2}{2N_o R} + 2 \right)}} \right) \quad (5.2.3-2)$$

With probability $1 - P_{DET}$, the squelch is down for at least one sample during the message; thus

$$1 - P_{DET} = P_{DEL} + P_{MISS}$$

But $P_{MISS} = (1 - \alpha_1)(1 - \beta_1)^{M-1}$ is a very small number, so we may write

$$1 - P_{DET} \approx P_{DEL}$$

5.2.4 Design Considerations

In selecting the squelch thresholds L_1 and L_2 , tradeoffs among the quantities we have just introduced must be considered. For example, typically a maximum value of $P_{FS} = \alpha_0$ might be specified, either directly or perhaps from a specified FSR via Figure 5.2.2-2. This determines the normalized threshold $L_1/N_o R$ and hence (for a given signal-to-noise ratio, $A_{sc}^2/2N_o R$), α_1 . With these quantities fixed, P_{DET} may be varied within limits by varying $L_2/N_o R$, but

as P_{DET} is increased, so is the fraction of time the squelch is up when no message is present, and the average duration of false starts. Figure 5.2.4 shows the variations of P_{DET} and P_{DEL} versus SNR for three values of P_{FS} and various choices of the second threshold L_2/N_0R . Curves are shown for both 64-bit and 4160-bit message lengths. Also included is a table showing the probability of π_{Up} from Equation 5.2.2-1 as a function of the fraction L_2/L_1 .

5.2.5 Squelch Analysis in the Absence of RF Carrier

The calculations of means and variances at the squelch filter output in Section 5.2.1 assumes that the RF carrier is on at all times. Under certain conditions (e.g., spacecraft over the horizon) the RF carrier will not be present. In this case, the AGC will amplify the receiver input noise and the response of the squelch filter to this noise may be significant. Since the squelch should inhibit decoding in this mode, the squelch filter response when no carrier is present should be considered in establishing the thresholds.

By considering the characteristics of the AGC, and employing techniques similar to those used in Section 5.2.1, we can obtain the squelch filter output mean μ_{NC} and standard deviation σ_{NC} under the condition that the carrier is absent. Then, for a specified false start probability P_{FS} , L_1 must be chosen so that both

$$Q \left(\frac{L_1 - \mu_0}{\sigma_0} \right) \leq P_{FS}$$

and

$$Q \left(\frac{L_1 - \mu_{NC}}{\sigma_{NC}} \right) \leq P_{FS}$$

Equivalently, we must choose

$$L_1 \geq \max \left\{ \sigma_0 Q^{-1}(P_{FS}) + \mu_0, \sigma_{NC} Q^{-1}(P_{FS}) + \mu_{NC} \right\}$$

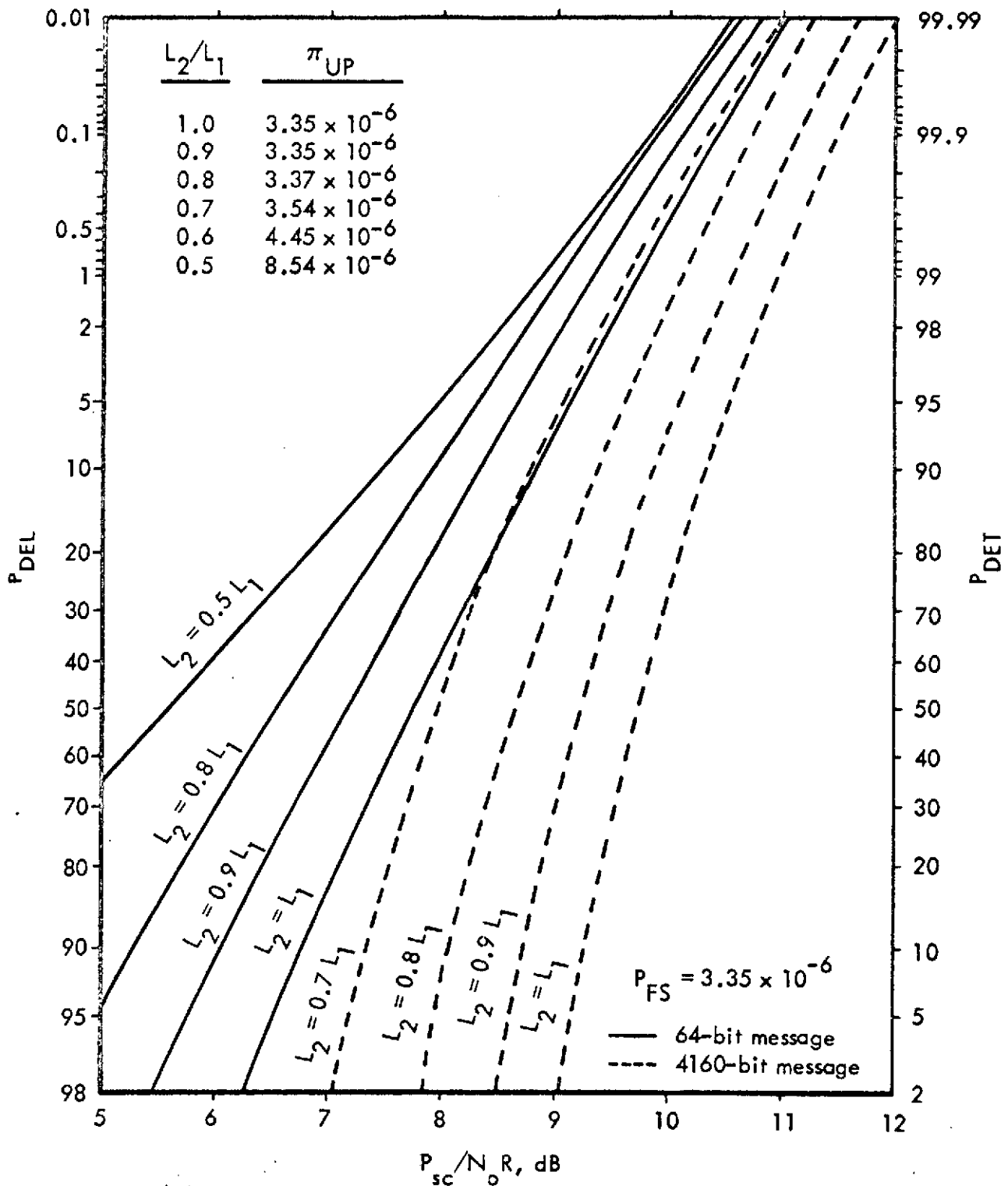


Figure 5.2.4(a). Detection and Deletion Probability

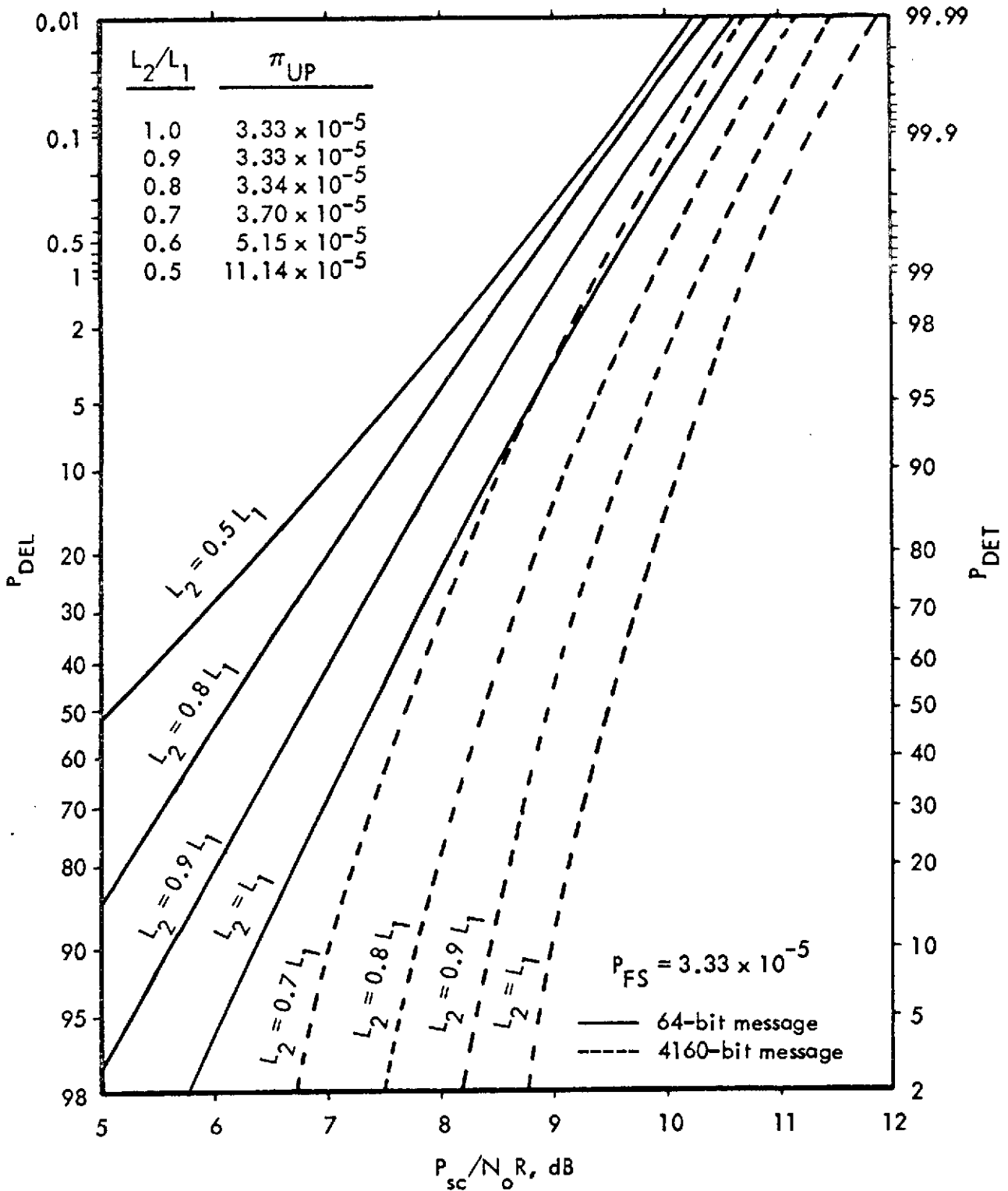


Figure 5.2.4(b). Message Detection and Deletion Probability

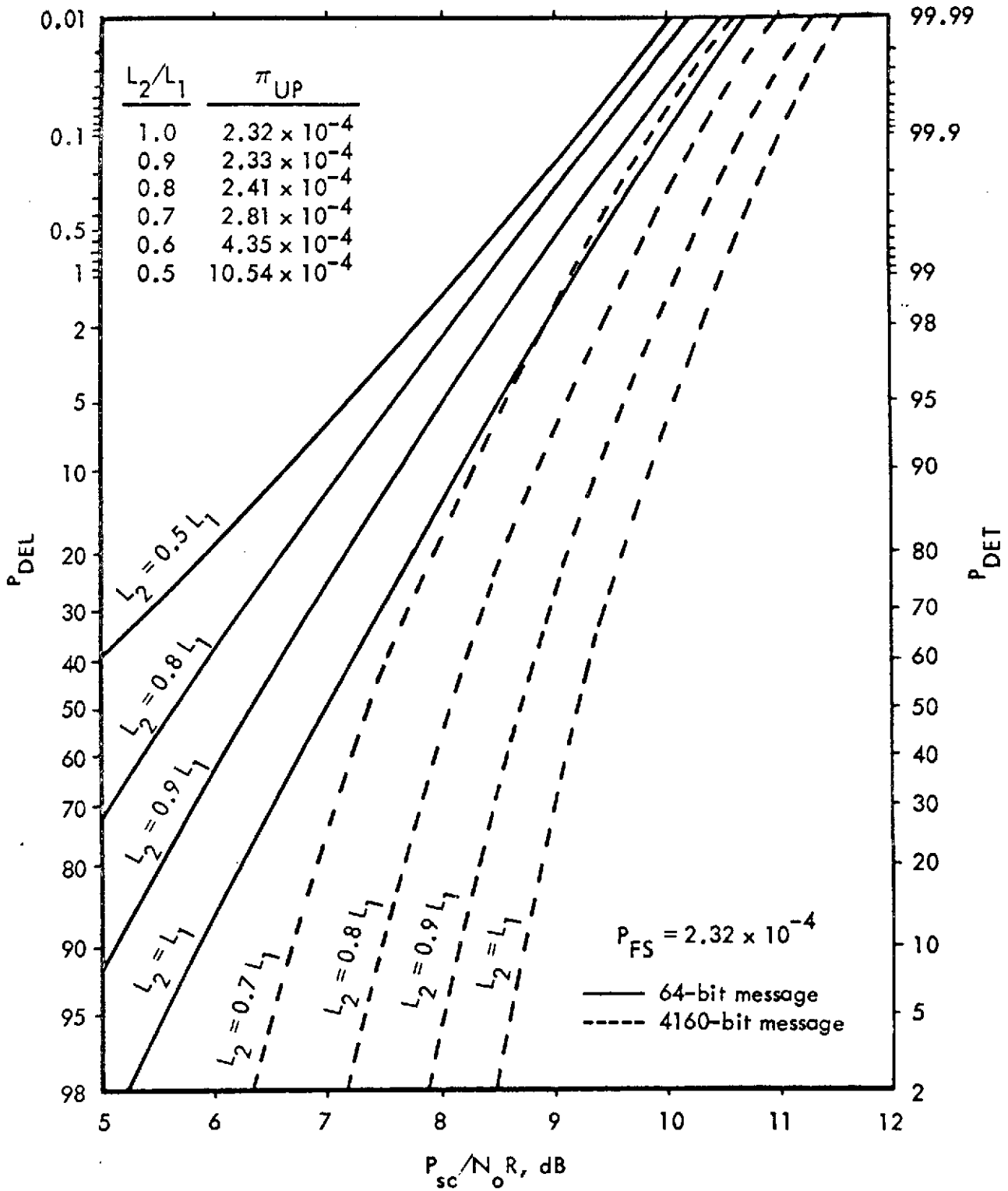


Figure 5.2.4(c). Message Detection and Deletion Probability

Typical of applications of interest here, it is the carrier-absent condition which determines the value of L_1 .

5.3 Bit Error Probability

In this section the bit error probability P_e of the demodulators of Figures 5.1.1-1 and 5.1.2 is determined. Degradation in performance due to subcarrier and clock jitter is estimated, and appropriate adjustments to the error probability formulas obtained in Section 2.1 are made. The noise in the subcarrier bandwidth is assumed to be white Gaussian noise with spectral density $N_o/2$.

The normalized output of the suboptimum PSK-AM detector, assuming perfect subcarrier and clock synchronization, is given by

$$z(t) = \pm \sqrt{\eta E_b} + n$$

where n is a zero-mean Gaussian random variable with variance $N_o/2$. The effect of synchronization errors is to reduce the magnitude of the first term, which is the response to the PSK-AM signal. The reduction due to bit timing error has been considered in Section 2.4, where the signal response under conditions of small bit synchronization error is given by Equation 2.4.2-1. If in addition the local oscillator phase differs from the actual subcarrier phase by an amount ϕ , the effect is an additional reduction by a factor $\cos \phi$. Thus the detector response to signal alone is

$$z(T+\tau) = \pm \sqrt{\eta E_b} \left[1 - 2 (1 + m_{cl} \cos \theta_{cl}) \frac{|\tau|}{T} \right] \cos \phi \quad (5.3-1)$$

The analogous expression for a PSK-Summed Clock signal is

$$z(T+\tau) = \pm \sqrt{\eta E_b} \left[1 - 2 \frac{|\tau|}{T} \right] \cos \phi$$

which is just Equation 5.3-1 with $m_{cl} = 0$.

If $P_{e|\tau, \phi}$ denotes the error probability conditioned on synchronization errors τ and ϕ , then

$$P_{e|\tau, \phi} = Q \left(\sqrt{\frac{2\eta E_b}{N_o}} \left[1 - 2(1 + m_{cl} \cos \theta_{cl}) \frac{|\tau|}{T} \right] \cos \phi \right) \quad (5.3-2)$$

where the appropriate expression for PSK-Summed Clock is obtained by taking $m_{cl} = 0$. The bit error probability is found by averaging $P_{e|\tau, \phi}$ over τ and ϕ :

$$P_e = \iint P_{e|\tau, \phi} p(\tau, \phi) d\tau d\phi \quad (5.3-3)$$

With perfect synchronization, $\tau = 0$ and $\phi = 0$ with probability one, so that

$$P_e = Q \left(\sqrt{\frac{2\eta E_b}{N_o}} \right)$$

Equations 5.3-1 through 5.3-2 indicate the manner in which performance is degraded due to clock and subcarrier jitter. The most meaningful measure of degradation would be the amount that the subcarrier power must be increased over that required to achieve a specified P_e under conditions of perfect synchronization; that is, for PSK-Summed Clock, for example, if

$$P_e = Q \left(\sqrt{\frac{2\eta E^*}{N_o}} \right) = E_{\tau, \phi} \left\{ Q \left(\sqrt{\frac{2\eta E_b}{N_o}} \left(1 - 2 \frac{|\tau|}{T} \right) \cos \phi \right) \right\}$$

then the degradation in dB at that value of P_e would be $10 \log (E_b/E^*)$.

Unfortunately, degradation so defined is difficult to calculate and depends on the specified P_e . Alternatively, degradation is defined here as the average reduction in the magnitude of the detector output at the sampling time (due to signal alone) caused by jitter. Furthermore, in order to separate the effects of clock and subcarrier jitter, we assume that τ and ϕ are uncorrelated. Thus, the total degradation, D , is

$$D = D_{sc} + D_{cl} \quad (5.3-4)$$

where

$$D_{sc} = -20 \log_{10} E \left[\cos \phi \right] \quad (5.3-5)$$

and

$$D_{cl} = -20 \log_{10} E \left\{ \left[1 - 2 (1 + m_{cl} \cos \theta_{cl}) \frac{|\tau|}{T} \right] \right\} \quad (5.3-6)$$

with the proviso that D_{cl} for PSK-Summed Clock is obtained by taking $m_{cl} = 0$. We proceed to derive expressions relating D_{sc} and D_{cl} to signal-to-noise ratios.

5.3.1 Degradation Due to Subcarrier Phase Jitter

The subcarrier tracking loop is analyzed here to determine the relationship between subcarrier signal-to-noise ratio and D_{sc} as given by Equation 5.3-5.

The output of the equivalent band-pass filter in the tracking loop of Figure 5.1.1-1 or 5.1.2 can be written

$$e_x(t) = A_x \cos(2\omega_{sc}t + 2\theta_{sc}) + n_x(t) \quad (5.3.1-1)$$

where, since $B_f \ll B_{sc}$, $n_x(t)$ can be assumed to be Gaussian with zero mean and variance σ_x^2 . Representing $n_x(t)$ in quadrature components, this becomes

$$e_x(t) = A_x \cos(2\omega_{sc} t + 2\theta_{sc}) + n_{cx}(t) \cos(2\omega_{sc} t + 2\theta_{sc}) \\ + n_{sx}(t) \sin(2\omega_{sc} t + 2\theta_{sc})$$

where

$$\overline{n_{cx}^2(t)} = \overline{n_{sx}^2(t)} = \sigma_x^2$$

Rewriting this,

$$e_x(t) = R_x(t) \cos(2\omega_{sc} t + 2\theta_{sc} + \psi(t))$$

where

$$R_x(t) = \sqrt{\left[A_x + n_{cx}(t)\right]^2 + n_{sx}^2(t)}$$

and

$$\psi(t) = \tan^{-1} \left[\frac{n_{sx}(t)}{A_x + n_{cx}(t)} \right]$$

Interest here lies in the phase $\psi(t)$ which can be approximated for large signal-to-noise ratio as

$$\psi(t) \approx \frac{n_{sx}(t)}{A_x}$$

with mean square value

$$\overline{\psi^2(t)} \approx \frac{\overline{n_{sx}^2(t)}}{A_x^2} = \frac{\sigma_x^2}{A_x^2} = \frac{1}{2\text{SNR}_x}$$

where SNR_x is the signal-to-noise ratio of Equation 5.3.1-1.

The subcarrier phase jitter is given by

$$\phi(t) = \frac{1}{2} \psi(t)$$

so

$$\overline{\phi^2(t)} = \frac{1}{4} \overline{\psi^2(t)} \approx \frac{1}{8\text{SNR}_x}$$

For small $\phi(t)$,

$$\overline{\cos \phi(t)} \approx 1 - \frac{1}{2} \overline{\phi^2(t)} \approx 1 - \frac{1}{16\text{SNR}_x}$$

Inserting this in Equation 5.3-5,

$$D_{sc} = -20 \log_{10} \left[1 - \frac{1}{16\text{SNR}_x} \right] \quad (5.3.1-2)$$

The signal-to-noise ratio SNR_x is related to the subcarrier signal-to-noise ratio

$$\text{SNR}_{sc} = \frac{P_{sc}}{N_o B_{sc}}$$

as follows. The signal-to-noise ratio out of the limiter is [5-3]

$$\text{SNR}_L \approx \frac{\text{SNR}_{sc} (1 - 2\text{SNR}_{sc})}{4/\pi + \text{SNR}_{sc}} \quad (5.3.1-3)$$

This expression assumes that the limiter is a bandpass limiter (i.e., that the hard-limiting is followed by a bandpass filter which passes only the fundamental component of the hard-limited signal). The resulting noise output is thus narrowband relative to the process immediately after hard-limiting; assuming that this noise process is adequately modelled as band-limited white Gaussian noise, the square-law detector analysis of [5-2] applies since the frequency doubler is implemented by a squaring operation. Following the development in [5-2], it can be shown that

$$\text{SNR}_x \approx \frac{(\text{SNR}_L)^2}{2 [1 + 2\text{SNR}_L]} \cdot \frac{B_{sc}}{B_t} \quad (5.3.1-4)$$

Using Equations 5.3.1-2 through 5.3.1-4, D_{sc} is shown as a function of SNR_{sc} in Figure 5.3.1.

5.3.2 Degradation Due to Clock Phase Jitter

The effect of clock phase jitter can be analyzed in a manner similar to the subcarrier phase jitter. The output of the clock extracting circuit is given as

$$e_{cl}(t) = A_{cl} \cos(\omega_{cl}t + \theta_{cl}) + n_{cl}(t)$$

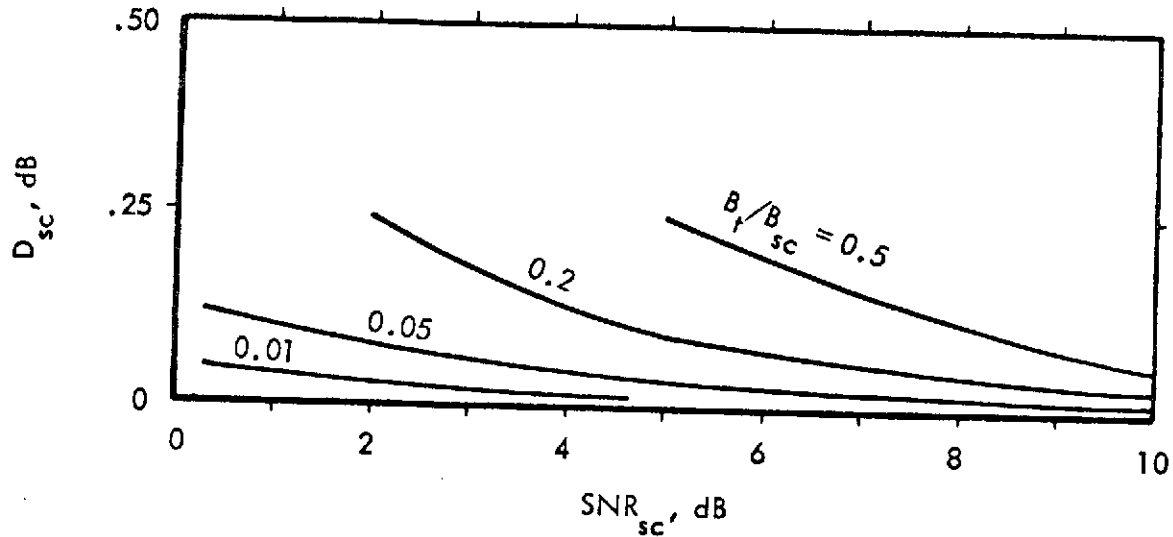


Figure 5.3.1. Degradation Due to Reference Subcarrier Phase Jitter

It is shown in Section 2.2 that whether the clock is AM or Summed, $n_{cl}(t)$ can be assumed to be Gaussian with output signal-to-noise ratio equal to the received signal-to-noise ratio,

$$SNR_{cl} = \frac{A_{cl}^2}{2 \sigma_{cl}^2} = \frac{P_{cl}}{N_o B_{cl}}$$

where P_{cl} is the power in the clock signal.

As before, $n_{cl}(t)$ causes a phase error $\phi(t)$ such that, for high signal-to-noise ratios,

$$\phi(t) \approx \frac{n_{cl,s}(t)}{A_{cl}}$$

The relation between timing error τ and phase error $\phi(t)$ is

$$\tau = \phi \frac{T}{2\pi}$$

We are interested in the average of the magnitude,

$$\overline{|\tau|} = \frac{T}{2\pi} \overline{|\phi|} = \frac{T}{2\pi A_{cl}} \overline{|n_{cl,s}(t)|}$$

But $n_{cl,s}(t)$ is a zero-mean Gaussian process with variance σ_{cl}^2 ; the mean of the magnitude of such a process is [5-4]

$$\overline{|n_{cl,s}(t)|} = \sqrt{\frac{2}{\pi}} \sigma_{cl}$$

Thus

$$\frac{\overline{|\tau|}}{T} = \frac{1}{2\pi \sqrt{\pi} \text{SNR}_{cl}}$$

so that

$$D_{cl} = -20 \log_{10} \left[1 - \frac{1 + m_{cl} \cos \theta_{cl}}{\pi \sqrt{\pi} \text{SNR}_{cl}} \right]$$

where the degradation for a Summed Clock system is obtained by setting $m_{cl} = 0$.

The degradation for PSK-Summed Clock and PSK-AM Clock with $\theta_{cl} = \pi$ and $m_{cl} = 0.5$ is illustrated in Figure 5.3.2. For SNR_{cl} in excess of 10 dB, the degradation is small, with the AM Clock approximately 0.25 dB better than the Summed Clock at $\text{SNR}_{cl} = 10$. Since $B_{sc} \gg B_{cl}$, this means that very little of the actual power transmitted needs to be in the clock signal. This conclusion, and the values of D_{cl} obtained here, are in agreement with what would be expected from consideration of the results given in Section 2.3.

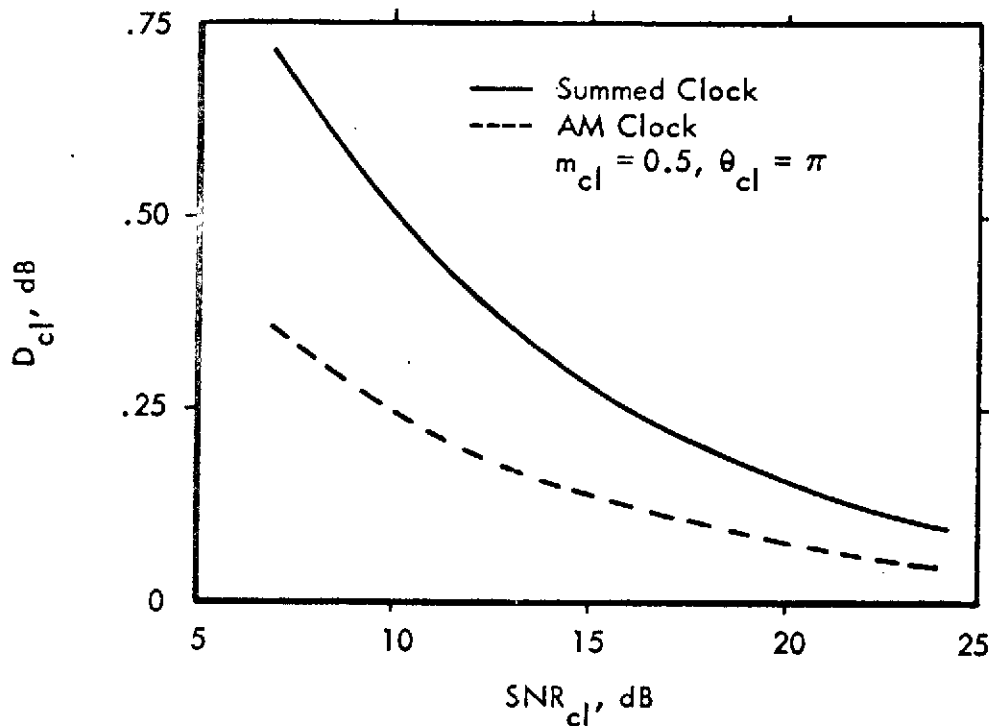


Figure 5.3.2. Degradation Due to Clock Phase Jitter

5.3.3 Degradation Due to Use of Suboptimum Demodulator

As we have noted, the receiver of Figure 5.1.1-1 is suboptimum. It is shown in Section 2.1.2 that the correlator output of the suboptimum detector is reduced from that of the optimum detector by an amount $\sqrt{\eta}$, when η is the fraction of the total signal power which is associated with the pure PSK subcarrier. From Equation 2.1.2-2

$$\eta = \frac{1}{1 + m_{cl}^2/2}$$

Therefore

$$D_{\text{SUBOPT}} = -10 \log_{10} (\eta) \quad .$$

For $m_{cl} = 0.5$, for example, use of the suboptimum receiver rather than the optimum receiver costs only 0.5 dB. Degradation versus clock modulation index is plotted in Figure 5.3.3.

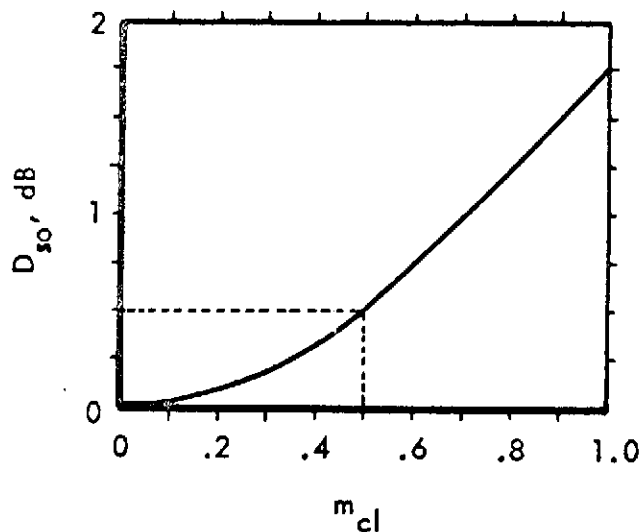


Figure 5.3.3. Degradation in Suboptimum PSK Detector Performance

5.4 Message Error Probability

A quantity of critical interest in command systems is the probability of correctly transmitting a command, which we denote P_{CORR} . Correct transmission is effected when (1) all bits are detected correctly, and (2) the squelch remains up for the entire message. Thus we have

$$\begin{aligned}
 P_{\text{CORR}} &= \Pr \left\{ \text{no bit errors in message, message detected} \right\} \\
 &= \Pr \left\{ \text{no bit errors in message} \mid \text{detection} \right\} \cdot P_{\text{DET}}
 \end{aligned}$$

Since $B_s \ll B_{sc}$, the correlation between the events "no bit errors" and "detection" is small. Thus we can approximate P_{CORR} as

$$P_{\text{CORR}} = \Pr \left\{ \text{no bit errors in message} \right\} P_{\text{DET}}$$

If the message consists of L bits, this becomes

$$P_{\text{CORR}} = (1 - P_e)^L P_{\text{DET}} \quad (5.4-1)$$

Equation 5.4-1 was evaluated for PSK with $\eta = 1$ for several values of P_{FS} ; the results are shown in Figure 5.4. When a clock is present, $\eta < 1$, so that P_{CORR} is reduced from the value shown. However, data taken for $\eta = 0.8$ and $\eta = 0.9$ indicates that the degradation is not significant.

5.5 RFI Effects in the Subcarrier Bandpass

Radio frequency interference (RFI) can affect the performance of a communications receiver in various ways. It is obvious that the presence of sufficient interference power can completely disrupt operation of a receiver, as in the case of large amounts of thermal noise. RFI in the RF carrier demodulation structure can possibly capture the receiver, causing the receiver to essentially ignore a desired signal. Deleterious effects are also possible in the absence of a desired signal. Depending upon the type of RF carrier modulation and the characteristics of the interfering signal, it is possible for interference to be translated into the subcarrier passband. A special case of such involving interference due to two systems sharing a common RF channel has been considered in Section 4.2. In general, these considerations have shown the manner in which interference is translated from RF to the subcarrier passband. In the presence of a desired signal, subcarrier interference can degrade performance in a manner similar to thermal noise, depending upon the nature of the interfering signal. Interference in the absence of a desired signal can cause the receiver to false alarm.

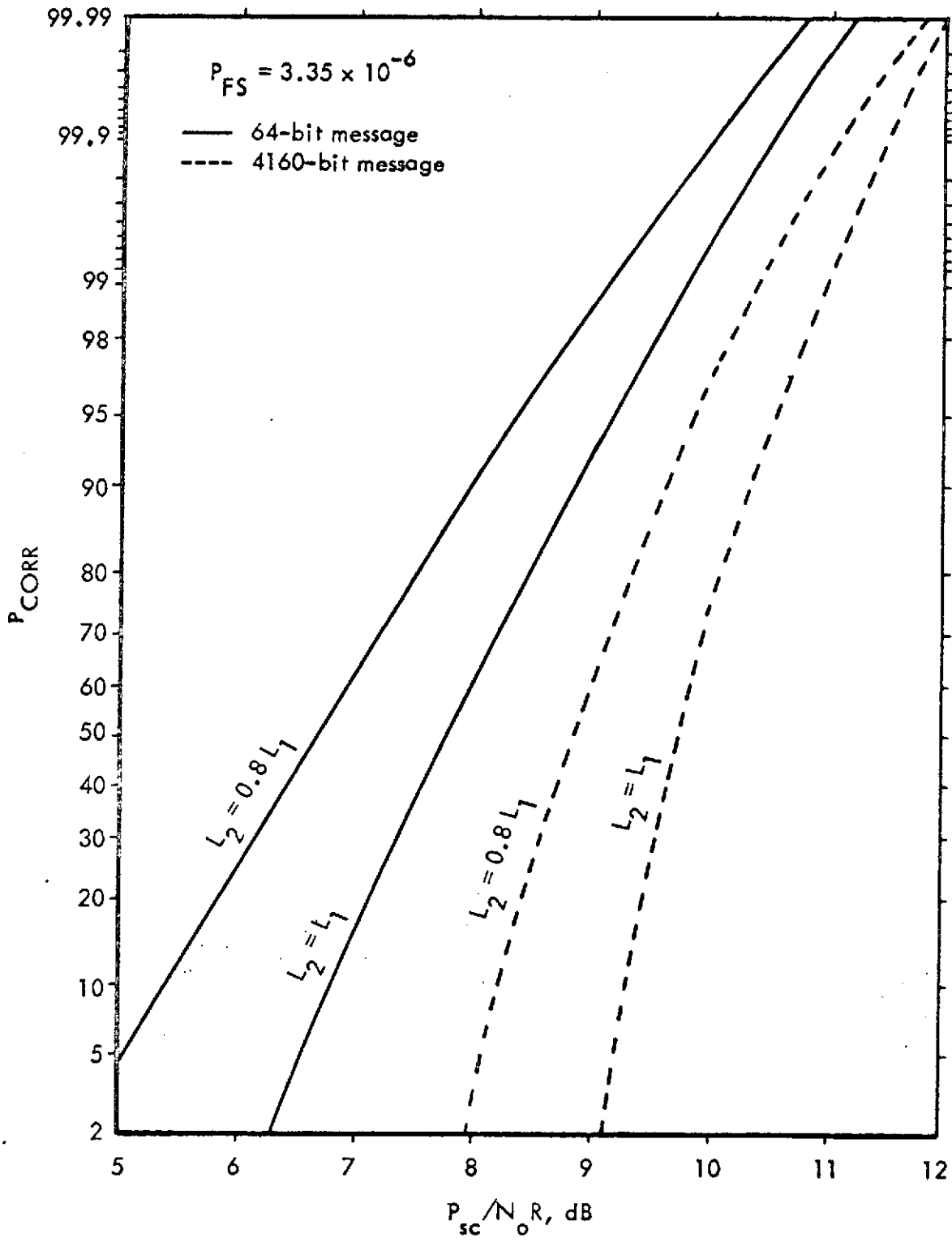


Figure 5.4(a). Probability of Correct Message

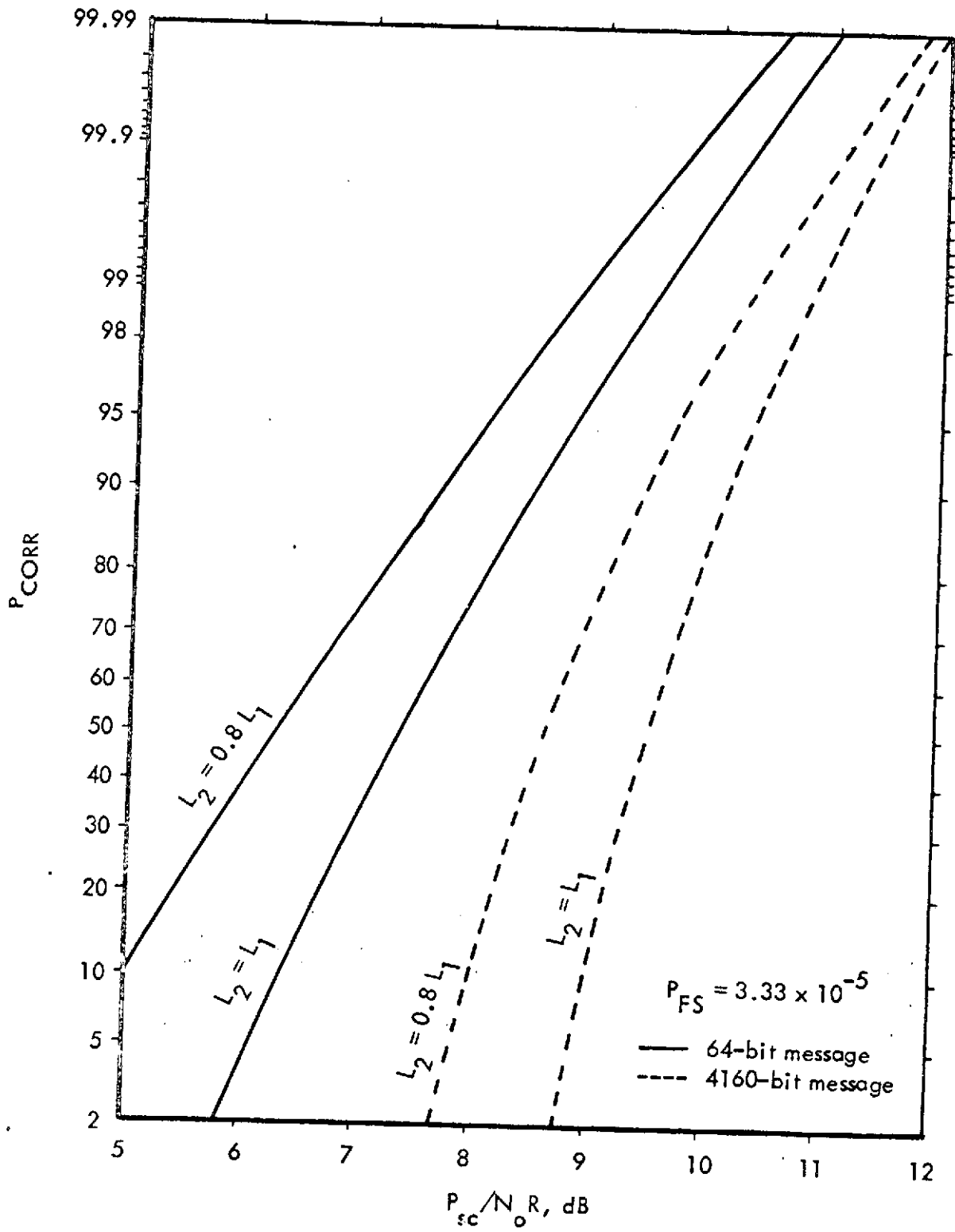


Figure 5.4(b). Probability of Correct Message

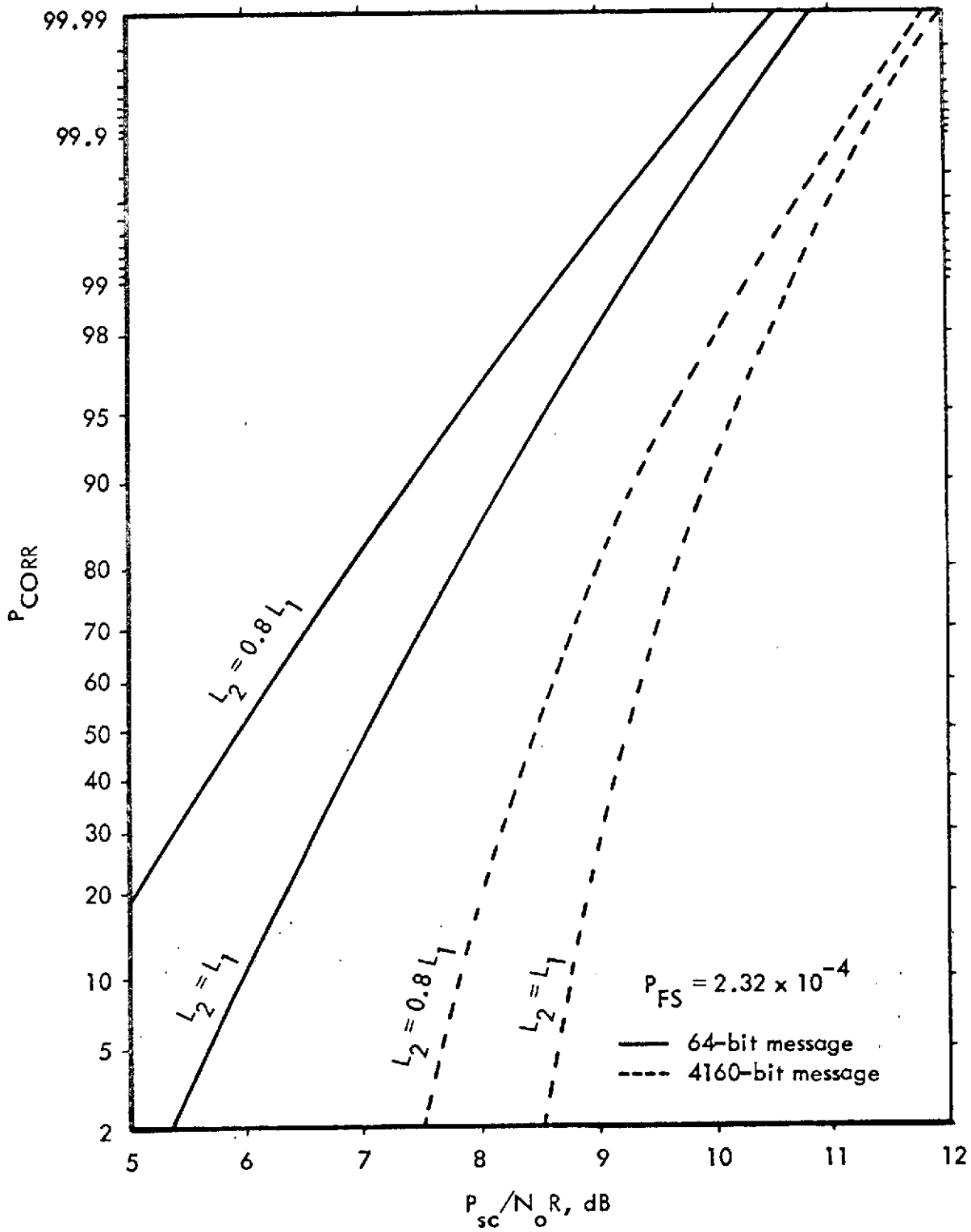


Figure 5.4(c). Probability of Correct Message

Under certain restrictive assumptions, the problem of RFI in the sub-carrier passband is addressed in the following paragraphs, and estimates of RFI effects are presented. Major emphasis here is placed upon the effects of RFI upon squelch operation. Although RFI effects are not restricted to squelch operation, major concern for such exists because squelch operation primarily determines the false start and message detection or deletion probabilities. It is assumed that an additive interfering signal exists in the subcarrier passband which can be expressed as

$$e_{si}(t) = A_{si} \sin \left[(\omega_{sc} + \Delta\omega)t \right] , \quad |\Delta f| < B_{sc}/2 .$$

5.5.1 Effects of RFI on Message False Alarm

In the absence of a desired signal, but when an interfering signal lies in the passband B_{sc} , the noise statistics at the output of the squelch filter are given by Equations 5.2.1-1 and 5.2.1-2 by changing A_{sc} to A_{si} in these expressions. The presence of RFI acts to increase the probability of false starts, and subsequently message false alarm, by contributing power to the squelch in addition to increasing the squelch noise power relative to that of the signal-absent case.

It is sufficient to state that the presence of RFI signal power in the squelch bandpass which is on the order of the noise power will cause false starts and message false alarms if no protective measures are taken to prevent such. A possible means of reducing false alarms in such a case would be to require that the clock signal level be above a specified value, in addition to the requirement that the squelch be up before initiating decoder action. Another possibility would be to structure the preamble such that the decoder must recognize a sequence of bits as opposed to a single bit change (e.g., a specified code word such as an address).

Some additional theoretical analysis, based upon the assumed interference, indicates the manner in which RFI increases the message false alarm probability. Employing the Gaussian statistics of Equations 5.2.1-1 and 5.2.1-2, the message false alarm probability can be expressed in terms of

$$P_{MFA} = \sum_{m=M}^{\infty} P_F(m) ,$$

and in the situation under consideration here

$$P_F(m) = \alpha_1 \beta_1^{m-1} (1 - \beta_1) \quad , \quad (5.5.1-1)$$

where A_{sc} is replaced by A_{si} in Equations 5.2.3-1 and 5.2.3-2. Recall that the squelch threshold is established in terms of the rms value of the noise for a given false start probability in the presence of thermal noise. Such a value can be employed in Equation 5.5.1-1 to determine message false alarm probability as a function of the ratio of interference signal power to thermal noise power.

Although the practicality of the above results are questionable, in that they depend upon the nature of the interference, this approach does indicate how RFI effects influence message false alarms.

5.5.2 Effects of RFI on Message Deletion Probability

Determination of the effects of RFI upon message deletion or detection probability requires consideration of the presence of a desired signal plus interference. This can be expressed by

$$e_{sc}(t) = A_{sc}(t) \cos(\omega_{sc} t) + A_{si} \sin \left[(\omega_{sc} + \Delta\omega) t \right]$$

where $A_{sc}(t)$ represents subcarrier modulation. The output of the squelch low pass filter for large desired signal-to-interference ratios is given approximately by the expression

$$e_s(t) = \frac{A_{sc}}{2} \left\{ A_{sc} + A_{si} \sin(\Delta\omega t) \right\} \quad , \quad \Delta f < B_s$$

In the event that $\Delta f = 0$, the desired subcarrier level can increase or decrease according to the interference level and phase relative to that of the subcarrier. The worst case corresponds to $A_{sc} - A_{si}$ in brackets above.

It should be noted that the presence of the interference signal component above is due to the existence of a beat frequency at the input of the envelope detector, as described in Section 4.2. The interference into the squelch's

threshold device is therefore represented by the interference component above, causing a time variation about the desired signal level. It is meaningless to consider an average effect; however, a worst case condition is meaningful when considered in conjunction with message deletion probability. The worst case corresponds to the minimum value of the above expression,

$$e_s(t)_{\min} = \frac{A_{sc}}{2} (A_{sc} - A_{si})$$

In terms of detection probability, degradation due to RFI can be determined by replacing A_{sc} in Equations 5.2.3-1 and 5.2.3-2 by

$$A_{sc} (1 - \sqrt{P_{si}/P_{sc}})$$

The degradation factor for detection probability is defined as

$$D_{DET} = -20 \log_{10} (1 - \sqrt{P_{si}/P_{sc}})$$

and plotted in Figure 5.5.2 as a function of the ratio of unmodulated subcarrier power-to-interference power.

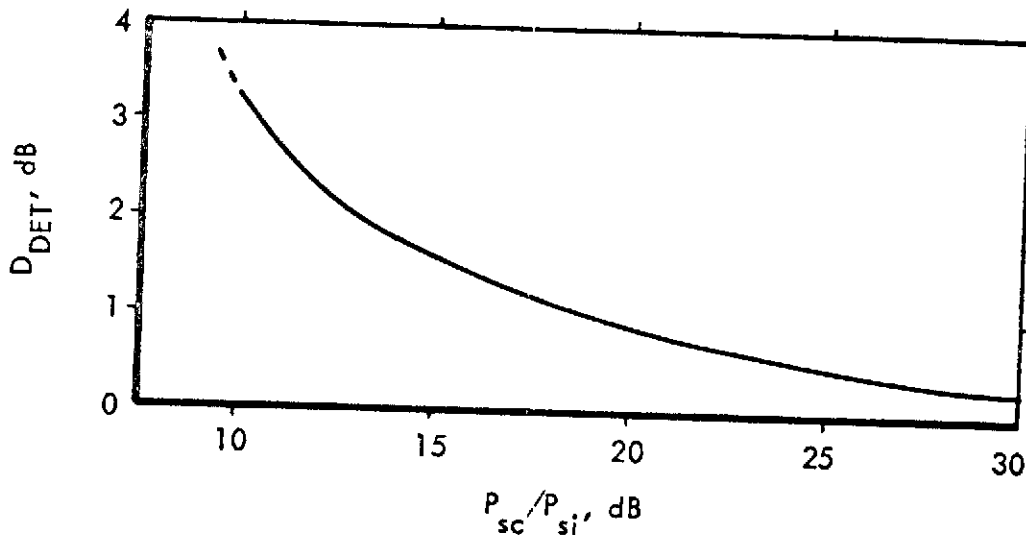


Figure 5.5.2. Degradation of Detection Probability Due to RFI in Subcarrier Passband

5.6 Coding for Error Detection and Correction

In order to assure correct command message transmission, the VHF command system utilizes one or several verification modes to compare the bitstream actually transmitted to the intended bitstream. Verification can be effected at the output of the command encoder and/or via the transmitted signal. Another verification mode exists in retransmission of the bitstream, from the spacecraft to the ground, for comparison with the intended message. In this case, errors can be introduced during retransmission which were not present originally. This problem is amplified due to the fact that the spacecraft's transmitter is power limited.

In addition to utilization of verification schemes, further reliability can be provided by error detecting and/or correcting codes. This kind of scheme is attractive when it is more economical to increase equipment complexity than to increase transmitter power, and when some expansion of the transmission bandwidth can be tolerated.

In a coded system, more bits are transmitted over the channel than are contained in the message. The extra bits, or redundant bits, are selected in such a way that a rule exists whereby with high probability, occurrence of errors during transmission can be detected, and, in some cases, the positions in error can be located and the errors corrected. The system bandwidth is expanded by a factor equal to the ratio of the number of bits transmitted per unit time to the number of message bits per unit time. The reciprocal of this number is called the code rate (not to be confused with data rate). Thus, a rate = $1/2$ system transmits twice as many bits per unit time as the message source generates, and requires twice the bandwidth that would be required if the message bits themselves were transmitted.

Since the considerations with regard to coding are different for uplink and downlink, they will be discussed separately.

5.6.1 Uplink Coding

Generally speaking, coding systems achieving extremely small error rates require extremely complicated decoders. In the uplink, where the decoder must be on board the spacecraft and where transmitter power is not critical, only a very modest coding scheme, if any at all, is called for. One possibility would be a scheme which attempts to detect errors in the received sequence, but requests retransmission of erroneous data rather than attempting to locate and correct the errors. Systems of this kind can be easily implemented and can provide moderate increase in reliability. Consider, for example, use of an extended Hamming Code [5-5] of length 16 and rate $11/16$. To use this code, message bits are grouped

into blocks of 11 bits and for each such block a codeword of 16 bits is transmitted. The mapping of message blocks into codewords is accomplished by a simple logic circuit. A simple decoder exists for this code, which is capable of detecting all patterns of three or fewer transmission errors. Suppose the transmitter expends E_s joules of energy per transmitted bit, and $E_s/N_0 = 3$ dB, for example. Assuming PSK modulation, the bit error probability is

$$p = Q \left(\sqrt{\frac{2E_s}{N_0}} \right) = 0.02289$$

The decoder fails to detect errors in a block of 16 transmitted bits only if four or more of the bits are in error. Thus,

$$\Pr \{ \text{undetected error} \} \leq \sum_{k=4}^{16} \binom{16}{k} p^k (1-p)^{16-k} = 0.00040$$

Now the probability that a block is received without an error is $(1-p)^{16} = 0.69039$. All blocks except those with no errors and those with errors which are undetected must be retransmitted. Therefore, the fraction of blocks requiring retransmission is

$$1 - (1-p)^{16} - \Pr \{ \text{undetected error} \} = 0.30921 \\ \approx 31\%$$

Similarly, 31% of the retransmissions will require another retransmission, and so on. The average number of transmissions required per block is

$$1 + (.30921) + (.30921)^2 + \dots = \frac{1}{1-0.30921} \\ = 1.4476$$

The average energy expended per message bit is then

$$E_b = E_s \times \left(\frac{16}{11} \right) \times (1.4476) = (2.1056) E_s$$

so that $E_b/N_0 = 6.2$ dB. An uncoded PSK system with this E_b/N_0 ratio would exhibit error rate $P_e = 0.00188$. This is the probability of an (undetected) bit error. A reasonable quantity to compare with the block undetected error probability of the coded system would be the probability of receiving a block of 11 consecutive bits in which at least one bit is in error:

$$\Pr \left\{ \text{undetected error in 11 bits} \right\} = 1 - (1 - P_e)^{11} = 0.02049$$

The coded system is seen to perform considerably better than an uncoded system of equal signal energy. An uncoded system which has the same undetected error probability (in an 11-bit block) as the coded system would require $E_b/N_0 = 8.9$ dB, or about a 2.7 dB increase in signal energy.

The numerical results of this section are intended only as examples of the gains that could be achieved by coding. Much lower undetected error probability could be achieved by using more sophisticated codes. However, it should be noted that in the system under consideration here, a built-in error detection scheme is present in the form of the verification loop via downlink. If the downlink is designed to be extremely reliable, then virtually all uplink errors will be detected by the verification loop, without extra error detection equipment. If the verification loop will always be in operation, and if the downlink is reliable, then use of coding in the uplink is probably not justified. On the other hand, if it is desired to limit use of the downlink, and/or the downlink is not extremely reliable, then use of forward error detection in the uplink might be economical.

5.6.2 Downlink Coding

In the downlink, where transmitter power is at a premium and the decoder is on the ground, sophisticated coding schemes can be used to good advantage. The best codes for such applications appear to be rate - 1/2 convolutional codes. (Although lower-rate codes are somewhat more efficient with respect to transmitter power, the simplicity of the rate - 1/2 encoder is, in most applications, worth the extra dB or so it costs.) A simple example of a convolutional

encoder is shown in Figure 5.6.2-1. Each transmitted bit is a linear combination of the present message bit and the m previous bits; the encoder is thus said to have memory m . The probability of error with these codes decreases exponentially with m , while encoder complexity increases proportionally with m . Hence, powerful codes can be implemented with simple equipment on board the spacecraft.

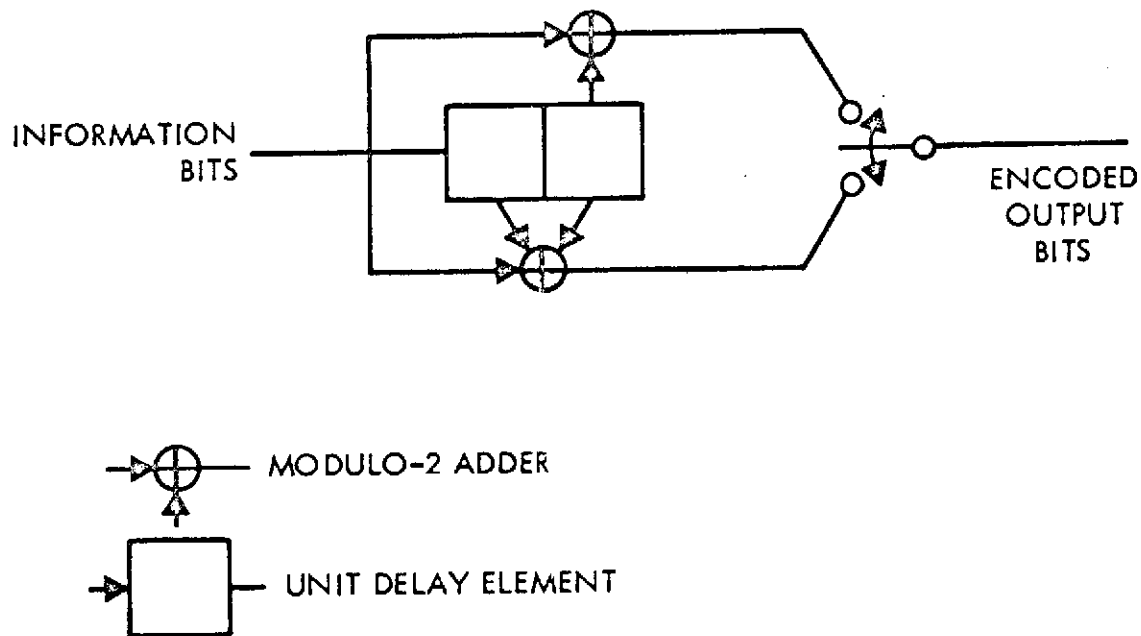


Figure 5.6.2-1. A Rate - 1/2, $m = 2$ Convolutional Encoder (Generators: 101, 111)

The optimum decoding rule for convolutional codes is due to Viterbi [5-6]. The amount of computation per decoded bit performed by this decoder is proportional to 2^m , and the decoder is, therefore, practical only for short codes. Some curves of error rate for Viterbi decoding of short convolutional codes are given in Figure 5.6.2-2. There is one set of curves for the case in which hard decisions are made at the output of the correlator, and another set for the case in which the correlator output is quantized into eight levels. Eight-level quantization is seen to be significantly better than two-level quantization, but it turns out that very little is gained by using more than eight levels.

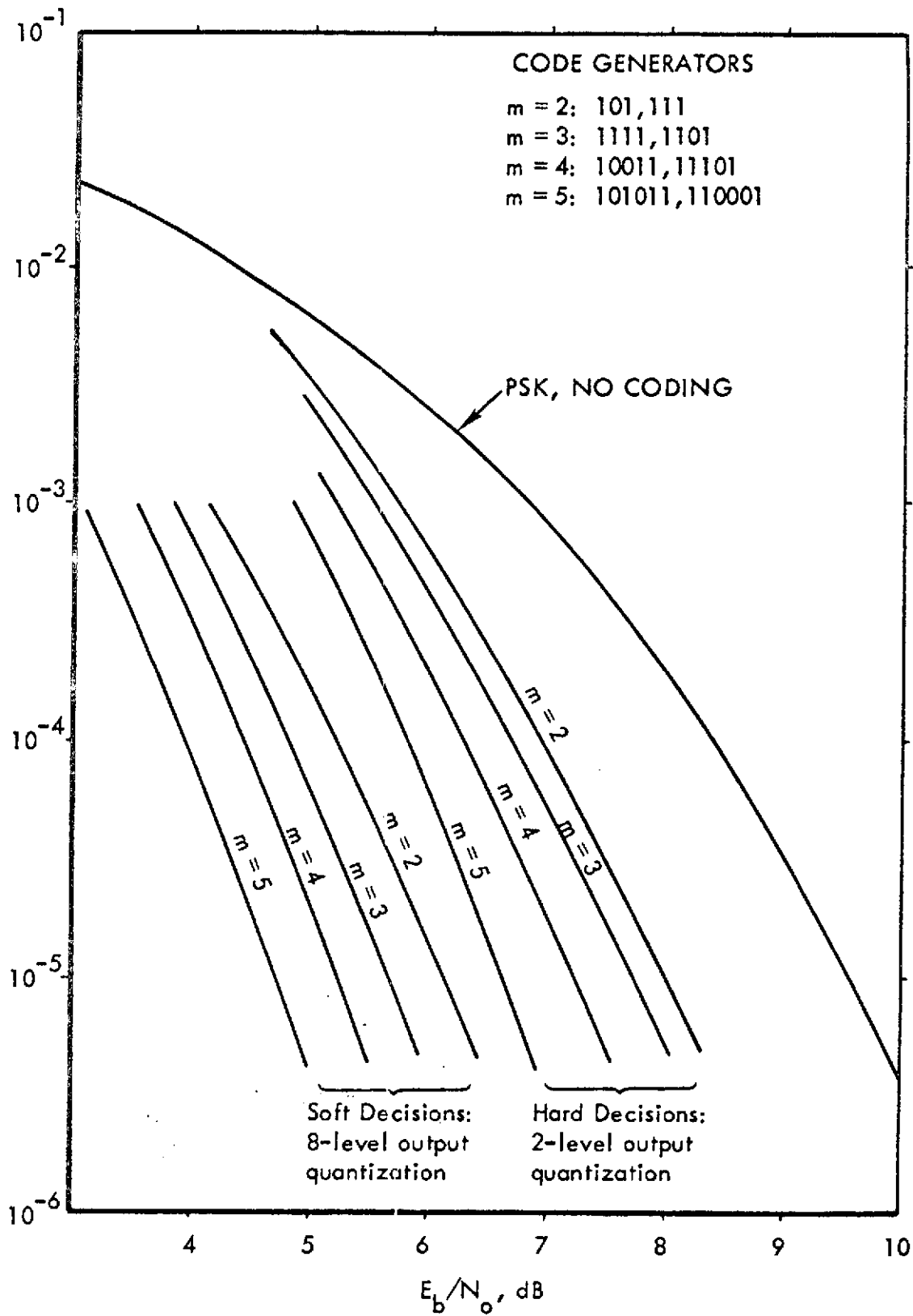


Figure 5.6.2-2. Performance of Rate-1/2 Convolutional Codes with Viterbi Decoding

The impracticality of the Viterbi algorithm for long codes is a significant restriction, since very low error rates require very long codes. An alternative decoding procedure, for which the complexity or amount of computation is relatively insensitive to code memory, is sequential decoding. The amount of computation a sequential decoder performs is a random variable, depending on the pattern of errors introduced during transmission. In order for the average number of computations per decoded bit to be at an acceptable level, it is necessary to operate at about a 3 dB higher value of E_b/N_o than with other decoding methods. For rate - 1/2 codes with hard decisions, E_b/N_o must exceed 4.5 dB; when 8-level quantization is used the minimum becomes about 3 dB. For any E_b/N_o above the minimum value, however, error probability can be made as small as desired (without increase in E_b/N_o) by making m large, with insignificant increase in decoder complexity.

It is important to note that both Viterbi decoding and sequential decoding work well only if the channel is memoryless; that is, if bit errors occur independently. In the system under study, this can be assumed to be the case if the transmission errors are due only to the presence of additive white noise. If transmission errors tend to occur in clusters or "bursts", a different coding scheme, designed for burst error correction, should be used.

Another feature of the present system which may have an effect is the finite message length. Claims made for coded systems are generally made under the assumption of a potentially infinite message sequence; when the message length is finite, the performance may be different. When short codes are used, so that the message length is several times the encoder memory, the effect will be minimal, but when m is large, some degradation from ideal performance should be expected. In any case, it is advisable to encode and decode a "tail" of m zeros at the end of each message. The purpose of the tail is to allow the last few message bits to affect the same number of transmitted bits as the earlier message bits. In the absence of such a tail, that is, when encoding and decoding ceases as soon as the last message bit is processed, the last bits of the message will exhibit a higher probability of error than the other bits because, in effect, fewer parity checks are available on them than on the earlier bits.

5.7 Performance Margin Criterion for PCM/PSK Demodulators

Performance of the optimum PCM/PSK demodulation structure with application to VHF Command Systems has been discussed previously in this section, as well as in Section 2. The difference in optimum performance and the performance expected from a realizable demodulator is the margin of performance. Thus, the margin of performance accounts for implementation losses resulting from use of non-ideal subsystems and components, and nonideal signal structures. Establishment of a margin criterion must also incorporate reasonable hardware complexity and costs.

The PSK demodulators of interest here accommodate signal structures where the clock signal is transmitted with the PSK subcarrier, including AM and Summed Clocks. Another factor which contributes to the margin of performance is therefore the division of total subcarrier power between the unmodulated subcarrier and the clock; that is, the power associated with making bit decisions and that associated with providing the clock.

The margin of performance is established here on the basis of bit error performance, and under energy limited conditions as opposed to peak amplitude limited conditions. Thus, in both clock systems of interest, the performance provided by the total energy in the information and clock bearing signals is being compared with the performance of an ideal, optimum PSK demodulator which uses the same total energy.

5.7.1 AM Clock System

Consideration here is given to establishing a margin of performance applicable to the PSK demodulation structure shown in Figure 5.1.1-1. This configuration accommodates demodulation of a signal structure where the clock is amplitude modulated on the subcarrier.

Optimum bit error performance of a PCM/PSK demodulator is given in Table 2.1.3 as

$$P_e = Q \left(\sqrt{\frac{2E_b}{N_o}} \right), \quad (5.7.1-1)$$

where E_b is the bit energy, and N_o is the single-sided noise spectral density. The demodulator depicted by Figure 5.1.1-1 is suboptimum. This configuration was selected on the basis that it is less complex than an optimum demodulator, but the reduction in bit error performance relative to optimum performance is typically small. Since the total average power in the subcarrier passband (i.e., power out of the receiver's first detector) is shared between the clock and the bit decision process, the effective value of E_b in Equation 5.7.1-1 is reduced in accordance with the efficiency factor, η . It is recalled that η is the fraction of the total bit energy which goes into making the bit decision. Thus, as shown in Table 2.1.3, the bit error probability for the PSK-AM suboptimum demodulator is

$$P_e = Q \left(\sqrt{\frac{2\eta E_b}{N_o}} \right) \quad , \quad (5.7.1-2)$$

with the relationship between m_{cl} and η being

$$\eta = \frac{1}{1 + m_{cl}^2/2}$$

Figure 5.3.3 shows this degradation as a function of clock modulation index, m_{cl} . Maximum degradation is 1.76 dB, corresponding to 100% modulation ($\eta = 0.67$). Employing the results of Figure 2.3-1, more representative is the degradation corresponding to 50% modulation ($\eta = 0.89$); that is, 0.51 dB a factor to be taken into account in establishing the margin of performance.

5.7.1.1 Subcarrier and Clock Reference Phase Jitter

Phase jitter on the subcarrier and clock reference signals is a further cause of degraded PSK demodulator performance. In Section 5.3, degradation in bit error performance due to phase jitter was determined and shown in both cases, as expected, to be a function of signal-to-noise ratio. This requires that the contribution of phase jitter to the margin of performance be determined on the basis of a realistic signal-to-noise ratio. The margin established here is based upon a 13 dB signal-to-noise ratio in the bit rate bandwidth.

With the clock signal-to-noise ratio given by

$$SNR_{cl} = \frac{m_{cl}^2}{2} \frac{P_{sc}}{N_o R} \frac{R}{B_{cl}} \quad ,$$

the value, 13 dB, in the bit rate bandwidth yields a 11 dB signal-to-noise ratio in the clock bandwidth for 50% amplitude modulation. From Figure 5.3.2, the degradation due to clock phase jitter is seen to contribute about 0.2 dB degradation for a clock phase of π radians.

The 13 dB signal-to-noise ratio in the bit rate bandwidth corresponds to 9 dB in the subcarrier passband, $B_{sc} = 4R$. From Figure 5.3.2, the degradation due to subcarrier phase jitter is seen to be less than 0.2 dB for this case.

5.7.1.2 Effects of Bandlimiting Upon Bit Error Performance

Bandlimiting the PSK signal affects the bit error performance by reducing the bit energy through suppression of spectral sidebands. In addition, bandlimiting causes intersymbol interference which also increases the bit error probability. Optimum performance of a synchronous PSK demodulator is obtained only when the effective bandwidth preceding the demodulator is infinite in width. In practice, this suggests that the bandwidth should be large compared to the equivalent bandwidth of the demodulator. Under such conditions, the deleterious effects of bandlimiting are minimized.

In the application here, the subcarrier passband tends to bandlimit the PSK signal. The actual bandlimiting effect is dependent upon the need to isolate the PSK signal from signal structures in adjacent bands. Upper bounds on bit error probability which correspond to bandlimiting NRZ-PSK signals are illustrated in Figure 5.7.1.2 [5-7]. These data are presented for several values of the product, $B_{sc}T$. Substantiating results have been obtained independently [5-8]. Although these results are based upon the use of ideal filters, use of realizable filters (e.g., a three pole Butterworth filter) will lead to results which do not differ greatly. That is, a realizable filter can be closely approximated by an unrealizable filter with delay.

Of particular interest here are the results from Figure 5.7.1.2 for an effective bandwidth equal to four times the bit rate, $B_{sc}T = 4$. It is noted that the worst case degradation in bit error performance due to reduced bit energy and intersymbol interference is about 0.8 dB at a bit error rate corresponding to 13 dB signal-to-noise ratio in the bit rate bandwidth. This value of degradation is used in establishing the margin of performance, and it should be a conservative value for these purposes when coupled with the clock parameters, $m_{c1} = 0.5$ and $\theta_{c1} = \pi$ radians.

5.7.1.3 Margin of Performance

Various factors which must be incorporated into the determination of the performance margin for a PSK-AM demodulator have been discussed above. In addition to these, some account must be made for implementation losses. Such a loss is exemplified by a "threshold offset" in the threshold device associated with making bit decisions, this being a result of tolerances in component values. Since the effects of bandlimiting can be considered as a form of implementation loss also, we estimate the total implementation losses to be 2 dB, a number which includes the 0.8 dB degradation due to bandlimiting.

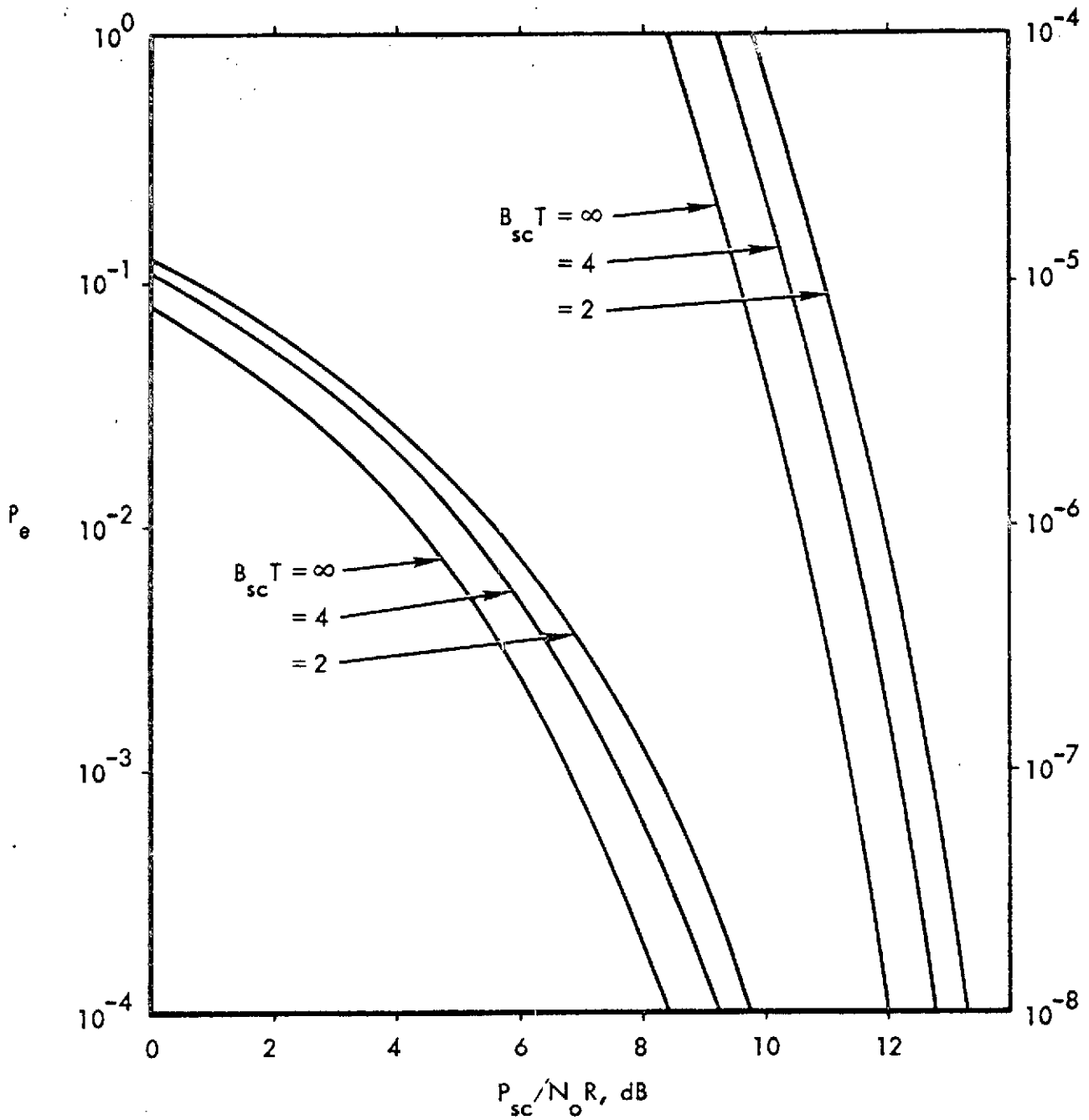


Figure 5.7.1.2. Upper Bounds on Bit Error Probability

Itemization of the various factors which have been established to yield the margin of performance is as follows:

Suboptimum demodulator ($m_{cl} = 0.5$)	0.5 dB
Subcarrier phase jitter	0.2 dB
Clock phase jitter	0.2 dB
Implementation losses	<u>2.0 dB</u>
TOTAL MARGIN	2.9 dB

The 2.9 dB margin of performance established here is based upon assumptions of 50% modulation of the subcarrier by the clock and a 13 dB signal-to-noise ratio requirement in the bit rate bandwidth. If required, adjustment in the margin for different values of modulation index, signal-to-noise ratio and bandlimiting can be made with the aid of the data presented.

5.7.2 Summed Clock System

Consideration here is given to establishing a margin of performance applicable to the PSK demodulation structure of Figure 5.1.2 for the Summed Clock system. Again, there is degradation from optimum performance attributed to power sharing between the clock and the bit decision process. Degradation due to reference subcarrier and clock phase jitter is again based upon the requirement for 13 dB signal-to-noise ratio in the bit rate bandwidth. Degradation due to subcarrier reference phase jitter is essentially equal to that for the AM Clock system.

In this case, the clock is added to the PSK subcarrier with a clock-to-subcarrier amplitude ratio of α , where the relationship between α and η is given by

$$\eta = \frac{1}{1 + \alpha^2} \quad (5.7.2-1)$$

As shown in Table 2.1.3, the bit error probability for the PSK-Summed demodulator is given by Equation 5.7.1-2, with η for this case defined above. From Figure 2.3-1, an appropriate division of power can be selected to correspond to $\eta = 0.89$ ($\alpha = 0.35$) as in the PSK-AM case.

With the clock signal-to-noise ratio in this case given by

$$\text{SNR}_{cl} = \alpha^2 \frac{P_{sc}}{N_o R} \frac{R}{B_{cl}}$$

13 dB in the bit rate bandwidth again yields 11 dB of clock signal-to-noise ratio for $\eta = 0.89$ ($\alpha = 0.35$). From Figure 5.3.2, degradation due to clock jitter is seen to be about 0.4 dB.

In the Summed Clock case, the effects of bandlimiting of interest here correspond to an effective bandwidth equal to four times the bit rate, $B_{scT} = 4$ in Figure 5.7.1.2. Corresponding to a bit error rate resulting from a 13 dB signal-to-noise ratio in the bit rate bandwidth, the degradation is seen to be approximately 0.8 dB or less, since Figure 5.7.1.2 depicts an upper bound on the bit error probability.

5.7.2.1 Margin of Performance

The major factors which contribute to establishing the margin of performance for the Summed Clock system of PSK demodulation have been presented above. Accounting for implementation losses as before, these factors are itemized as:

Power division factor ($\alpha = 0.35$)	0.5 dB
Subcarrier phase jitter	0.2 dB
Clock phase jitter	0.4 dB
Implementation losses	<u>2.0 dB</u>
TOTAL MARGIN	3.1 dB

The 3.1 dB margin of performance given above is based upon a 13 dB signal-to-noise ratio in the bit rate bandwidth and a clock-to-subcarrier summing ratio of 0.35. As in the case of the PSK-AM demodulator margin, information is provided to make necessary adjustments to the margin under conditions different from those assumed here.

5.7.3 Comparative Performance

The foregoing results show that the performance of the PSK-AM and PSK-Summed demodulator are equal to within several tenths dB under the assumed conditions. The difference is attributed to an optimum choice of clock phase in the PSK-AM case. If $\theta_{c1} = \pm \pi/2$ radians were selected, the margin in each case would be approximately the same.

It should be emphasized at this point that the performance margins given are for energy-limited conditions, the conditions under which the PSK demodulators would probably be tested. However, if either demodulator is tested as an integral part of a total receiver system, the system and demodulator would operate under peak-limited conditions. Figure 2.3-2 indicates that the PSK-Summed demodulator performs best under this condition.

5.8 Summary and Conclusions

Theoretical analyses have been conducted and reported which are concerned with the prime objectives of a command system, that of correct transmission of command data in as efficient a manner as possible. PSK demodulators for the AM and Summed Clock systems have been defined. Using a basic hysteresis squelch strategy, various probabilities associated with correct message transmission have been computed, including bit error, message error, message deletion and false start probabilities. Emphasis has been placed upon investigation of system parameters which significantly influence these probabilities. Theoretical data are graphically presented which cover a range of parameter values such as false start rates and squelch threshold levels. Consideration is also given to effects of RFI upon squelch operation. This effect is estimated for selected interfering signals.

Further factors influencing operation of a PSK demodulator include phase jitter on the reference subcarrier and clock. Degradation due to such has been computed and presented here. A criterion has been established for evaluating a PSK demodulator's performance relative to theoretical. This margin is shown to be 2.9 dB and 3.1 dB respectively for the AM and Summed Clock systems.

Finally, error detection and correction coding schemes are considered in view of constraints imposed by receive complexity and available power. Consideration here has been given to typical uplink and downlink applications.

References

- [5-1] Gardner, F. M., Phaselock Techniques, John Wiley and Sons, New York, 1966, pp. 167-169.
- [5-2] Davenport, W. B., Jr., and W. L. Root, An Introduction to the Theory of Random Signals and Noise, McGraw-Hill Book Co., New York, 1958, pp. 257-267.
- [5-3] Gardner, F. M., *ibid.*, pp. 169.
- [5-4] Papoulis, A., Probability, Random Variables and Stochastic Processes, McGraw-Hill Book Co., New York 1965, pp. 147.
- [5-5] Peterson, W. W. and E. J. Weldon, Jr., Error Correcting Codes, Second Edition, MIT Press, Cambridge, Mass., 1972, pp. 117-119.
- [5-6] Viterbi, A. J., "Error Bounds for Convolutional Codes and an Asymptotically Optimum Decoding Algorithm", IEEE Trans. on Information Theory, Vol. IT-13, April 1967, pp. 260-269.
- [5-7] Hartmann, H. P., "Degradation of Signal-to-Noise Ratio Due to IF Filtering", IEEE Trans. on Aerospace and Electronic Systems, Vol. AES 5, No. 1, January 1969.
- [5-8] Jones, J. J., "Filter Distortion and Intersymbol Interference Effects on PSK Signals", IEEE Trans. on Communication Technology, Vol. COM-19, No. 2, April 1971.

6.0 UPLINK CARRIER MODULATION

The subcarrier signals discussed previously are transmitted to the spacecraft by one of several RF modulation schemes. The purpose of this section is to determine how the RF parameters affect overall system performance.

The principal results of this section are formulas relating bit error probability to carrier-to-noise power ratio. To derive these results, the output signal and noise characteristics of the RF detector are obtained. Then, with suitable approximations and assumptions, the error probability results for subcarrier detectors derived in Section 2 are employed. (The formulas used are those assuming perfect synchronization, so that degradation due to jitter, as determined in Section 5, must be accounted for separately.) Analytical expressions relating P_e to the ratio C/N_0R , where C is the unmodulated carrier power, N_0 is the one-sided noise power spectral density, and R is the data rate, are obtained for AM and narrowband PM. These expressions are subject to an additional threshold constraint; that is, they are valid only for ratios of C/N_0R in excess of some threshold value depending on a choice of p (and in the PM case, β).

The chief obstruction to obtaining analytical relationships between P_e and C/N_0R for an FM uplink is that for typical values of the modulation index β , the operating point lies well below threshold, where the additive white Gaussian noise model for the detector input fails. Approximate results are obtained by ignoring the non-Gaussian character of the noise and using an empirical formula for the output noise spectral density. In addition, a lower bound on P_e is obtained, the form of which indicates that the usual "wideband FM improvement" cannot be exploited in these transmission schemes.

Amplitude, frequency and phase modulators with conventional demodulators are discussed in Sections 6.1 - 6.3. In Section 6.4 we study the response of receivers of one kind to signals of another kind. Finally, Doppler effects and their impact on RF and subcarrier demodulator design are considered in Section 6.5.

6.1 AM Carrier Modulation

When the subcarrier amplitude-modulates the RF carrier, the resulting transmitted signal has the form

$$e_c(t) = A_c \left[1 + m_c e_{sc}(t) \right] \cos \omega_c t \quad (6.1-1)$$

where A_c is the amplitude of the unmodulated carrier, m_c is the RF modulation index, ω_c is the angular carrier frequency, and $e_{sc}(t)$ is the subcarrier signal, which may be PSK or FSK, with AM or Summed Clock. We assume $|e_{sc}(t)| \leq 1$ (with equality for some t); the subcarrier signal is therefore peak - constrained, and when applying results from Section 2, we will use formulas appropriate to peak constraints.

When $m_c < 1$ and the received signal-to-noise ratio is sufficiently high, the signal can be demodulated by the receiver shown in Figure 6.1-1. The bandpass filter is assumed to be wide enough to pass $e_c(t)$ with negligible degradation, so that the filter output is

$$y_1(t) = e_c(t) + n(t)$$

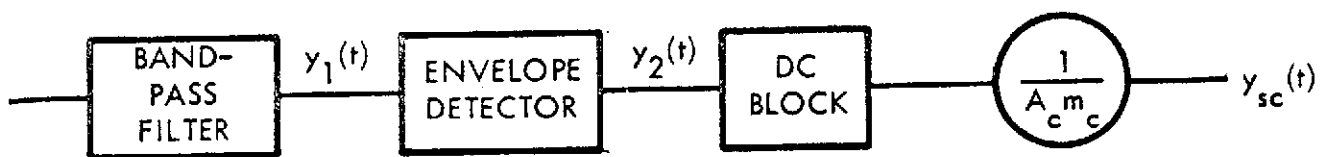


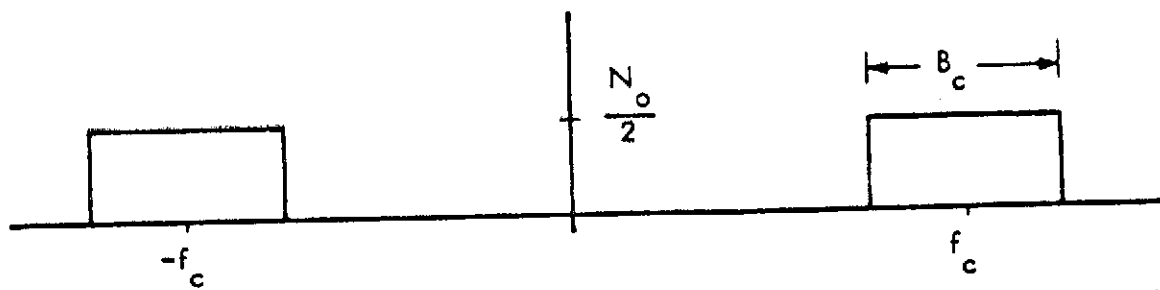
Figure 6.1-1. AM Receiver

where $n(t)$ has the spectral density illustrated in Figure 6.1-2(a). This narrowband noise process can be represented in the form

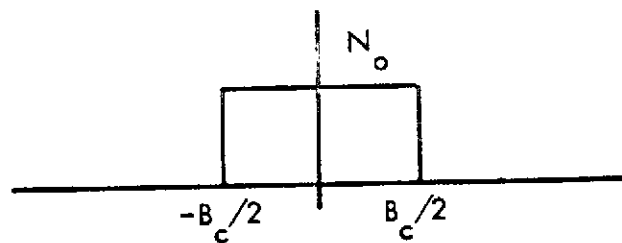
$$n(t) = n_c(t) \cos \omega_c t + n_s(t) \sin \omega_c t$$

where the quadrature components $n_c(t)$ and $n_s(t)$ both have the power spectral density of Figure 6.1-2(b). The input to the envelope detector can then be written

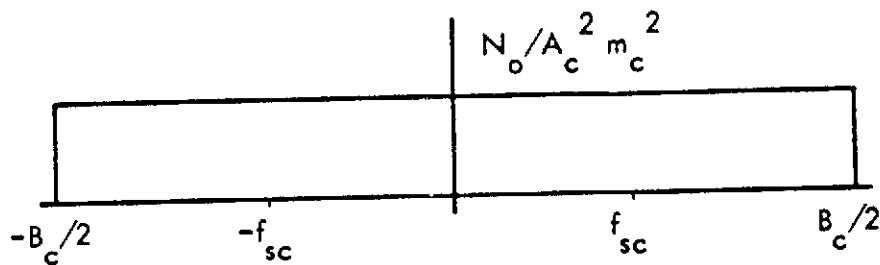
$$y_1(t) = \left[A_c (1 + m_c e_{sc}(t)) + n_c(t) \right] \cos \omega_c t + n_s(t) \sin \omega_c t$$



(a)



(b)



(c)

Figure 6.1-2. Noise Spectra Associated with AM Receiver (High C/N_oR)

The output of the envelope detector, assuming ideal envelope extraction, is

$$y_2(t) = \sqrt{\left[A_c (1 + m_c e_{sc}(t)) + n_c(t) \right]^2 + n_s^2(t)} \quad (6.1-2)$$

When the received signal-to-noise ratio is high, the first term under the radical will, with high probability, be considerably greater than the second.

Under this assumption we may neglect $n_s(t)$ and say

$$y_2(t) \approx A_c (1 + m_c e_{sc}(t)) + n_c(t) \quad (6.1-3)$$

Following the dc block and the scalar multiplication we have

$$y_{sc}(t) = e_{sc}(t) + n_{sc}(t)$$

where

$$n_{sc}(t) = \frac{n_c(t)}{A_c m_c}$$

Thus $n_{sc}(t)$ has the power spectral density shown in Figure 6.1-2(c). Since the spectrum is flat over the frequency band of interest, we may assume that it remains flat outside this band; i.e., that the input to the subcarrier detector consists of the signal $e_{sc}(t)$ in the presence of additive white Gaussian noise of spectral density $N_o/A_c^2 m_c^2$. The results of Section 2 can now be applied, except that the N_o appearing in the formulas there must be replaced by $2N_o/A_c^2 m_c^2$ (since a noise spectral density of $N_o/2$ was assumed in deriving those formulas).

If the subcarrier modulation is PSK with AM Clock, then from Table 2.1.4, with $a = 1$, we obtain

$$P_e = Q \left(\sqrt{\frac{A_c^2}{2N_o R} m_c^2 \frac{\eta}{2 - \eta + 2 \sqrt{2\eta(1-\eta)}}} \right)$$

Recognizing that $A_c^2/2$ is the power in the pure carrier term, and denoting this as C , we can rewrite this as

$$P_e = Q \left(\sqrt{\frac{C}{N_o R} \frac{m_c^2 \eta}{2 - \eta + 2 \sqrt{2\eta(1-\eta)}}} \right)$$

For Summed Clock, we obtain

$$P_e = Q \left(\sqrt{\frac{C}{N_o R} \frac{m_c^2 \eta}{1 + 2 \sqrt{\eta(1-\eta)}}} \right)$$

The corresponding expressions for noncoherent FSK are*

$$P_e = \frac{1}{2} \exp \left\{ - \frac{C}{2N_o R} \frac{m_c^2 \eta}{2 [2 - \eta + 2 \sqrt{2\eta(1-\eta)}]} \right\} \quad \text{AM Clock}$$

$$P_e = \frac{1}{2} \exp \left\{ - \frac{C}{2N_o R} \frac{m_c^2 \eta}{2 [1 + 2 \sqrt{\eta(1-\eta)}]} \right\} \quad \text{Summed Clock}$$

The results are illustrated in Figure 6.1-3 for $\eta = 8/9$, the approximate optimum value determined in Section 2.3, and $m_c = 0.8$, the modulation index specified in the VHF PCM/FSK Command Standard [2-2].

*Here and hereafter we will tabulate results only for PSK and noncoherent FSK, and only for Summed Clock and AM Clock with suboptimum receiver, because these are the only cases of significant practical interest.

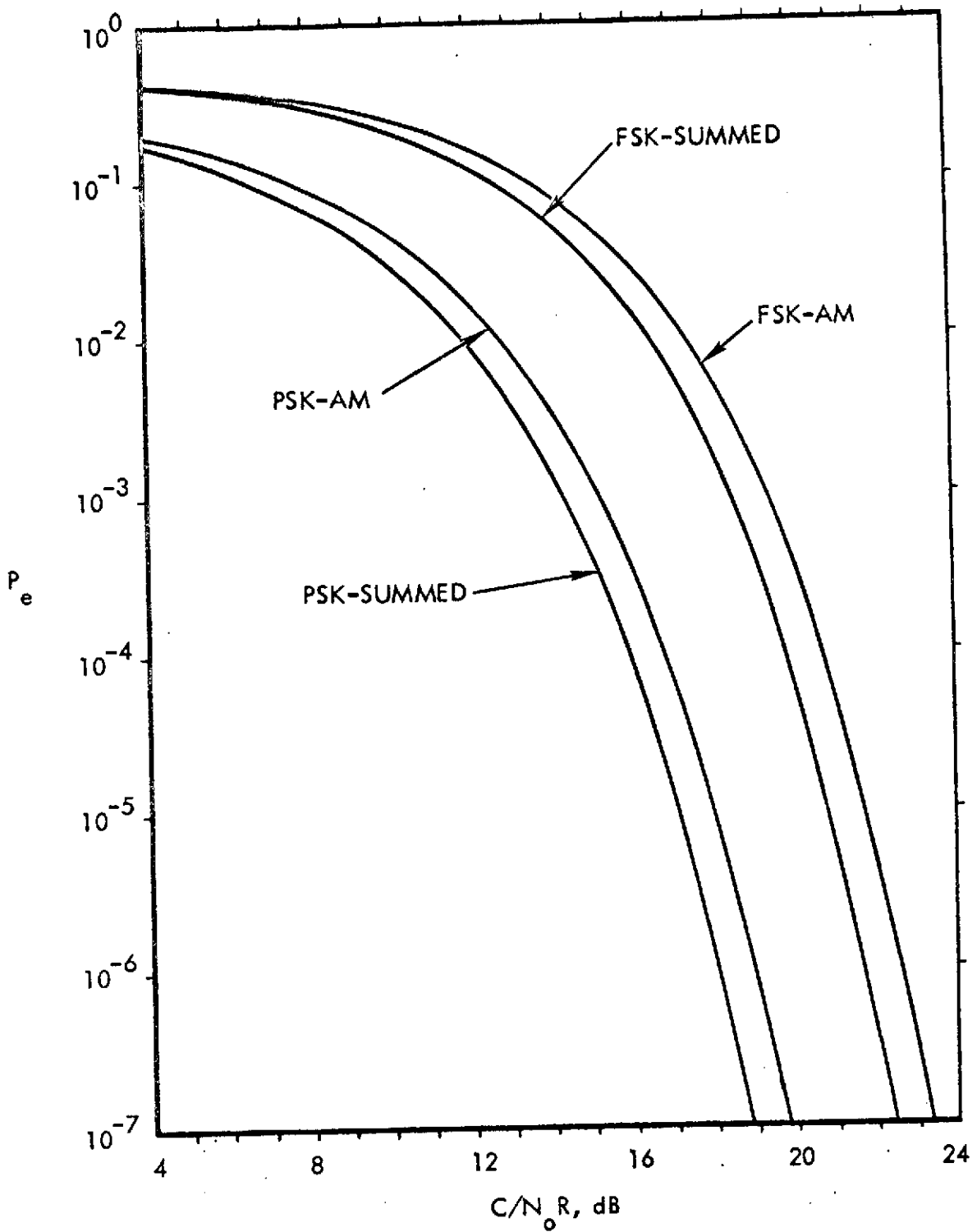


Figure 6.1-3. Error Probability for AM Uplink Above Threshold, $m_c = 0.8$

Although the curves of Figure 6.1-3 show a wide range of C/N_0R , our derivation is only valid at high signal-to-noise ratios, since a critical step in the derivation was to neglect the quadrature noise term appearing in Equation 6.1-2. Because of the nonlinearity of the envelope detector, at low signal-to-noise ratios, receiver performance degrades rapidly from that shown in the curves, giving rise to a receiver threshold effect. Thus, the results we have obtained apply only above threshold, i.e., at sufficiently high signal-to-noise ratios for the assumption of signal plus Gaussian noise into the PSK or FSK detector to apply with high probability. Below threshold, determination of overall receiver performance (P_e versus C/N_0R) is complicated by the fact that the noise into the PSK or FSK detector is decidedly non-Gaussian, and the usual formulas for error probability do not apply. It would appear that computer simulation is the most promising means to determine the dependence of P_e on C/N_0R near threshold.

It is generally accepted [6-1], [6-2], that the envelope detector threshold occurs in the vicinity of 0 to 10 dB received signal-to-noise ratio; this is usually of little practical significance since signal quality requirements usually call for much higher signal-to-noise ratio than this. However, in our application, note from Figure 6.1-3 that error probability of 10^{-7} requires in the vicinity of 20 dB signal-to-noise ratio in the bit-rate bandwidth. Since $B_c \approx 2pR$ and $p \geq 6$, the required signal-to-noise ratio in the RF bandwidth is 11 dB or more below this. Thus systems of the kind we are discussing could operate in the region where the threshold effect is a consideration.

Threshold problems can be avoided by using a synchronous receiver. It can be shown that such a receiver behaves in accordance with the curves of Figure 6.1-3 for all values of C/N_0R ; that is, there is no threshold effect. The synchronous receiver is considerably more complex than the envelope receiver, because of the need to synchronize to the received carrier.

The most practical approach to dealing with the problem appears to be simply to operate in the threshold region and suffer whatever losses of efficiency are incurred. The difficulty is determining just what the loss is. While considerable effort has been expended on analyzing envelope detectors below threshold, the analyses have generally dealt with output signal-to-noise ratios, and not the spectral and statistical properties of the output noise process. Knowledge of output SNR is insufficient to determine overall performance, because, as we have noted, unless the noise into the PSK or FSK detector is Gaussian with a flat spectrum, the error probability of the detector is unknown.

The standard analyses of envelope detectors (e.g., [6-3], [6-4]) indicate that above threshold, output SNR varies linearly with input SNR, while below threshold, output SNR varies with the square of the input SNR. The receiver characteristic thus has the rough form of Figure 6.1-4 where for convenience we take the threshold to occur at 0 dB.

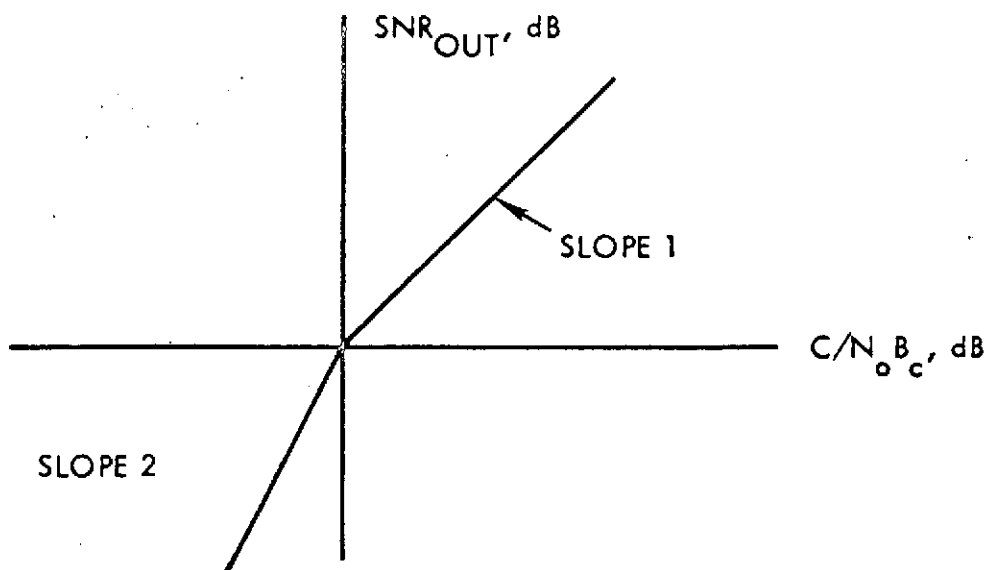


Figure 6.1-4. Performance Curve for AM Receiver

If we assume that the fact that below threshold, the noise is nonwhite and non-Gaussian has no significant effect on the PSK detector error probability, then we would expect the overall P_e versus $C/N_o R$ curve to have the appearance of Figure 6.1-5; here $(C/N_o R)^*$ is the value corresponding to $C/N_o B_c = 1$, and γ is a constant depending on η , m_c , and the kind of synchronization scheme used. While this is probably a satisfactory rough approximation to the behavior of P_e , more careful means must be employed to obtain specific values.

6.2 FM and Noncoherent PM Carrier Modulation

If the subcarrier signal angle modulates the RF carrier, the resulting signal is

$$e_c(t) = A_c \cos [\omega_c t + \phi(t)] \quad (6.2-1)$$

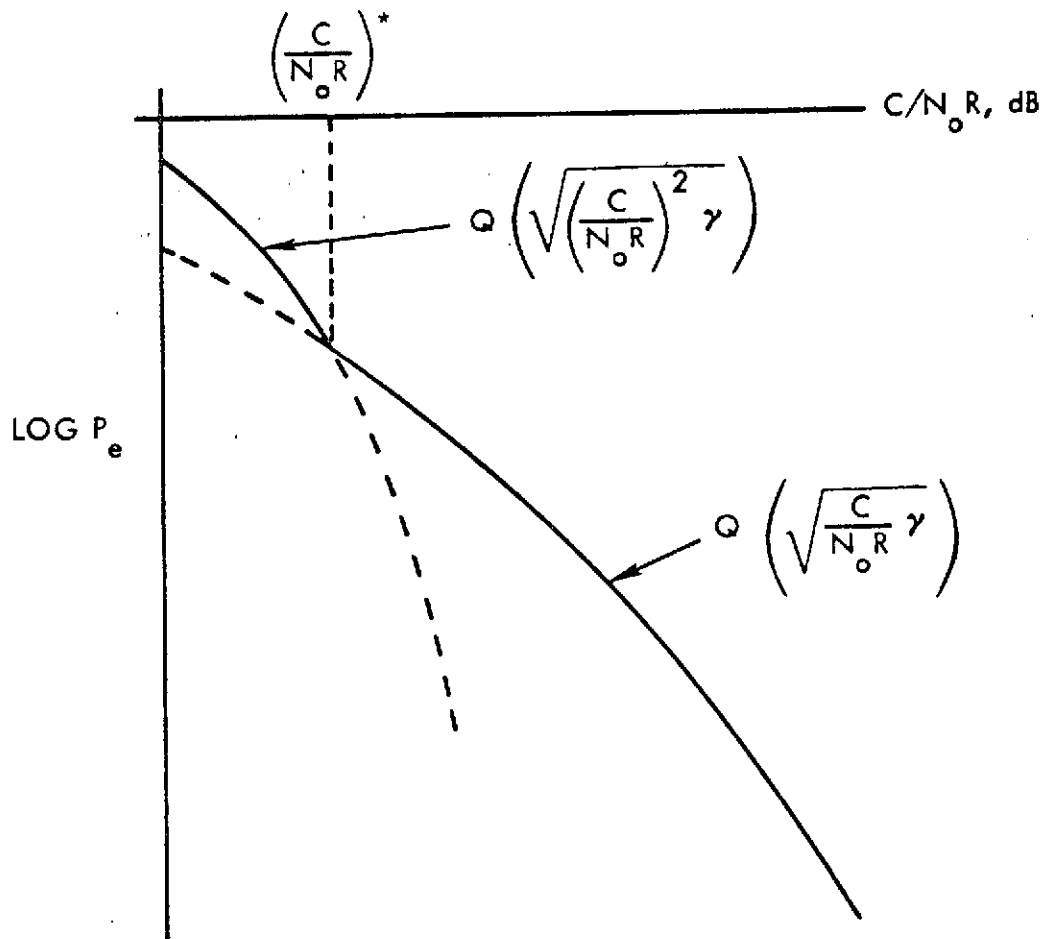


Figure 6.1-5. Approximate Error Probability Curve for PSK/AM

where for FM

$$\phi(t) = k \int_{t_0}^t e_{sc}(s) ds$$

and for PM

$$\phi(t) = k e_{sc}(t)$$

Since FM by $e_{sc}(t)$ is the same as PM by $\int e_{sc}(t) dt$, any FM receiver can be converted to a PM receiver by integrating its output. A phase demodulator constructed this way is called a noncoherent phase demodulator. In the next section we will consider a different kind of phase demodulator which synchronizes to a pure carrier component in the received signal and demodulates coherently.

The receiver to be considered in this section is that shown in Figure 6.2-1. The discriminator is a device whose output is the instantaneous frequency of the input. It can be shown [6-2] that if the bandwidth of the bandpass filter is wide enough to pass $e_c(t)$ with negligible distortion, then the instantaneous frequency of $y_1(t)$ is

$$y_2(t) = \frac{d}{dt} \left[\omega_c t + \phi(t) + \tan^{-1} \left\{ \frac{n_1(t)}{A_c + n_2(t)} \right\} \right]$$

where $n_1(t)$ and $n_2(t)$ are band-limited white Gaussian noise processes with spectral density N_0 .



Figure 6.2-1. FM Receiver

When the input signal-to-noise ratio is high, $A_c \gg n_1(t)$ and $A_c \gg n_2(t)$ with high probability. Under this assumption, we have the approximation

$$\tan^{-1} \left\{ \frac{n_1(t)}{A_c + n_2(t)} \right\} \approx \tan^{-1} \left\{ \frac{n_1(t)}{A_c} \right\} \approx \frac{n_1(t)}{A_c} \quad (6.2-2)$$

so that

$$y_2(t) \approx \omega_c + \frac{d\phi}{dt} + \frac{1}{A_c} \frac{dn_1}{dt}$$

Following the dc block we have

$$y_3(t) \approx \frac{d\phi}{dt} + \frac{1}{A_c} \frac{dn_1}{dt} \quad (6.2-3)$$

The high signal-to-noise ratio condition leading to Equation 6.2-2 gives rise to a threshold similar to that just observed in connection with the envelope detector. A generally accepted threshold value [6-2] for the discriminator-type receiver is at $C/N_o B_c = 10$. As before, translating to $C/N_o R$ increases the threshold value considerably. For example, from Figure 3.3.2-3, a PSK/FM signal with $\beta = 2$ has 98% of its power within $3f_{sc}$ on each side of f_c ; thus $B_c \approx 2 \cdot 3 f_{sc} = 6 pR$, and the threshold is at

$$\frac{C}{N_o R} = \frac{C}{N_o B_c} \cdot \frac{B_c}{R} = 60 p$$

For the minimum value of $p = 6$, this yields a 25.5 dB threshold, well above the $C/N_o R$ which would be required for reasonable P_e if there were no threshold effect. Thus, typical operating points lie well below threshold.

As before, performance of the system cannot be exactly determined; however, it is possible to approximate the performance by replacing the discriminator noise output by white Gaussian noise of spectral density $S(f_{sc})$, where $S(f)$ is the actual discriminator output noise power spectral density. An empirical formula for $S(f)$ with the signal format under discussion is

$$S(f) = 1.5 B_{IF} e^{-1.2r} + 0.7 \beta f_{sc} e^{-r} (1 - e^{-r})^2 + \frac{(1 - e^{-r})^2}{2r B_{IF}} f^2$$

where $r = C/N_o B_{IF}$ and B_{IF} is the IF bandwidth, taken here for simplicity to be the Carson's Rule bandwidth $B_{IF} = 2(\beta + 1) f_{sc}$. Using this we obtain the curves of Figure 6.2-2. In these curves, $\eta = 0.89$ is used, although there is no guarantee that this value is optimum, since it was obtained under the assumption of white Gaussian noise.

Also shown in Figure 6.2-2 is a lower bound to P_e . This bound, which uses $\eta = 1.0$ for simplicity, is obtained by noting that the correlation coefficient between two PSK/FM signals with FM modulation index β is $J_0(2\beta)$. Thus using Equation 2.1-1,

$$P_e = Q \left(\sqrt{\frac{C}{N_o R} (1 - J_0(2\beta))} \right) \quad (6.2-4)$$

for a receiver which demodulates coherently at RF and subcarrier. Equation 6.2-4 is thus a fairly conservative lower bound to P_e for both PSK/FM and FSK/FM for any value of η . This equation also shows that the "FM improvement" generally expected in analog FM systems is not available here since as β becomes large, $J_0(2\beta)$ approaches zero and the bound becomes independent of β (rather than decreasing with increasing β , as FM improvement would require).

To consider the case of phase modulation, we note from Table 3.4 that for the modulation indices of interest, $\beta \leq 0.5$, the RF bandwidth is approximately the same as that for an AM uplink. Thus the threshold constraint is not as severe as in FM, so we carry out the analysis assuming that the approximation in Equation 6.2-2 is valid. As with the AM analysis, however, the results must be interpreted with the threshold condition in mind.

For PM, $\phi(t) = k e_{sc}(t)$. Since the constant k is the phase modulation index, we relabel it β , so that from Equation 6.2-3, we have

$$y_3(t) = \beta \frac{de_{sc}}{dt} + \frac{1}{A_c} \frac{dn_1}{dt}$$

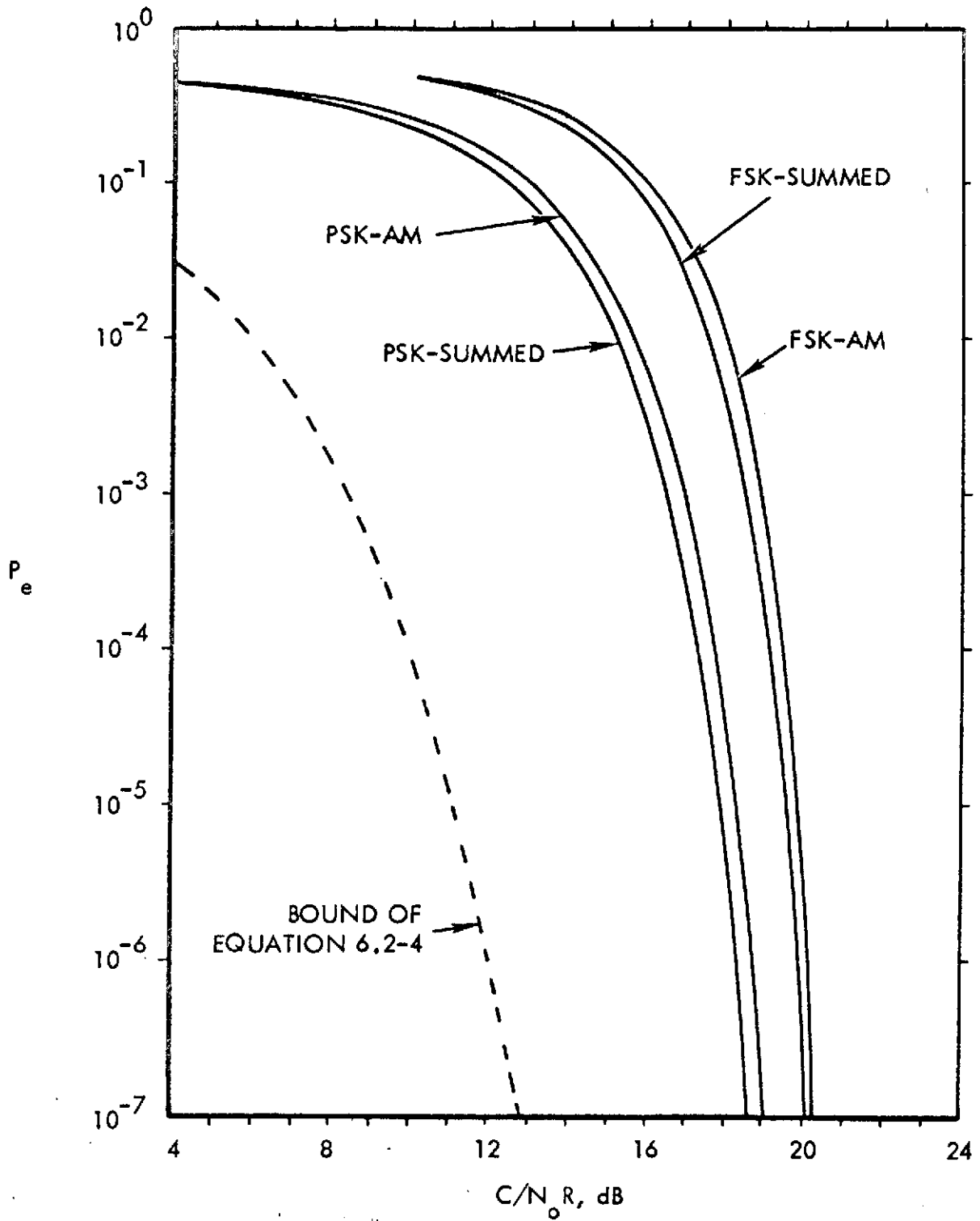


Figure 6.2-2. Approximate Bit Error Probability for FM Uplink with $\beta = 2$ and $p = 6$

The appropriate receiver is, as we have noted before, simply the FM receiver of Figure 6.2-1 followed by an integrator. The integrator output is

$$y_{sc}(t) = e_{sc}(t) + n_{sc}(t)$$

where $n_{sc}(t)$ is band-limited white noise of spectral density

$$\frac{N_o^2}{A_c^2 \beta^2}$$

Removing the band-limitation and making appropriate substitutions into the formulas of Table 2.1.4 yields

$$P_e = Q \left(\sqrt{\frac{C}{N_o R} \beta^2 \frac{\eta}{2-\eta + 2\sqrt{2\eta(1-\eta)}}}} \right) \quad \text{PSK-AM/PM}$$

$$P_e = Q \left(\sqrt{\frac{C}{N_o R} \beta^2 \frac{\eta}{1 + 2\sqrt{\eta(1-\eta)}}}} \right) \quad \text{PSK-Summed/PM}$$

$$P_e = \frac{1}{2} \exp \left\{ - \frac{C}{2N_o R} \beta^2 \frac{\eta}{2[2-\eta + 2\sqrt{2\eta(1-\eta)}]} \right\} \quad \text{FSK-AM/PM}$$

$$P_e = \frac{1}{2} \exp \left\{ - \frac{C}{2N_o R} \beta^2 \frac{\eta}{2[1 + 2\sqrt{\eta(1-\eta)}]} \right\} \quad \text{FSK-Summed/PM}$$

Error probability curves for PM with $\beta = 0.5$ are shown in Figure 6.2-3. The parameter η is chosen as $8/9$ in all cases.

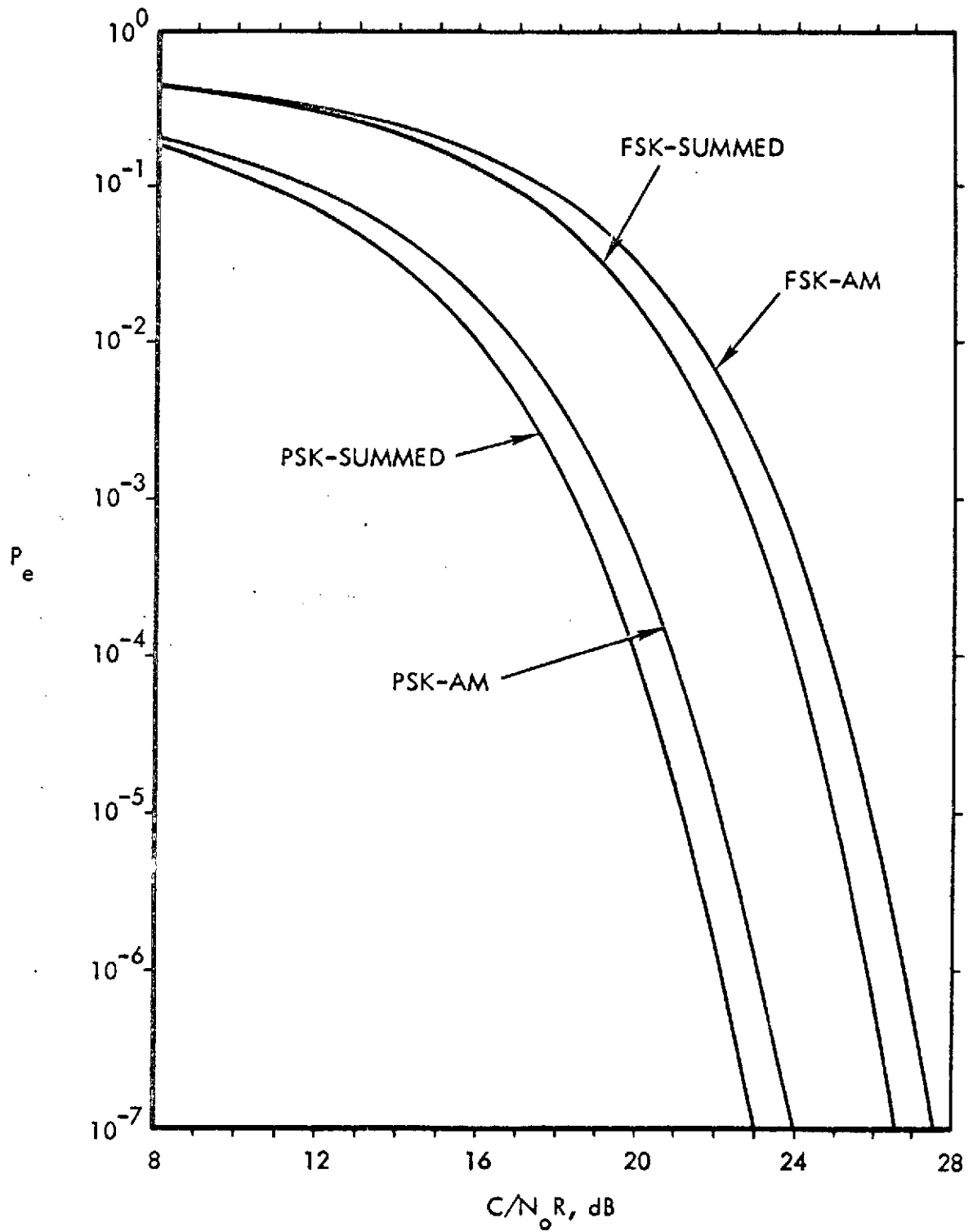


Figure 6.2-3. Error Probability for PM Uplink Above Threshold, $\beta = 0.5$

6.3

Coherent PM Carrier Modulation

When phase modulation is used with a sufficiently small modulation index, the device shown in Figure 6.3-1 can be used to demodulate the signal. Since it operates by synchronizing to a carrier component in the received signal, it is called a coherent PM demodulator. For simplicity, we first consider the special case of PSK subcarrier with no clock; i.e.,

$$e_c(t) = A_c \cos \left[\omega_c t + \beta e_{sc}(t) \right] \quad (6.3-1)$$

where

$$e_{sc}(t) = x(t) \sin \omega_{sc} t$$

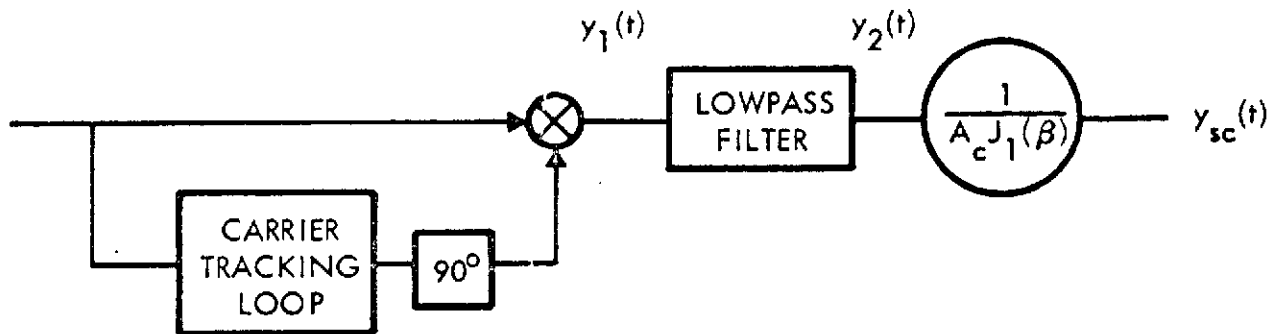


Figure 6.3-1. Coherent PM Receiver

Here $x(t)$ is a random signal which maintains a constant value ± 1 over each bit interval.

From Equation 6.3-1, we obtain

$$\begin{aligned} e_c(t) &= A_c \cos(\beta x(t) \sin \omega_{sc} t) \cos \omega_c t \\ &\quad - A_c \sin(\beta x(t) \sin \omega_{sc} t) \sin \omega_c t \end{aligned} \quad (6.3-2)$$

Since $x(t) = \pm 1$, and since cosine is even and sine is odd,

$$\begin{aligned} \cos(\beta x(t) \sin \omega_{sc} t) &= \cos(\beta \sin \omega_{sc} t) \\ &= J_0(\beta) + 2 \sum_{k=1}^{\infty} J_{2k}(\beta) \cos 2k \omega_{sc} t \end{aligned}$$

and

$$\begin{aligned} \sin(\beta x(t) \sin \omega_{sc} t) &= x(t) \sin(\beta \sin \omega_{sc} t) \\ &= x(t) \left[2 \sum_{k=0}^{\infty} J_{2k+1}(\beta) \cos(2k+1) \omega_{sc} t \right] \end{aligned}$$

where $J_k(\cdot)$ is the Bessel function of the first kind of order k . Substituting into Equation 6.3-2 yields

$$\begin{aligned} e_c(t) &= A_c J_0(\beta) \cos \omega_c t \\ &+ A_c \sum_{k=1}^{\infty} J_{2k}(\beta) \left[\cos(\omega_c + 2k \omega_{sc}) t + \cos(\omega_c - 2k \omega_{sc}) t \right] \\ &+ A_c x(t) \sum_{k=0}^{\infty} J_{2k+1}(\beta) \left[\cos(\omega_c + (2k+1) \omega_{sc}) t \right. \\ &\left. - \cos(\omega_c - (2k+1) \omega_{sc}) t \right] \end{aligned} \tag{6.3-3}$$

When $e_c(t)$ is multiplied by a sinusoid in phase quadrature with the carrier, the result is:

$$\begin{aligned}
 y_1(t) &= -e_c(t) \sin \omega_c t \\
 &= A_c J_1(\beta) e_{sc}(t) + A_c x(t) \sum_{k=1}^{\infty} J_{2k+1}(\beta) \sin(2k+1) \omega_{sc} t \\
 &\quad + \text{terms of frequency near } 2\omega_c
 \end{aligned}$$

If ω_{sc} is greater than the bandwidth of $x(t)$ then the low-pass filter can be chosen such that the first term is passed and all remaining terms blocked, yielding an output

$$y_2(t) = A_c J_1(\beta) e_{sc}(t) \quad (6.3-4)$$

$$y_{sc}(t) = e_{sc}(t)$$

The fact that $x_{sc}(t)$ can be recovered without distortion regardless of β (as long as $J_1(\beta) \neq 0$) depends strongly on the fact that $x_{sc}(t)$ was assumed to be a pure PSK signal; as we will see later, in general, distortion will result unless β is small.

In the presence of noise, the accuracy with which the receiver can lock onto the carrier depends on the signal-to-noise ratio in the tracking loop, which in turn is proportional to $J_0^2(\beta)$. In addition, the output signal-to-noise ratio is proportional to $J_1^2(\beta)$. The system thus operates best at a value of β for which $J_0^2(\beta)$ and $J_1^2(\beta)$ are both large. Plots of $J_0(\beta)$ and $J_1(\beta)$ for $0 \leq \beta \leq 2$ are shown in Figure 6.3-2, along with the small- β approximations:

$$J_0(\beta) \approx 1 - \frac{\beta^2}{4} \quad , \quad J_1(\beta) \approx \frac{\beta}{2}$$

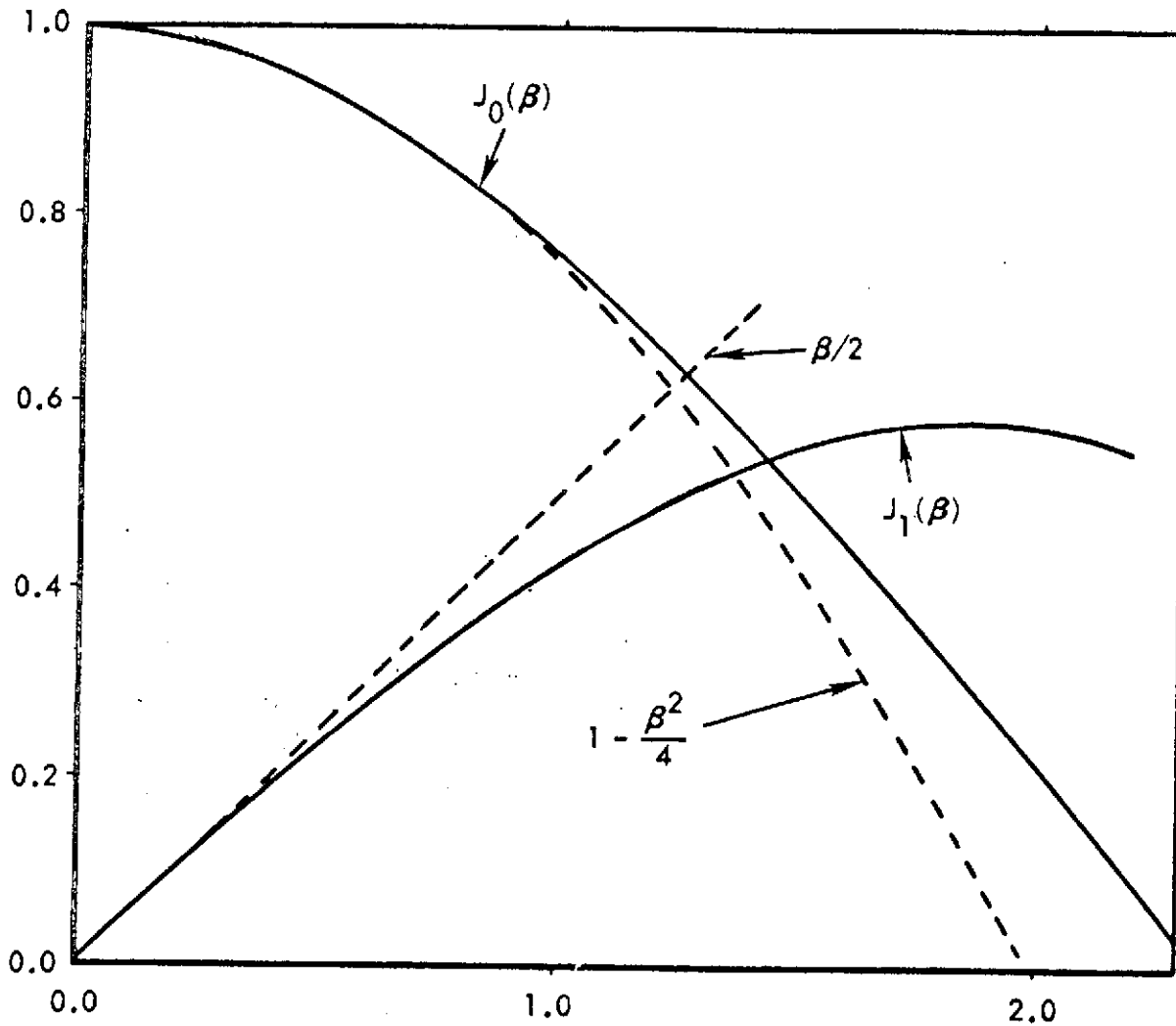


Figure 6.3-2. $J_0(\beta)$ and $J_1(\beta)$, With Small- β Approximations

As an alternative approach to analyzing the coherent PM receiver, suppose that the input is given by Equation 6.3-1, but the restriction is to pure PSK subcarrier signals is removed. If the carrier tracking loop achieves exact synchronization, then

$$\begin{aligned}
 y_1(t) &= -A_c \cos \left[\omega_c t + \beta e_{sc}(t) \right] \sin \omega_c t \\
 &= \frac{A_c}{2} \sin \beta e_{sc}(t) - \frac{A_c}{2} \sin \left[2\omega_c t + \beta e_{sc}(t) \right]
 \end{aligned}$$

The second term is rejected by the filter, leaving

$$y_2(t) = \frac{A_c}{2} \left[\sin \beta e_{sc}(t) \right]_{lp}$$

where $[\cdot]_{lp}$ denotes the low-pass components of the enclosed signal. If β is small, say $\beta \leq 0.5$, then

$$\sin \left[\beta e_{sc}(t) \right] \approx \beta e_{sc}(t) \quad (6.3-5)$$

so that

$$y_2(t) \approx \frac{A_c \beta}{2} e_{sc}(t)$$

We note that this agrees with Equation 6.3-4 when $J_1(\beta)$ is replaced by its approximate value $\beta/2$.

When β is not small, the approximation of Equation 6.3-5 fails and considerable distortion of the signal may result. We have seen that if $e_{sc}(t)$ is pure PSK, this is not the case, but if $e_{sc}(t)$ consists of PSK with a Summed Clock term, then $\sin \beta e_{sc}(t)$ contains contributions at all frequencies of the form $n\omega_{cl}$, $\omega_{sc} \pm n\omega_{cl}$, $2\omega_{sc} \pm n\omega_{cl}$, etc., which are in the passband of the filter and which may be non-negligible.

If the input to the receiver of Figure 6.3-1 is the PM signal $e_c(t)$ with added white Gaussian noise of spectral density $N_0/2$, and if β is small enough for Equation 6.3-5 to hold, then under the assumption of perfect carrier synchronization, the output is found to be

$$y_{sc}(t) = e_{sc}(t) + n_{sc}(t)$$

where $n_{sc}(t)$ is band-limited white Gaussian noise of spectral density $N_0/A_c^2 \beta^2$. Since this is the same noise spectrum found in Section 6.2 for the noncoherent receiver, we conclude that the performance of the coherent and noncoherent receivers agree, provided that the signal-to-noise ratio is high enough that carrier synchronization errors are negligible. With this condition the curves of Figure 6.2-3 apply for coherent PM.

6.4 Cross-Coupling Between RF Systems

In this section we determine the response of one type of RF receiver to a received signal at the same carrier frequency, but with a different type of RF modulation. This problem is of interest when, for example, two missions are assigned the same RF channel but use different carrier modulation schemes. The results of this section would indicate the extent to which the receiver aboard one spacecraft would respond to signals directed to the other. It is important to remember that these results are (in general) only valid when the desired signal is off; when the received signal consists of desired signal plus interfering signal, we have an RFI problem, rather than a cross-coupling problem. This problem can be approached using the techniques of Section 4.

6.4.1 Cross-Coupling Between Angle - and Amplitude - Modulation Systems

An angle-modulated RF signal has the form indicated by Equation 6.2-1, in which $\phi(t)$ involves the subcarrier signal $e_{sc}(t)$. Since such a signal has constant envelope, an envelope detector does not respond to the signal, and therefore there is no cross-coupling into an AM receiver.

An AM signal has the form of Equation 6.1-1. Conventional angle modulation receivers employ limiters at the input to remove spurious amplitude fluctuations. When an AM signal is received, the limiter removes the modulation. Since the resulting signal has constant phase, the response of the demodulator is zero.

6.4.2 Cross-Coupling Between FM and PM

The instantaneous phase of a frequency-modulated signal is

$$\omega_c t + k \int_{t_0}^t e_{sc}(s) ds$$

while the instantaneous frequency of a phase-modulated signal is

$$\omega_c + \beta \frac{de_{sc}}{dt}$$

Hence, if a PM receiver demodulates an FM signal, the output is proportional to

$$\int e_{sc}(t) dt$$

and if an FM receiver demodulates a PM signal, the output is proportional to

$$\omega_c + \beta \frac{de_{sc}}{dt}$$

These results are displayed in Table 6.4.2, in which the RF detector outputs are given, to within a scale factor, for all types of receiver with all possibilities of received signal.

Table 6.4.2. Cross-Coupling Between FM and PM

Receiver	Receiver Input		
	AM	FM	PM
AM	$e_{sc}(t)$	0	0
FM	0	$e_{sc}(t)$	$\frac{de_{sc}}{dt}$
PM	0	$\int e_{sc}(t) dt$	$e_{sc}(t)$

6.5 Doppler Considerations

In this section we estimate the magnitude of the frequency shift due to relative motion between spacecraft and transmitter. Our purpose is to determine what design modifications are necessary to compensate for the frequency uncertainty.

A sinusoid of frequency f undergoes a frequency shift by an amount $v_t f/c$, where c is the speed of light, and v_t is the component of spacecraft velocity in the direction of the transmitter. We assume a worst-case velocity component of

$$v_t = 13 \text{ km/sec (7 nautical mi/sec)}$$

so that $v_t/c = 4.33 \times 10^{-5}$.

Uplink carrier frequencies are near 150 MHz, so that the worst-case Doppler is approximately 6.5 kHz. Thus unless an attempt is made to track the carrier, the RF and IF bandwidths must be 13 kHz wider than actually required to accommodate the signal. For example, if the RF modulation is AM or relatively narrowband angle modulation, then as noted in Section 3.3, the signal bandwidth is a few times the subcarrier frequency, and since f_{sc} can be as low as 7 kHz, widening of the filter passbands enough to accommodate frequency shift can significantly increase the amount of noise power in the RF detector input, causing degradation of performance.

As another example of the effect of Doppler variations, we consider its impact on the design of the coherent PM demodulator discussed in Section 6.3. For simplification, we assume that the subcarrier modulation is PSK with no clock. Then $\eta = 1$, and we have

$$P_e = Q \left(\sqrt{\frac{C}{N_o R}} \beta^2 \right) \quad (6.5-1)$$

This is plotted for several values of β in the range of interest in Figure 6.5.

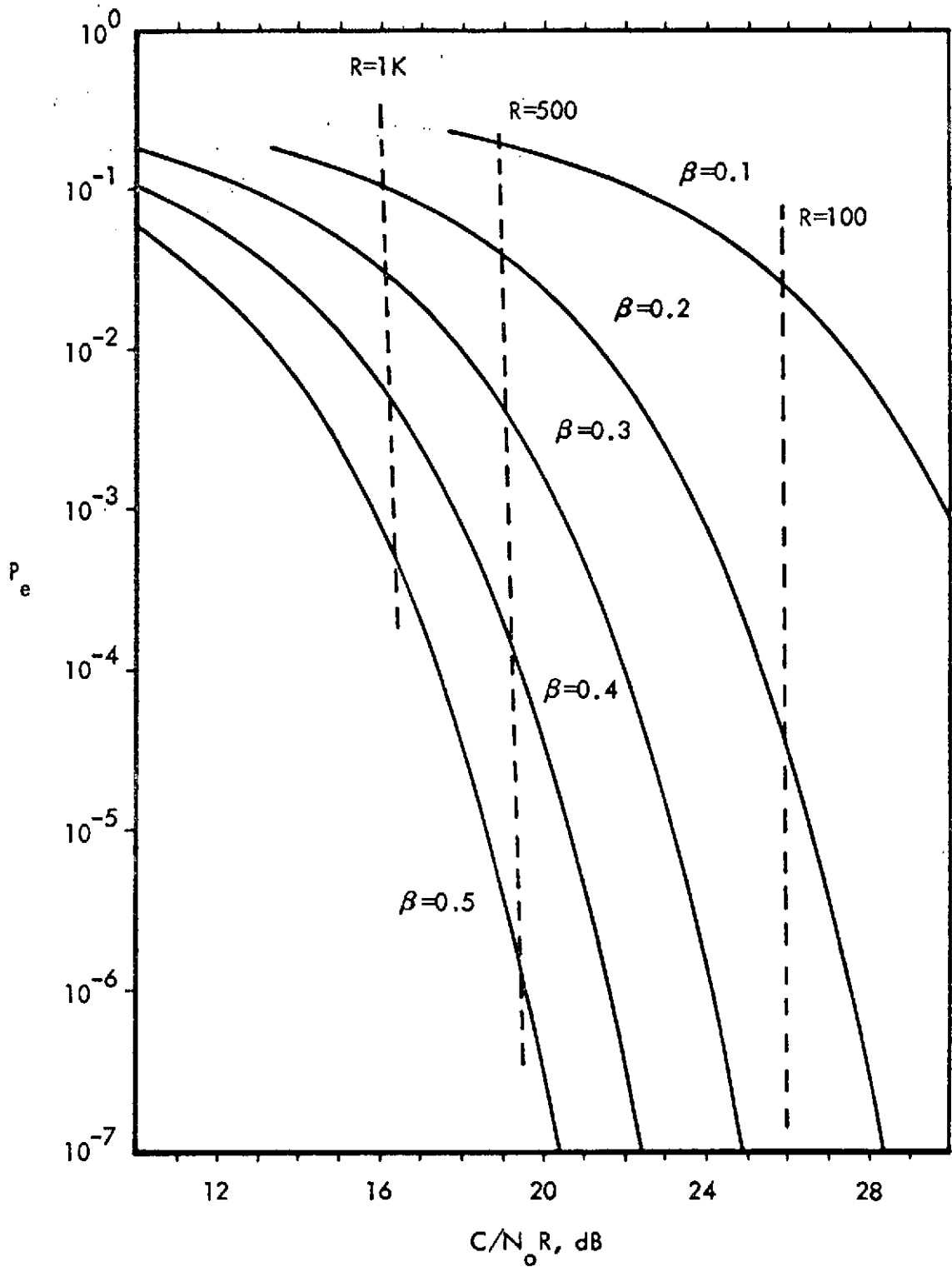


Figure 6.5. Error Probability for PSK/PM, $0.1 \leq \beta \leq 0.5$

Recall from Equation 6.3-3 that the received signal contains a pure carrier term of the form

$$A_c J_0(\beta) \cos(\omega_c t)$$

to which the receiver must lock before reliable demodulation can take place. The frequency uncertainty requires that the carrier tracking loop have some bandwidth B_0 , related to the Doppler and Doppler rate in a manner depending on the characteristics of the tracking method. If we require 10 dB signal-to-noise ratio in the carrier tracking loop, and assume a nominal value of 4 kHz for B_0 , then we must have

$$\frac{A_c^2 J_0^2(\beta)}{2N_o B_0} = \frac{C}{N_o R} J_0^2(\beta) \cdot \frac{R}{4 \text{ kHz}} \geq 10 \quad (6.5-2)$$

Equation 6.5-2 establishes, for given data rate R and modulation index β , minimum allowable values of $C/N_o R$ for reliable carrier tracking. Thus, we have an effect analogous to the threshold effect seen in Sections 6.1 and 6.2; i.e., at low values of $C/N_o R$, performance is degraded from that predicted by Equation 6.5-1 because of poor carrier tracking. The thresholds implied by Equation 6.5-2 are shown in Figure 6.5 for several bit rates.

The spacecraft velocity also causes a shift in the subcarrier frequency; however, since subcarrier frequencies are at most 15 kHz, the worst case frequency shift is given by

$$\frac{v_t}{c} f_{sc} \leq 4.33 \times 10^{-5} \times 15 \times 10^3 = 0.63 \text{ Hz}$$

This shift is less than 10% of even the least allowable bit rate, and therefore less than 5% of the least possible subcarrier bandwidth. Therefore the Doppler effects on the design and operations of the subcarrier detector are negligible.

6.6 Summary

This section has addressed certain problems associated with the RF carrier portion of the command system. Results relating P_c to $C/N_0 R$, where C is the RF carrier power, are obtained for AM, FM, and PM RF modulation in conjunction with the subcarrier keying and clock transmission schemes discussed earlier. The threshold effect associated with conventional receivers is discussed and its effect on system operating characteristics is considered.

Another problem considered in this section is the response of one kind of receiver to a received signal of another kind. These cross-coupling effects are determined and listed for all combinations of receiver and transmitted signal.

Finally, the frequency shifts at RF and subcarrier due to spacecraft motion are determined. Some implications of Doppler effects on RF system design are discussed. It is also shown that the frequency shift at subcarrier is negligible.

6.7 References

- [6-1] Schwartz, M., W. R. Bennett, and S. Stein, Communication Systems and Techniques, McGraw Hill, New York, 1966, pp. 100 ff.
- [6-2] Viterbi, A. J., Principles of Coherent Communication, McGraw Hill, New York, 1966, pp. 174 ff.
- [6-3] Davenport, W. B., and W. L. Root, Random Signals and Noise, McGraw Hill, New York, 1958, pp. 265 ff.
- [6-4] Middleton, D., An Introduction to Statistical Communication Theory, McGraw Hill, New York, 1960, pp. 563 ff., 636 ff.

7.0 DOWNLINK CARRIER MODULATION

The downlink transmission schemes used for command verification differ from those in the uplink in several respects. For example, the usual baseband signal is biphase PCM; NRZ signals are not used. No clock is transmitted along with the data. The baseband signal directly frequency or phase modulates the RF carrier, without the intermediate step of subcarrier modulation which is employed in the uplink. Finally, since the transmitter is on board the spacecraft, power limitations are of more significance than in the uplink.*

In this section, various aspects of the downlink are investigated, with emphasis on those features which are peculiar to the downlink, and relying as much as possible on results and techniques developed previously. First some comments on biphase PCM are made. Then the RF signals resulting from PM or FM modulation by a biphase baseband signal are studied. Finally, some observations concerning the power constraint, as it relates to the reliability requirements, are made.

7.1 Biphase PCM

In biphase PCM the baseband signal consists of a sequence of pulses $s_0(t)$ or $s_1(t)$ with the form

$$s_0(t) = \begin{cases} +1 & 0 \leq t < T/2 \\ -1 & T/2 \leq t < T \end{cases}$$

$$s_1(t) = -s_0(t)$$

The power spectrum of a random biphase PCM signal can be shown to be [7-1]:

$$S(f) = T \frac{\sin^4(\pi fT/2)}{(\pi fT/2)^2}$$

*Gains and other characteristics of ground antennas are found in "Handbook of NASA/GSFC Tracking, Data Acquisition and Communication Antennas", No. X-525-64-222, October 1964.

which is illustrated in Figure 7.1. Note that there is very little signal power near dc, so that the signal can be ac-coupled without significant distortion. This is one of the principal reasons for using biphase rather than NRZ signals. Another reason is that since at least one sign change per bit interval is guaranteed, bit synchronization directly from the signal is facilitated.

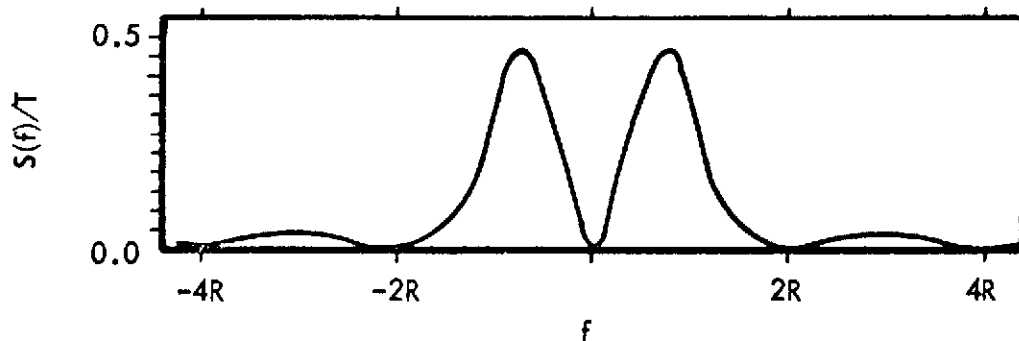


Figure 7.1. Random Biphase PCM Power Spectrum

In the following sections we investigate the signals resulting from phase or frequency modulation of a carrier by a biphase PCM signal.

7.2 PCM/PM

The general form of a PM signal with PCM modulation is

$$e_c(t) = A_c \cos \left[\omega_c t + \beta x(t) + \theta_c \right] \quad (7.2-1)$$

where $x(t)$ is a biphase PCM signal. We adopt the convention of referring to such signals as PCM/PM, reserving the designation PSK for such signals in which $\beta = \pi/2$.

Expanding Equation (7.2-1) yields

$$\begin{aligned} e_c(t) &= A_c \cos \left[\beta x(t) \right] \cos (\omega_c t + \theta_c) \\ &\quad - A_c \sin \left[\beta x(t) \right] \sin (\omega_c t + \theta_c) \end{aligned}$$

But since for any t , $x(t) = \pm 1$, this can be written

$$\begin{aligned} e_c(t) &= A_c \cos \beta \cos (\omega_c t + \theta_c) \\ &\quad - A_c x(t) \sin \beta \sin (\omega_c t + \theta_c) \end{aligned} \tag{7.2-2}$$

The first term in Equation 7.2-2 is a pure carrier term while the second is a pure antipodal biphasic PSK term.

Power spectra of such signals can be determined using the techniques developed in Section 3. Spectra for $\beta = 1$ and $\beta = \pi/2$ are shown in Figure 7.2-1.

For receiving stations which do not have the capability of extracting the carrier from a PSK signal, β should be chosen in such a way that enough power is left in the pure carrier to allow reliable acquisition and tracking. For example, the appropriate standard [7-2] requires that at least 10% of the transmitted power be left in the pure carrier term. From Equation 7.2-2, this requirement means that $\cos^2 \beta \geq 0.1$, or $\beta \leq 1.25$. When the receiving station is capable of obtaining carrier synchronization directly from the received PSK signal, the most efficient modulation index is $\beta = \pi/2$, which suppresses the carrier entirely and devotes all the transmitted power to the data. It should be noted, however, that values of β equal to 1.25, 1.1 and 1, for example, corresponding to 10, 20 and 30 percent of the power in the carrier, yield 0.5 dB, 1 dB and 1.5 dB losses in the PSK component, respectively. The 0.5 dB to 1 dB loss might provide a good trade for reduced receiver complexity realized by tracking the carrier directly. This is contrasted with the frequency doubling, tracking and dividing scheme typically employed to reconstruct the carrier in PSK, and finally resolving a phase ambiguity.

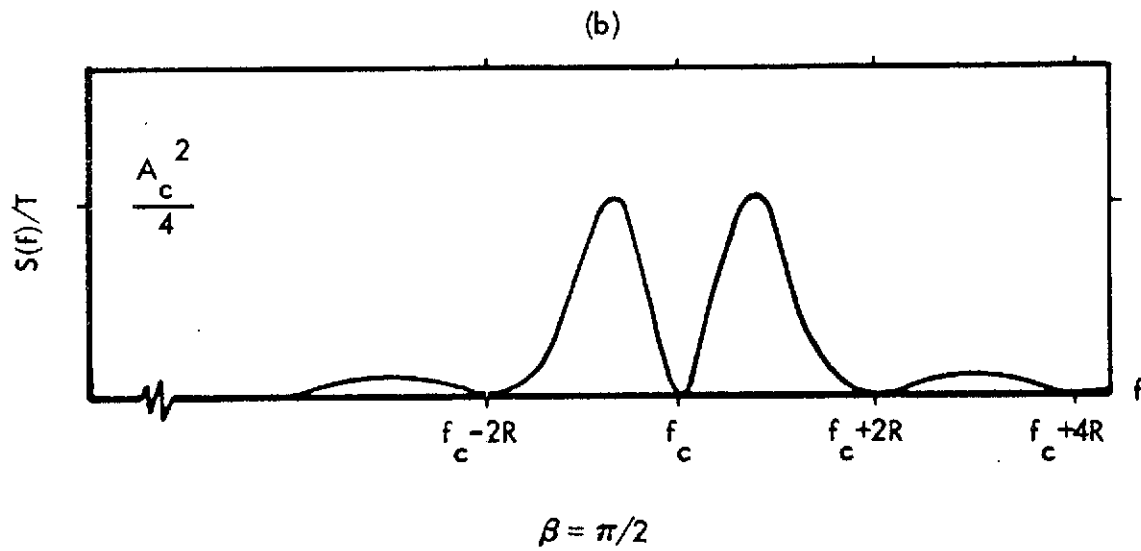
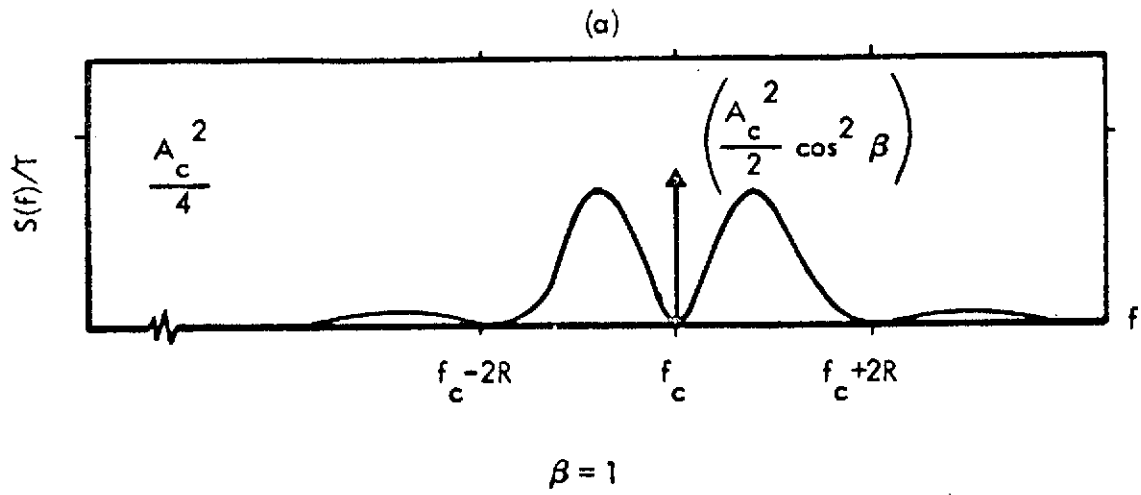


Figure 7.2-1. Power Spectra of PCM/PM

We have seen in Section 2.1 that the optimum receiver for antipodal biphase PSK ($\beta = \pi/2$) is a correlator similar to that of Figure 2.1.1-1 (except that the local signal to be multiplied must be a biphase sinusoid rather than a pure sinusoid). We also noted that the error probability is given by

$$P_e = Q \left(\sqrt{\frac{2E_b}{N_o}} \right)$$

where E_b is the energy in each bit interval of the biphase PSK signal. It has just been shown that for any β , a biphase PSK signal can be written as the sum of a pure carrier and an antipodal biphase PSK signal with bit energy

$$E_b = \frac{A_c^2 \sin^2 \beta}{2} T$$

If $\omega_c \gg 2\pi R$, the response of the correlator to the pure carrier is negligible, and so the correlator is the optimum receiver for any β . Letting $C = A_c^2/2$ and noting that $T = 1/R$, we have for the optimum receiver,

$$P_e = Q \left(\sqrt{\frac{2 C \sin^2 \beta}{N_o R}} \right) \quad (7.2-3)$$

Equation 7.2-3 can also be derived by considering the biphase PCM/PM signals as points in a signal space of two dimensions. The geometry is shown in Figure 7.2-2. The length of each vector is the square root of the signal energy, $A_c \sqrt{T/2}$, and the vectors are inclined at angles $\pm\beta$ to the $\phi_1(t)$ - axis. The error probability of such a signal set is given by [7-3]:

$$P_e = Q \left(\frac{d}{\sqrt{2N_o}} \right)$$

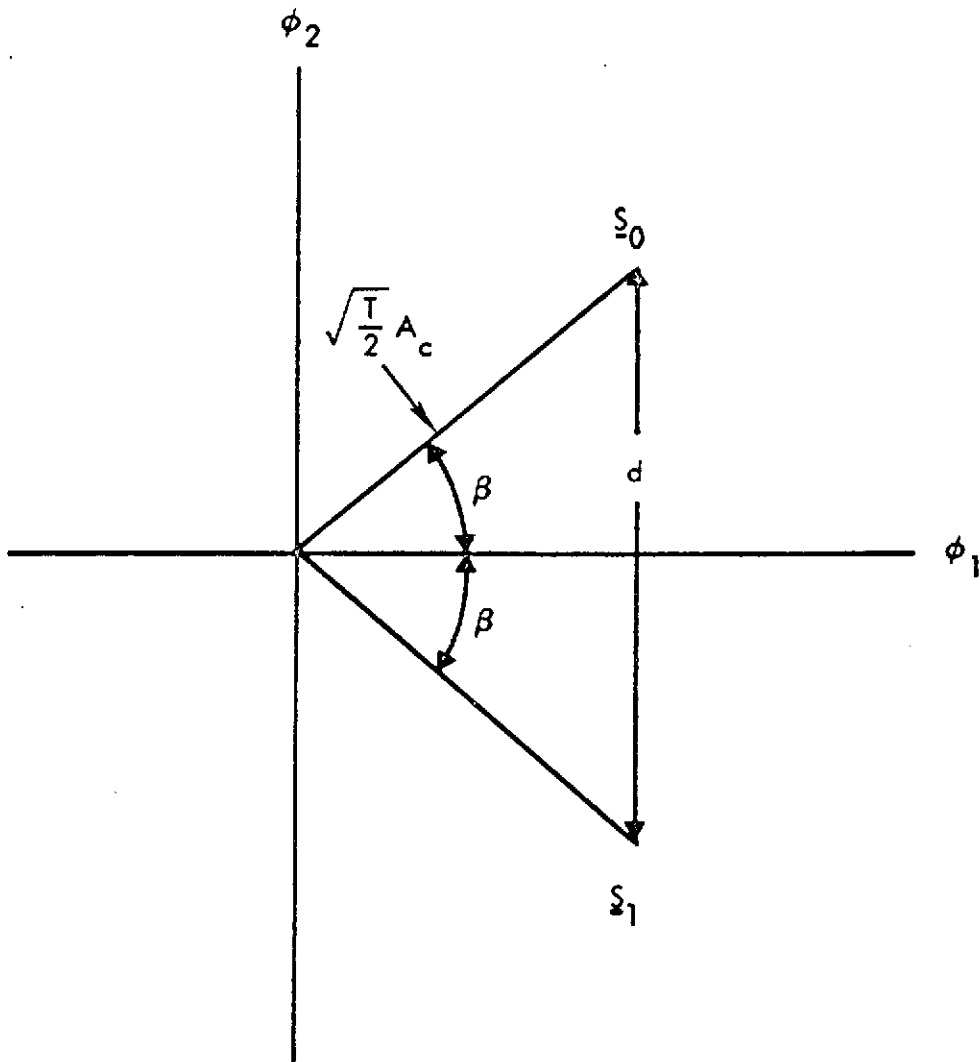


Figure 7.2-2. Signal Space Model for PCM/PM

where d is the Euclidean distance between the signal vectors. From Figure 7.2-2,

$$d = 2 \sqrt{\frac{T}{2}} A_c \sin \beta$$

which leads to Equation 7.2-3. This geometric approach also shows that $\beta = \pi/2$ is the optimum choice to minimize P_e , and that nothing is gained by increasing β to values greater than $\pi/2$.

The use of FM rather than PM as the RF downlink modulation affords some simplification since a noncoherent receiver can be used. As noted in Section 2.1, the optimum receiver for such a signal is essentially the same matched filter-envelope detector receiver shown in Figure 2.1.1-2, except that the filters are matched to split-phase pulses. If the signals are orthogonal, the error probability is given by

$$P_e = \frac{1}{2} e^{-E_b/2N_o} = \frac{1}{2} e^{-C/2N_o R} \quad (7.3-1)$$

The signals can be shown to be orthogonal if $|f_1 - f_0| T$ is an even integer. If this quantity, which is the PCM/FM modulation index, is not an even integer, but f_0 and f_1 , are sufficiently far apart that a filter tuned to f_1 responds negligibly to f_0 and vice-versa, then P_e is approximated by Equation 7.3-1. A somewhat simpler receiver for these signals consists of filters matched to f_0 and f_1 over half of a bit interval, followed by envelope detectors, with post-detection combining of the detector outputs at times $T/2$ and T . The error probability when such a receiver is used is given by [7-4]

$$P_e = \frac{1}{2} e^{-C/2N_o R} \left(1 + \frac{C}{8N_o R} \right) \quad (7.3-2)$$

Power spectra of biphase PCM/FM signals have been obtained by Hartmann [7-1] using an approach similar to that of Section 3. As an example, the (one-sided) spectrum for a modulation index of 2 is shown in Figure 7.3. This is chosen since it is the least modulation index for which the signals are exactly orthogonal. The spectrum is seen to contain impulses at the mark and space frequencies as well as a continuous part exhibiting nulls at f_0 and f_1 . These features are typical of PCM/FM power spectra with even integer modulation indices.

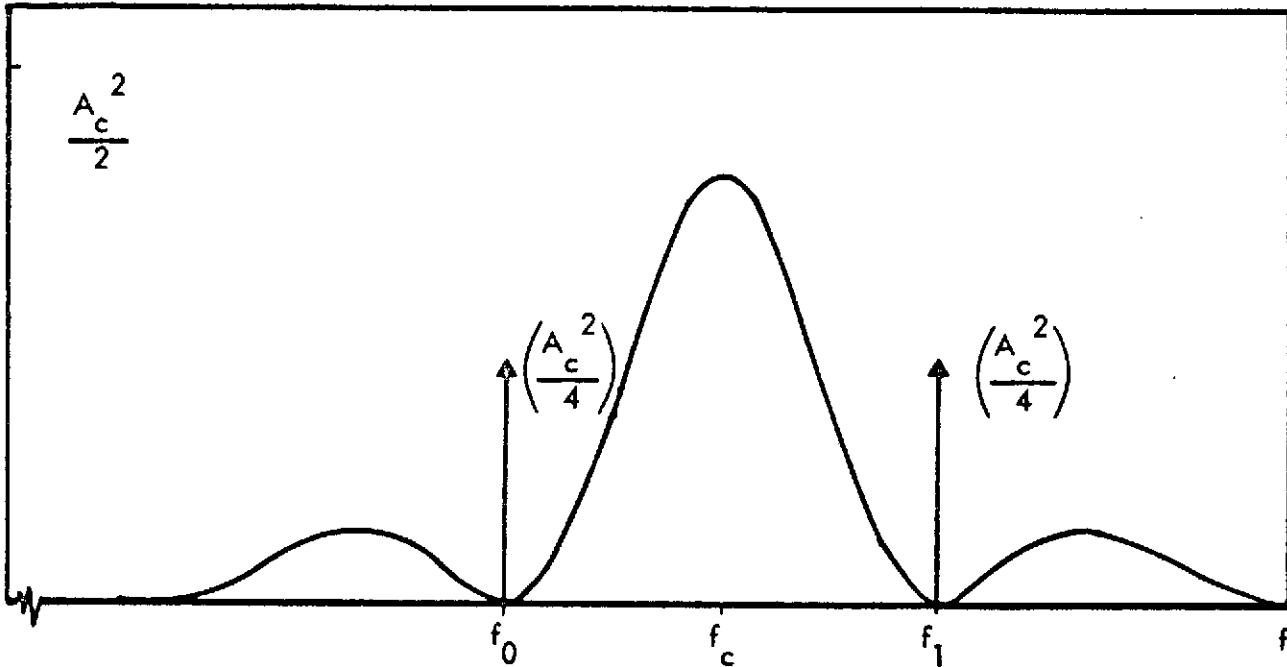


Figure 7.3. PCM/FM Power Spectrum

7.4 Downlink Reliability Requirements

Since decoded commands are transmitted to the ground via the telemetry downlink for purposes of verification, it is necessary that the downlink be at least as reliable as the uplink and preferably much more reliable. The reason for this is that whenever the command relayed via downlink disagrees with that which was transmitted, the command must be repeated. If the downlink error probability is, say, an order of magnitude greater than the uplink error probability, then most of the disagreements between transmitted and received messages will be due to errors in the downlink, and therefore, most of the repeated commands are actually repeats of commands which were initially received correctly on board the spacecraft. A high-reliability downlink ensures that almost all detected errors occurred in the uplink, and thus very few unnecessary retransmissions are incurred.

The bit error probability results of Equations 7.2-3, 7.3-1 and 7.3-2 are shown in Figure 7.4. From these plots we see that bit error probabilities of the order of 10^{-5} or less require 10 dB or more C/N_0R . Because of the limitation on spacecraft transmitter power, it is desirable to operate at as low a value of C/N_0R as possible, with particular interest in the intermediate range of 7 dB or so. Figure 7.4 indicates that P_e is unacceptably high at this value of C/N_0R ,

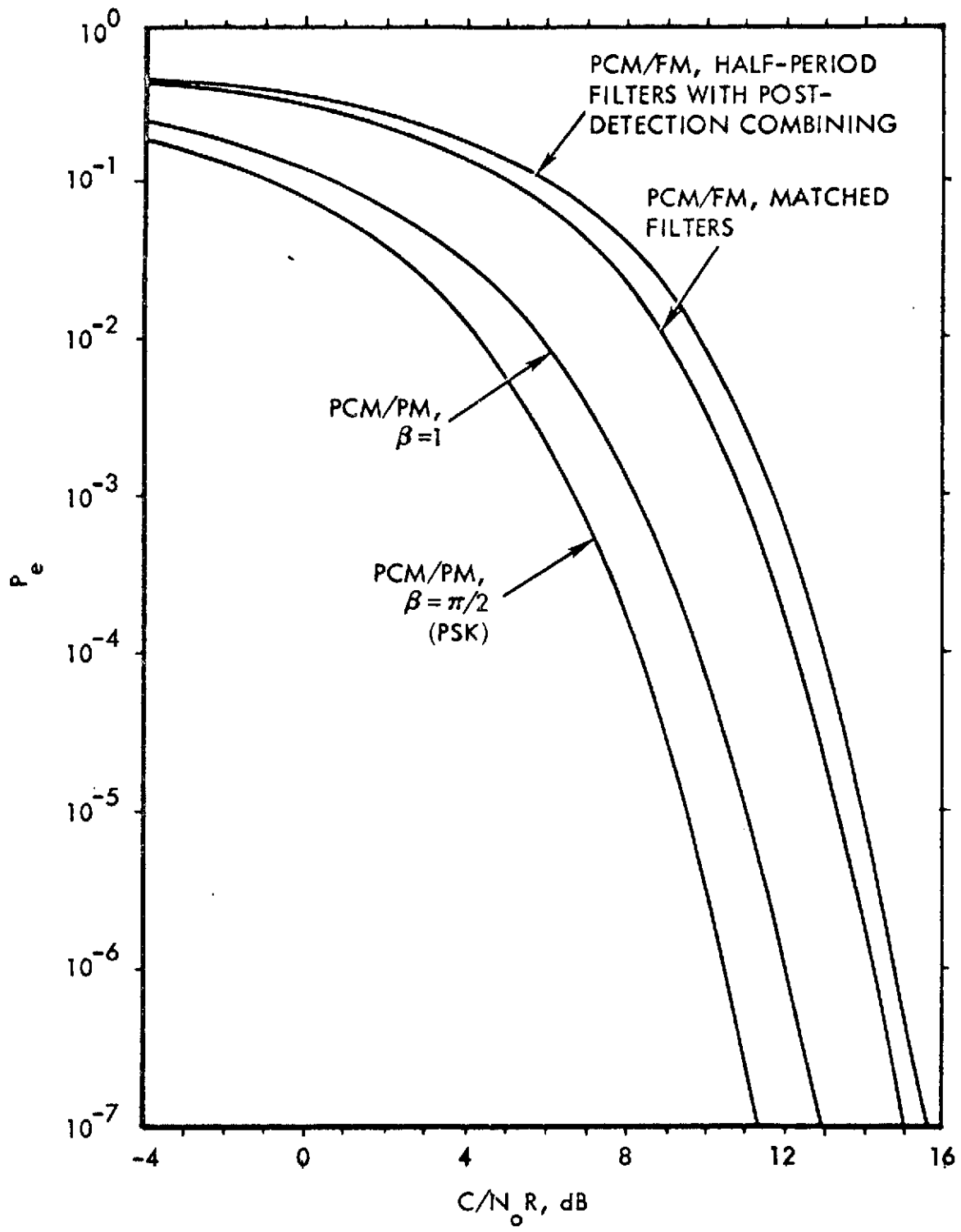


Figure 7.4. Error Probabilities for PCM/PM and PCM/FM

even for the most efficient modulation scheme. This suggests the use of coding in the downlink. As discussed in Section 5.6, substantial gains can be obtained with relatively simple encoding equipment on board the spacecraft and decoding equipment of moderate complexity on the ground. For example, referring to Figure 5.6.2-2, P_e of 10^{-5} or less can be obtained at 6.6 dB E_b/N_0 with a memory 5, rate 1/2 nonsystematic convolutional code with Viterbi decoding and hard decisions at the receiver. With soft decisions, the required E_b/N_0 drops to 4.7 dB. These values represent gains of 3 dB and 4.9 dB, respectively, over the 9.6 dB required to achieve $P_e = 10^{-5}$ in an uncoded system. While these gains are given for antipodal PSK, comparable coding gains would be expected with any PCM/PM or PCM/FM transmission scheme. We conclude that with the use of coding in the downlink, the necessary reliability can be obtained at intermediate values of C/N_0R with equipment of moderate complexity.

7.5 Summary

During this task effort, certain aspects of the telemetry downlink with application to command verification have been studied. Signal structures and spectra representing PCM/PM and PCM/FM signals, where the PCM is biphase rather than NRZ, are considered. Error probability associated with these systems are also discussed and data are graphically presented.

Concerning PCM/PM, various values of the peak phase deviation, β , are considered. Based upon the fact that $\beta = \pi/2$ (i.e., PSK) provides the best bit error performance, other values of β and the corresponding degradation in performance are investigated. It is shown that values of β equal to 1.25, 1.1 and 1, for example, corresponding to 10, 20 and 30 percent of the power in the carrier, yield 0.5 dB, 1 dB and 1.5 dB degradation in performance relative to PSK. The 0.5 dB to 1 dB loss might provide a good trade for reduced receiver complexity realized by tracking the carrier directly. Factors to be considered include the following. Typically, a frequency doubler, tracking and divider technique is employed to reconstruct the carrier for PSK, producing a phase ambiguity which must be resolved. In PCM/PM, a carrier tracking phase locked loop can be employed when sufficient power is allocated to the carrier. In the latter case the tracking loop is operating at a lower signal-to-noise ratio, depending upon the loop bandwidth. The loop bandwidth in both cases is determined by the frequency uncertainty and the requirement upon acquisition time. Finally, it should be noted that the frequency uncertainty is doubled in the PSK case.

Regarding error probability, it is shown that even the most efficient modulation scheme provides an error probability which is unacceptably high for command verification purposes when operating in the intermediate signal-to-noise ratio range (e.g., 7 dB) of interest. However, sufficient gain from coding is available to reduce the error probability to an acceptable level for typical values of C/N_0R . The coding gain can be obtained with the use of relatively simple encoding and decoding equipment.

7.6

References

- [7-1] Hartmann, H. P., "Spectrum of Manchester Coded FSK", IEEE Trans. Comm., Vol. COM-20, pp. 1001-1004, October 1972.
- [7-2] Aerospace Data System Standards, Part III, Section 1, Ratio Frequency and Modulation Standard for Space-to-Ground Telemetry.
- [7-3] Wozencraft, J. M., and I. M. Jacobs, Principles of Communication Engineering, Wiley, New York, 1965.
- [7-4] Gonsalves, R. A., "Performance of Manchester Coded FSK", IEEE Trans. on Aerospace and Electronic Systems, Vol. AES-6, pp. 598-599, July 1970; Vol. AES-7, p. 395, March 1971.